

## **INFORMATION TO USERS**

**This manuscript has been reproduced from the microfilm master. UMI films the text directly from the original or copy submitted. Thus, some thesis and dissertation copies are in typewriter face, while others may be from any type of computer printer.**

**The quality of this reproduction is dependent upon the quality of the copy submitted. Broken or indistinct print, colored or poor quality illustrations and photographs, print bleedthrough, substandard margins, and improper alignment can adversely affect reproduction.**

**In the unlikely event that the author did not send UMI a complete manuscript and there are missing pages, these will be noted. Also, if unauthorized copyright material had to be removed, a note will indicate the deletion.**

**Oversize materials (e.g., maps, drawings, charts) are reproduced by sectioning the original, beginning at the upper left-hand corner and continuing from left to right in equal sections with small overlaps.**

**ProQuest Information and Learning  
300 North Zeeb Road, Ann Arbor, MI 48106-1346 USA  
800-521-0600**

**UMI<sup>®</sup>**



**UNIVERSITY OF OKLAHOMA  
GRADUATE COLLEGE**

**BRIDGE WEIGH-IN-MOTION (WIM) ALGORITHM FOR  
ESTIMATING AXLE WEIGHTS, AXLE SPACING, AND OTHER  
TRUCK PARAMETERS**

**A Dissertation**

**SUBMITTED TO THE GRADUATE FACULTY**

**in partial fulfillment of the requirements for the**

**degree of**

**DOCTOR OF PHILOSOPHY**

**By**

**SARAH K. LEMING**

**Norman, Oklahoma**

**2002**

UMI Number: 3073701

UMI<sup>®</sup>

---

UMI Microform 3073701

Copyright 2003 by ProQuest Information and Learning Company.  
All rights reserved. This microform edition is protected against  
unauthorized copying under Title 17, United States Code.

---

ProQuest Information and Learning Company  
300 North Zeeb Road  
P.O. Box 1346  
Ann Arbor, MI 48106-1346

**© Copyright by SARAH K. LEMING 2002  
All Rights Reserved**

**BRIDGE WEIGH-IN-MOTION (WIM) ALGORITHM FOR ESTIMATING AXLE WEIGHTS, AXLE SPACING, AND OTHER TRUCK PARAMETERS**

**A Dissertation APPROVED FOR THE  
SCHOOL OF AEROSPACE AND MECHANICAL ENGINEERING**

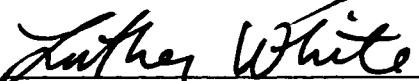
**BY**

  
\_\_\_\_\_  
**Dr. Harold Stalford (Committee Chair)**

  
\_\_\_\_\_  
**Dr. Charles Bert**

  
\_\_\_\_\_  
**Dr. Kuang-Hua Chang**

  
\_\_\_\_\_  
**Dr. Robert Anex**

  
\_\_\_\_\_  
**Dr. Luther White**

# Table of Contents

|   |       |
|---|-------|
| Table of Contents .....                               | iv    |
| List of Figures .....                                 | viii  |
| List of Tables .....                                  | xiv   |
| Abstract .....  | xviii |
| 1. WIM Systems and Force Identification Methods ..... | 1     |
| 1.1 In-Service WIM Systems .....                      | 3     |
| 1.2 Force Identification Methods .....                | 9     |
| 2. Bridge Models .....                                | 16    |
| 2.1 Combination Models .....                          | 17    |
| 2.2 Multiple Beam Models .....                        | 20    |
| 2.3 Single Beam Models .....                          | 21    |
| 2.4 My Models .....                                   | 22    |
| 2.5 Static Beam .....                                 | 24    |
| 2.6 Finite Element Model .....                        | 24    |
| 2.7 Solution of the Differential Equation .....       | 26    |
| 2.8 Static Beam Bending Equation .....                | 27    |
| 2.9 Dynamic Beam .....                                | 28    |
| 2.10 $R(s,z)$ .....                                   | 31    |
| 2.11 Reduced Order Model .....                        | 32    |
| 2.12 Sensor Location .....                            | 34    |
| 2.13 Chapter Conclusions .....                        | 37    |
| 2.14 Bridge Models Appendix .....                     | 38    |

|  |           |
|--|-----------|
| <b>3. Truck Models .....</b>                                       | <b>41</b> |
| <b>3.1 3D Truck Models .....</b>                                   | <b>43</b> |
| <b>3.2 2D Truck Models .....</b>                                   | <b>44</b> |
| <b>3.3 1D Truck Models .....</b>                                   | <b>46</b> |
| <b>3.4 Static Weight .....</b>                                     | <b>52</b> |
| <b>3.5 Numerical Parameters Used in Static Truck Models .....</b>  | <b>52</b> |
| <b>3.6 Numerical Parameters Used in Dynamic Truck Models .....</b> | <b>53</b> |
| <b>4. Bridge/Truck Interaction .....</b>                           | <b>56</b> |
| <b>4.1 Iterative Solutions .....</b>                               | <b>56</b> |
| <b>4.2 Other Methods .....</b>                                     | <b>57</b> |
| <b>4.3 Direct Integration .....</b>                                | <b>57</b> |
| <b>4.4 Truck Crossing the Bridge .....</b>                         | <b>58</b> |
| <b>4.5 Static Bridge/Static Truck .....</b>                        | <b>60</b> |
| <b>4.6 Static Bridge/Dynamic Truck .....</b>                       | <b>61</b> |
| <b>4.7 Dynamic Bridge/Static Truck .....</b>                       | <b>64</b> |
| <b>4.8 Dynamic Bridge/Dynamic Truck .....</b>                      | <b>65</b> |
| <b>5. Optimization and Problem Statement .....</b>                 | <b>68</b> |
| <b>5.1 The Optimization Routine .....</b>                          | <b>68</b> |
| <b>5.2 Problem Statement .....</b>                                 | <b>73</b> |
| <b>6. Static Bridge/Static Truck .....</b>                         | <b>77</b> |
| <b>6.1 Static Bridge/Static Truck Problem .....</b>                | <b>77</b> |
| <b>6.2 Uniform Sampling Method .....</b>                           | <b>80</b> |
| <b>6.3 Discontinuities in the Derivatives .....</b>                | <b>80</b> |

|  |     |
|--|-----|
| 6.4 Random Sampling Method .....                                     | 90  |
| 6.5 Chapter Conclusions and Contributions .....                      | 100 |
| 7. Dynamic Bridge/Static Truck .....                                 | 102 |
| 7.1 Dynamic Bridge/Static Truck-Speed and Axle Spacing Known .....   | 102 |
| 7.2 Dynamic Bridge/Static Truck-Speed and Axle Spacing Unknown ..... | 107 |
| 7.3 Chapter Conclusions .....  | 117 |
| 8. Static Bridge/Dynamic Truck .....                                 | 119 |
| 8.1 The Measured Profile .....                                       | 119 |
| 8.2 Approximating the Force .....                                    | 120 |
| 8.3 Parameter Identification-Optimization Routine .....              | 125 |
| 8.4 Parameter Identification-Force Objective Function .....          | 126 |
| 8.5 Parameter Identification-Deflection Objective Function .....     | 133 |
| 8.6 Chapter Conclusions .....  | 143 |
| 9. Dynamic Bridge/Dynamic Truck .....                                | 146 |
| 9.1 Simulating the Truck and Bridge-Full Model .....                 | 147 |
| 9.2 Approximate Force Model .....                                    | 148 |
| 9.3 WIM Algorithm.....   | 152 |
| 9.4 Parameter Identification.....                                    | 152 |
| 9.5 Optimization Results .....                                       | 154 |
| 9.6 Numerical Results .....  | 177 |
| 9.7 Conclusions and Contributions .....                              | 197 |
| 10. Conclusions and Future Work .....                                | 200 |
| 10.1 Conclusions.....  | 200 |

|                              |            |
|------------------------------|------------|
| <b>10.2 Future Work.....</b> | <b>204</b> |
| <b>11. References.....</b>   | <b>206</b> |

# List of Figures

|   |    |
|---|----|
| Figure 1.1 Flowchart of WIM Systems .....   | 5  |
| Figure 1.2 Force Identification Methods .....   | 10 |
| Figure 2.1 Flowchart of Bridge Models in the Literature .....   | 17 |
| Figure 2.2 Finite Element Model of Bridge .....   | 23 |
| Figure 2.3 Sample Deflection Profile of the Static Bridge Midpoint Deflection .....                   | 25 |
| Figure 2.4 Sample Deflection Profile of the Midpoint Deflection Using the Dynamic<br>Beam Model ..... | 29 |
| Figure 2.5 Error Using Modes 1, 2, 3, 5, 7 in the Reduced Order Model .....                           | 33 |
| Figure 2.6 Error Using Modes 1, 2, 3, 4, 5, 6, 7 in the Reduced Order Model .....                     | 33 |
| Figure 2.7 Deflection at Each Node Due to a Moving Point Force .....                                  | 35 |
| Figure 2.8 Sine Term at Each Node For Three Modes .....   | 36 |
| Figure 3.1 Flowchart of Truck Models in the Literature .....  | 42 |
| Figure 3.2 'Quarter-Car' Model Used in This Work .....  | 48 |
| Figure 4.1 Flowchart of Bridge/Truck Interaction Literature .....                                     | 56 |
| Figure 4.2 Time intervals for the Truck Crossing the Bridge .....                                     | 59 |
| Figure 5.1 General Outline of Optimization Routine .....  | 69 |
| Figure 6.1 Time Frames for the Truck Crossing the Bridge .....  | 80 |
| Figure 6.2 Midpoint Deflection Profile for the Static Bridge/Static Truck .....                       | 81 |
| Figure 6.3 Changes in Force Position for Variations in Axle Spacing For a Fixed Speed at<br>T1 .....  | 83 |
| Figure 6.4 Changes in Force Position for Variations in Axle Spacing For a Fixed Speed at<br>T2 .....  | 86 |

|  |     |
|--|-----|
| Figure 6.5 Changes in Force Position for Variations in Speed For Axle Spacing at T1 ..               | 87  |
| Figure 6.6 Changes in Force Position for Variations in Speed For a Fixed Axle Spacing at<br>T2 ..... | 87  |
| Figure 6.7 Front Axle Weight Estimates With Noise (Random Sampling) .....                            | 92  |
| Figure 6.8 Rear Axle Weight Estimates With Noise (Random Sampling Method) .....                      | 92  |
| Figure 6.9 Percent Error in Front Axle Weight Estimates (Random Sampling Method) ..                  | 94  |
| Figure 6.10 Percent Error in Front Axle Weight ( $10^{-4}$ m Noise) .....                            | 94  |
| Figure 6.11 Percent Error in Rear Axle Weight .....  | 95  |
| Figure 6.12 Percent Error in Rear Axle Weight Estimates ( $10^{-4}$ m Noise) .....                   | 95  |
| Figure 6.13 Percent Error in Front Axle Weight (a).....  | 96  |
| Figure 6.14 Percent Error in Front Axle Weight (b).....  | 96  |
| Figure 6.15 Percent Error in Front Axle Weight (c).....  | 97  |
| Figure 6.16 Percent Error in Front Axle Weight (d).....  | 97  |
| Figure 6.17 Percent Error in Rear Axle Weight (a).....   | 98  |
| Figure 6.18 Percent Error in Rear Axle Weight (b).....   | 98  |
| Figure 6.19 Percent Error in Rear Axle Weight (c).....   | 99  |
| Figure 6.20 Percent Error in Rear Axle Weight (d).....   | 99  |
| Figure 7.1 Weight 1 (Front) Estimates With Noise Using 1 Measurement .....                           | 105 |
| Figure 7.2 Weight 2 (Rear) Estimates With Noise Using 1 Measurement .....                            | 106 |
| Figure 7.3 Percent Error in Rear Axle Weight Estimates Using 1 Sensor .....                          | 106 |
| Figure 7.4 Percent Error in Front Axle Weight Estimates Using 1 Sensor .....                         | 107 |
| Figure 7.5 Static Beam Mode Shapes .....   | 108 |
| Figure 7.6 Front Axle Weight Estimates With Noise Using 3 Sensors .....                              | 111 |

|  |            |
|--|------------|
| <b>Figure 7.7 Rear Axle Weight Estimates With Noise Using 3 Measurements .....</b>         | <b>111</b> |
| <b>Figure 7.8 Percent Error in the Front Axle Weight Estimates Using 3 Measurements ..</b> | <b>112</b> |
| <b>Figure 7.9 Percent Error in the Rear Axle Weight Estimates Using 3 Measurements ...</b> | <b>112</b> |
| <b>Figure 7.10 Percent Error in the Front Axle Weight Estimates (a).....</b>               | <b>113</b> |
| <b>Figure 7.11 Percent Error in the Front Axle Weight Estimates (b).....</b>               | <b>113</b> |
| <b>Figure 7.12 Percent Error in the Front Axle Weight Estimates (c).....</b>               | <b>114</b> |
| <b>Figure 7.13 Percent Error in the Front Axle Weight Estimates (d).....</b>               | <b>114</b> |
| <b>Figure 7.14 Percent Error in the Rear Axle Weight Estimates (a).....</b>                | <b>115</b> |
| <b>Figure 7.15 Percent Error in the Rear Axle Weight Estimates (b).....</b>                | <b>115</b> |
| <b>Figure 7.16 Percent Error in the Rear Axle Weight Estimates (c).....</b>                | <b>116</b> |
| <b>Figure 7.17 Percent Error in the Rear Axle Weight Estimates (d).....</b>                | <b>116</b> |
| <b>Figure 8.1 Truck Response With and Without Interaction Effects .....</b>                | <b>122</b> |
| <b>Figure 8.2 Truck Axle Forces .....</b>  | <b>127</b> |
| <b>Figure 8.3 Front Axle Weight Estimates With Noise Using Force Objective Function ..</b> | <b>130</b> |
| <b>Figure 8.4 Rear Axle Weight Estimates With Noise Using Force Objective Function ..</b>  | <b>130</b> |
| <b>Figure 8.5 Midpoint Deflection Profile for Static and Dynamic Truck Models .....</b>    | <b>134</b> |
| <b>Figure 8.6 Front Axle Weight Estimates (Deflection Objective Function) .....</b>        | <b>136</b> |
| <b>Figure 8.7 Rear Axle Weight Estimates (Deflection Objective Function) .....</b>         | <b>136</b> |
| <b>Figure 8.8 Percent Error in Front Axle Weight (Deflection Objective Function) .....</b> | <b>137</b> |
| <b>Figure 8.9 Percent Error in Rear Axle Weight (Deflection Objective Function) .....</b>  | <b>137</b> |
| <b>Figure 8.10 Percent Error in Front Axle Weight (a).....</b>                             | <b>138</b> |
| <b>Figure 8.11 Percent Error in Front Axle Weight (b).....</b>                             | <b>138</b> |
| <b>Figure 8.12 Percent Error in Front Axle Weight (c).....</b>                             | <b>139</b> |

|   |     |
|---|-----|
| Figure 8.13 Percent Error in Front Axle Weight (d).....   | 139 |
| Figure 8.14 Percent Error in Rear Axle Weight (a).....  | 140 |
| Figure 8.15 Percent Error in Rear Axle Weight (b).....  | 140 |
| Figure 8.16 Percent Error in Rear Axle Weight (c).....  | 141 |
| Figure 8.17 Percent Error in Rear Axle Weight (d).....  | 141 |
| Figure 9.1 Dynamic Bridge/Dynamic Truck and Static Bridge/Static Truck Deflection<br>Profiles ..... | 148 |
| Figure 9.2 Dynamic Bridge/Dynamic Truck and Static Bridge/Static Truck Deflection<br>Profiles.....  | 149 |
| Figure 9.3 Front Axle Weight Estimates With Noise .....   | 154 |
| Figure 9.4 Rear Axle Weight Estimates With Noise .....  | 155 |
| Figure 9.5 Percent Error in Front Axle Weight (a) .....   | 156 |
| Figure 9.6 Percent Error in Front Axle Weight (b) .....   | 156 |
| Figure 9.7 Percent Error in Front Axle Weight (c) .....   | 157 |
| Figure 9.8 Percent Error in Front Axle Weight (d) .....   | 157 |
| Figure 9.9 Percent Error in Rear Axle Weight (a) .....  | 158 |
| Figure 9.10 Percent Error in Rear Axle Weight (b) .....   | 158 |
| Figure 9.11 Percent Error in Rear Axle Weight (c) .....   | 159 |
| Figure 9.12 Percent Error in Rear Axle Weight (d) .....   | 159 |
| Figure 9.13 Front Axle, Low Mode, Frequency Estimate (a).....                                       | 160 |
| Figure 9.14 Front Axle, Low Mode, Frequency Estimate (b).....                                       | 161 |
| Figure 9.15 Front Axle, Low Mode, Frequency Estimate (c).....                                       | 161 |
| Figure 9.16 Front Axle, Low Mode, Frequency Estimate (d).....                                       | 162 |

|  |     |
|--|-----|
| Figure 9.17 Front Axle, Low Mode, Damping Estimate (a).....    | 162 |
| Figure 9.18 Front Axle, Low Mode, Damping Estimate (b).....    | 163 |
| Figure 9.19 Front Axle, Low Mode, Damping Estimate (c).....    | 163 |
| Figure 9.20 Front Axle, Low Mode, Damping Estimate (d).....    | 164 |
| Figure 9.21 Front Axle, High Mode, Frequency Estimate (a)..... | 164 |
| Figure 9.22 Front Axle, High Mode, Frequency Estimate (b)..... | 165 |
| Figure 9.23 Front Axle, High Mode, Frequency Estimate (c)..... | 165 |
| Figure 9.24 Front Axle, High Mode, Frequency Estimate (d)..... | 166 |
| Figure 9.25 Front Axle, High Mode, Damping Estimate (a).....   | 166 |
| Figure 9.26 Front Axle, High Mode, Damping Estimate (b).....   | 167 |
| Figure 9.27 Front Axle, High Mode, Damping Estimate (c).....   | 167 |
| Figure 9.28 Front Axle, High Mode, Damping Estimate (d).....   | 168 |
| Figure 9.29 Rear Axle, Low Mode, Frequency Estimate (a).....   | 168 |
| Figure 9.30 Rear Axle, Low Mode, Frequency Estimate (b).....   | 169 |
| Figure 9.31 Rear Axle, Low Mode, Frequency Estimate (c).....   | 169 |
| Figure 9.32 Rear Axle, Low Mode, Frequency Estimate (d).....   | 170 |
| Figure 9.33 Rear Axle, Low Mode, Damping Estimate (a).....     | 170 |
| Figure 9.34 Rear Axle, Low Mode, Damping Estimate (b).....     | 171 |
| Figure 9.35 Rear Axle, Low Mode, Damping Estimate (c).....     | 171 |
| Figure 9.36 Rear Axle, Low Mode, Damping Estimate (d).....     | 172 |
| Figure 9.37 Rear Axle, High Mode, Frequency Estimate (a).....  | 172 |
| Figure 9.38 Rear Axle, High Mode, Frequency Estimate (b).....  | 173 |
| Figure 9.39 Rear Axle, High Mode, Frequency Estimate (c).....  | 173 |

|   |            |
|---|------------|
| <b>Figure 9.40 Rear Axle, High Mode, Frequency Estimate (d)</b> ..... | <b>174</b> |
| <b>Figure 9.41 Rear Axle, Low Mode, Damping Estimate (a)</b> .....    | <b>174</b> |
| <b>Figure 9.42 Rear Axle, Low Mode, Damping Estimate (b)</b> .....    | <b>175</b> |
| <b>Figure 9.43 Rear Axle, Low Mode, Damping Estimate (c)</b> .....    | <b>175</b> |
| <b>Figure 9.44 Rear Axle, Low Mode, Damping Estimate (d)</b> .....    | <b>176</b> |

# List of Tables

|  |     |
|--|-----|
| Table 2.1 Properties Used in Beam Model .....  | 24  |
| Table 2.2 Sine Term for Each Mode .....  | 37  |
| Table 3.1 Numerical Static Truck Parameters .....  | 53  |
| Table 3.2 Numerical Parameters for Dynamic Truck Models.....                                 | 54  |
| Table 6.1 Upper and Lower Bounds for Optimization Parameters .....                           | 79  |
| Table 6.2 Average Error in Truck Parameters Using the Random Sampling Method ....            | 93  |
| Table 6.3 Maximum Error in Truck Parameters Using the Random Sampling Method ..              | 93  |
| Table 7.1 Upper and Lower Bounds for Optimization Parameters .....                           | 104 |
| Table 7.2 Average Errors in Axle Weight Estimates With Noise- .....                          | 107 |
| Table 7.3 Upper and Lower Bounds for Optimization Parameters- .....                          | 109 |
| Table 7.4 Average Axle Weight Error for the Multiple Sensor- .....                           | 110 |
| Table 7.5 Maximum Axle Weight Error for the Multiple Sensor.....                             | 110 |
| Table 8.1 Upper and Lower Bounds for Optimization Parameters .....                           | 126 |
| Table 8.2 Average Error in Axle Weight Estimates Using the Force Objective Function<br>..... | 129 |
| Table 8.3 Front Axle Frequency Estimates (Force Objective Function).....                     | 131 |
| Table 8.4 Front Axle Damping Ratio Estimates (Force Objective Function) .....                | 132 |
| Table 8.5 Rear Axle Frequency Estimates (Force Objective Function) .....                     | 132 |
| Table 8.6 Rear Axle Damping Ratio Estimates (Force Objective Function) .....                 | 133 |
| Table 8.7 Average Percent Error in Axle Weight (Deflection Objective Function) .....         | 135 |
| Table 8.8 Maximum Percent Error in Axle Weight (Deflection Objective Function) ...           | 135 |
| Table 8.9 Front Axle Frequency Estimates (Deflection Objective Function).....                | 142 |

|   |            |
|---|------------|
| <b>Table 8.10 Front Axle Damping Ratio Estimates (Deflection Objective Function) .....</b>  | <b>142</b> |
| <b>Table 8.11 Rear Axle Frequency Estimates (Deflection Objective Function) .....</b>       | <b>143</b> |
| <b>Table 8.12 Rear Axle Damping Ratio Estimates (Deflection Objective Function) .....</b>   | <b>143</b> |
| <b>Table 9.1 Average Error in Axle Weights Using Unlimited Optimization Iterations ....</b> | <b>154</b> |
| <b>Table 9.2 Truck 1 Estimates .....</b>  | <b>177</b> |
| <b>Table 9.3 Truck 2 Estimates .....</b>  | <b>178</b> |
| <b>Table 9.4 Truck 3 Estimates .....</b>  | <b>179</b> |
| <b>Table 9.5 Truck 4 Estimates .....</b>  | <b>180</b> |
| <b>Table 9.6 Truck 5 Estimates.....</b>   | <b>181</b> |
| <b>Table 9.7 Truck 6 Estimates .....</b>  | <b>182</b> |
| <b>Table 9.8 Truck 7 Estimates .....</b>  | <b>183</b> |
| <b>Table 9.9 Truck 8 Estimates .....</b>  | <b>184</b> |
| <b>Table 9.10 Truck 9 Estimates .....</b>   | <b>185</b> |
| <b>Table 9.11 Truck 10 Estimates .....</b>  | <b>186</b> |
| <b>Table 9.12 Truck 11 Estimates .....</b>  | <b>187</b> |
| <b>Table 9.13 Truck 12 Estimates .....</b>  | <b>188</b> |
| <b>Table 9.14 Truck 13 Estimates .....</b>  | <b>189</b> |
| <b>Table 9.15 Truck 14 Estimates .....</b>  | <b>190</b> |
| <b>Table 9.16 Truck 15 Estimates.....</b>   | <b>191</b> |
| <b>Table 9.17 Truck 16 Estimates .....</b>  | <b>192</b> |
| <b>Table 9.18 Truck 17 Estimates .....</b>  | <b>193</b> |
| <b>Table 9.19 Truck 18 Estimates .....</b>  | <b>194</b> |
| <b>Table 9.20 Truck 19 Estimates .....</b>  | <b>195</b> |

**Table 9.21 Truck 20 Estimates .....196**

# Acknowledgements

I would like to thank my committee as well as my professor Dr. Harold Stalford for their assistance in completing this work. I would also like to thank Sandia National Laboratories for giving me the opportunity to complete my work there, as well as Kent Pfeiffer, my mentor at Sandia, for his support and assistance over the last year.

I would also like to thank my parents for their backing and encouragement while completing this work. Without their help (with everything from school to the laundry!), I could have never gotten through all of the ups and downs of college and graduate school. And, last but not least, I would like to thank my friend Angela for not only giving me a place to crash while finishing this work, but also for making sure that I had *a lot* of fun along the way.

# Abstract

In this work, we discuss the development of a bridge weigh-in-motion (WIM) algorithm to predict axle weights to within 1% for  $\pm 1 \times 10^{-6}$  m measurement noise. WIM systems that use bridges as scales are already in limited use, but they are only able to predict axle weights to within 10-15%, in part due to the models used to represent the bridge and the truck. We are proposing a method to estimate truck axle weights, axle spacing, and speed that includes the dynamic properties of both the bridge and the truck, as well as the static effects of the truck weight, therefore, improving the axle weight estimates. Estimates of the truck's dynamic properties, including natural frequencies, damping ratios, and initial conditions, are also found.

To identify the truck, the deflection profiles over time at given measurement locations are calculated. An optimization routine is then employed to determine the set of truck parameters that produces the closest match to the "measured" deflection profile. Throughout this work, the bridge is modeled as a simply-supported Euler beam. Two truck models are used to represent the truck. The first treats each axle of the truck as a moving point force and considers only the static weight of each axle. Using this static truck model, only axle weights and axle spacing are unknown and treated as optimization parameters. The second truck model is a 2 degree-of-freedom 'quarter-car' model that represents the static weight as well as the dynamic behavior of the truck. The coupled bridge/truck equations of motion are developed and integrated to expressly include the interaction between the two. In this model, the static axle weights and axle spacing are again unknown as are the natural frequencies, damping ratios, and initial conditions of

each mode of each axle. Both truck models assume that the truck travels at a constant speed, and that the truck's total time on the bridge is known from another source.

The final algorithm is developed in stages using increasing levels of complexity in the models. In the first case, the static bridge model, which neglects the inertial properties of the bridge, is used in conjunction with the moving point force model. In the second, the dynamic properties of the bridge are included, and the moving point force model is again used to excite the bridge. In the third and fourth cases, the dynamic, 'quarter-car' model of the truck is used to excite the static and dynamic bridge respectively.

To identify the relevant properties of the dynamic truck, an approximate model of the force applied by each axle is assumed. The force is assumed to be the superposition of the static weight of each axle and a homogeneous solution of the 'quarter-car' equations of motion. This homogeneous solution consists of two damped oscillatory modes, in which the natural frequencies, damping ratios, and initial conditions are unknown and are used as optimization parameters along with the static weight and axle spacing.

In the dynamic bridge/dynamic truck system, it is necessary to integrate the differential equations of motion of the coupled bridge/truck system. To do this, it is necessary to transform the truck system of equations in terms of the unknown parameters in the homogeneous solution. This transformation is the first major contribution of this dissertation. The transformation allows the original system of equations, which is expressed in terms of the physical parameters stiffness, damping, and mass, to be written in terms of the modal parameters of the truck. Expressing the truck system in this manner eliminates the need for additional optimization parameters but still allows the integration of the coupled bridge/truck equations inside the optimization routine.

It is necessary to integrate the bridge/truck equations of motion at each iteration of the optimization routine. It was found that approximately 7,000 iterations were necessary to identify the truck. Each integration takes approximately 5 seconds, resulting in approximately 10-12 hours of computation time for each truck. This lengthy time scale prevents real-time identification of each truck.

The second major contribution of this dissertation is the ability to determine static axle weights very accurately, as well as the dynamic properties of each axle. Other authors have considered identifying the static weight or the total applied force of the truck but expressly identifying the natural frequencies, damping ratios and initial conditions of each axle is unique to this method. Since the dynamic properties of the truck are included in the approximate force model, they are therefore determined by the optimization routine. This algorithm determines not only the static axle weight and axle spacing of the truck, but also provides very accurate estimates of the natural frequencies and damping ratios of each axle. The estimation of the dynamic properties of each axle is unique to this algorithm and provides useful information about the passing truck.

Using this algorithm, axle weights could be determined to within 0.019% for zero measurement noise. The natural frequency and damping ratio of each axle's low mode could be determined to within 0.5 Hz and 0.8% (of critical damping) respectively. The properties of each axle's high mode could be determined to within 1.3 Hz and 3.1% (of critical damping). Measurement noise was also added to the deflection profiles to determine its effect on the algorithm's performance. With the addition of measurement noise of  $\pm 1 \times 10^{-6}$  m, estimates of axle weights remained within 0.03%. The frequency and damping of the low mode could be found within 0.85 Hz and 2.1% (of critical damping)

and the high mode could be identified to within 1.9 Hz and 3.4% (of critical damping). The largest measurement noise examined was  $\pm 1 \times 10^{-4}$  m. With this level of noise, the error in axle weight estimates remained below 1.15%. The natural frequency and damping of the low mode could be determined within 2 Hz and 3.6%, and the high mode was determined to within 4.4 Hz and 14% (of critical damping).

# **Chapter 1**

## **WIM Systems and Force Identification**

### **Methods**

A great deal of work has been done over the years on modeling, simulating, and identifying the characteristics and behavior of highway bridges and vehicles, both independently of one another and of the coupled systems. This work has been especially useful in aiding in bridge design and maintenance, as well as for developing regulations for truck loads and traffic control.

In recent times, there has been a great deal of attention paid to the condition of the nation's roads and bridges. In 1989, the Federal Highway Administration gave a substandard rating to 41% of the bridges in the U.S. highway system ("Exclusive, 1989). The poor condition of the nation's roads and bridges is, in part, due to the increased number and weight of the heavy truck traffic traveling these highways (Cebon, 1999). In 1987, it was estimated that the repair and replacement of the faulty bridges would require a \$2.65 billion investment annually for the next 20 years ("Fragile", 1988). The potential for this exorbitant expense has prompted even more work to be done to effectively model bridges and trucks, as well as their interaction with one another.

Vehicle-induced bridge vibration is a significant contribution to the degradation of the surface and structure of highway bridges. While not typically the cause of catastrophic bridge failure, it does contribute to surface wear and concrete cracking,

which can lead to corrosion (Cebon, 1999). Understanding and potentially reducing this vibration could lead to the extension of the services lives of many bridges and roadways, resulting in significant monetary savings for the responsible agencies.

Improving the condition of bridges and extending their service lives is two-fold. It would be possible to better design bridges to be less susceptible to truck-induced vibration or to reduce the effects of vibration through some sort of structural control. Better regulation and design of truck suspensions and loads would also be beneficial to the condition of both the bridges and roadways. One way to accomplish the latter would be to better enforce truck weight regulations on the nation's highways. This is the focus of this work-to develop a system to determine truck weights as they traverse a highway bridge based on the vibration of that bridge.

The standard method of weighing trucks and enforcing weight regulations is through the use of stationary weigh stations. These stations require trucks to exit the highway and be weighed while at rest on scales. The weigh stations are manned at all times while operational. While the use of static scales is the simplest and most obvious method of monitoring truck loads on the highway, it is not always the most effective. Besides being costly to staff and maintain, they are easily and often avoided by drivers of overweight vehicles since their location can be known miles in advance through driver communication (Snyder, 1992). For these reasons, there has been a great deal of work to develop weigh-in-motion (WIM) systems to reduce the dependency on static weigh stations.

There are currently several types of WIM systems in limited use around the world. The majority of them fall into three main categories-systems mounted *on* the road

surface, systems installed *in* the roadbed, and systems that use bridges as scales. While there are advantages and disadvantages to all types of systems, their use is becoming more desirable and commonplace as the need to monitor traffic grows. Many patents have been issued for different types of systems, and a study on the effectiveness of WIM systems was performed by the Transportation Research Board in 1986 (Transportation Research Board, 1986). Descriptions of a few of the primary systems are given in the following section.

A chart outlining several individual WIM systems is given below in Figure 1.1. The systems described are representative of the types of systems currently in commercial production and use around the world.

### **1.1 In-Service WIM Systems**

One common type of WIM system essentially consists of scales embedded in the surface of the road aligned with the wheel paths of oncoming vehicles. The standard design of these systems is a steel frame housing various numbers of load cells or other electromechanical devices to measure the force from a passing vehicle. A piece of the road surface is removed and the system is placed level with the road surface. Typically, two of these frames are installed in each lane to align with the wheel paths of oncoming vehicles. Patents for the systems developed by Yamanaka (Yamanaka, 1974) and Tamamura (Tamamura, 1977) issued to the same company (Yamato Scale Company, Limited) outline two systems of this type. In Yamanaka's system, one platform is embedded in the pavement in the path of the vehicle. The signal recorded at the front and rear edges of the platform are averaged to yield the weight of the vehicle. Tamamura's

system is similar, but it averages the response from several smaller platforms placed in a series along the wheel path. The systems proposed by Mills (Mills, 1990) and Loshbough (Loshbough, 1991) are similar to the others, although the construction details of the frame and platform over which the truck passes vary slightly. All of the systems average a very few measurements of the force applied by the truck over time and/or space to yield the total weight and axle weights of the vehicle.

**In-Service WIM Systems**

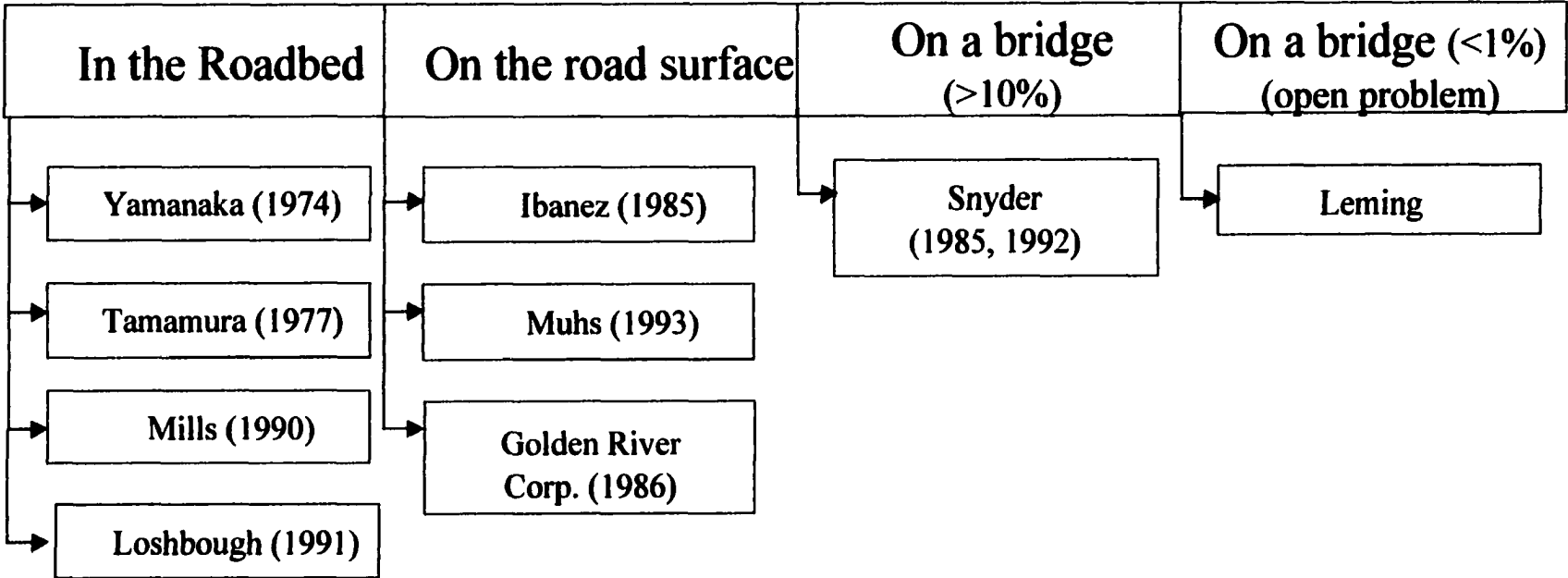


Figure 1.1 Flowchart of WIM Systems

A study performed by the Transportation Research Board (Transportation Research Board, 1986) examined operational and installation problems and performance of a number of commercially produced systems similar to the ones described above. Although the companies' products described above were not specifically discussed, systems with similar installation and operation were evaluated. It was found that such systems were quite useful in obtaining truck information in multi-lane, high traffic environments, because each lane could accommodate an individual system, making simultaneous, uncoupled measurements possible. Initial installation of the systems was cited as a problem since traffic had to be diverted and large pieces of the roadway surface removed to house the WIM apparatus. It was also found that, since these systems are placed in a hole in the roadway surface material, it was possible for them to work loose over time as the surrounding surface material degraded. This problem was solved by constructing another slab in the bottom of the hole to which the frame was bolted, making installation even more time consuming and expensive. The problem of scale avoidance was also not solved by such a system. Once the systems were identified by drivers, changing lanes or straddling lanes if the systems were installed in multiple lanes provided unusable information. Some systems were modified to correct for this problem by creating a continuous platform that spanned all lanes. While this method prevented avoiding the scale, it did not allow for independent measurements of side-by-side vehicles. Despite many of the problems, at the time of publication of the Transportation Research Board's report, this type of WIM system was the most widely used.

Another type of WIM system that is growing in popularity is placed temporarily on the road surface. Typically the housings of these systems consist of a rubber or

elastomeric pad that is fixed to the roadway surface in the wheel path of the vehicles. Different types of electric or optical sensors are imbedded in these pads to measure the force imparted by a truck. Steel sheets separated by layers of rubber are used as parallel-plate capacitive sensors in the Golden River Corporation Design (Transportation Research Board, 1986). As the rubber is compressed, the change in capacitance is measured and correlated to a truck weight. Ibanez (Ibanez, 1985) and Muhs (Muhs, 1993) use a similar rubber pad, but embed optical fibers and attenuating devices that, when compressed by a passing vehicle, attenuate the light passed through the fibers. The measured light intensity is then correlated to a weight. Other systems use inductive loops rather than capacitors or optical fibers to detect the force.

These very portable, surface-mounted systems are growing in popularity around the U.S. They have been found to be quite reliable since there are few moving parts and they are simple to install, reducing the potential for human error. They are also much less expensive than the embedded systems discussed previously, and installation is simpler, much faster (an hour as opposed to multiple days), and, consequently, much less expensive. It has been found that these types of systems are more susceptible to intentional damage by drivers than the below-the-surface models since heavy braking can quickly deteriorate the rubber pads in which the sensors are installed. It was also found that it was necessary to install such systems on very smooth sections of roadway as surface irregularities caused a serious degradation in performance (Transportation Research Board, 1986).

The bridge WIM in motion system developed by Snyder (Snyder, 1985, 1992, Transportation Research Board, 1986) is one of the few of its kind in use in the U.S. It

consists of a system of strain gages installed on the girders underneath a bridge deck to record the bridge's response to a passing vehicle over time. Each bridge is individually calibrated using a slowly moving test truck to determine its response to the moving load. Axle sensors at the entrance and exit of the bridge are installed to determine the number and spacing of the axles as well as the vehicle speed. Details of the authors' algorithm to determine axle weight will be discussed in the following section.

Although Snyder's system is one of few bridge WIM systems in use in the U.S, it was found to perform very well by the Transportation Research Board. Once a bridge was instrumented, the strain gages and associated electronics remained functional for long periods of time and did not require recalibration often. The axle sensors at the entrance and exit of the bridge were cited as the primary problem with the hardware of the system, since they required stopping traffic to install, were easily damaged by vehicles, and were difficult to install in damp or below freezing conditions. Errors in the system's weight estimates cited by the inventor (Snyder, 1985) were on the order of 10-15%. It is the opinion of this author that this level of error is due in part to the algorithm used to deduce weight from the measured strain record, as will be discussed in a subsequent section.

Although several construction, installation, and operational variations exist in commercial WIM devices, the above outlines the primary structure of existing systems. Due to the need for more effective traffic monitoring, WIM is becoming an attractive alternative and addition to stationary weigh stations, prompting extensive and on-going work in the area. In the following section, algorithms associated with moving force identification will be addressed.

## **1.2 WIM Methods**

The primary goal of any WIM system is to accurately estimate axle weights and/or gross weights of vehicles in motion. Therefore, while the structure of the system is important, designing the hardware is not the only aspect to WIM. Developing an algorithm that accurately predicts these weights is also a necessary part of solving the WIM problem. Several authors, as well as the inventors of the systems described in the previous section, have worked to develop methods to determine truck characteristics from WIM data. A chart of some of the contributions in this area is given below in Figure 1.2. The methods used in many of the in-service systems described above as well as work from other authors studying the moving force identification problem are included.

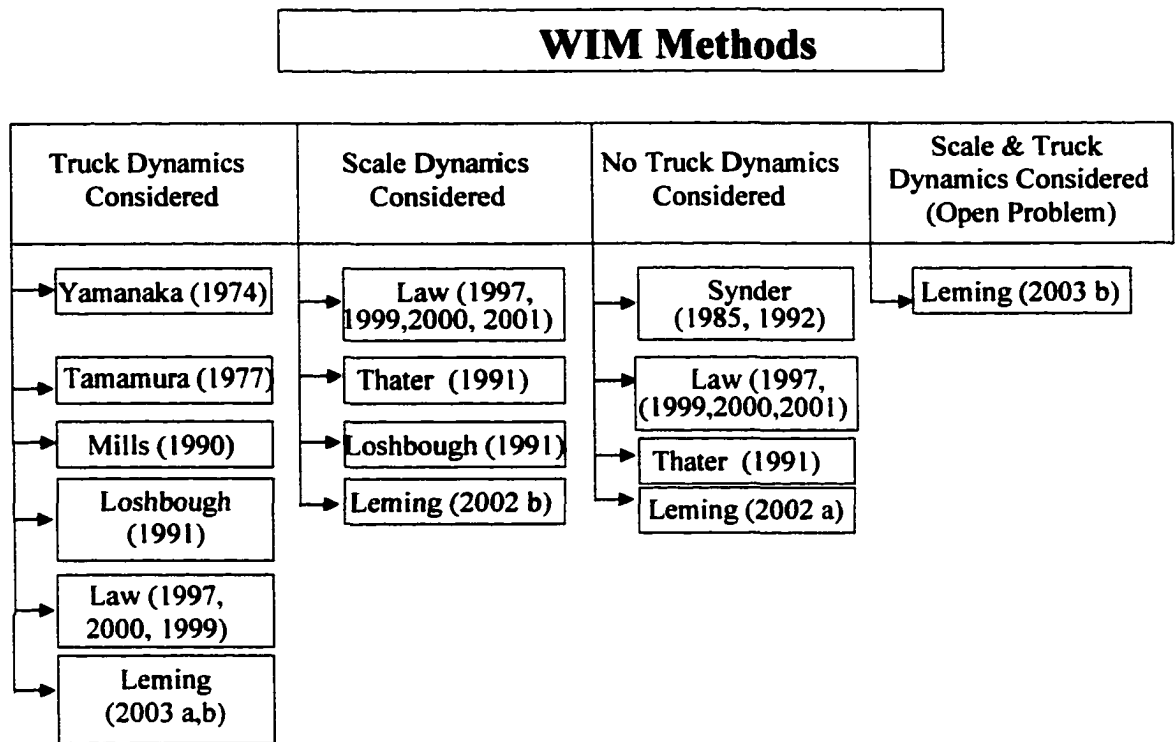


**Figure 1.2 Force Identification Methods**

To develop an algorithm to accurately predict truck characteristics from data acquired while the vehicle is in motion, it is necessary to first understand precisely what is being measured. As a vehicle moves along a real roadway or bridge, it does not apply a constant force over time. Irregularities in the road surface or interaction with a bridge or platform over which it travels can potentially excite the dynamics of the vehicle's suspension and tires, resulting in a time-varying force to be applied by the vehicle. Further details of this tire force will be discussed in a later chapter, but to examine the problem of moving force identification in regards to a truck, it is important to recognize that what is being measured is not necessarily a constant force.

Varying levels of complexity in the models and algorithms used to predict static weight from time-varying data exist in the literature and the in-service systems. Some

inventors, such as Ibanez and Muhs (Ibanez, 1985, Muhs, 1993) do not consider the dynamic nature of the vehicle or the weighing device over which it travels, but rather make measurements over a short period of time and ignore the time-varying aspect of the tire force. Other inventors use a method of averaging a very few measurements made of each axle over time to account for the time varying nature of the tire force. The systems developed by Yamanaka (Yamanaka, 1974) and Mills (Mills, 1990) make two measurements at the leading and trailing edges of the plate as an axle passes over and averages them to obtain an estimate of the static weight. In a similar method, Tamamura (Tamamura, 1977) averages the force measurements obtained from a series of 2-4 successive platforms to estimate the weight.

It could also be said that the dynamic properties of the scale, whether it be a platform embedded in the pavement or a bridge structure, such as in Snyder's work (Snyder, 1985, 1992), must be considered to obtain accurate measurements of the tire force. Loshbough's system (Loshbough, 1991) handles the problem of scale platform dynamics by designing the platform to have a natural frequency far from that of the truck's so that the two do not interact and successive measurements of tire force do not contain the effects of the vibrating scale platform.

The system designed by Snyder (Snyder, 1985, 1992) uses a bridge structure as a scale platform. This means that the weighing platform is much larger and more flexible than the other systems discussed, and the vehicle remains on the platform for a much longer period of time. Measurements of the strain in the bridge girders are made continuously over time, so there are many measurements to work with. Each bridge is characterized by an influence line (the bending moment at a given measurement location

versus force position along the bridge for a unit load). This influence line can be approximated by the influence line of a beam with equivalent geometry and bending properties as the sum of the girders or by direct measurement. To obtain the influence line directly, a slowly moving truck passes over the bridge, and measurements are made at each of the sensor locations. The truck travels across the bridge slowly enough that neither the bridge dynamics nor the truck dynamics are excited. The magnitude of the line is then normalized by the weight of the truck.

Axle sensors at the entrance and exit of the bridge record the number and spacing of the axles, and the speed is also calculated using this information. Assuming a constant speed, the position of each axle is therefore known at every point in time. A system of equations is generated at each time step that relates the measured strain to the product of the appropriate value along the influence line for each axle and the unknown axle weights. To solve this system of equations, it is necessary that there be at least as many measurement locations as axles of the truck. The equations are then solved for the unknown axle weights at each time step. To account for the dynamic nature of both the bridge and the truck, the axle weights obtained at each time step are then averaged to give an approximate static weight. The estimates of axle weight reported by the author (Snyder, 1985) show errors up to 15%. Although Snyder does not speculate on the origin of this error, recent studies in the literature indicate that this is approximately equal to the error found in simulating a bridge's response to a dynamic truck crossing a bridge when the interaction between the truck and the bridge is neglected, as it is in Snyder's model, (Green and Cebon, 1997).

Other authors in the literature are also working on the identification of moving forces from bridge response information. Some of the work involves attempting to eliminate the dynamic properties of the measured signal to extract the only the static response. Thater et al. (Thater, et al., 1991) developed a method to filter the dynamic bridge response using the pre-determined response of the bridge to a slowly moving vehicle (“static” response). They had previously determined that using conventional filtering methods were not effective for separating the dynamic and static responses of the bridge. Working in the frequency domain, it was assumed that the static and dynamic responses of the bridge at 0 Hz to the same truck were equal. An FFT was performed on both the static bridge response due to the calibration test truck and the measured dynamic response of an unknown truck. The magnitude of the dynamic response at 0 Hz was then scaled by the magnitude of the static response to the calibration truck at 0 Hz to determine the unknown weight. While this method provided some improvement in weight estimates over the existing bridge WIM techniques, errors of 5% using simulated data were still observed.

Another group, Law, et al. (Law, 1997, 1999, 2000, 2001) is also working on the moving force identification problem, although their goal is not to extract the static weight of a simulated truck crossing a bridge, but rather to identify numerically the total force applied by the truck. Modeling the bridge as a simply supported Euler beam, two types of moving forces are examined. First, a static point force moving at a constant speed along the beam is used to excite the bridge. Next, a simple vehicle model that includes interaction with the bridge due to the displacement of the bridge under each contact point is used. Details of this vehicle model will be discussed in a later chapter.

For both the moving point force and the vehicle model, the differential equation of motion for the deflection of an Euler beam (neglecting damping) is developed. For the point force analysis, a closed form solution is obtained for the deflection of the beam as a function of space and time, and expressions for the bending moment and acceleration are derived from this. Either the moment or acceleration at a given sensor location is used as the measured bridge response, and the number of measurement locations is greater than or equal to the number of point forces moving across the beam. A system of equations for each point in time is then formulated based on the measured bridge response and the closed form solution with the magnitudes of the point forces assumed to be unknown. Solving these equations leads to an estimate of the magnitude of each point force for each instant in time. In the point force case, these estimates are averaged to determine the magnitudes of all point forces.

To determine the magnitude of the moving vehicle model's force, coupled differential equations of the vehicle and the bridge are formulated. This formulation will be discussed in greater detail in a later chapter along with the model. To first obtain the "measured" (obtained through simulation) bridge response to the vehicle model, the coupled, nonlinear equations are numerically integrated to obtain deflection, moment, and acceleration profiles at the sensor locations over time. Using the same method as above, a system of equations is formed for each time step using either bending moment or acceleration as the measured quantity. The equations are then solved for the magnitude of the applied force at each time step. This method was not intended to determine axle weights, but rather to identify the magnitude of the applied force at each instant. Random white noise of various magnitudes was also added to the measured signal to determine the

performance. Using this method, errors in force magnitude estimates of both the point force and the vehicle model ranged from 6-24% for the smallest noise level.

The goal of our work is to develop an algorithm that relates a measured bridge response to a set of truck parameters including axle weights, axle spacing and speed that produced the bridge response. In certain cases, speed is assumed to be known from an independent sensor. Different models of both the truck and the bridge are examined which include both moving point forces and moving vehicle models. The effect of the bridge dynamics on our ability to determine truck properties is also examined by first neglecting and then including the inertia of the bridge. A simply supported Euler beam model is used to represent the dominant behavior of the bridge, and both point force and one-dimensional axle models described in later chapters are used to simulate a truck. An optimization routine minimizes the least-squares difference between the measured profiles and the simulated ones and modifies relevant truck parameters to obtain the best approximation of the truck characteristics. The different models and combinations of models used as well as the optimization technique will be outlined throughout the remainder of this work.

# **Chapter 2**

## **Bridge Models**

Examining the response of bridges to different loadings is a large area of research, focusing on a variety of different driving forces. Response to wind, earthquake and vehicle loading comprise a significant portion of the work in structural dynamics. A portion of this work deals with modeling bridges to obtain their response to excitation by vehicles. Many authors are also working in this area and using a variety of different types of models. These models vary in structure as well as in level of complexity. A chart outlining some of the contributions in the area of bridge model construction and solution is given below in Figure 2.1. The works have been categorized by the geometric properties of the model.

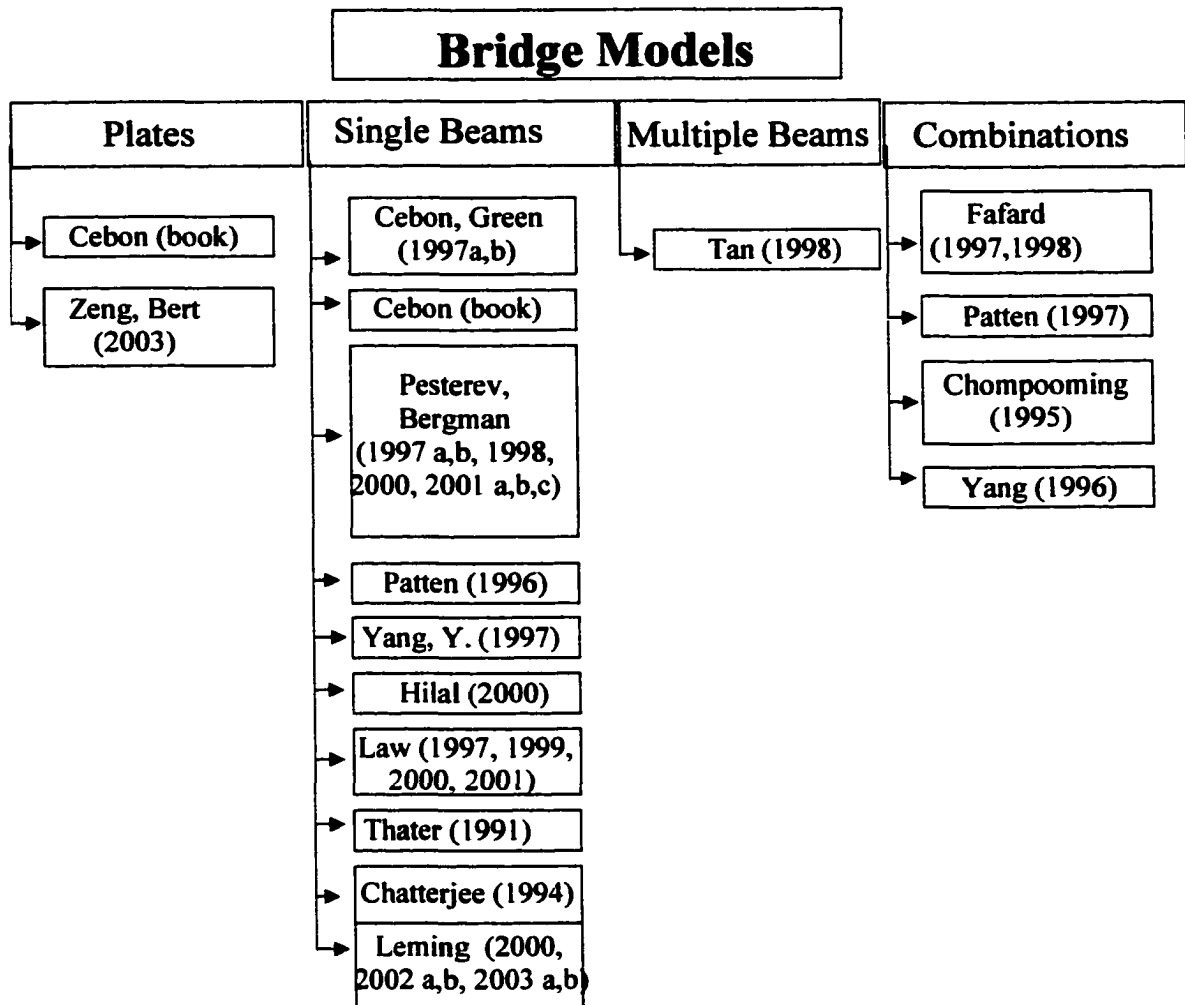


Figure 2.1 Flowchart of Bridge Models in the Literature

## 2.1 Combination Models

Different authors use varying degrees of complexity to model bridges, depending on their purpose. Some of the most complex models are finite element representations of a given bridge that include a variety of elements, including plates, beam, solids, shells and bars. One such model developed by Patten and Sun (Sun, 1997) included the bridge's superstructure and piers for use in the design of a vibration mitigation system. It was a 4,800 degree of freedom (DOF) model composed of three types of beam elements, thin shell, bar, and solid elements, and 811 nodes. The accuracy of the model was

verified experimentally, and it was found that the first eight natural frequencies matched those of the actual bridge upon which the model was based to within 3%. Higher modes, up to the 14<sup>th</sup>, were also predicted with slightly less accuracy. To use this model more efficiently, a coarser meshing technique was used which resulted in only 225 DOF but maintained the accuracy in predicting the first ten modes of the bridge (Patten, 1999).

The model was based on an in-service interstate highway bridge on I-35 N near Purcell, Oklahoma. Since this bridge is the basis for other models used in the body of this text, some important conclusions drawn from Patten's work should be discussed here, although geometric and construction details will be given in the following section. First, the first two modes of the bridge were found to be bending modes of frequencies 2.5 and 3.0 Hz. Higher modes were torsion and combinations of torsion and bending (Sun, 1997). It was also found that standard trucks crossing this bridge excited only those modes below 10 Hz (the first fourteen modes for the actual bridge). An even simpler model of this bridge was also used in much of the practical application of this group's work. It was found that modeling this bridge as a simply supported beam with the appropriate mass, stiffness, and damping properties gave sufficient performance and computational efficiency to design the authors' vibration control system. Time domain measurements compared favorably with those from the actual bridge and the full-scale finite element model (FEM), making it attractive for estimating deflection. It is on this simplified beam model that the bridge models used in the following chapters are based.

Other authors have also constructed finite element models that are combinations of a variety of elements. One common method for doing this is to model the bridge deck using plate/shell elements and to model the girders independently using beam elements.

Fafard (Fafard et al., 1998, Fafard and Bennur, 1997) and Chompooming (Chompooming and Yener, 1995) both constructed this type of model. Fafard's model also included the parapet and a sidewalk on one side of the bridge and modeled them using beam elements. The model also used a non-uniform set of bending properties to more fully capture the cracks and irregularities in the concrete deck. This model was quite accurate in predicting the modal characteristics of the first ten modes, but showed large variations of up to 70% in the prediction of strain along the bridge for various vehicle induced loadings. The authors attribute a significant portion of this error to the fact that the surface roughness of the actual bridge is not included in the model, which would change the response of the simulated vehicle model. Variations in the actual vehicle dynamics and the simulated one were also cited as a source of error in these calculations. Chompooming's model was very similar in structure to Fafard's although it included only the deck and the girders and not the parapet or any other parts of the bridge structure. The majority of their work dealt with the influence of vehicle parameters, which will be discussed in the following chapters.

Many of these combination-type models most accurately predict the finer points of the bridge response, including many modes and a variety of mode shapes, but they can also be computationally intensive and time consuming to use. Simplified models that include important features of the bridge response are often developed to predict specific aspects of interest to the author. In Cebon's book (Cebon, 1999), two simplified models were developed and compared to experiment and to each other. The first model was a mesh of orthotropic plate elements mounted on flexible supports. To incorporate the effect of the girders, the plate elements were given different stiffnesses along the

direction of the girders than in the other direction. In the second model, the beam was approximated as a simply-supported beam with mass and stiffness properties representative of the deck and girder cross sections. The responses of both models were then compared to measured data from the actual bridge. It was found that the beam model predicted only four of the first eight modes while the plate model was relatively accurate for them all. However, in examining time domain data, it was found that both the plate and the beam model gave accurate and nearly identical deflection information when compared to the measured response to various loads. This was attributed to the fact that the two dominant modes of this particular bridge were bending modes and were represented well by both models. The author concludes that either model would suffice for accurately obtaining deflection information for this bridge, but computation time and complexity would influence the choice of model.

## **2.2 Multiple Beam Models**

Other models of highway bridges that use only beams have also been examined. These models typically represent the bridge as either a single beam along the direction of the bridge or as a grillage or mesh of beams to include both transverse deflections and torsional effects. One such grillage model of a bridge was constructed by Tan (Tan, et al. 1998). The model used beam longitudinal beam elements to represent the girders and transverse diaphragms to represent the torsional stiffness. The two types of elements were pinned at their intersection to ensure equal deflections at these nodes. The stiffness and geometric spacings were tuned so that the static deflections measured from an actual

bridge corresponded to ones simulated using the model, but does not compare the dynamic response of the two.

### **2.3 Single Beam Models**

One of the simplest types of models used to simulate a bridge's response is a single or multi-span beam. As discussed previously, this type of model captures the dominant behavior of many types of bridges (Cebon, 1999, Patten, et al. 1999), although it does not include the torsional effects of the bridge deck. In terms of computational efficiency, however, beam models are usually considered much more practical for actual use. Extensive work has been done using beam models to examine not only bridge response, but also interaction effects between vehicles and bridges. Different methods of solving the coupled systems have also been proposed. Pesterev and Bergman (Pesterev and Tavrizov, 1994 a,b, Pesterev and Bergman, 1997 a,b, 1998, 2000, Pesterev et al, 2001 a,b) did extensive work developing efficient and accurate methods to solve the bridge-truck interaction problem using a beam model. Their emphasis, however, was on the solution rather than the model, and details of their work will be discussed in the next chapter.

Many other authors also use beam models to study the interaction between vehicles and bridges. Yang (Yang, Y. 1995, 1997) used such a model to study the interaction between railway bridges and trains. They used regular beam elements of appropriate cross-section and properties where the train was not in contact and proposed an "interaction" element where the train was in contact. This element included the mass, stiffness, and damping of the combined beam/vehicle system. Hilal (Hilal and Zibdeh,

2000) used beam models with a variety of boundary conditions to examine the effects of acceleration, deceleration, and uniform motion of a moving point force and obtained a closed form solution for the deflection profile. Chatterjee (Chatterjee et al., 1994) used a multi-span beam model that allowed torsion of the beam due to eccentric loads. The bridge on which this model was based had much higher frequencies in torsion than in bending, meaning that it was torsionally stiff. This resulted in a negligible change in bridge deflection when torsional coupling was included, indicating that, for this bridge, the eccentricity of the vehicle with respect to the center-line of the beam had did not have an effect on bridge behavior. Results were not given for a less torsionally stiff bridge.

Because of the computational efficiency, beam models were chosen to use in the rest of this work. Single span, simply supported beams are used to determine the bridge response to a variety of load conditions. We also examine the effect of the inertia of the beam on the response of the bridge to a loading and on our ability to identify that load. Details of these models are given in the following sections.

## **2.4 My Models**

The goal of this work was to identify the axle weights, axle spacing, and speed of a truck passing over a bridge based on the deflection response of the bridge. To do this, it was necessary to develop a model of the bridge that would be representative of the principal behavior of the bridge when subjected to vehicular loading. An in-service highway bridge spanning Walnut Creek on I-35 N near Purcell, Oklahoma was the basis for the simplified beam models used in this work. The original bridge consisted of a reinforced concrete deck and five steel I-beam girders spanning the entire length of the bridge. The four-span bridge was supported by three equally spaced piers and two end

abutments. The right-hand traffic lane was centered over the second girder (near east) and the left-hand lane was centered between the fourth and fifth girders (near and far west) (Sun et al., 1997). For simplicity, a single span beam model based on the above-described bridge was developed for this work. It is important to note that this model and the force identification method could easily be extended to include more lanes.

The general model consisted of eight beam elements and nine nodes. It was found that this number of elements was sufficiently large to accurately represent the displacement while still remaining computationally efficient. The use of eight elements was also advantageous, because it provided nodes at locations that were desirable for measurements, the midpoint, the quarter-length point, and the three-quarter-length point. A diagram of this model is given below with the potential sensor locations marked in Figure 2.2. A discussion of these sensor locations will be given below in section 2.4.

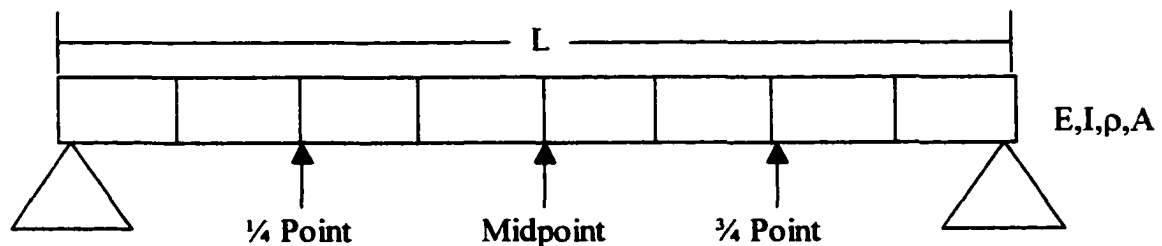


**Figure 2.2 Finite Element Model of Bridge**

Each node was given two degrees of freedom (DOF), vertical displacement and in-plane rotation. The boundary conditions of the simply supported beam were such that the displacements at the first and last nodes were fixed. In total, this model had 16 DOF. The properties of the beam were determined to correlate with the measured properties of the second span of the Walnut Creek Bridge. These properties are given below in Table 2.2.1.

**Table 2.2.1 Properties Used in Beam Model**

|              |                                    |
|--------------|------------------------------------|
| L            | 30.48 m                            |
| EI (product) | $7.36 \times 10^{10} \text{ Nm}^2$ |
| $\rho A$     | $3.35 \times 10^4 \text{ kg/m}$    |

Two versions of this beam model were used in this work. The first, termed the “static” model, did not include the inertia of the beam, the solution of which was a series of static calculations through time. The second, the “dynamic” beam, included the inertia of the beam and was solved continuously.

## **2.5 Static Beam**

Three methods of solving the static beam response were used, the finite element method, the direct solution of the differential equation of motion of the beam for a moving point force, and static beam bending equations. Details of the solution for a moving vehicle model will be given in the Interaction chapter of this work.

## **2.6 Finite Element Model**

The first solution method used the finite element model and properties given above. The elemental stiffness matrix  $K_e$  was derived using the standard beam element equations and is given below in Equation (2.1). The global stiffness matrix was assembled using standard finite element method and will not be given here for the sake of brevity.

$$K_e = \frac{EI}{L^3} \begin{bmatrix} 12 & 6L & -12 & 6L \\ 6L & 4L^2 & -6L & 2L^2 \\ -12 & -6L & 12 & -6L \\ 6L & 2L^2 & -6L & 4L^2 \end{bmatrix} \quad (2.1)$$

For the moving point force problem, a static calculation of the beam deflection was performed at each time step to determine the displacement of each node. Although the same beam model was used for a moving vehicle model, a slightly different solution method was employed and will be discussed in Chapter 4. In both cases, however, the governing equation of the bridge deflection was given by

$$\bar{F}(t) = \mathbf{K}_G \bar{x}(t) \quad (2.2)$$

the solution of which is given by

$$\bar{x}(t) = \mathbf{K}_G^{-1} \bar{F}(t) \quad (2.3)$$

where  $K_G$  is the global stiffness matrix of the beam,  $x(t)$  is the deflection and rotation at each node, and  $F(t)$  is a vector of the applied force at each node.

The term ‘deflection profile’ will be used throughout this work to define the deflection as a function of time at a given sensor location. An example of a profile using the static bridge finite element model is given below.

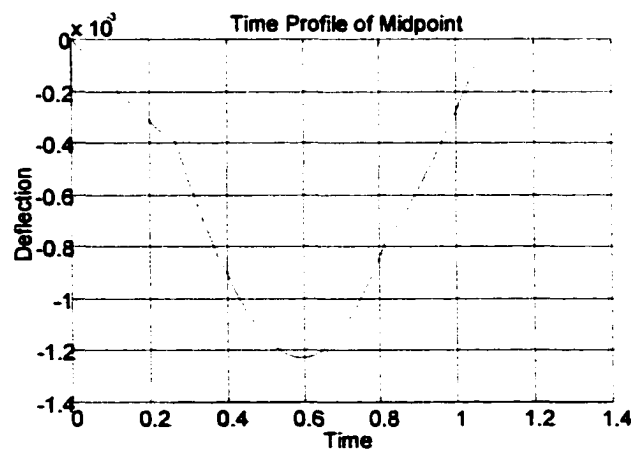


**Figure 2.3 Sample Deflection Profile of the Static Bridge Midpoint Deflection**

The measurement equation, giving the beam deflection at the sensor location is given by

$$\begin{aligned}
\bar{y} &= C_B \bar{x} \\
C_B &= [0_{3 \times 32}] \\
C_B(1,8) &= 1 && \text{for midpoint deflection} \\
C_B(2,4) &= 1 && \text{for quarter point deflection} \\
C_B(3,12) &= 1 && \text{for three - quarter point deflection}
\end{aligned} \tag{2.4}$$

for three sensor locations. For only one sensor located at the span midpoint,  $C_B$  is a  $1 \times 32$  vector and  $C_B(1,8)=1$ .

## 2.7 Solution of the Differential Equation

The second method for determining the deflection profile of a static beam subjected to a moving force involves the solution of the partial differential equation of bending for a beam. This method of solution assumed a moving point force, although it was expanded for use with a moving vehicle model. For this section, however, we will limit our discussion to moving point forces only.

The differential equation of bending for a Bernoulli-Euler beam is given by

$$EI \frac{\partial^4 w(x,t)}{\partial z^4} = \delta(x - \tilde{x}(t))P \tag{2.5}$$

where  $w(x,t)$  is the vertical displacement of the beam as a function of time and horizontal distance along the length,  $x$ ,  $P$  is the force, and  $\tilde{x}(t)$  is the location of the force as a function of time. A solution to this equation in terms of the mode shapes of the beam can be written as

$$w(x,t) = \sum_{i=1}^{\infty} \phi_i(x) V_i(t) \tag{2.6}$$

For a simply supported beam, the mode shapes,  $\phi_i(x)$ , can be written as

$$\phi_i(x) = \sin \frac{i\pi x}{L} \tag{2.7}$$

Substituting Equations (2.6) and (2.7) into Equation (2.5) and multiplying both sides by  $\sin \frac{j\pi x}{L}$  leads to

$$EI \sum_{i=1}^{\infty} \left( \frac{i\pi}{L} \right)^4 \sin \frac{i\pi x}{L} \sin \frac{j\pi x}{L} V_i(t) = P \delta(x - \tilde{x}(t)) \sin \frac{j\pi x}{L} \quad (2.8)$$

If Equation (2.8) is integrated with respect to  $x$  from 0 to  $L$ , the right-hand side becomes zero except where  $x = \tilde{x}(t)$ . The equation then becomes

$$EI \sum_{i=1}^{\infty} \left( \frac{i\pi}{L} \right)^4 \left( \frac{L}{2\pi} \right) \frac{\sin(i-j)\pi}{i-j} V_i(t) = P \sin \frac{j\tilde{x}(t)}{L} \quad (2.9)$$

The left-hand side of Equation (2.9) is zero unless  $i=j$ , when it is undefined. Applying L'Hospital's rule with respect to the quantity  $i-j$ , the left-hand side becomes

$$EI \sum_{i=1}^{\infty} \left( \frac{i\pi}{L} \right)^4 \left( \frac{L}{2} \right) V_i(t) = P \sin \frac{i\tilde{x}(t)}{L} \quad (2.10)$$

The above equation gives an expression for the time-dependent portion of the solution to Equation (2.4). The complete solution to Equation (2.5) is therefore given by

$$w(x,t) = \frac{2P}{EIL \left( \frac{\pi}{L} \right)^4} \sum_{i=1}^{\infty} \left( \frac{1}{i} \right)^4 \sin \frac{i\pi x}{L} \sin \frac{i\tilde{x}(t)}{L} \quad (2.11)$$

Evaluating Equation (2.11) at the sensor locations generated deflection profiles of the same nature as in Figure 2.3. It was determined that using 4-5 terms of the series expansion in Equation (2.11) gave the best approximation to the finite element deflection profiles. Equation (2.11) was evaluated at  $x=L/2$ ,  $L/4$ ,  $3L/4$  to measure the deflection profile.

## 2.8 Static Beam Bending Equations

The standard equations for static beam bending were also used to evaluate the deflection profiles of the beam. The deflections due to each force at a given location are found using the standard expressions for the inverse of beam stiffness and are given below (Gere, 1997).  $H_1$  is used if the  $x < b$ , and  $H_2$  is used if  $x > b$ , where  $x$  is the location of the applied force along the beam.

$$\begin{aligned} H_1(x, b) &= \frac{bx(b^2 - L^2 + x^2)}{6EIL} \\ H_2(x, a) &= \frac{(a - L)(a^2 - 2aL + (L - x)^2)(L - x)}{6EIL} \end{aligned} \quad (2.12)$$

where  $b_i = L - x_i$ , and  $a_i + b_i = L$ . The deflection of the beam is given below in three different time frames which determine how many axles on the beam at a given time. The details of the truck motion will be given in Chapter 3.  $W_1$  and  $W_2$  are the front and rear axle weights of the truck,  $a$  is the spacing between the weights, and  $v$  is the truck speed. The subscripts  $i$  and  $j$  depend on the relative location of the sensors and each applied force.

$$\begin{aligned} w(x, t) &= -H_i(x, b_1)W_1 && \text{when } 0 \leq t \leq \frac{a}{v} \\ w(x, t) &= -H_i(x, b_1)W_1 - H_j(x, b_2)W_2 && \text{when } \frac{a}{v} \leq t \leq \frac{L}{v} \\ w(x, t) &= -H_i(x, b_2)W_2 && \text{when } \frac{L}{v} \leq t \leq \frac{L+a}{v} \end{aligned} \quad (2.13)$$

The sensors are located at the midpoint and/or the quarter-point and three-quarter-point ( $x=L/2, L/4, 3L/4$ ). The deflections at these locations would be given by evaluating Equation (2.13) at these points.

## 2.9 Dynamic Beam

The second version of the beam model used in this work included the inertial effects of the bridge and was termed the “dynamic” bridge model. The same eight

element, nine node geometric model of the simply supported beam was used, but the mass of the beam was included in the development. The figure below illustrates a deflection profile of the midpoint deflection of the beam using this model compared with one from the static model.

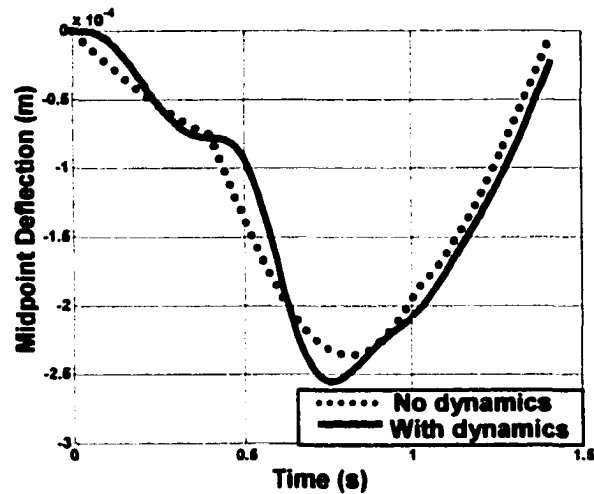


**Figure 2.4 Sample Deflection Profile of the Midpoint Deflection Using the Dynamic Beam Model**

A consistent mass matrix for a beam element was developed using the parameters given in Table 2.2.1, and is given below in Equation (2.14). The same element stiffness matrix was used as in the static model, Equation (2.1). The global mass and stiffness matrices were assembled using the standard finite element method.

$$M_e = \frac{\rho AL}{420} \begin{bmatrix} 156 & 22L & 54 & -13L \\ 22L & 4L^2 & 13L & -3L^2 \\ 54 & 13L & 156 & -22L \\ -13L & -3L^2 & -22L & 4L^2 \end{bmatrix} \quad (2.14)$$

The damping in bridges is typically quite low (approximately 2% of critical) (Cebon, book). The measured values of the damping in the Walnut Creek Bridge are

quite close to 2% for the first eight modes of the actual bridge. Using the 2% damping, the global damping matrix is therefore given by

$$\mathbf{C}_G = 0.04\mathbf{M}_G (\mathbf{M}_G^{-1}\mathbf{K}_G)^{1/2} \quad (2.15)$$

where  $M_G$  and  $K_G$  are the global mass and stiffness matrices respectively.

The discretized equations of motion for the beam becomes

$$\mathbf{M}_G \ddot{\bar{x}}(t) + \mathbf{C}_G \dot{\bar{x}}(t) + \mathbf{K}_G \bar{x}(t) = \bar{F}(t) \quad (2.16)$$

where  $x(t)$  is again the displacement and rotation of the nodes, and  $F(t)$  is a vector of force applied at each node.

To conveniently integrate these equations, it is necessary to reduce the set of second order differential equations to a set of first order ones

$$\begin{aligned} \dot{\bar{x}}_B &= \mathbf{A}_B \bar{x}_B + \mathbf{B}_B(t) \bar{f}(t) \\ \bar{y} &= \mathbf{C}_B \bar{x}_B \end{aligned} \quad (2.17)$$

where  $\bar{x}_B = [\bar{x} \quad \dot{\bar{x}}]^T$  and  $A_B$  and  $B_B(t)$  are given below.  $f(t)$  is the time force vector. This quantity will be discussed for individual truck models in later chapters.  $C_B$  varies depending on which of the three potential sensor locations are being measured.

$$\mathbf{A}_B = \begin{bmatrix} \mathbf{0}_{16 \times 16} & \mathbf{I}_{16 \times 16} \\ -\mathbf{M}_G^{-1}\mathbf{K}_G & -\mathbf{M}_G^{-1}\mathbf{C}_G \end{bmatrix} \quad \mathbf{B}_B = \begin{bmatrix} \mathbf{0}_{16 \times 16} \\ \mathbf{M}_G^{-1} \end{bmatrix} \mathbf{R}(s, z) \quad (2.18)$$

$$\begin{aligned} \mathbf{C}_B &= [\mathbf{0}_{3 \times 32}] \\ \mathbf{C}_B(1,8) &= 1 && \text{for midpoint deflection} \\ \mathbf{C}_B(2,4) &= 1 && \text{for quarter point deflection} \\ \mathbf{C}_B(3,12) &= 1 && \text{for three - quarter point deflection} \end{aligned} \quad (2.19)$$



where  $R(s, z)$  describes the distribution of the force and moment due to the load between the nodes as described below.

## 2.10 $R(s, z)$

For a force applied at a position  $z$ ,  $0 \leq z \leq L$ ,  $0 \leq s \leq L/8$

For  $z \in E_i$ , and  $0 \leq s \leq L/8$ , the  $32 \times 1$  vector (or  $32 \times 2$  for two axes)  $\mathbf{R}(s, z)$  is formed from an  $36 \times 1$  (or  $36 \times 2$ ) vector  $\mathbf{r}(s, z)$  whose elements are defined below. Each column of  $\mathbf{R}(s, z)$  represents the location of an individual axle.

$$\begin{aligned}
 r(s, z)_{2i-1} &= \frac{1}{L^3} (2s^3 - 3s^2L + L^3) \\
 r(s, z)_{2i} &= \frac{1}{L^3} (s^3L - 2s^2L^2 + sL^3) \\
 r(s, z)_{2i+2} &= \frac{1}{L^3} (-2s^3 + 3s^2L) \\
 r(s, z)_{2i+2} &= \frac{1}{L^3} (s^3L - s^2L^2)
 \end{aligned} \tag{2.20}$$

All other  $r(s, z)_j = 0$  for  $2i - 2 > j > 2i + 2$

The boundary conditions are such that the deflections at the endpoints of the span are zero. For this reason the 1<sup>st</sup>, 17<sup>th</sup>, 19<sup>th</sup>, and 35<sup>th</sup> rows of  $\mathbf{r}(s, z)$  are removed ( $r(s, z)_1 = [ \ ]$ ,  $r(s, z)_{17} = [ \ ]$ , etc.) to form  $\mathbf{R}(s, z)$ .

## **2.11 Reduced Order Model**

For computational efficiency, two reduced order models of the dynamic bridge were also developed. It was found that 99.5% of the midpoint deflection was expressed by the first, third, fifth and seventh modes. The simplest reduced order model contained only these modes and was produced using a transformation algorithm in MATLAB. The second reduced order model used the first seven modes of the beam and was used with in the dynamic bridge/dynamic truck section of the work. The even numbered modes were included to improve the deflection estimates at the quarter and three-quarter points. The deflection from the reduced order models was compared to the full-order model to determine the contribution of the higher modes. The two figures below show the error between the reduced-order model and the full-order model at each of the three sensor locations for two different combinations of modes. The first, Figure 2.5, shows the error using modes 1, 2, 3, 5, 7. The second, Figure 2.6, includes the even modes 4 and 6 and was the model used for the larger reduced-order model. Adding the fourth and sixth modes reduced the maximum error from  $1 \times 10^{-6} \text{m}$  to  $2 \times 10^{-7} \text{m}$ . This was considered a significant enough improvement to justify the added complication in the model.

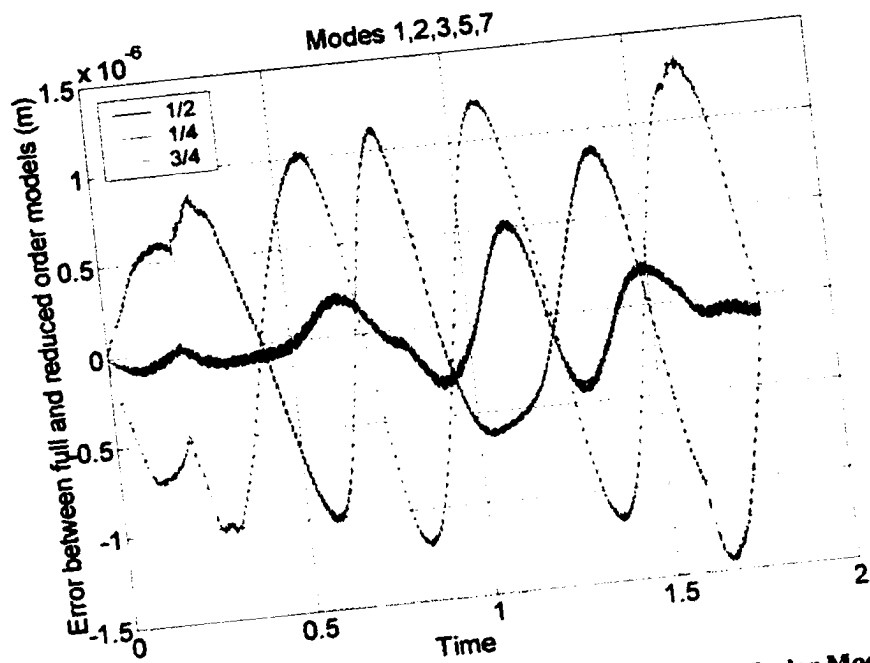


Figure 2.5 Error Using Modes 1, 2, 3, 5, 7 in the Reduced Order Model

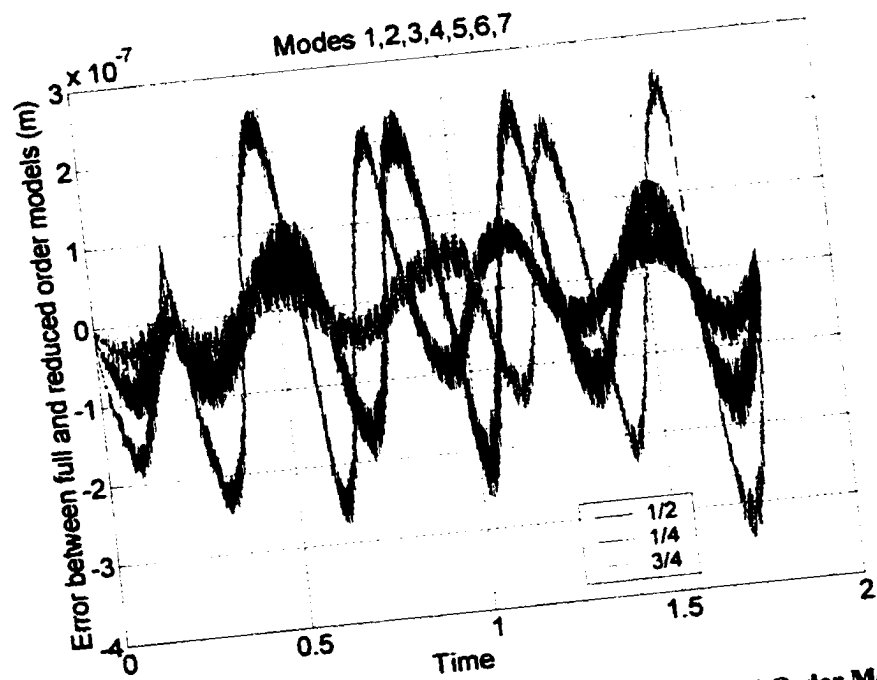


Figure 2.6 Error Using Modes 1, 2, 3, 4, 5, 6, 7 in the Reduced Order Model

The modal coordinate vector for either reduced order model,  $z$ , can be expressed as

$$\bar{z} = \mathbf{T}\bar{x}_B \quad (2.21)$$

where  $T$  is the appropriate transformation matrix for each model and both will be given in an Appendix to this chapter. Rewriting the system of equations in terms of these modal coordinates gives

$$\begin{aligned} \dot{\bar{z}} &= \mathbf{T}\mathbf{A}_B\mathbf{T}^{-1}\bar{z} + \mathbf{T}\mathbf{B}_B f(t) = \tilde{\mathbf{A}}\bar{z} + \tilde{\mathbf{B}}f(t) \\ \bar{y} &= \mathbf{C}_B\mathbf{T}^{-1}\bar{z} = \tilde{\mathbf{C}}\bar{z} \end{aligned} \quad (2.22)$$

The new state matrix  $\tilde{A}$  for each model is in block diagonal form with  $A_i$  along the diagonal.

$$\mathbf{A}_i = \begin{bmatrix} \sigma_i & \beta_i \\ -\beta_i & \sigma_i \end{bmatrix} \quad (2.23)$$

where  $\sigma_i = \xi_i \omega_i$  and  $\beta_i = \omega_i \sqrt{1 - \xi_i^2}$ .  $\omega_i$  is the natural frequency in radians of the mode and  $\xi_i$  is the damping ratio.  $\xi_i = 0.02$  for all  $i=1,7$ .

The bridge models described above are each used in a different phase of the truck identification problem. The truck models used with each bridge models and the solution methods employed to solve each coupled system are discussed in the following two chapters.

## 2.12 Sensor Locations

The locations of the measurements used in this work were selected based on their information content and the use of symmetry. First, consider the deflection at each of the seven interior nodes (not at the supports) for the static beam. Since static beam bending is

the dominant behavior of the beam, the sensor locations are chosen using the static beam model. The midpoint deflection has the largest magnitude so it is an obvious choice for one sensor location. The deflection over time at each node for a moving point force is shown below in Figure 2.7.

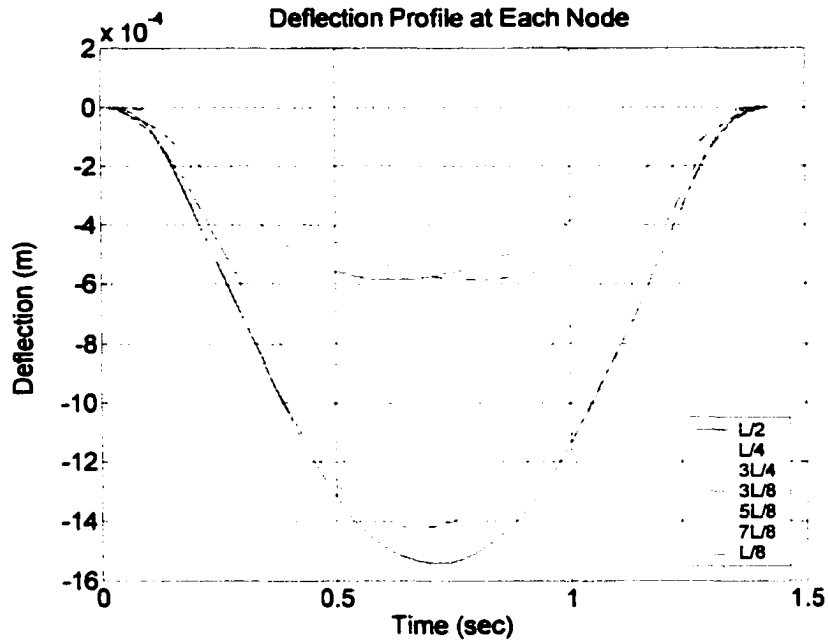


Figure 2.7 Deflection at Each Node Due to a Moving Point Force

Clearly, the midpoint deflection profile has the largest magnitude for the same weight, so it was chosen as the first sensor location. The static deflection of the beam is

given by Equation (2.11). The  $\left(\frac{1}{i}\right)^4 \sin \frac{i\pi x}{L}$  term in Equation (2.11) determines the

magnitude of the response based on the measurement location. This expression can be

rewritten in terms of the locations of the nodes as  $\left(\frac{1}{i}\right)^4 \sin \frac{i\pi n}{8}$  where  $n$  is the node

number, and  $i$  is the mode number. A plot of the absolute value of this term is shown for the first three modes below in Figure 2.8. The magnitude of the sine term is scaled by

$\left(\frac{1}{i}\right)^4$  for the  $i^{\text{th}}$  mode. For the first mode, the midpoint ( $n=4$ ) has the largest magnitude.

The next largest responses for the first mode are at  $n=3, 5$  ( $x=3L/8, 5L/8$ ). For the second mode,  $n=2, 6$  ( $x=L/4, 3L/4$ ) have the largest responses. Although it is small, the magnitude of the sine term for the third mode is larger for the  $n=2, 6$  ( $x=L/4, 3L/4$ ) than for the  $n=3, 5$  ( $x=3L/8, 5L/8$ ). Based on the magnitudes of the deflection at each node due to each of the first three modes, the quarter-point and the three-quarter-point ( $x=L/4, 3L/4$  or  $n=2, 6$ ) were selected for the locations of the other two sensors. This sensor combination also provided an evenly distributed, symmetric arrangement of sensors.

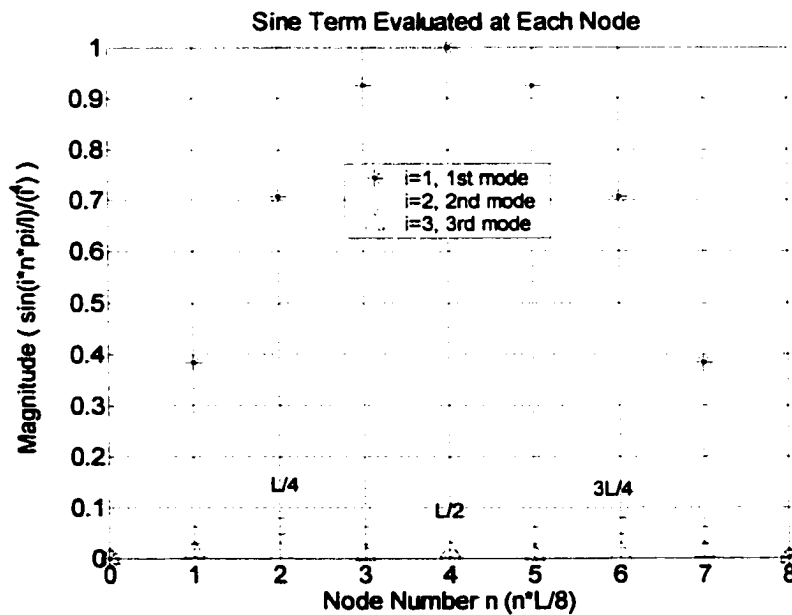


Figure 2.8 Sine Term at Each Node For Three Modes

The magnitudes of the  $\sin \frac{i\pi x}{L}$  term for each sensor location for the first eight modes are given in the table below. Neither of three sensor location reflects the fourth or the eighth modes. This was not considered significant since the magnitude of each mode

decreases by  $i^4$ , and the contribution to the deflection by higher modes decreases rapidly.

The magnitude  $\left(\frac{1}{i}\right)^4$  was 0.0039 for the fourth mode and 0.0123 for the third mode.

**Table 2.2 Sine Term For Each Mode**

| Sensor Location | Sine Term              | i=1          | i=2 | i=3          | i=4 | i=5           | i=6 | i=7           | i=8 |
|-----------------|------------------------|--------------|-----|--------------|-----|---------------|-----|---------------|-----|
| $x=L/2$         | $\sin \frac{i\pi}{2}$  | 1            | 0   | -1           | 0   | 1             | 0   | -1            | 0   |
| $x=L/4$         | $\sin \frac{i\pi}{4}$  | $1/\sqrt{2}$ | 1   | $1/\sqrt{2}$ | 0   | $-1/\sqrt{2}$ | -1  | $-1/\sqrt{2}$ | 0   |
| $x=3L/4$        | $\sin \frac{i3\pi}{4}$ | $1/\sqrt{2}$ | -1  | $1/\sqrt{2}$ | 0   | $-1/\sqrt{2}$ | 1   | $1/\sqrt{2}$  | 0   |

### 2.13 Chapter Conclusions

The bridge models and sensor equations described in sections 2.4-2.12 are used throughout the rest of this work in combination with two truck models that are described in Chapter 3. The static bridge model is used in Chapters 6 and 7 to examine the static bridge/static truck and static bridge/dynamic truck systems. The combined bridge/truck models will be used to identify important truck parameters from the deflection profiles at the sensor locations.

## 2.14 Bridge Models Appendix

The matrices shown on the following pages are used to form the transformation matrices used in the reduced order model of the dynamic bridge model. The first,  $T_{s7}^T$ , selects the first seven modes of the full-scale bridge model. The second,  $T_{s4}^T$ , selects the first four odd modes of the bridge model. The complete transformation matrices are formed by

$$T = \begin{bmatrix} T_{sj} & 0_{nx16} \end{bmatrix}$$

where  $j$  is the number of modes used in the model.

Seven Modes (1-7)

$T_{s7}^T =$

|          |          |          |          |          |          |          |          |          |          |          |          |          |          |
|----------|----------|----------|----------|----------|----------|----------|----------|----------|----------|----------|----------|----------|----------|
| -9.7E-01 | 1.9E-02  | -9.3E-01 | 1.9E-02  | 8.4E-01  | -1.7E-02 | -7.2E-01 | 1.4E-02  | -5.7E-01 | 1.1E-02  | -4.2E-01 | 8.5E-03  | 2.8E-15  | 4.0E-01  |
| -1.3E-01 | 2.6E-03  | -2.6E-01 | 5.1E-03  | 3.6E-01  | -7.3E-03 | -4.3E-01 | 8.6E-03  | -4.3E-01 | 8.6E-03  | -3.7E-01 | 7.4E-03  | 2.4E-15  | 3.8E-01  |
| 1.8E+00  | -3.6E-02 | 1.3E+00  | -2.6E-02 | -6.4E-01 | 1.3E-02  | -1.1E-14 | -1.3E-15 | -4.4E-01 | 8.8E-03  | -6.0E-01 | 1.2E-02  | 3.8E-15  | 7.4E-01  |
| 2.4E-01  | -4.8E-03 | 3.6E-01  | -7.2E-03 | -2.8E-01 | 5.6E-03  | -6.7E-15 | -8.1E-16 | -3.3E-01 | 6.6E-03  | -5.2E-01 | 1.0E-02  | 3.2E-15  | 7.1E-01  |
| -1.4E+00 | 2.7E-02  | 1.5E-15  | -2.1E-15 | -1.2E+00 | 2.4E-02  | 1.4E+00  | -2.9E-02 | 8.1E-01  | -1.6E-02 | 3.5E-14  | -7.4E-15 | -6.6E-16 | 5.7E-01  |
| -3.1E-01 | 6.3E-03  | -2.6E-01 | 5.1E-03  | -1.5E-01 | 3.0E-03  | 4.3E-01  | -8.6E-03 | 1.8E-01  | -3.6E-03 | -3.7E-01 | 7.4E-03  | 1.8E-15  | 9.3E-01  |
| 7.4E-01  | -1.5E-02 | -1.3E+00 | 2.6E-02  | 1.5E+00  | -3.1E-02 | 1.8E-14  | 4.4E-15  | 1.1E+00  | -2.1E-02 | 6.0E-01  | -1.2E-02 | -4.8E-15 | 3.1E-01  |
| 3.4E-01  | -6.8E-03 | 1.7E-15  | -6.5E-16 | 3.9E-01  | -7.9E-03 | 4.9E-15  | 3.1E-15  | 4.7E-01  | -9.3E-03 | 8.2E-14  | -1.3E-14 | -7.4E-16 | 1.0E+00  |
| -6.0E-15 | -9.2E-15 | 1.9E+00  | -3.7E-02 | -6.1E-16 | -3.4E-15 | -1.4E+00 | 2.9E-02  | -2.1E-15 | 1.2E-14  | 8.5E-01  | -1.7E-02 | -5.1E-15 | -1.3E-13 |
| -3.1E-01 | 6.3E-03  | 2.6E-01  | -5.1E-03 | -1.5E-01 | 3.0E-03  | -4.3E-01 | 8.6E-03  | 1.8E-01  | -3.6E-03 | 3.7E-01  | -7.4E-03 | -2.8E-15 | 9.3E-01  |
| -7.4E-01 | 1.5E-02  | -1.3E+00 | 2.6E-02  | -1.5E+00 | 3.1E-02  | -3.6E-14 | -3.9E-15 | -1.1E+00 | 2.1E-02  | 6.0E-01  | -1.2E-02 | -3.0E-15 | -3.1E-01 |
| 2.4E-01  | -4.8E-03 | -3.6E-01 | 7.2E-03  | -2.8E-01 | 5.6E-03  | -1.6E-14 | 6.3E-16  | -3.3E-01 | 6.6E-03  | 5.2E-01  | -1.0E-02 | -3.6E-15 | 7.1E-01  |
| 1.4E+00  | -2.7E-02 | 4.2E-15  | -1.5E-15 | 1.2E+00  | -2.4E-02 | 1.4E+00  | -2.9E-02 | -8.1E-01 | 1.6E-02  | -7.5E-14 | 5.4E-15  | -6.0E-17 | -5.7E-01 |
| -1.3E-01 | 2.6E-03  | 2.6E-01  | -5.1E-03 | 3.6E-01  | -7.3E-03 | 4.3E-01  | -8.6E-03 | -4.3E-01 | 8.6E-03  | 3.7E-01  | -7.4E-03 | -2.6E-15 | 3.8E-01  |
| -1.8E+00 | 3.6E-02  | 1.3E+00  | -2.6E-02 | 6.4E-01  | -1.3E-02 | 2.3E-14  | -2.8E-16 | 4.4E-01  | -8.8E-03 | -6.0E-01 | 1.2E-02  | 4.0E-15  | -7.4E-01 |
| 9.7E-01  | -1.9E-02 | -9.3E-01 | 1.9E-02  | -8.4E-01 | 1.7E-02  | -7.2E-01 | 1.4E-02  | 5.7E-01  | -1.1E-02 | -4.2E-01 | 8.5E-03  | 3.1E-15  | -4.0E-01 |

Four Modes

$$T_{s4}^T =$$

|          |          |          |          |          |          |          |          |
|----------|----------|----------|----------|----------|----------|----------|----------|
| -9.7E-01 | 1.9E-02  | 8.4E-01  | -1.7E-02 | -5.7E-01 | 1.1E-02  | 2.8E-15  | 4.0E-01  |
| -1.3E-01 | 2.6E-03  | 3.6E-01  | -7.3E-03 | -4.3E-01 | 8.6E-03  | 2.4E-15  | 3.8E-01  |
| 1.8E+00  | -3.6E-02 | -6.4E-01 | 1.3E-02  | -4.4E-01 | 8.8E-03  | 3.8E-15  | 7.4E-01  |
| 2.4E-01  | -4.8E-03 | -2.8E-01 | 5.6E-03  | -3.3E-01 | 6.6E-03  | 3.2E-15  | 7.1E-01  |
| -1.4E+00 | 2.7E-02  | -1.2E+00 | 2.4E-02  | 8.1E-01  | -1.6E-02 | -6.6E-16 | 5.7E-01  |
| -3.1E-01 | 6.3E-03  | -1.5E-01 | 3.0E-03  | 1.8E-01  | -3.6E-03 | 1.8E-15  | 9.3E-01  |
| 7.4E-01  | -1.5E-02 | 1.5E+00  | -3.1E-02 | 1.1E+00  | -2.1E-02 | -4.8E-15 | 3.1E-01  |
| 3.4E-01  | -6.8E-03 | 3.9E-01  | -7.9E-03 | 4.7E-01  | -9.3E-03 | -7.4E-16 | 1.0E+00  |
| -6.0E-15 | -9.2E-15 | -6.1E-16 | -3.4E-15 | -2.1E-15 | 1.2E-14  | -5.1E-15 | -1.3E-13 |
| -3.1E-01 | 6.3E-03  | -1.5E-01 | 3.0E-03  | 1.8E-01  | -3.6E-03 | -2.8E-15 | 9.3E-01  |
| -7.4E-01 | 1.5E-02  | -1.5E+00 | 3.1E-02  | -1.1E+00 | 2.1E-02  | -3.0E-15 | -3.1E-01 |
| 2.4E-01  | -4.8E-03 | -2.8E-01 | 5.6E-03  | -3.3E-01 | 6.6E-03  | -3.6E-15 | 7.1E-01  |
| 1.4E+00  | -2.7E-02 | 1.2E+00  | -2.4E-02 | -8.1E-01 | 1.6E-02  | -6.0E-17 | -5.7E-01 |
| -1.3E-01 | 2.6E-03  | 3.6E-01  | -7.3E-03 | -4.3E-01 | 8.6E-03  | -2.6E-15 | 3.8E-01  |
| -1.8E+00 | 3.6E-02  | 6.4E-01  | -1.3E-02 | 4.4E-01  | -8.8E-03 | 4.0E-15  | -7.4E-01 |
| 9.7E-01  | -1.9E-02 | -8.4E-01 | 1.7E-02  | 5.7E-01  | -1.1E-02 | 3.1E-15  | -4.0E-01 |

# **Chapter 3**

## **Truck Models and Dynamics**

Another important aspect to modeling the response of a bridge to a truck is the model of the truck used. Existing models vary in complexity and in the truck properties they include. A chart outlining many of the authors developing truck models is given below in Figure 3.1.

# Truck Models

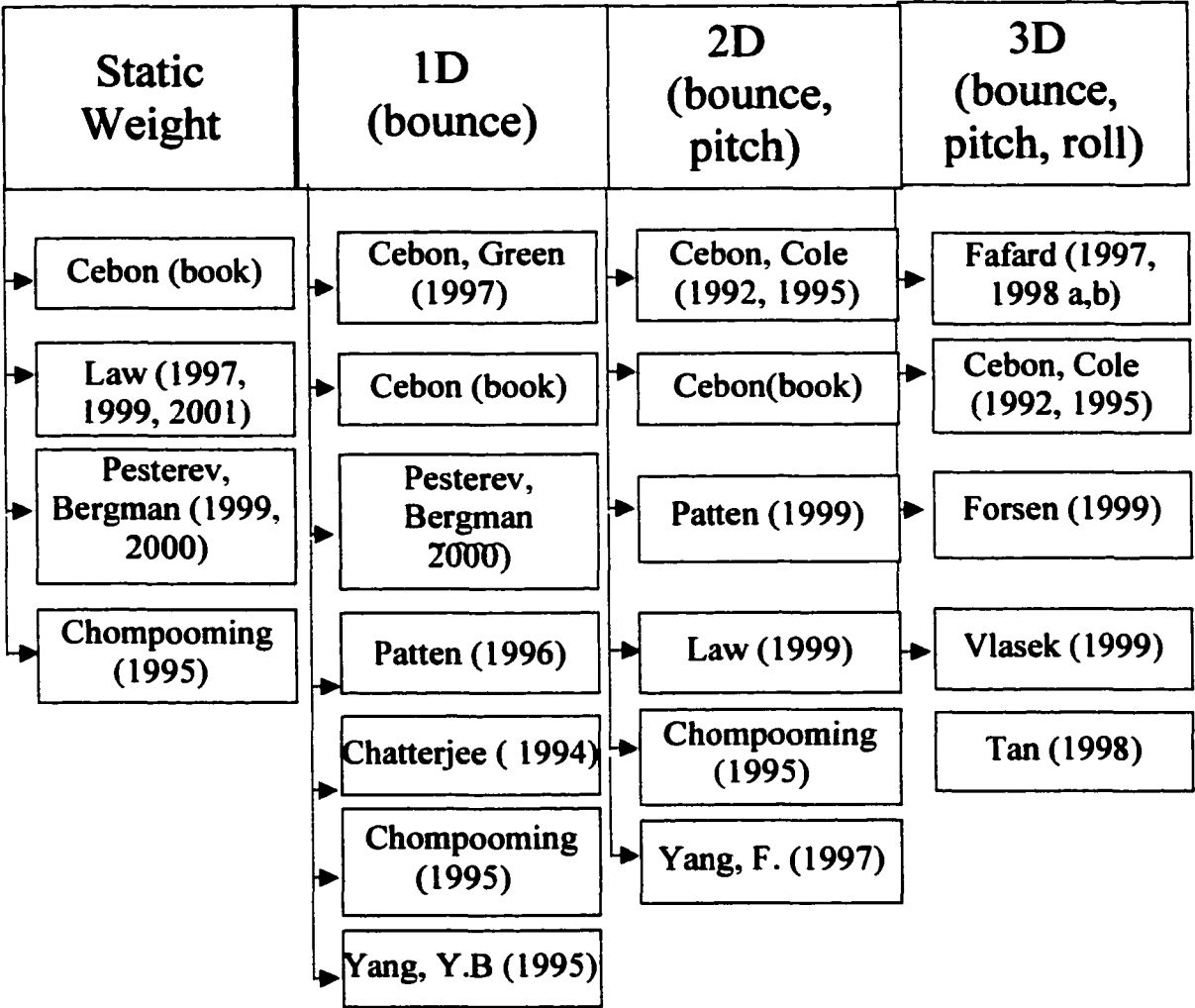


**Figure 3.1 Flowchart of Truck Models in the Literature**

### **3.1 3D Truck Models**

Many of the existing truck models are quite complex and include the vertical displacement (bounce) of the truck's tractor and/or trailer, as well as the pitch and roll of the truck. These models typically represent each wheel pair on an axle and are three-dimensional representations. One such model is described by Fafard (Fafard and Bennur, 1997). It is an 18 DOF three-dimensional model that includes the tractor (cab) and two trailers. It assumes that each body of the model is a rigid mass connected to linear suspension systems. For each of the two trailers, a rigid mass is connected to four spring/damper sets that represent the linear behavior of a multileaf suspension system. At each of these four points, the tire is represented by another mass and spring/damper set approximating the stiffness and damping of the tire pairs. The tractor is a rigid mass with two spring/damper sets and two tire assemblies to represent the single axle common to most vehicles of this type. It was also assumed that each tire remained in contact with the bridge or road at all times. This model included the bounce, pitch and roll of all three of the truck's bodies. A similar model that included only one trailer was also described in another work (Fafard et al., 1998). The numerical values for the stiffnesses and dampings were determined experimentally from a fully instrumented test truck.

In another work, the Fafard and Henchi describe a similar model of simpler truck that also included the bounce, pitch and roll (Henchi et al., 1998). The truck was a dump truck that had a trailer and cab attached as one body. Three axles, one under the cab and two under the rear of the trailer, were again modeled using the appropriate linear properties of a multileaf suspension system. The entire truck was modeled as one mass

connected to four spring/damper systems for the suspension systems at each tire. Four tire assemblies were also included and were the points of contact to the road surface. The properties of the two rear axles were combined and modeled as two rear suspension and tire assemblies on either side of the truck. The model had seven DOF in total and described the bounce, pitch and roll of the vehicle.

Another three-dimensional model is described by Forsen (Forsen, 1999). A solid modeling and finite element package is used to model the truck as 23 bodies connected by joints, springs and dampers for a total of 74 DOF. The tires of this truck were modeled as three-dimensional rigid rings that included sidewall stiffness and belt mass. The stiffness, damping and mass parameters were verified from data collected from a fully instrumented test truck passing over several types of obstacles and various speeds. After proper tuning, it was found that this model very closely represented the motion of the test truck although it was computationally quite complex.

### **3.2 2D Truck Models**

Cole and Cebon (Cole and Cebon, 1992) developed two models of a tractor and single trailer combination and compared the contributions from bounce, roll, and pitch for a variety of conditions. The first model was three-dimensional and similar in structure to the single trailer model described by Fafard and included 21 DOF. The model was validated experimentally and found to accurately represent the tire force applied by the test truck.

Several conclusions were drawn by the authors regarding the relative contributions of the components of the truck motion. Truck motion can typically be

described by two modes, the “sprung mass mode” which have frequencies of 1-4 Hz, and the “unsprung mass mode” of frequency 10-15 Hz. The authors found that, for the sprung mass mode, the contribution to the tire force due to the roll was negligible compared to the bounce. For the higher unsprung mass mode, the bounce and roll had similar magnitudes. It was also found that, for the majority of trucks, the contribution to the tire force by the unsprung mass mode is typically small compared to the sprung mass mode. This led to the conclusion that the roll component of the motion could be neglected for most trucks, making a two-dimensional model adequate.

Cole and Cebon then investigated the use of a two-dimensional model similar to “half” the three-dimensional one. Instead of representing each tire pair of each axle separately, each axle was condensed into a single suspension and tire assembly. It was found that two- and three-dimensional models compared favorably in the sprung mass mode (1-4 Hz) where the majority of the tire force originates, but differed for the unsprung mass mode (10-15 Hz) due to the omission of the roll component of the motion. It was also found that, at highway speeds, the three-dimensional model showed less excitation of the roll modes than at lower ones, indicating that the two-dimensional model was sufficient for representing trucks traveling at higher speeds. The authors concluded that the two-dimensional model gave an adequate representation of the tire force for the majority of trucks and required approximately one-tenth the computation time of the three-dimensional model, making it desirable for any type of real-time study.

Other authors have also used two-dimensional truck models in their work. Patten (Patten et al., 1999) used a model similar in structure to Cole and Cebon’s with parameters determined experimentally from a test truck. Chompooming (Chompooming

and Yener, 1995) described a four DOF two-dimensional model to examine bridge/truck interaction. This model consists of a rigid mass connected to two suspension and tires assemblies, allowing for bounce and pitch. The suspension is represented by a spring and a damper, and each tire is a mass/spring/damper assembly. The tire assembly's spring and damper are assumed to remain in contact with the bridge or road at all times. Yang (Yang, F. and Fonder, 1996) reduced the complexity of the two-dimensional model even further, combining each suspension and tire assembly into a single spring and damper.

### **3.3 1D Truck Models**

In another work by Cebon (Cebon, 1999) two models were compared that represented the majority of truck dynamics. One was a two-dimensional, three DOF model termed the 'walking-beam model'. It consisted of a rigid mass connected by a spring and damper to a rigid beam. The rigid beam joined the two axles and contacted the surface with two spring/damper assemblies. The mass was allowed vertical displacement, while the beam was given vertical displacement and rotation. The walking-beam model displayed a large pitching vibration in the frequency range of 8-15 Hz, which is representative of only a small percentage of typical truck suspensions. The second model is a one-dimensional, two DOF 'quarter car' model. This model consisted of a large sprung mass representative of the load on an axle and a smaller unsprung mass typical of tires. The two masses were connected by a spring and a damper with properties representative of a typical suspension. The unsprung mass was connected to the surface by a spring and a damper corresponding to the tire properties. This model generated its main tire force due to the low-frequency sprung mass motion (1.5-4 Hz), which made it

representative of the axle properties of the majority of trucks in use. The author cited this model as very representative of the behavior of each axle in the majority of trucks and indicated that multiple quarter-car models could be used in series to represent the multiple axles of a larger truck.

Cebon's 'quarter-car' model is similar to the model cited by Patten (Patten, et al. 1996). This model is also given the name 'quarter-car' model. This version of the 'quarter-car' model is depicted in Figure 3.2 and will be used throughout the remainder of this work. Any number of these quarter-car models can be combined to represent the axles of a given truck configuration.

The equations of motion for the  $i^{th}$  quarter car are given below where  $y_B(\tilde{x}_i, t)$  is the vertical deflection under the axle at the axle's lateral position  $\tilde{x}_i$ , and  $x_u$  and  $x_s$  are the vertical displacements of the unsprung and sprung masses. The equilibrium positions are taken relative to zero bridge displacement.

$$\begin{aligned} M_{si} \ddot{x}_{si} + K_{si}(x_{si} - x_{ui}) + C_{si}(\dot{x}_{si} - \dot{x}_{ui}) &= M_{si}g \\ M_{ui} \ddot{x}_{ui} + K_{si}(x_{ui} - x_{si}) + C_{si}(\dot{x}_{ui} - \dot{x}_{si}) + K_{ui}(x_{ui} - y_B(\tilde{x}_i, t)) &= M_{ui}g \end{aligned} \quad (3.1)$$

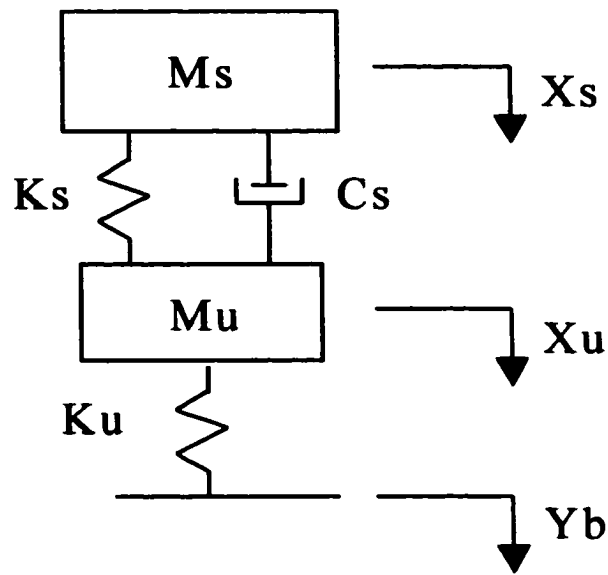


**Figure 3.2 'Quarter-Car' Model Used in This Work**

The total force applied to the bridge or road by each axle is given by

$$F_i(t) = -W_i + k_{u_i}(x_{u_i}(t) - y_B(x_i, t)) \quad (3.2)$$

This model is used throughout this work to illustrate the effect of the weight of the truck and the coupling between the bridge deflection and the truck. Details of this interaction will be discussed in the following chapter.

It became necessary throughout this work to examine the homogeneous solution of the differential equations of motion of the truck; in other words, to examine the truck's behavior without the bridge interaction term  $y_B$  in Equation (3.1). This would be the case if the truck were traveling across a roadway or "infinitely stiff" bridge.

Because the dynamic portion of the force is determined by the motion of the unsprung mass,  $x_u$ , this quantity is of the greatest interest in this work. The homogenous solutions for  $x_u$  of both axles have the form of two damped oscillatory modes as given in Equation (3.3) below.

$$\begin{aligned}Xu_1 &= A_{11}e^{-\alpha_{11}(t-t_1)}\sin(\beta_{11}(t-t_1)+\phi_{11})+A_{12}e^{-\alpha_{12}(t-t_1)}\sin(\beta_{12}(t-t_1)+\phi_{12}) \\Xu_2 &= A_{21}e^{-\alpha_{21}(t-t_2)}\sin(\beta_{21}(t-t_2)+\phi_{21})+A_{22}e^{-\alpha_{22}(t-t_2)}\sin(\beta_{22}(t-t_2)+\phi_{22})\end{aligned}\quad (3.3)$$

The time shifts in each expression,  $t_1$  and  $t_2$ , are the times at which each axle enters the bridge. The constants  $A_{ij}$  and  $\phi_{ij}$  depend on the initial conditions of each axle upon entering the bridge. The constants  $\alpha_{ij}$  and  $\beta_{ij}$  determine the damping and frequency of oscillation of the axle and can be related to the more familiar quantities  $\xi$  and  $\omega_n$  through the following relations, where  $\xi$  is the damping coefficient of each mode and  $\omega_n$  is the natural frequency of the mode.

$$\alpha = \xi\omega_n \quad \text{and} \quad \beta = \omega_n\sqrt{1-\xi^2}\quad (3.4)$$

It is often useful to write the second order differential equations of motion for such a system in terms of multiple first order differential equations. The truck system given in Equation (3.1) for both axles could therefore be written as

$$\begin{aligned}\dot{\bar{x}}_T &= \mathbf{A}_T\bar{x}_T + \mathbf{B}_Ty_B \\ \bar{y}_T &= \mathbf{B}_u\bar{x}_T = \begin{bmatrix} xu_1 \\ xu_2 \end{bmatrix} = \bar{x}_u\end{aligned}\quad (3.5)$$

where

$$\mathbf{A}_T = \begin{bmatrix} \mathbf{0}_{4 \times 4} & \mathbf{I}_{4 \times 4} \\ \tilde{\mathbf{A}}_{Ts} & \tilde{\mathbf{A}}_{Td} \end{bmatrix}, \quad \tilde{\mathbf{A}}_{Td} = \begin{bmatrix} -\mathbf{M}s^{-1}\mathbf{C} & \mathbf{M}s^{-1}\mathbf{C} \\ \mathbf{M}u^{-1}\mathbf{C} & -\mathbf{M}u^{-1}\mathbf{C} \end{bmatrix}\quad (3.6a, b)$$

$$\tilde{\mathbf{A}}_{Ts} = \begin{bmatrix} -\mathbf{M}s^{-1}\mathbf{K}s & \mathbf{M}s^{-1}\mathbf{K}s \\ \mathbf{M}u^{-1}\mathbf{K}s & -\mathbf{M}u^{-1}(\mathbf{K}s + \mathbf{K}u) \end{bmatrix}\quad (3.6c)$$

$$\mathbf{M}u^{-1} = \begin{bmatrix} \frac{1}{mu_1} & 0 \\ 0 & \frac{1}{mu_2} \end{bmatrix}, \quad \mathbf{K}s = \begin{bmatrix} ks_1 & 0 \\ 0 & ks_2 \end{bmatrix}, \quad \mathbf{M}s^{-1} = \begin{bmatrix} \frac{1}{ms_1} & 0 \\ 0 & \frac{1}{ms_2} \end{bmatrix}\quad (3.6d)$$

$$\mathbf{B}_T = \begin{bmatrix} \mathbf{0}_{6 \times 2} \\ \mathbf{M}\mathbf{u}^{-1}\mathbf{K}\mathbf{u} \end{bmatrix} \text{ for 2 axles, } \mathbf{B}_T = \begin{bmatrix} \mathbf{0}_{3 \times 2} \\ ku_i / mu_i \end{bmatrix} \text{ for the } i^{\text{th}} \text{ axle} \quad (3.6e)$$

where  $\bar{\mathbf{x}}_T = [x_{s1}, x_{s2}, x_{u1}, x_{u2}, \dot{x}_{s1}, \dot{x}_{s2}, \dot{x}_{u1}, \dot{x}_{u2}]^T$ .

The quantities  $\alpha_{ij}$  and  $\beta_{ij}$  are the real and imaginary parts of the eigenvalues of the matrix  $A_T$ . As shown later in this work, expressing the truck state matrices in terms of the quantities  $\alpha_{ij}$  and  $\beta_{ij}$  was found to be useful. The transformation to this form will be discussed here, but the importance of this form will become apparent in later chapters. For the remainder of this discussion, the transformation from the physical quantities discussed above to the modal properties  $\alpha_{ij}$  and  $\beta_{ij}$  will be applied to only one axle, although the state matrix for both axles (like Equation (3.6a)) would be of the same form.

It was necessary to rewrite the truck state matrices  $A_T$  and  $B_T$  in terms of the quantities  $\alpha_{ij}$  and  $\beta_{ij}$  rather than the physical properties in Equation (3.6d). The development of Equations (3.7)-(3.12) were provided by Stalford (Stalford, October, 2002). To do this, let us first define the quantities

$$\lambda_1^2 = \alpha_1^2 + \beta_1^2 \quad \text{and} \quad \lambda_2^2 = \alpha_2^2 + \beta_2^2 \quad (3.7)$$

The single subscript on each quantity is because the following derivation is for one axle only. The nomenclature would be similar to that used above for both axles. The quantities  $\alpha_1$ ,  $\alpha_2$ , and  $\beta_1$ ,  $\beta_2$  are the absolute values of the real and imaginary parts of the eigenvalues of the state matrix  $A_T$ . To further the development of the transformed truck system, let us also define the following quantities.

$$\begin{aligned}
c_3 &= \alpha_1 + \alpha_2 \\
c_2 &= \lambda_1^2 + \lambda_2^2 + 4\alpha_1\alpha_2 \\
c_1 &= \alpha_2\lambda_1^2 + \alpha_1\lambda_2^2 \\
c_0 &= \lambda_1^2\lambda_2^2
\end{aligned} \tag{3.8}$$

The following four equations can be solved for  $\sigma_1$ ,  $\sigma_2$ ,  $\theta_1^2$ , and  $\theta_2^2$  in terms of  $c_3$ ,  $c_2$ ,  $c_1$ , and  $c_0$ .

$$\begin{aligned}
\sigma_1 + \sigma_2 &= c_3 \\
\theta_1^2 + \theta_2^2 &= c_2 \\
\sigma_1\theta_2^2 - \sigma_2\theta_1^2 &= c_1 \\
\theta_1^2\theta_2^2 - \theta_1^2\theta_1^2\frac{\sigma_2}{\sigma_1} &= c_0
\end{aligned} \tag{3.9}$$

The solutions to the equations in Equation (3.9) are given below. These values are used to form the transformed representation of the  $A_T$  matrix.

$$\begin{aligned}
\sigma_1 &= \frac{c_1^2}{c_1c_2 - c_0c_3} \\
\sigma_2 &= c_3 - \sigma_1 \\
\theta_1^2 &= \frac{c_0}{c_1}\sigma_1 \\
\theta_2^2 &= c_2 - \theta_1^2
\end{aligned} \tag{3.10}$$

The above quantities are now in terms of the known quantities  $\alpha_1$ ,  $\alpha_2$ , and  $\beta_1$ ,  $\beta_2$ . The  $A_T$  and  $B_T$  matrices can now be written in terms of these quantities as

$$\mathbf{A}_T = \begin{bmatrix} \mathbf{0}_{2 \times 2} & \mathbf{I}_{2 \times 2} \\ -\theta_1^2 & \theta_1^2 & -2\sigma_1 & 2\sigma_1 \\ \theta_1^2\frac{\sigma_2}{\sigma_1} & -\theta_2^2 & 2\sigma_2 & -2\sigma_2 \end{bmatrix} \text{ and } \mathbf{B}_T = \begin{bmatrix} \mathbf{0}_{3 \times 1} \\ \theta_2^2 - \theta_1^2\frac{\sigma_2}{\sigma_1} \\ \sigma_1 \end{bmatrix} \tag{3.11}$$

This transformation has been repeatedly verified and is an equivalent representation of the  $A_T$  and  $B_T$  matrices given in Equations (3.6a) and (3.6e).

A relationship between  $ku_i$  and  $W_i$  using the quantities described above was also developed and used in Chapter 9. This expression is given below.

$$ku_i = W_i \left( \theta_1^2 - \theta_2^2 \frac{\sigma_2}{\sigma_1} \right) \quad (3.12)$$

This expression was used to eliminate  $ku$  as an optimization parameter in Chapter 9.

### 3.4 Static Weight

The simplest model of a truck crossing a bridge is a static weight. Many authors, including the ones listed in Figure 3.1, have examined the problem of a point force moving across a bridge. In two sections of this work, the truck is modeled as a point force of magnitude equal to the axle weight of a truck traveling at a constant speed across the beam bridge model. Details of this problem will be discussed in a later chapter.

### 3.5 Numerical Parameters Used in the Static Truck Models

Below is a table giving the numerical parameters of the trucks used in the two chapters describing the use of the static truck models (Chapters 6 and 7). Table 3.1 only gives the parameters for the trucks whose results are shown in this work although the algorithms were tested using many other truck configurations.

**Table 3.1 Numerical Static Truck Parameters**

| Static Truck No. | Front Axle Weight ( $W_1$ ) | Rear Axle Weight ( $W_2$ ) | Axle Spacing | Speed  |
|------------------|-----------------------------|----------------------------|--------------|--------|
| 1                | $4.96 \times 10^4$ N        | $1.38 \times 10^5$ N       | 5 m          | 25 m/s |
| 2                | $4.96 \times 10^4$ N        | $2.3 \times 10^5$ N        | 7 m          | 30 m/s |
| 3                | $4.96 \times 10^4$ N        | $1.59 \times 10^5$ N       | 7 m          | 25 m/s |
| 4                | $4.96 \times 10^4$ N        | $2.72 \times 10^5$ N       | 5 m          | 35 m/s |
| 5                | $7.01 \times 10^4$ N        | $1.38 \times 10^5$ N       | 5 m          | 25 m/s |
| 6                | $7.01 \times 10^4$ N        | $2.3 \times 10^5$ N        | 7 m          | 30 m/s |
| 7                | $7.01 \times 10^4$ N        | $1.59 \times 10^5$ N       | 7 m          | 25 m/s |
| 8                | $7.01 \times 10^4$ N        | $2.72 \times 10^5$ N       | 5 m          | 35 m/s |
| 9                | $8.48 \times 10^4$ N        | $1.38 \times 10^5$ N       | 5 m          | 25 m/s |
| 10               | $8.48 \times 10^4$ N        | $2.3 \times 10^5$ N        | 7 m          | 30 m/s |
| 11               | $8.48 \times 10^4$ N        | $1.59 \times 10^5$ N       | 7 m          | 25 m/s |
| 12               | $8.48 \times 10^4$ N        | $2.72 \times 10^5$ N       | 5 m          | 35 m/s |
| 13               | $1.2 \times 10^5$ N         | $1.38 \times 10^5$ N       | 5 m          | 25 m/s |
| 14               | $1.2 \times 10^5$ N         | $2.3 \times 10^5$ N        | 7 m          | 30 m/s |
| 15               | $1.2 \times 10^5$ N         | $1.59 \times 10^5$ N       | 7 m          | 25 m/s |
| 16               | $1.2 \times 10^5$ N         | $2.72 \times 10^5$ N       | 5 m          | 35 m/s |

### 3.6 Numerical Parameters Used in the Dynamic Truck Models

Below is a table of the parameters used in the dynamic truck models discussed in this work. The parameters are given in terms of their physical values (stiffness, damping, mass) as shown in Figure 3.2 as well as the equivalent natural frequencies and damping ratios. The initial conditions for each axle,  $X0_i$ , are also given in the table. The notation used is a vector of the truck states equal to  $x_T = [x_s \quad x_u \quad \dot{x}_s \quad \dot{x}_u]^T$ . The natural frequencies and damping ratios are given in terms of the axle number  $i$  and the mode number  $j$ , as  $\omega_{nij}$  and  $\xi_{ij}$ .

**Table 3.2 Numerical Parameters for Dynamic Truck Models**

| Parameter                                    | 1                        | 2                         | 3                         | 4                         | 5                         | 6                          | 7                        | 8                        | 9                        | 10                       |                          |
|--|--------------------------|---------------------------|---------------------------|---------------------------|---------------------------|----------------------------|--------------------------|--------------------------|--------------------------|--------------------------|--------------------------|
| <b>W1 (N)</b>                                | 9.8E4                    | 9.8E4                     | 9.8E4                     | 9.8E4                     | 9.8E4                     | 1.15E5                     | 1.24E5                   | 1.24E5                   | 1.19E5                   | 1.18E5                   |                          |
| <b>Ku1 (N/m)</b>                             | 3.5E6                    | 3.5E6                     | 3.5E6                     | 3.5E6                     | 3.5E6                     | 4.2E6                      | 4.2E6                    | 4.9E6                    | 10.1E6                   | 3.5E6                    |                          |
| <b>Ks1 (N/m)</b>                             | 2E6                      | 2E6                       | 2E6                       | 2E6                       | 2E6                       | 2.4E6                      | 2.4E6                    | 1.8E6                    | 4.2E6                    | 2.6E6                    |                          |
| <b>Ms1 (kg)</b>                              | 8,900                    | 8,900                     | 8,900                     | 8,900                     | 8,900                     | 10,680                     | 11,570                   | 11,570                   | 11,125                   | 11,125                   |                          |
| <b>Mu1 (kg)</b>                              | 1,100                    | 1,100                     | 1,100                     | 1,100                     | 1,100                     | 1,100                      | 1,100                    | 1,100                    | 1,100                    | 1,100                    |                          |
| <b>Cs1 (Ns/m)</b>                            | 4E4                      | 4E4                       | 4E4                       | 4E4                       | 4E4                       | 4E4                        | 4E4                      | 4E4                      | 4E4                      | 8E4                      |                          |
| <b><math>\omega_{n11}</math> (Hz)</b>        | 1.91                     | 1.91                      | 1.91                      | 1.91                      | 1.91                      | 1.89                       | 1.82                     | 1.70                     | 2.59                     | 1.62                     |                          |
| <b><math>\xi_{11}</math> (%)</b>             | 7.2                      | 7.2                       | 7.2                       | 7.2                       | 7.2                       | 6.1                        | 5.9                      | 8.5                      | 5.4                      | 16.7                     |                          |
| <b><math>\omega_{n12}</math> (Hz)</b>        | 11.27                    | 11.27                     | 11.27                     | 11.27                     | 11.27                     | 12.35                      | 12.35                    | 12.39                    | 18.20                    | 11.09                    |                          |
| <b><math>\xi_{12}</math> (%)</b>             | 27.6                     | 27.6                      | 27.6                      | 27.6                      | 27.6                      | 24.9                       | 24.8                     | 24.4                     | 16.7                     | 50.0                     |                          |
| <b>X0<sub>1</sub></b><br>(m, m, m/s,<br>m/s) | -0.01<br>-0.01<br>0<br>0 | -0.01 -<br>0.01<br>0<br>0 | -0.01 -<br>0.01<br>0<br>0 | -0.01 -<br>0.01<br>0<br>0 | -0.01 -<br>0.01<br>0<br>0 | -0.01 -<br>-0.15<br>0<br>0 | -0.05<br>-0.15<br>0<br>0 | -0.05<br>-0.15<br>0<br>0 | -0.05<br>-0.15<br>0<br>0 | -0.05<br>-0.15<br>0<br>0 | -0.05<br>-0.15<br>0<br>0 |
| <b>a</b>                                     | 5                        | 5                         | 5                         | 5                         | 6                         | 6                          | 6                        | 4                        | 4                        | 4                        |                          |
| <b>v</b>                                     | 25                       | 25                        | 30                        | 30                        | 25                        | 25                         | 35                       | 35                       | 30                       | 25                       |                          |
|  |                          |                           |                           |                           |                           |                            |                          |                          |                          |                          |                          |
| <b>W2 (N)</b>                                | 9.8E4                    | 1.24E5                    | 1.50E5                    | 9.8E4                     | 1.42E5                    | 1.68E5                     | 1.93E5                   | 1.91E5                   | 1.41E5                   | 1.74E5                   |                          |
| <b>Ku2 (N/m)</b>                             | 3.5E6                    | 3.5E6                     | 3.5E6                     | 3.5E6                     | 7E6                       | 8.4E6                      | 8.4E6                    | 9.3E6                    | 7.1E6                    | 4.5E6                    |                          |
| <b>Ks2 (N/m)</b>                             | 2E6                      | 2E6                       | 2E6                       | 3E6                       | 4E6                       | 4.8E6                      | 4.8E6                    | 2.3E6                    | 5E6                      | 2.6E6                    |                          |
| <b>Ms2 (kg)</b>                              | 8,900                    | 13,350                    | 14,240                    | 8,900                     | 13,353                    | 16,020                     | 18,512                   | 18,512                   | 13,350                   | 16,688                   |                          |
| <b>Mu2 (kg)</b>                              | 1,100                    | 1,100                     | 1,100                     | 1,100                     | 1,100                     | 1,100                      | 1,200                    | 1,000                    | 1,100                    | 1,100                    |                          |
| <b>Cs2 (Ns/m)</b>                            | 4E4                      | 4E4                       | 4E4                       | 4.8E4                     | 4.8E4                     | 6E4                        | 6E4                      | 6.8E4                    | 5.6E4                    | 6E4                      |                          |
| <b><math>\omega_{n21}</math> (Hz)</b>        | 1.91                     | 1.67                      | 1.50                      | 2.12                      | 2.19                      | 2.19                       | 2.04                     | 1.60                     | 2.36                     | 1.58                     |                          |
| <b><math>\xi_{21}</math> (%)</b>             | 7.2                      | 6.4                       | 5.9                       | 6.2                       | 5.6                       | 6.4                        | 5.9                      | 12.9                     | 5.6                      | 5.8                      |                          |
| <b><math>\omega_{n22}</math> (Hz)</b>        | 11.27                    | 11.27                     | 11.27                     | 12.35                     | 15.95                     | 17.48                      | 16.72                    | 17.12                    | 16.79                    | 12.76                    |                          |
| <b><math>\xi_{22}</math> (%)</b>             | 27.6                     | 27.1                      | 26.9                      | 25.9                      | 19.2                      | 17.5                       | 16.7                     | 19.1                     | 18.4                     | 46.8                     |                          |
| <b>X0<sub>2</sub></b><br>(m, m, m/s,<br>m/s) | -0.01<br>-0.01<br>0<br>0 | -0.01<br>-0.01<br>0<br>0  | -0.01<br>-0.01<br>0<br>0  | -0.01<br>-0.01<br>0<br>0  | -0.01<br>-0.01<br>0<br>0  | -0.01<br>-0.15<br>0<br>0   | -0.05<br>-0.15<br>0<br>0 | -0.05<br>-0.15<br>0<br>0 | -0.05<br>-0.15<br>0<br>0 | -0.05<br>-0.15<br>0<br>0 | -0.01<br>-0.05<br>0<br>0 |

| Parameter                                    | 11    | 12     | 13     | 14     | 15     | 16     | 17    | 18     | 19     | 20     |
|--|-------|--------|--------|--------|--------|--------|-------|--------|--------|--------|
| <b>W1 (N)</b>                                | 9.7E4 | 9.8E4  | 9.9E4  | 1.32E5 | 1.32E5 | 1.5E5  | 9.8E4 | 1.06E5 | 9.7E4  | 9.8E4  |
| <b>Ku1 (N/m)</b>                             | 4.5E6 | 4.5E6  | 3.5E6  | 3.5E6  | 3.5E6  | 3.5E6  | 3.5E6 | 3.2E6  | 3.2E6  | 2.6E6  |
| <b>Ks1 (N/m)</b>                             | 2.6E6 | 2.6E6  | 2.6E6  | 2.6E6  | 2.6E6  | 7E6    | 2E6   | 2E6    | 3E6    | 2E6    |
| <b>Ms1 (kg)</b>                              | 8900  | 8900   | 8900   | 12460  | 12460  | 14240  | 8900  | 9790   | 8900   | 8900   |
| <b>Mu1 (kg)</b>                              | 1000  | 1100   | 1300   | 1100   | 1100   | 1100   | 1100  | 1000   | 1000   | 1100   |
| <b>Cs1 (Ns/m)</b>                            | 6E4   | 6E4    | 3E4    | 4E4    | 4E4    | 6E4    | 6E4   | 4E4    | 7.2E4  | 4E4    |
| $\omega_{n11}$ (Hz)                          | 2.18  | 2.18   | 1.89   | 1.61   | 1.61   | 1.66   | 1.91  | 1.78   | 2.09   | 1.79   |
| $\xi_{11}$ (%)                               | 9.6   | 9.5    | 5.4    | 6.2    | 6.2    | 5.9    | 10.9  | 6.6    | 7.4    | 6.0    |
| $\omega_{n12}$ (Hz)                          | 13.39 | 12.78  | 10.41  | 11.27  | 11.27  | 12.06  | 11.16 | 11.44  | 12.49  | 10.38  |
| $\xi_{12}$ (%)                               | 38.0  | 36.5   | 19.2   | 27.1   | 27.1   | 37.9   | 41.8  | 29.7   | 49.8   | 30.3   |
| <b>X0<sub>1</sub></b><br>(m, m, m/s,<br>m/s) | -0.01 | 0.05   | 0.05   | -0.05  | -0.05  | 0      | -0.01 | -0.01  | -0.01  | 0.01   |
|  | -0.05 | 0.05   | 0.05   | 0.05   | 0.05   | 0      | -0.01 | -0.01  | -0.01  | 0.01   |
|  | 0     | 0      | 0      | -0.01  | -0.01  | -0.01  | 0     | 0      | 0      | 0      |
|  | 0     | -0.01  | -0.01  | 0.01   | 0.01   | -0.01  | 0     | 0      | 0      | 0      |
| <b>a</b>                                     | 4     | 6      | 8      | 10     | 10     | 8      | 5     | 6      | 5      | 5      |
| <b>v</b>                                     | 25    | 25     | 25     | 30     | 25     | 35     | 25    | 25     | 35     | 35     |
|  |       |        |        |        |        |        |       |        |        |        |
| <b>W2 (N)</b>                                | 9.8E4 | 1.17E5 | 1.17E5 | 1.45E5 | 1.57E5 | 1.78E5 | 9.8E4 | 1.47E5 | 1.52E5 | 1.24E5 |
| <b>Ku2 (N/m)</b>                             | 3.6E6 | 3.6E6  | 3.5E6  | 3.5E6  | 8.7E6  | 7.0E6  | 7.0E6 | 6.6E6  | 6.6E6  | 3.9E6  |
| <b>Ks2 (N/m)</b>                             | 2.1E6 | 2.1E6  | 2E6    | 2E6    | 8E6    | 8.1E6  | 3.2E6 | 2.6E6  | 2.6E6  | 2.6E6  |
| <b>Ms2 (kg)</b>                              | 8900  | 10675  | 10675  | 13781  | 14952  | 17110  | 8900  | 13721  | 14234  | 11629  |
| <b>Mu2 (kg)</b>                              | 1100  | 1300   | 1300   | 1100   | 1100   | 1100   | 1100  | 1300   | 1300   | 1100   |
| <b>Cs2 (Ns/m)</b>                            | 6E4   | 6E4    | 3.2E4  | 4E4    | 8.4E4  | 12E4   | 6E4   | 8E4    | 4.8E4  | 4E4    |
| $\omega_{n21}$ (Hz)                          | 1.95  | 1.78   | 1.72   | 1.53   | 2.64   | 2.35   | 2.50  | 1.87   | 1.83   | 1.70   |
| $\xi_{21}$ (%)                               | 10.7  | 9.7    | 5.5    | 5.9    | 6.6    | 7.7    | 9.8   | 12.3   | 5.9    | 6.9    |
| $\omega_{n22}$ (Hz)                          | 11.39 | 10.51  | 10.40  | 11.26  | 19.75  | 18.74  | 15.27 | 13.34  | 13.38  | 11.69  |
| $\xi_{22}$ (%)                               | 40.9  | 37.5   | 19.0   | 26.9   | 16.0   | 25.1   | 30.3  | 19.7   | 34.1   | 26.1   |
| <b>X0<sub>2</sub></b><br>(m, m, m/s,<br>m/s) | -0.01 | 0.05   | 0.05   | 0.05   | 0.05   | 0      | -0.01 | -0.01  | -0.01  | -0.01  |
|  | -0.05 | 0.05   | 0.05   | 0.05   | 0.05   | 0      | -0.01 | -0.01  | -0.01  | -0.01  |
|  | 0     | 0      | 0      | -0.05  | -0.05  | 0.01   | 0     | 0      | 0      | 0      |
|  | 0     | -0.01  | -0.01  | -0.05  | -0.05  | -0.01  | 0     | 0      | 0      | 0      |

# Chapter 4

## Bridge/Truck Interaction

Different methods are commonly used to examine the interaction effects between a truck and a bridge depending on the types of models used and the desired efficiency of the computations. Below is a chart outlining the methods in the literature to be discussed.

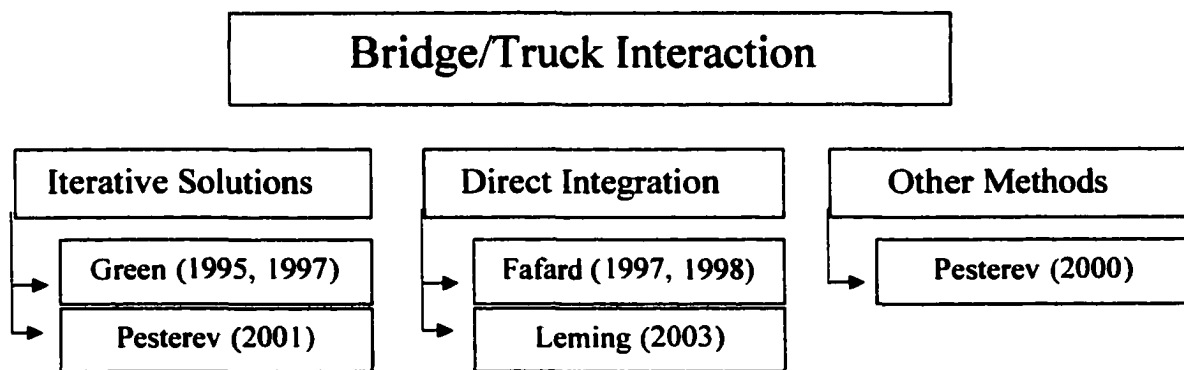


Figure 4.1 Flowchart of Bridge/Truck Interaction Literature

### 4.1 Iterative Solutions

A common method of treating the interaction between the bridge and the truck is the use of an iterative solution. Green (Green and Cebon, 1995, Green et. al, 1997) used one such iterative solution to solve the coupled bridge/truck system. At each time step, the vehicle response was calculated and the resulting force due to the weight and displacement of the individual masses applied to the bridge. The bridge response was then calculated and applied back into the truck model to recalculate the force due to the truck. This procedure was repeated at each time step until a convergence tolerance was

reached. Pesterev (Pesterev and Bergman, 2001) used another iterative method to solve the coupled system. The solution of the bridge response was broken into two parts-the eigenvalue expansion, which did not contain a discontinuity and one function that contained the moving discontinuity due to the moving force from the truck. The response of the beam from the eigenvalue expansion was then substituted back into the truck model to get the interaction forces. The resulting motion of the truck was then used to formulate a new total force due to the truck, which was then applied to the bridge. The process was repeated until the portion of the solution that contained the discontinuity converged to a solution. The total bridge response was then the sum of the eigenvalue expansion and the iterative solution. Methods such as these are supposed to be faster than directly integrating the equations.

#### **4.2 Other Methods**

Pesterev also proposed another method for solving the coupled system (Pesterev and Bergman, 2000). The homogeneous solution of the bridge differential equation was found with the use of static Green functions. A second term in the solution resulted from directly integrating the truck equations to find the truck response. The homogeneous solution and the integrated truck response were then combined to give the total bridge response.

#### **4.3 Direct Integration**

The most straightforward method for solving the coupled bridge/truck system is to numerically integrate the differential equations of the system. This has been done by many authors, although their methods of integration vary slightly. In the work described

in this dissertation, two methods are used to solve the coupled bridge/truck differential equations. In the first, the coupled bridge/truck differential equations are integrated directly. In the second, only the truck differential equations are integrated using an analytic expression for the bridge deflection. The common features of both methods will now be discussed.

#### **4.4 Truck Crossing the Bridge**

To discuss the interaction between the truck and the bridge, it is first necessary to describe the truck's motion across the beam. The following text applies to all four combinations of truck and bridge models used in this work, but is used in this context to examine the bridge/truck interaction solution.

For a two-axle truck model, the time that it takes for the truck to cross the bridge can be divided into three intervals. A schematic of these three intervals is shown in Figure 4.2. The distance between the two axles is  $a$ ,  $v$  is the constant speed at which they move, and  $L$  is length of the beam.

During each of the three time frames given in Figure 4.2, different descriptions of the interaction due to the bridge deflection apply and will be discussed in the following sections.

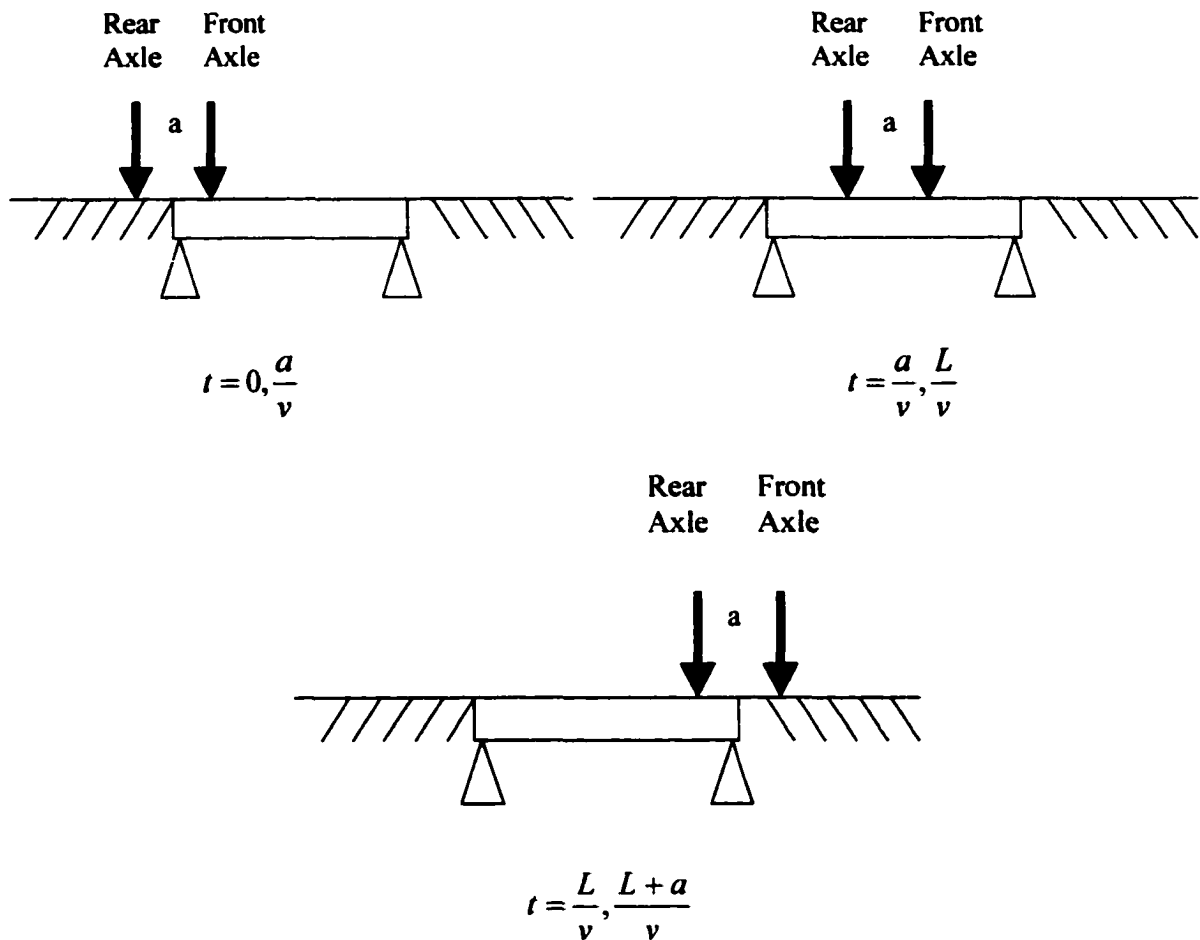


**Figure 4.2 Time intervals for the Truck Crossing the Bridge**

Each of the following four sections contains details of the interaction present with each pair of bridge and truck models. In the cases involving the static truck (or moving point force), the interaction is not what is classically considered 'bridge/truck interaction'-the excitation of the dynamics of the truck by bridge deflection-but rather a discussion on the effect on the beam due to the applied forces.

#### 4.5 Static Bridge/Static Truck

In this case, the static bridge model from Chapter 2 is deflected due to two moving point forces. The total force applied by each axle is of constant magnitude equal to the weight of the axle and moves across the beam with a constant speed  $v$ . Therefore, the total force applied by each axle is given by  $F_i = -W_i$ .

The deflections due to each force at a given location is found using the standard expressions for the inverse of beam stiffness found in Gere (Gere, 1997) and are given below.  $H_1$  is used if the  $x < b$ , and  $H_2$  is used if  $x > b$ , where  $x$  is the location of the applied force along the beam.

$$\begin{aligned} H_1(x, b) &= \frac{bx(b^2 - L^2 + x^2)}{6EIL} \\ H_2(x, a) &= \frac{(a - L)(a^2 - 2aL + (L - x)^2)(L - x)}{6EIL} \end{aligned} \quad (4.1)$$

where  $b_i = L - x_i$ , and  $a_i + b_i = L$ .

When only one axle is on the beam, the deflection along the beam is due only to the force applied by that axle. While both axles are on the beam, the deflection of the entire beam is the sum of the deflection to the front axle and the deflection due to the rear axle. This is simply a superposition of the solutions of the differential equation of bending for the static beam discussed in Chapter 2. The total deflection of the beam can be written as

$$\begin{aligned} w(x, t) &= -H_i(x, b_1)W_1 && \text{when } 0 \leq t \leq \frac{a}{v} \\ w(x, t) &= -H_i(x, b_1)W_1 - H_j(x, b_2)W_2 && \text{when } \frac{a}{v} \leq t \leq \frac{L}{v} \\ w(x, t) &= -H_i(x, b_2)W_2 && \text{when } \frac{L}{v} \leq t \leq \frac{L+a}{v} \end{aligned} \quad (4.2)$$

where the subscripts  $i$  and  $j$  on  $H$  are determined by the location of the measurement relative to the location of the force. An upward deflection of the beam is defined as positive.

#### 4.6 Static Bridge/Dynamic Truck

In this case, the static model of the bridge described in Chapter 2 is driven by two quarter-car models described in Chapter 3. As discussed in Chapter 3, the total force applied by each quarter car is given by

$$F_i(t) = -W_i + ku_i(xu_i(t) - y_B(x_i, t)) \quad (4.3)$$

To calculate this force, it is necessary to determine  $y_B(x, t)$ . As discussed above, when only one axle is on the beam, the deflection under that axle  $y_B(x_i, t)$  is due only to the force applied by that axle and can be called  $\delta_{ii}$  (deflection at the  $i^{\text{th}}$  axle due to the  $i^{\text{th}}$  axle). While both axles are on the beam, the deflection under the first axle  $y_B(x_1, t)$ , is due to both the force applied by the first axle,  $\delta_{11}$  and to the force applied by the second axle,  $\delta_{12}$  (deflection at 1 due to 2). The total deflection at  $x_1$  is the sum of  $\delta_{11}$  and  $\delta_{12}$ . The same is true for the deflection at  $x_2$ .

Each deflection is given by

$$\begin{aligned} \delta_{ii} &= H_1(x_i, b_i)F_i = H_{1i}F_{ii} \\ \delta_{12} &= H_2(x_1, a_2)F_2 = H_{12}F_2 \\ \delta_{21} &= H_1(x_2, b_1)F_1 = H_{21}F_1 \end{aligned} \quad (4.4)$$

where  $H(x, b)$  is defined above.

During the first time interval,  $t = 0, \frac{a}{v}$ , depicted in Figure 4.2, the deflection under the first axle is due only to the force applied by the first axle. The deflection  $y_B(x_1, t)$ , is therefore given by

$$y_B(x_1, t) = H_1(x_1, b_1)F_1(t) \text{ where } x_1 = a_1 \quad (4.5)$$

where  $x_1$  is the horizontal location of the front axle along the beam, and  $F_1$  is the force imparted by the front axle at the given time. A similar expression is true during the third time interval,  $t = \frac{L}{v}, \frac{L+a}{v}$ , when only the rear axle is on the beam.

$$y_B(x_2, t) = H_2(x_2, b_2)F_2(t) \text{ where } x_2 = a_2 \quad (4.6)$$

During the middle time interval,  $t = \frac{a}{v}, \frac{L}{v}$ , both axles are on the beam and the deflection under each axle is the sum of the deflection due to that axle and the deflection due to the other axle. In matrix form, this can be expressed as

$$y_B = \begin{bmatrix} H_{11} & H_{12} \\ H_{21} & H_{22} \end{bmatrix} \begin{bmatrix} F_1 \\ F_2 \end{bmatrix} = [H]\bar{F} \quad (4.7)$$

Throughout the rest of the text, these inverse stiffnesses will be expressed as  $H_{ij}$ , where  $\delta_{ij} = H_{ij}F_j$ . The subscript  $i$  on  $H_i(x, b)$  relating to the relative locations of the force and measurement has been dropped for clarity but are still calculated as described above. These expressions are similar to Equations (4.2) in the previous section but depend on the *total force* from the truck rather than just the static weight.

Substituting Equation (4.7) into Equation (4.3) leads to a vector representation of the force imparted by the axles to the beam given by

$$\begin{aligned}
F &= Q(KuXu + W) \text{ where } Q = [I + HKu]^{-1}, \\
Ku &= \begin{bmatrix} ku_1 & 0 \\ 0 & ku_2 \end{bmatrix}, Xu = \begin{bmatrix} xu_1 \\ xu_2 \end{bmatrix}, W = \begin{bmatrix} W_1 \\ W_2 \end{bmatrix}, \\
Y_B &= \begin{bmatrix} y_B(x_1, t) \\ y_B(x_2, t) \end{bmatrix}
\end{aligned} \tag{4.8}$$

The parameters  $ku_1$  and  $ku_2$  are the unsprung mass stiffnesses shown in Chapter 3,  $W_1$  and  $W_2$  are the total weights of the front and rear axles respectively, and  $xu_1$  and  $xu_2$  are the positions of the unsprung masses at a given time.

$F$  can be rewritten as

$$\begin{aligned}
F - W &= (Q - I)W + KuXu + (Q - I)KuXu \\
&= Ku(Xu - Y_B)
\end{aligned} \tag{4.9}$$

The equations of motion for each axle are given in Chapter 3, but are restated here for simplicity.

$$\begin{aligned}
M_{si} \ddot{x}_{si} + K_{si}(x_{si} - x_{ui}) + C_{si}(\dot{x}_{si} - \dot{x}_{ui}) &= M_{si}g \\
M_{ui} \ddot{x}_{ui} + K_{si}(x_{si} - x_{ui}) + C_{si}(\dot{x}_{ui} - \dot{x}_{si}) + K_{ui}(x_{ui} - y_B(\tilde{x}_i, t)) &= M_{ui}g
\end{aligned} \tag{4.10}$$

Substituting the expression given in Equation (4.9) for  $Ku(Xu - Y_B)$  into Equation (4.10) and rewriting the second order differential equations of motion as eight first order differential equations gives the following representation of the truck system.

$$\dot{\bar{x}} = [A + \Delta A(t)]\bar{x} + B(t)\bar{W} \tag{4.11}$$

where  $\bar{x} = [x_{s1}, x_{s2}, x_{u1}, x_{u2}, \dot{x}_{s1}, \dot{x}_{s2}, \dot{x}_{u1}, \dot{x}_{u2}]^T$  and

$$A = \begin{bmatrix} \mathbf{0}_{4 \times 4} & \mathbf{I}_{4 \times 4} \\ \tilde{A}_{Ts} & \tilde{A}_{Td} \end{bmatrix}, \tilde{A}_{Td} = \begin{bmatrix} -Ms^{-1}C & Ms^{-1}C \\ Mu^{-1}C & -Mu^{-1}C \end{bmatrix} \tag{4.12a,b}$$

$$\tilde{A}_{Ts} = \begin{bmatrix} -Ms^{-1}Ks & Ms^{-1}Ks \\ Mu^{-1}Ks & -Mu^{-1}(Ks + Ku) \end{bmatrix} \tag{4.12c}$$

$$\mathbf{Mu}^{-1} = \begin{bmatrix} \frac{1}{mu_1} & 0 \\ 0 & \frac{1}{mu_2} \end{bmatrix}, \mathbf{Ks} = \begin{bmatrix} ks_1 & 0 \\ 0 & ks_2 \end{bmatrix}, \mathbf{Ms}^{-1} = \begin{bmatrix} \frac{1}{ms_1} & 0 \\ 0 & \frac{1}{ms_2} \end{bmatrix}, \bar{\mathbf{W}} = \begin{bmatrix} -W_1 \\ -W_2 \end{bmatrix} \quad (4.12d-g)$$

$$\Delta\mathbf{A}(t) = \begin{bmatrix} \mathbf{0}_{4 \times 4} & \mathbf{I}_{4 \times 4} \\ \mathbf{0}_{2 \times 2} & \mathbf{0}_{2 \times 2} \\ \mathbf{0}_{2 \times 2} & -\mathbf{Mu}^{-1}(\mathbf{I} - \mathbf{Q})\mathbf{Ku} \\ & \mathbf{0}_{4 \times 4} \end{bmatrix} \quad (4.13)$$

$$\mathbf{B}(t) = \begin{bmatrix} \mathbf{0}_{6 \times 2} \\ \mathbf{Mu}^{-1}(\mathbf{I}_{2 \times 2} - \mathbf{Q}) \end{bmatrix} \quad (4.14)$$

These equations are integrated over time to determine  $Xu$  and the force applied by the truck. The equations given in Equations (4.11-4.14) represent the system only at the times at which both axles are on the beam. The system is modified to include only the appropriate axles during the other two time intervals, but maintains the same form.

#### 4.7 Dynamic Bridge/Static Truck

The dynamic bridge/static truck is similar to the static bridge/static truck case in that the deflection of the bridge is due to the sum of the deflections due to the individual truck weights. This is apparent from the system of equations of motion for the dynamic bridge case given in Chapter 2 and restated here.

$$\begin{aligned} \dot{\bar{x}}_B &= \mathbf{A}_B \bar{x}_B + \mathbf{B}_B(t) \bar{f}(t) \\ \bar{y} &= \mathbf{C}_B \bar{x}_B \end{aligned} \quad (4.15)$$

where

$$\mathbf{A}_B = \begin{bmatrix} \mathbf{0}_{16 \times 16} & \mathbf{I}_{16 \times 16} \\ -\mathbf{M}_G \mathbf{K}_G & -\mathbf{C}_G \end{bmatrix} \quad \mathbf{B}_B(t) = \begin{bmatrix} \mathbf{0}_{16 \times 16} \\ \mathbf{M}_G^{-1} \end{bmatrix} \mathbf{R}(s, z) \quad (4.16)$$

$$\bar{f}(t) = - \begin{bmatrix} W_1 \\ W_2 \end{bmatrix} \quad (4.17)$$

For the times when only one axle is on the bridge,  $\mathbf{R}(s, z)$  contains one column representing the force and moment distribution due to the weight to the appropriate nodes and one column of zeros since the effect of the axle that is not on the bridge is zero. When both axles are on the bridge,  $\mathbf{R}(s, z)$  contains two nonzero columns that result in an input into the system that is a weighted sum of the two axle weights. It is through the matrix  $\mathbf{R}(s, z)$  that the superposition of the effects of the weights enters the system.

#### 4.8 Dynamic Bridge/Dynamic Truck

In this section, we examine the coupled differential equations of the dynamic bridge model from Chapter 2 and the quarter-car model from Chapter 3. The derivation of the coupled differential equations (4.18-4.24) discussed in this section were provided by Stalford (Stalford, September, 2002). The coupled bridge/truck equations are integrated over time to give the motion of the coupled system.

Referring back to Chapter 2, the first order system of equations for the dynamic bridge model is given by

$$\begin{aligned} \dot{\bar{x}}_B &= \mathbf{A}_B \bar{x}_B + \mathbf{B}_B(t) \bar{F}(t) \\ \bar{y}_B &= \mathbf{C}(x_1, x_2) \bar{x}_B \end{aligned} \quad (4.18)$$

where  $x_1$ , and  $x_2$  are the positions of the front and rear axles as a function of time,  $F(t)$  is the force imparted by the truck, and all  $B$  subscripted variables are properties of the

bridge given in Chapter 2.  $y_B$  is the deflection of the bridge under each axle, and  $C(x_1, x_2) = R(s, z)^T$  where the elements and form of  $R(s, z)$  are given in Chapter 2.

A similar system of equations can be written for the truck.

$$\begin{aligned}\dot{\bar{x}}_T &= \mathbf{A}_T \bar{x}_T + \mathbf{B}_T y_B \\ \bar{y}_T &= \mathbf{B}_u \bar{x}_T = \begin{bmatrix} xu_1 \\ xu_2 \end{bmatrix} = \bar{x}_u\end{aligned}\quad (4.19)$$

where  $A_T$  is given by the expression for  $A$  in Equation (4.12a) above. The nomenclature has been modified in this section for clarity. Expressions for  $B_T$  and  $B_u$  are given below in Equations (4.20a) and (4.20b).

$$\mathbf{B}_T = \begin{bmatrix} \mathbf{0}_{6 \times 2} \\ \mathbf{M}\mathbf{u}^{-1}\mathbf{K}\mathbf{u} \end{bmatrix} \text{ for 2 axles, } \mathbf{B}_T = \begin{bmatrix} \mathbf{0}_{3 \times 2} \\ ku_i / mu_i \end{bmatrix} \text{ for the } i^{\text{th}} \text{ axle}\quad (4.20a)$$

$$\begin{aligned}\mathbf{B}_u &= \begin{bmatrix} 0 & 0 & 1 & 1 & 0 & 0 & 0 & 0 \end{bmatrix} \text{ for 2 axles and} \\ \mathbf{B}_u &= \begin{bmatrix} 0 & 1 & 0 & 0 \end{bmatrix} \text{ for 1 axle}\end{aligned}\quad (4.20b)$$

The force due to the truck is given by the expression in Equation (4.3) above. Substituting the expression for  $y_B(t)$  in Equation (4.18), and the expression for  $\bar{x}_u$  in Equation (4.19), the force can be written in vector form as

$$\bar{F}(t) = -\bar{W} + \mathbf{K}\mathbf{u}(\mathbf{B}_u \bar{x}_T - \mathbf{C}(x_1, x_2) \bar{x}_B)\quad (4.21)$$

Substituting Equation (4.21) into Equation (4.18) for the bridge dynamics gives

$$\dot{\bar{x}}_B = (\mathbf{A}_B - \mathbf{B}_B(t)\mathbf{K}\mathbf{u}\mathbf{C}(x_1, x_2))\bar{x}_B - \mathbf{B}_B(t)\bar{W} + \mathbf{B}_B(\tau)\mathbf{K}\mathbf{u}\mathbf{B}_u \bar{x}_T\quad (4.22)$$

Similarly, substituting the expression for  $y_B$  given in Equation (4.18) into Equation (4.19) gives the system of equations representing the dynamics of the truck.

$$\dot{\bar{x}}_T = \mathbf{A}_T \bar{x}_T + \mathbf{B}_T \mathbf{C}(x_1, x_2) \bar{x}_B\quad (4.23)$$

Writing Equations (4.22) and (4.23) in matrix form gives the final coupled differential equations of motion of the bridge/truck system.

$$\begin{bmatrix} \dot{\bar{x}}_B \\ \dot{\bar{x}}_T \end{bmatrix} = \begin{bmatrix} \mathbf{A}_B - \mathbf{B}_B(t)\mathbf{K}\mathbf{u}\mathbf{C}(\mathbf{x}_1, \mathbf{x}_2) & \mathbf{B}_B(t)\mathbf{K}\mathbf{u}\mathbf{B}_u \\ \mathbf{B}_T\mathbf{C}(\mathbf{x}_1, \mathbf{x}_2) & \mathbf{A}_T \end{bmatrix} \begin{bmatrix} \bar{x}_B \\ \bar{x}_T \end{bmatrix} + \begin{bmatrix} \mathbf{B}_B(t) \\ \mathbf{0}_{8 \times 2} \end{bmatrix} \overline{W} \quad (4.24a)$$

$$x_{T(front)} = 0 \quad t < 0 \quad \text{or} \quad t > \frac{L}{v} \quad (4.24b)$$

$$x_{T(rear)} = 0 \quad t < \frac{a}{v} \quad \text{or} \quad t > \frac{L+a}{v} \quad (4.24c)$$

It is important to note that the matrices and dimensions above referring to the truck are modified depending on which axles are on the bridge at a given time. The dimensions in Equation (4.24) refer specifically to the middle time frame when both axles are on the bridge. The system is modified during the other two time periods to reflect only the appropriate individual axle on the beam, but maintains the same form.

The “A” and “B” matrices of Equation (4.24a) are time-varying due to the truck’s moving across the bridge. As a result, one might conclude that the system described by Equations (4.24a-c) is a linear system with time-varying coefficients. This would be true for the case of a single axle moving across the bridge, although not so when two axles are considered. This is because the states of each axle are zero when that axle is off the bridge. We note that the states of the front axle jump from a nonzero state to a zero state upon leaving the bridge, and that the rear axle states jump from a zero state to a nonzero state when that axle enters the bridge. Consequently, since the truck states are making such jumps, the system described by Equations (4.24a-c) is a nonlinear system for the two-axle case treated in this dissertation.

# Chapter 5

## Optimization and Problem Statement

The optimization routine used to identify the truck parameters is a function in the MATLAB Optimization Toolbox called *fmincon*. It is a standard nonlinear, constrained optimization routine in which the user defines the form of the scalar objective function and constraints of the problem. A brief description of the algorithm used by the function is discussed in this chapter, although in-depth mathematical details are not given since they are not the focus of this work.

### 5.1 The Optimization Routine

A flowchart of the general method used by *fmincon* is given on the following page in Figure 5.1. The objective function  $f(\bar{x})$  used in this work is a quadratic of a least-squares form, and  $\bar{x}$  is a vector of optimization parameters. The algorithm *fmincon* uses a Sequential Quadratic Programming (SQP) method to minimize the quadratic objective function. The equality and inequality constraints  $G_i(\bar{x})$  are linear functions of the optimization parameters and include the lower and upper bounds of all parameters.

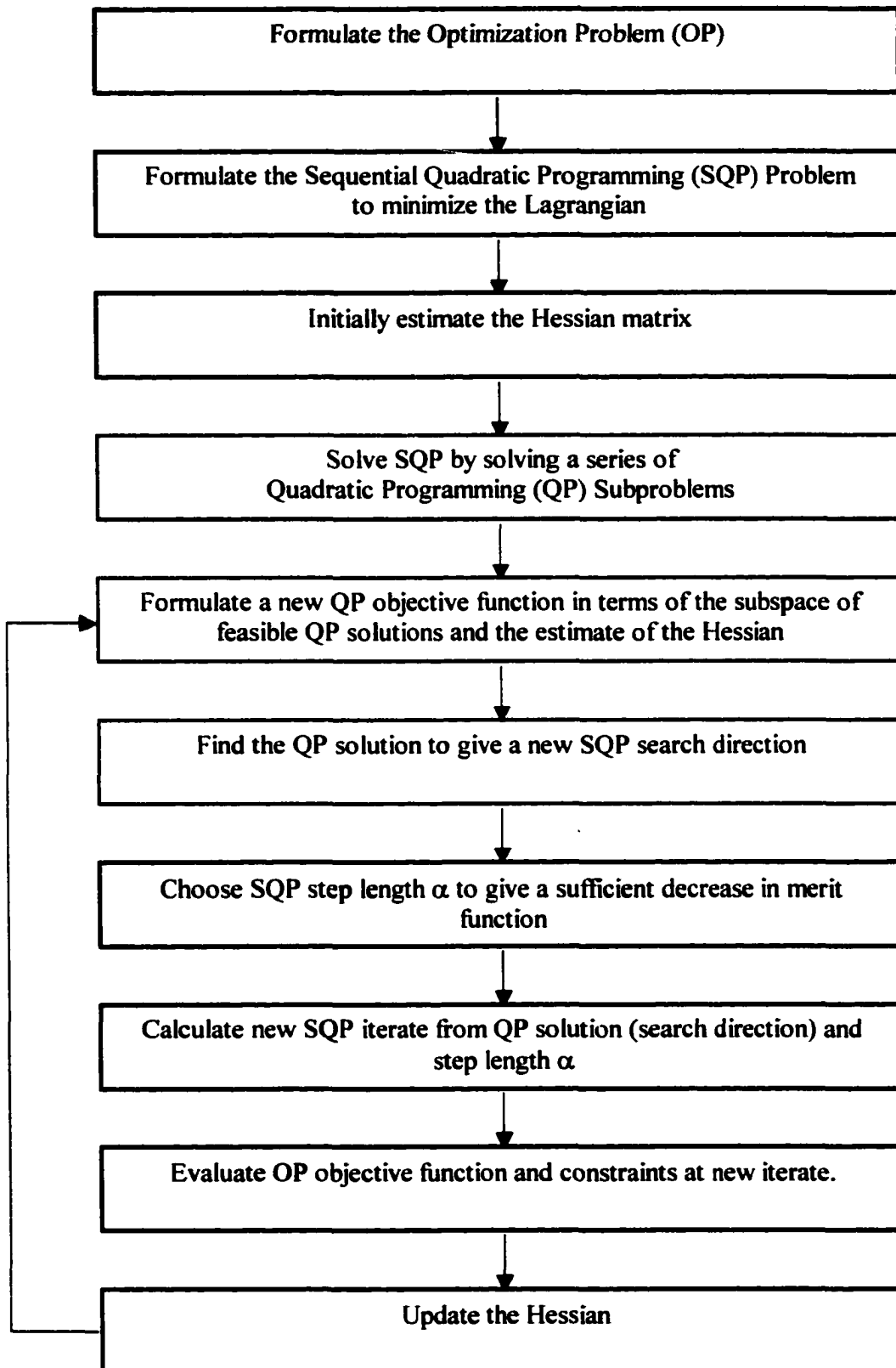


**Figure 5.1 General Outline of Optimization Routine**

The general procedure of SQP is to formulate a Quadratic Programming (QP) problem at each iteration of the optimization routine. This QP problem is then solved to determine the search direction and step size for the next iteration of the SQP problem. In the chart above in Figure 5.1, a brief description of the steps used to solve the general optimization problem (OP) is given. The chart is color-coded to represent the three different stages of the routine. The general optimization problem (OP) is given in black, the sequential quadratic programming (SQP) steps are shown in blue, and the quadratic programming (QP) problem steps are in red.

The formulation of the general optimization problem (OP) is given below where  $m_e$  is the number of equality constraints, and  $m$  is the total number of constraints.

$$\begin{aligned}
 \min_{x \in R^n} f(\bar{x}) \\
 G_i(\bar{x}) = 0 \quad i = 1..m_e \\
 G_i(\bar{x}) \leq 0 \quad i = m_e + 1..m \\
 x_l \leq x \leq x_u
 \end{aligned} \tag{5.1}$$

Many standard methods of solving constrained optimization problems revolve around the solution of the Kuhn-Tucker equations, which are necessary conditions for optimality for such a problem. The Kuhn-Tucker equations are stated below. The solution for the Lagrange multipliers  $\lambda_i$  which make Equation (5.2) true are the basis for the SQP method used by *fmincon*.

$$\begin{aligned}
 \nabla f(x^*) + \sum_{i=1}^m \lambda_i * G_i(x^*) = 0 \\
 \nabla G_i(x^*) = 0 \quad i = 1..m_e \\
 \lambda^* \geq 0 \quad i = m_e + 1..m
 \end{aligned} \tag{5.2}$$

The SQP problem solution is based on the Kuhn-Tucker equations. Its goal is to find a set of optimization parameters  $\bar{x}$  which minimize the Lagrangian given below.

$$L = f(x) + \sum_{i=1}^m \lambda_i g_i(x) \quad (5.3)$$

To do this, a QP subproblem is formulated at each iteration using second order information about the Lagrangian. The solution of the QP subproblem is used to form a new iterate in the SQP.

The objective function for the QP subproblem is given below.

$$\begin{aligned} \min_{d \in R^n} q(d) &= \frac{1}{2} d^T H_k d + \nabla f(x_k)^T d \\ \nabla g_i(x_k)^T d + g_i(x_k) &= 0 \quad i = 1 \dots m_e \\ \nabla g_i(x_k)^T d + g_i(x_k) &\leq 0 \quad i = m_e + 1 \dots m \end{aligned} \quad (5.4)$$

where  $H_k$  is the Hessian of the Lagrangian for the  $k^{\text{th}}$  iteration, and  $d$  is the new search direction for the SQP. In the first iteration, an estimate of the Hessian is made by the routine, although it is possible to use a user-given form. In subsequent iterations, the routine updates the Hessian based on the latest set of optimization parameters. This updating method will be briefly described later.

The solution method for the QP problem is an active-set method, since it is based upon an estimate of the active constraints at each solution point. The search direction is calculated to minimize the QP problem objective function and remain on the active constraint boundaries. A basis of a feasible subspace,  $Z_k$ , for the QP problem search direction  $\hat{d}_k$  is found which is orthogonal to the gradients of the active constraints. This means that a linear combination of the columns of  $Z_k$  would remain on the constraint

boundaries as required by the QP solution method. The QP search direction  $\hat{d}_k$  is a linear combination of the columns of  $Z_k$  given by  $\hat{d}_k = Z_k p$ .

The QP problem objective function is rewritten in terms of  $p$  as given below.

$$q(p) = \frac{1}{2} p^T Z_k^T H Z_k^T p + \nabla f(x_k)^T Z_k p \quad (5.5)$$

Since it is required that the Hessian  $H$  be positive definite, the minimum of the objective function  $q(p)$  occurs when  $\nabla q(p^*) = 0$ . Thus, the new search direction for the SQP problem is given by

$$d_k = Z_k p^* \quad (5.6)$$

The new SQP iterate is then given by  $x_{k+1} = x_k + \alpha d_k$ , where  $\alpha$  is the search step length. The step length is chosen to produce a sufficient decrease in a merit function defined below in Equation (5.7). The magnitude constituting a ‘sufficient decrease’ in the merit function is either defined by the user or predetermined by the routine based on the magnitude of the objective function. This merit function is a combination of the value of the objective function and penalty functions on all active constraints. The constraint penalties can also be prescribed by the user or determined by a predetermined method that will not be described here. Details can be found in the ‘Line Search and Merit Function’ documentation for MATLAB’s Optimization Toolbox.

$$\psi(\bar{x}_k) = f(\bar{x}_k) + \sum_{i=1}^{me} r_i g_i(\bar{x}_k) + \sum_{l=me+1}^m r_l \max\{0, g_l(\bar{x}_k)\} \quad (5.7)$$

Based on the new SQP iterate, an update of the Hessian to be used in the next iteration is then obtained using the BFGS (Broyden, Fletcher, Goldfarb, Shanno) method. This is a common steepest-descent method for updating the Hessian and will not be

described in detail here. Additional information on this method can be found in the 'Updating the Hessian' section of the Optimization Toolbox documentation or in works by its namesakes, Broyden, (Broyden, 1970), Fletcher, (Fletcher, 1970), Goldfarb, (Goldfarb, 1970), and Shanno (Shanno, 1970).

This process is repeated until a sufficiently small value of the general optimization problem (OP) objective function is found. This value is either prescribed by the user or defined automatically by the routine. It was found through extensive use of the *fmincon* function that appropriate scaling of the magnitude of the objective function could dramatically improve the performance of the routine due to the automatic scaling of step size and convergence values.

## **5.2 Problem Statement**

Using the bridge and truck models described in the previous two chapters and the optimization routine described in section 5.1, the method used to identify truck parameters discussed in the rest of this work is developed. The goal of this work is to develop a bridge weigh-in-motion (WIM) algorithm that is capable of estimating truck axle weights to within 1% of their true values from measured deflection profiles with 1 micron measurement errors. The measurement error is also increased from 1 micron to 100 microns to assess the algorithm's ability to estimate axle weights with imperfect measurements. To accurately identify axle weights, we found it necessary to determine other truck parameters such as natural frequency and damping ratios as well.

In both the static and dynamic truck models, axle spacing and speed are both needed to define the force applied by the truck. A relationship between these two

parameters is given based on the assumption that the entrance and exit times of each axle are known and used to determine the truck's total time on the bridge. As shown in Figure 4.2, the truck's total time on the bridge is given by

$$t_f = \frac{L + a}{v} \quad (5.8)$$

where  $a$  is axle spacing and  $v$  is the truck speed. It is assumed that this total time,  $t_f$ , was known, so an estimate of  $\hat{v}$  is found from each estimate of  $\hat{a}$  and is given by  $\hat{v} = \frac{L + \hat{a}}{t_f}$ .

This relationship is used throughout the rest of this work to determine an estimate of speed from an estimate of axle spacing.

The other truck parameters of interest changed depending on the complexity of the model used. When the dynamic truck model is used to simulate the bridge response, it became necessary to estimate the dynamic properties of each axle, including natural frequencies, damping ratios, and bridge interaction effects. It is found that the dynamic characteristics of the truck could be accurately estimated using this method and provided a more complete description of the effect of the truck on the bridge. While these properties of the truck are not the primary focus of this work, determining them was necessary to obtain accurate axle weight estimates.

Different combinations of the bridge and truck models described in the previous chapters are used to simulate the bridge/truck system. To begin to understand the bridge/truck system and formulate the optimization routine, the static bridge and static truck models are combined to generate the deflection profiles. This is the simplest system approximating the bridge/truck system and is used initially to examine this problem, as described in Chapter 6.

In Chapter 7, the dynamic bridge model, which included the inertial effects of the bridge, is used with the static truck model to represent the system. The addition of the bridge dynamics complicates the problem somewhat and allows the formulation of a reduced-order bridge model to be used in the optimization routine.

To better approximate the actual bridge/truck system, the dynamic truck model is used with the static and dynamic bridge models in Chapters 8 and 9 respectively. The use of the dynamic truck model required additional parameters to accurately describe the force imparted by the truck. In both Chapters 8 and 9, identification of the dynamic characteristics of each axle is required to accurately predict axle weights. Axle spacing is also still required to describe the truck, and the relationship between the speed and the axle spacing given in Equation (5.8) is used. In Chapter 8, the static bridge is excited by the dynamic truck. For this system, the truck's axle weights, axle spacing and dynamic properties are found, as well as the bridge/truck interaction effects. Two optimization parameters relating to the interaction effects are necessary to describe each axle. In Chapter 9, the dynamic bridge/dynamic truck system is examined. The axle weights, axle spacing, and dynamic characteristics of the truck are again found. In this chapter, however, the bridge/truck interaction effects are found directly from integrating the equations of motion and are not optimization parameters.

Chapters 6-9 describe the development of the weigh-in-motion algorithm in stages. The complexity of the models was increased in each stage to incorporate another aspect of the coupled bridge/truck system, until finally, the dynamic bridge/dynamic truck model was completed. Approaching the problem in this manner allowed each facet

**of the coupled system to be examined individually and the appropriate modifications in the optimization routine made to accurately predict the truck axle weights.**

# Chapter 6

## Static Bridge/Static Truck

First, we consider the simplest WIM problem—a static truck crossing a static bridge. The bridge is modeled as a static beam (neglecting inertial effects) as described in Chapter 2. Each axle of the truck is modeled as a moving point force with a constant speed and separated by a given axle spacing. The optimization routine described in Chapter 5 is used to minimize the difference between a measured deflection profile and one generated using the estimated truck parameters. Discontinuities in the derivative of the objective function with respect to the optimization parameter axle spacing require a modified sampling routine to be developed that uses random rather than the usual uniform sampling. This sampling method and the discontinuities are discussed.

### 6.1 Static Bridge/Static Truck Problem

The finite element model of a static beam described in Chapter 2 is used to initially simulate the truck crossing the bridge and obtain a profile of the midpoint deflection. Two moving point forces are used to represent the two axles of the truck. Because of the simplicity of the truck model, there are four unknown truck parameters to be identified: two axle weights,  $W_1$  and  $W_2$ , axle spacing  $a$ , and speed,  $v$ , although only three of these are used as optimization parameters. It is assumed that the truck's total time on the bridge is known, and the relationship between axle spacing and speed given in Equation (5.8) is used to determine speed. The total truck weight,  $W_t$ , is the sum of the

two axle weights. The deflection of the bridge due to the moving truck is calculated every 0.001 sec (1000 Hz sampling rate) in a series of static beam bending calculations based on the position of each axle at each point in time.

An optimization routine was used to minimize the difference between the measured deflection profile and the one generated using the estimated truck parameters. Two sampling methods for selecting the measured deflections were used to formulate the objective function in the optimization routine. A description of these sampling methods is in the following sections.

At each iteration of the optimization routine, a deflection profile due to the approximate truck parameters was generated using the series solution of the differential equation stated in Equation (2.10). This solution was the sum of the deflections due to each of the axle weights as given below. The deflection measurement was taken at the span midpoint  $x=L/2$ .

$$w\left(\frac{L}{2}, t\right) = \frac{2}{EIL\left(\frac{\pi}{L}\right)^4} \sum_{i=1}^{\infty} \left(\frac{1}{i}\right)^4 \sin \frac{i\pi}{2} \left( W_1 \sin \frac{i\pi \tilde{x}_1(t)}{L} + W_2 \sin \frac{i\pi(\tilde{x}_1(t) - a)}{L} \right) \quad (6.1)$$

In Equation (6.1), the position of the front axle  $\tilde{x}_1(t)$  is given by  $\tilde{x}_1(t) = vt$  where  $v$  is the speed of the truck. The position of the rear axle is given by  $\tilde{x}_1(t) - a$  since the two axles are separated by a constant axle spacing  $a$ . It was found that five terms in the series above were sufficient to accurately represent the deflection profile. There were three solutions available to solve the static beam problem—the finite element model, the series solution to the differential equation, and the expression for static beam bending given in Chapter 4. The series solution was used in the optimization routine rather than the finite element routine.

The objective function is then formulated using a least-squares difference between the measured and estimated deflections and is given below

$$J = \sum_{i=1}^N (\tilde{w}_i - w_i(\bar{p}))^2 \quad (6.2)$$

where  $\tilde{w}_i$  is the measured midpoint deflection at the  $i^{\text{th}}$  time step, and  $w_i(\bar{p})$  is the midpoint deflection generated using the estimated truck parameters,  $\bar{p}$ .

The optimization parameters contained in  $\bar{p}$  are the front and rear axle weights and the axle spacing. The relationship between axle spacing,  $a$ , and speed,  $v$ , determines the estimate of speed from each axle spacing estimate. A table of the upper and lower bounds of the remaining three optimization parameters is given below.

**Table 6.1 Upper and Lower Bounds for Optimization Parameters**

|               | Minimum Value | Maximum Value |
|---------------|---------------|---------------|
| a             | 2 m           | 15 m          |
| $W_1$ (front) | 0 N           | 500,000 N     |
| $W_2$ (rear)  | 0 N           | 500,000 N     |

An inequality constraint regarding the weight distribution between the axles is also used to constrain the optimization routine. This inequality constraint comes from typical truck configurations and is given below.

$$0.10W_2 \leq W_1 \leq 0.9W_2 \quad (6.3)$$

It is important to note that the optimization was also used without this constraint and results similar to those described in the following sections were obtained. This indicates that the optimization routine was not sensitive to this constraint, although this was not known during the initial formulation of this problem.

The two sampling methods used to select the time steps to be used in the optimization routine are discussed in the following sections.

## 6.2 Uniform Sampling Method

The first method of selecting points to use in the objective function was a uniform sampling method. Every tenth time step (100 Hz sampling rate) was used to formulate the objective function. The midpoint deflection at each of the selected time steps was calculated using the analytic expression given in Equation (6.1). Unacceptably large errors in estimated truck parameters, up to 320% in axle weight, were obtained using this method. This poor performance can be explained by the discontinuities in the derivatives of the deflection profile. These discontinuities are discussed in the following section.

## 6.3 Discontinuities in the Derivatives

As the truck passes over the bridge, three different force configurations occur. This is illustrated in Figure 4.2, which is repeated here for clarity.

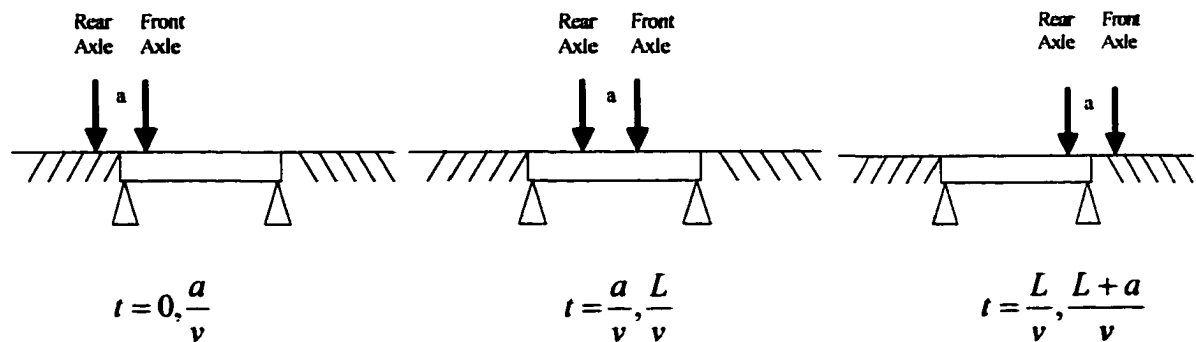


**Figure 6.1 Time Frames for the Truck Crossing the Bridge**

In the first time frame only the front axle is on the beam. In the second, both forces are acting on the beam, and, in the third time frame, only the rear axle is on the beam. A sample deflection profile is given below in Figure 6.2. The time at which the rear axle enters the bridge,  $t = \frac{a}{v}$ , is labeled  $T1$  in the figure. The time at which the front axle exits the bridge,  $t = \frac{L}{v}$ , is labeled  $T2$ . At both of these times, the force on the bridge changes abruptly due to the addition or subtraction of one of the forces. This is the cause of the discontinuities in the derivatives with respect to time of the deflection profile shown in Figure 6.2. These discontinuities in the derivative result in problems for the optimization routine.

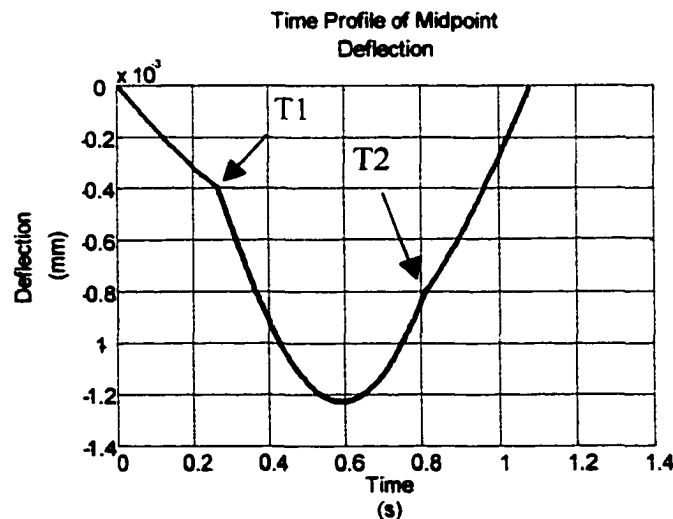


**Figure 6.2 Midpoint Deflection Profile for the Static Bridge/Static Truck**

The search method used by this and most optimization methods depends on the derivatives of the objective function with respect to the optimization parameters,  $\frac{\partial J}{\partial p_i}$ . It will be shown that the discontinuities in the derivatives of the deflection profile with

respect to the optimization parameters  $a$  and  $v$ ,  $\frac{\partial w(x,t)}{\partial a}$  and  $\frac{\partial w(x,t)}{\partial v}$ , lead to discontinuities in the objective function with respect to the optimization parameters  $a$  and  $v$  as well.

To understand these discontinuities better, it is necessary to recall the relationship between points in time and axle location along the beam. The front axle's position is given by  $\tilde{x}_f(t) = vt$  and the rear axle's position is related by  $\tilde{x}_r(t) = a$ . Using these relations, each point in time can then be related to a point in space for each axle.

The optimization routine selects values for the optimization parameters by making small changes in each parameter and calculating the value of the objective function and its derivatives using these parameters. Let us now consider the point in time of one of these discontinuities,  $T1$ . This is the time at which the rear axle, a distance  $a_0$  from the front axle, enters the beam. The actual axle spacing will be termed  $a_0$  for the remainder of this discussion for clarity. Assuming the speed parameter is fixed, Figure 6.3 shows the two different force conditions that could occur for small changes in the estimated axle spacing. The figure is not drawn to scale and is intentionally exaggerated for effect. The red arrow in Figure 6.3 indicates an increase in axle spacing of  $\Delta a$ . The blue arrow indicates a decrease of  $\Delta a$ . Clearly the force conditions resulting from these small changes are entirely different. For the increase in  $a$ , the rear axle is not on the beam and does not contribute to its deflection. For the decrease in  $a$ , the rear axle is on the beam and does contribute to the deflection. Recalling the relationship between time and space of the two axles, this would be equivalent to being to the left of  $T1$  (smaller time) in Figure 6.2 for the  $+\Delta a$  case, and to the right of it in the  $-\Delta a$  case. The derivatives of the

deflection profile are different in the two sections of the deflection curve (red and green in Figure 6.2) since the forcing conditions are different.

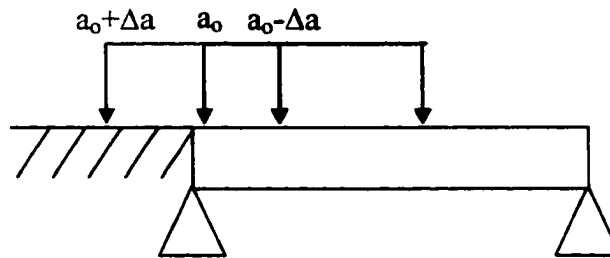


**Figure 6.3 Changes in Force Position for Variations in Axle Spacing For a Fixed Speed at T1**

Since the objective function is formulated using the midpoint deflection, it is now necessary to examine how these different forcing conditions result in a discontinuity in  $w\left(\frac{L}{2}, t\right)$  at these points.

In the case of  $a = a_0 + \Delta a$ , the rear axle is not on the beam and the midpoint deflection is due only to the force applied by the front axle. Reverting to the static beam bending expressions given in Chapter 4, this deflection is given by

$$w\left(\frac{L}{2}, t\right) = -W_1 H_2\left(\frac{L}{2}, a_1\right) \quad (6.4)$$

where  $H_2(x, a_1)$  is given below.  $a_1 = vt$  and  $b_1 = L - b_1$ . This derivation assumes that the axle spacing  $a_0$  is less than half the span length, although a similar derivation could be developed if  $a_0 > L/2$ .

$$H_2(x, a_1) = \frac{(a_1 - L)(a_1^2 - 2a_1L + (L - x)^2)(L - x)}{6EIL} \quad (6.5)$$

Substituting the measurement location,  $x = L/2$  into Equation (6.5), leads to

$$H_2\left(\frac{L}{2}, a_1\right) = \frac{(a_1 - L)\left(a_1^2 - 2a_1L + \left(\frac{L}{2}\right)^2\right)\left(\frac{L}{2}\right)}{6EIL} \quad (6.6)$$

The derivative of  $w\left(\frac{L}{2}, t\right)$  with respect to  $a$  is given by

$$\frac{\partial w\left(\frac{L}{2}, t\right)}{\partial a} = -W_1 \frac{\partial H_2\left(\frac{L}{2}, a_1\right)}{\partial a} \quad (6.7)$$

Since  $a_1$  does not depend on axle spacing  $a$ ,  $\frac{\partial H_2\left(\frac{L}{2}, a_1\right)}{\partial a} = 0$ , so  $\frac{\partial w\left(\frac{L}{2}, t\right)}{\partial a} = 0$ .

In the case of  $a = a_o - \Delta a$ , the deflection at the midpoint is due to the forces applied by both the axles.

$$w\left(\frac{L}{2}, t\right) = -W_1 H_2\left(\frac{L}{2}, a_1\right) - W_2 H_2\left(\frac{L}{2}, a_2\right) \quad (6.8)$$

where  $a_1$  is defined above and  $a_2 = a_1 - a$ . The derivative of the deflection with respect to  $a$  is then given by

$$\frac{\partial w\left(\frac{L}{2}, t\right)}{\partial a} = -W_1 \frac{\partial H_2\left(\frac{L}{2}, a_1\right)}{\partial a} - W_2 \frac{\partial H_2\left(\frac{L}{2}, a_2\right)}{\partial a} \quad (6.9)$$

As before,  $\frac{\partial H_2\left(\frac{L}{2}, a_1\right)}{\partial a} = 0$ , but  $\frac{\partial H_2\left(\frac{L}{2}, a_2\right)}{\partial a} \neq 0$ , since  $a_2$  depends on axle spacing  $a$ .

The derivative of  $H_2\left(\frac{L}{2}, a_2\right)$  with respect to axle spacing  $a$  is then given by

$$\frac{\partial H_2\left(\frac{L}{2}, a_2\right)}{\partial a} = \frac{1}{12EI} \left( 3a_2^2 \frac{\partial a_2}{\partial a} - 6a_2L \frac{\partial a_2}{\partial a} + \frac{9L^2}{4} \frac{\partial a_2}{\partial a} \right) \quad (6.10)$$

Recalling that  $a_2=vt-a$ ,  $\frac{\partial a_2}{\partial a} = -1$ . Substituting this expression into Equation (6.10) leads

to

$$\frac{\partial H_2\left(\frac{L}{2}, a_2\right)}{\partial a} = \frac{1}{12EI} \left( -3a_2 + 6a_2L + \frac{9L^2}{4} \right) \quad (6.11)$$

The derivative of the deflection with respect to axle spacing for  $a=a_o-\Delta a$ , is therefore given by

$$\frac{\partial w\left(\frac{L}{2}, t\right)}{\partial a} = 0 - W_2 \frac{\partial H_2\left(\frac{L}{2}, a_2\right)}{\partial a} - \frac{W_2}{12EI} \left( -3(vt-a) + 6(vt-a)L + \frac{9L^2}{4} \right) \quad (6.12)$$

Clearly, the derivatives of deflection with respect to axle spacing for the two force conditions generated by the small changes in axle spacing are not equal. For the first case

described,  $a=a_o+\Delta a$ ,  $\frac{\partial w\left(\frac{L}{2}, t\right)}{\partial a} = 0$ , but for the second where  $a=a_o-\Delta a$ ,  $\frac{\partial w\left(\frac{L}{2}, t\right)}{\partial a} \neq 0$ ,

but is given by Equation (6.12).

The fact that there is this discontinuity in the derivatives of the deflection with respect to axle spacing for small changes in  $a$  prevents the optimization routine from converging to the proper solution.

A similar condition occurs for points in time near  $T2$  with the same problem. A schematic of this scenario is given in Figure 6.4.

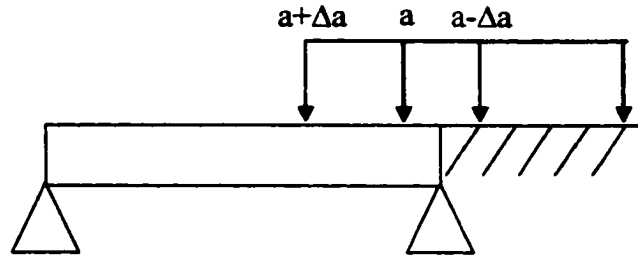


**Figure 6.4 Changes in Force Position for Variations in Axle Spacing For a Fixed Speed at T2**

At times near either  $T1$  or  $T2$ , the slope of the deflection profile changes with a change in axle spacing. Physically, this is equivalent to changing the forcing conditions on the bridge at a given time. Since there are discontinuities in the derivatives of the deflection profile with respect to axle spacing,  $\frac{\partial w(x,t)}{\partial a}$ , there are also discontinuities in the objective function with respect to  $a$ ,  $\frac{\partial J}{\partial a}$ . Mathematically, this can be expressed as

$$\begin{aligned}
 J &= \sum_{i=1}^n (\tilde{w}_i - w_i(\bar{p}))^2 \\
 \frac{\partial J}{\partial a} &= \sum_{i=1}^n -2(\tilde{w}_i - w_i(\bar{p})) \frac{\partial w_i(\bar{p})}{\partial a}
 \end{aligned}
 \tag{6.13}$$

The optimization routine requires that the derivatives of the objective function with respect to the optimization parameters,  $\frac{\partial J}{\partial p_i}$ , be continuous, so these points in time prevent the routine from converging.

A situation similar to the one described above occurs if speed were to be treated as an optimization parameter as well. Although  $v$  is not used explicitly as an optimization parameter in this section, we show below that the derivatives of the objective function

with respect to  $v$  would be discontinuous. In this case, discontinuities in the derivatives of the objective function with respect to  $v$  would result in convergence problems similar to those described above for axle spacing. These discontinuities are described below.

For a fixed axle spacing, a small change in the speed parameter results in the situations shown in Figure 6.5 and Figure 6.6. An argument akin to the one given for axle spacing can be made for the discontinuities due to the derivatives with respect to speed. For clarity, the true value of speed has been subscripted  $v_o$ .

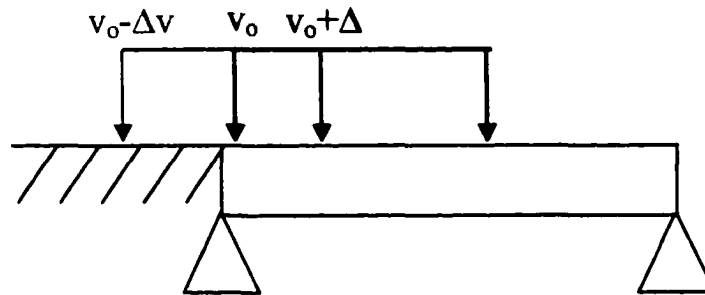


**Figure 6.5 Changes in Force Position for Variations in Speed For a Fixed Axle Spacing at T1**

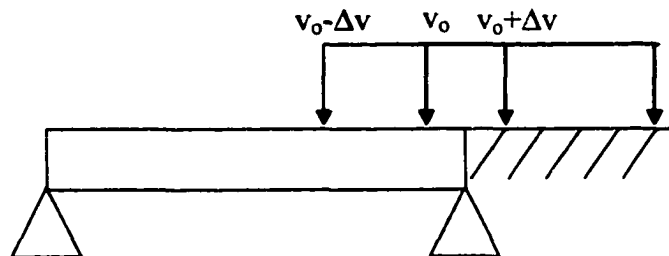


**Figure 6.6 Changes in Force Position for Variations in Speed For a Fixed Axle Spacing at T2**

As shown in Figure 6.5, a small change in  $v$ ,  $v=v_o-\Delta v$ , can place the rear axle off the beam (red). The midpoint deflection for this case can then be given by

$$w\left(\frac{L}{2}, t\right) = -W_1 H_2 \left(\frac{L}{2}, a_1\right) \quad (6.14)$$

where  $a_1 = vt$ . The derivative of the deflection with respect to speed is given by

$$\frac{\partial w\left(\frac{L}{2}, t\right)}{\partial v} = -W_1 \frac{\partial H_2\left(\frac{L}{2}, a_1\right)}{\partial v} \quad (6.15)$$

or

$$\frac{\partial H_2\left(\frac{L}{2}, a_1\right)}{\partial v} = \frac{1}{12EI} \left( 3a_1^2 \frac{\partial a_1}{\partial v} - 6a_1 L \frac{\partial a_1}{\partial v} + \frac{9L^2}{4} \frac{\partial a_1}{\partial v} \right) \quad (6.16)$$

In this case, however, the derivative of  $H_2$  with respect to  $v$  is not equal to zero since  $a_1$  depends on  $v$ . It is given by

$$\frac{\partial H_2\left(\frac{L}{2}, a_1\right)}{\partial v} = \frac{1}{12EI} \left( 3a_1^2 \frac{\partial a_1}{\partial v} - 6a_1 L \frac{\partial a_1}{\partial v} + \frac{9L^2}{4} \frac{\partial a_1}{\partial v} \right) \quad (6.17)$$

where  $a_1 = vt$  so  $\frac{\partial a_1}{\partial v} = t$ . Substituting this expression into Equation (6.17) and then substituting the result into Equation (6.15) leads to an expression for the derivative of the deflection for the case of,  $v = v_o - \Delta v$ .

$$\frac{\partial w\left(\frac{L}{2}, t\right)}{\partial v} = \frac{-W_1}{12EI} \left( 3a_1^2 t - 6a_1 L t + \frac{9L^2}{4} t \right) \quad (6.18)$$

For the case shown in Figure 6.6 where  $v = v_o - \Delta v$  (blue), both axles are on the beam, so both forces contribute to the deflection.

$$w\left(\frac{L}{2}, t\right) = -W_1 H_2\left(\frac{L}{2}, a_1\right) - W_2 H_2\left(\frac{L}{2}, a_2\right) \quad (6.19)$$

The derivative of the deflection for this case would be given by

$$\frac{\partial w\left(\frac{L}{2}, t\right)}{\partial v} = -W_1 \frac{\partial H_2\left(\frac{L}{2}, a_1\right)}{\partial v} - W_2 \frac{\partial H_2\left(\frac{L}{2}, a_2\right)}{\partial v} \quad (6.20)$$

An expression for  $\frac{\partial H_2\left(\frac{L}{2}, a_1\right)}{\partial v}$  is given in Equation (6.17) and would still apply here. A

similar expression for  $\frac{\partial H_2\left(\frac{L}{2}, a_2\right)}{\partial v}$  can be expressed as

$$\frac{\partial H_2\left(\frac{L}{2}, a_2\right)}{\partial v} = \frac{1}{12EI} \left( 3a_2^2 \frac{\partial a_2}{\partial v} - 6a_2 L \frac{\partial a_2}{\partial v} + \frac{9L^2}{4} \frac{\partial a_2}{\partial v} \right) \quad (6.21)$$

The parameter  $a_2 = a_1 - a$ , so  $\frac{\partial a_2}{\partial v} = \frac{\partial a_1}{\partial v} = t$ , so

$$\frac{\partial H_2\left(\frac{L}{2}, a_2\right)}{\partial v} = \frac{1}{12EI} \left( 3a_2^2 t - 6a_2 L t + \frac{9L^2}{4} t \right) \quad (6.22)$$

The total derivative  $\frac{\partial w\left(\frac{L}{2}, t\right)}{\partial v}$  is therefore given by Equation (6.20) where

$\frac{\partial H_2\left(\frac{L}{2}, a_1\right)}{\partial v}$  and  $\frac{\partial H_2\left(\frac{L}{2}, a_2\right)}{\partial v}$  are given Equations (6.17) and (6.22). The two

expressions for  $\frac{\partial w\left(\frac{L}{2}, t\right)}{\partial v}$  for both small changes in speed,  $v = v_o + \Delta v$  and  $v = v_o - \Delta v$  are not

equal. If speed is treated as an optimization parameter, this discontinuity in the derivative results in a discontinuity in the objective function given in Equation (6.13), similar to the axle spacing case.

Because the objective function contains discontinuities in the derivatives with respect to both  $a$  and  $v$ , the optimization routine may have convergence problems when points in time near these discontinuities are used in the objective function. Using the uniform sampling routine, measurements could be taken at or near these points in time and used to formulate the objective function. In this case, the discontinuities appear in the objective function derivatives and prevent the optimization routine from converging properly. To avoid this, an alternate sampling method was developed.

#### **6.4 Random Sampling Method**

To reduce the effect of the discontinuities in the objective function, a modified sampling method is adopted based on the idea of using randomly chosen inputs to identify unknown processes (Stalford, 1973). One half the number of time points as used in the original uniform sampling method (one-twentieth of the total sampled points, equivalent to a 50 Hz sampling rate) are chosen randomly to formulate the objective function. Each axle's location and the midpoint deflection are calculated at these time points using the analytic expression given in Equation (6.1). These randomly chosen points are used to formulate the objective function and compared to the corresponding time points of the measured deflection profile. The optimization procedure is repeated independently using six sets of randomly chosen time points. The truck parameters corresponding to the smallest final value of the objective function are selected as the best approximation.

The estimates of the truck parameters improved dramatically using the random sampling method for a variety of truck configurations. With zero measurement noise, the error in all three parameters is essentially zero ( $10^{-3}\%$ ). Uniform random noise was then added to the data to examine its effect on the performance of the algorithm. The amplitude of the noise is described as a percentage of the typical peak magnitude of the deflection profile, which was on the order of  $10^{-3}$  m. Noise to signal ratios of 0, 0.1%, 1%, and 10% ( $\pm 0$  m,  $10^{-6}$  m,  $10^{-5}$  m,  $10^{-4}$  m) were used to test the algorithm. Examples of estimated truck axle weights are shown in Figure 6.7 and Figure 6.8. The use of a random sampling method improved the results of the optimization routine by reducing the probability that a point used in the objective function would be at or near the discontinuities in the derivatives of the function. The truck configurations shown in the figures are given in Table 3.1.

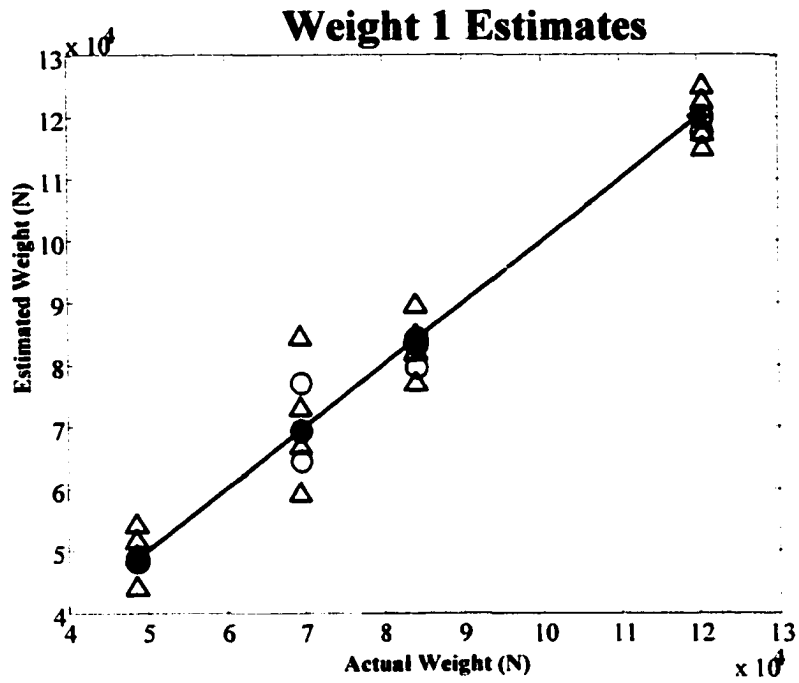


**Figure 6.7 Front Axle Weight Estimates With Noise (Random Sampling)**

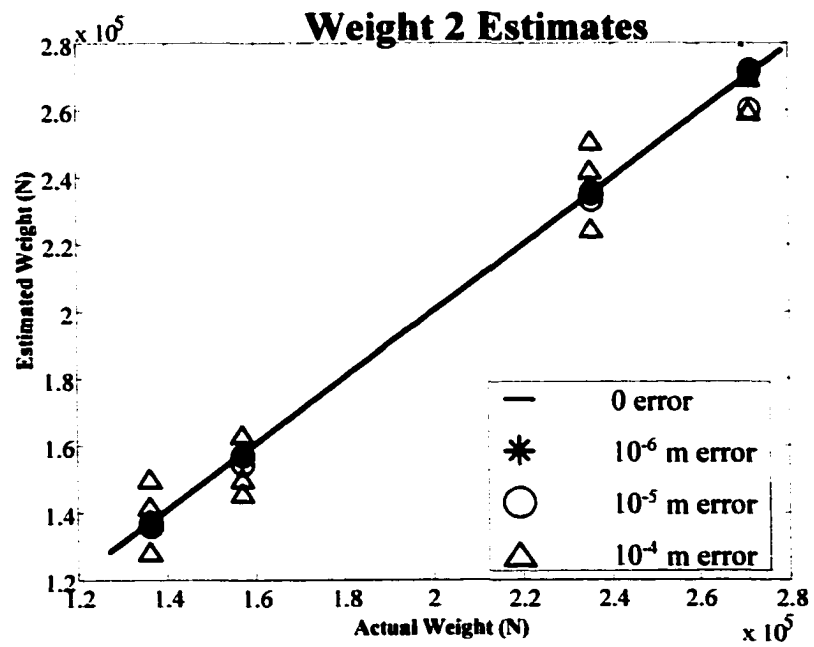


**Figure 6.8 Rear Axle Weight Estimates With Noise (Random Sampling Method)**

The average and maximum magnitudes of the error in each parameter are given in the following tables. It is important to note that the ‘average percent error’ is the average *magnitude* of the percent error in each parameter.

The average magnitude of the error in all truck parameters is less than 1% until the amplitude of the noise was  $\pm 10^{-4}$  m (10%). The table below gives the average error magnitude obtained for each parameter for the various noise levels using the random sampling method. The total weight is the sum of the two axle weights.

**Table 6.2 Average Error Magnitude in Truck Parameters Using the Random Sampling Method**

| Parameter         | 0           | $10^{-6}$ m | $10^{-5}$ m | $10^{-4}$ m |
|-------------------|-------------|-------------|-------------|-------------|
| Front Axle Weight | $10^{-3}\%$ | 0.036%      | 0.2%        | 2.7%        |
| Rear Axle Weight  | $10^{-3}\%$ | 0.040%      | 0.25%       | 3.1%        |

The maximum error magnitude in each truck parameter is given below in Table 6.3.

**Table 6.3 Maximum Error Magnitude in Truck Parameters Using the Random Sampling Method**

| Parameter         | 0                      | $10^{-6}$ m | $10^{-5}$ m | $10^{-4}$ m |
|-------------------|------------------------|-------------|-------------|-------------|
| Front Axle Weight | $4.5 \times 10^{-3}\%$ | 0.057%      | 0.33%       | 4.1%        |
| Rear Axle Weight  | $4.9 \times 10^{-3}\%$ | 0.062%      | 0.35%       | 4.9%        |

Figure 6.9 and Figure 6.10 below show the percent error in front axle weight estimates for the different noise levels. There is negligible error ( $\sim 10^{-4}\%$ ) in the axle spacing estimates for all noise levels, so no figures are given for these results. The x-axis in the

figures is the truck case numbers given in Table 3.1. The x-axis in Figures 6.10-6.20 is the truck case numbers.

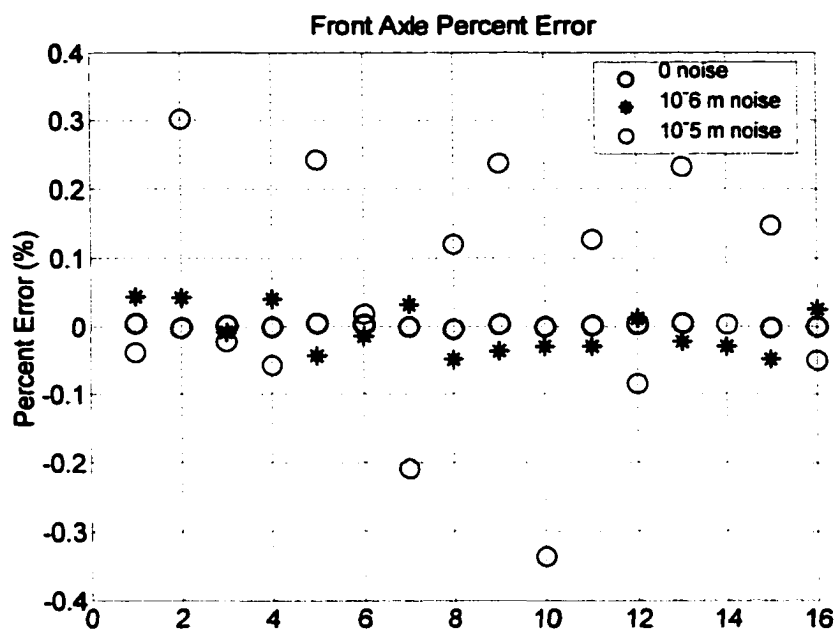


Figure 6.9 Percent Error in Front Axle Weight Estimates (Random Sampling Method)

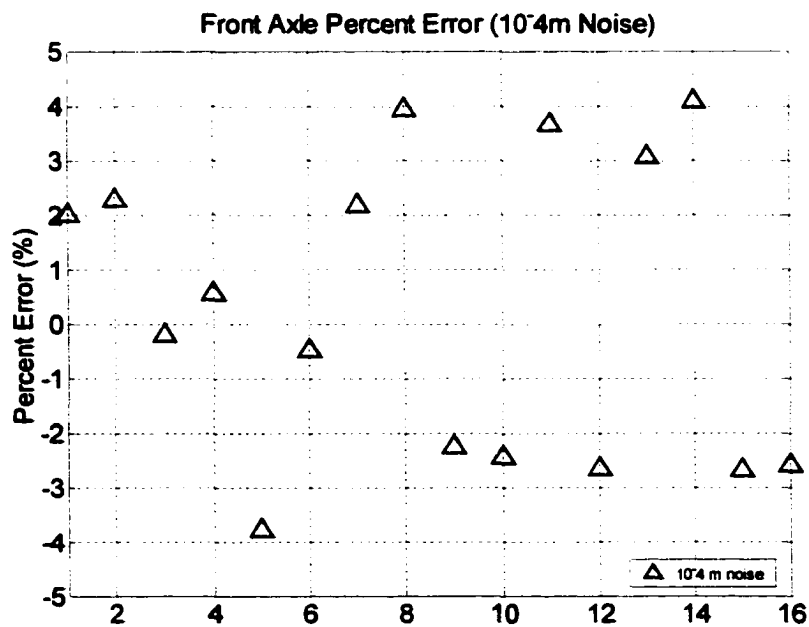


Figure 6.10 Front Axle Percent Error

Figure 6.11 and Figure 6.12 show the percent error in the rear axle weight estimates.

Again, the x-axis is the truck case number from Table 3.1.

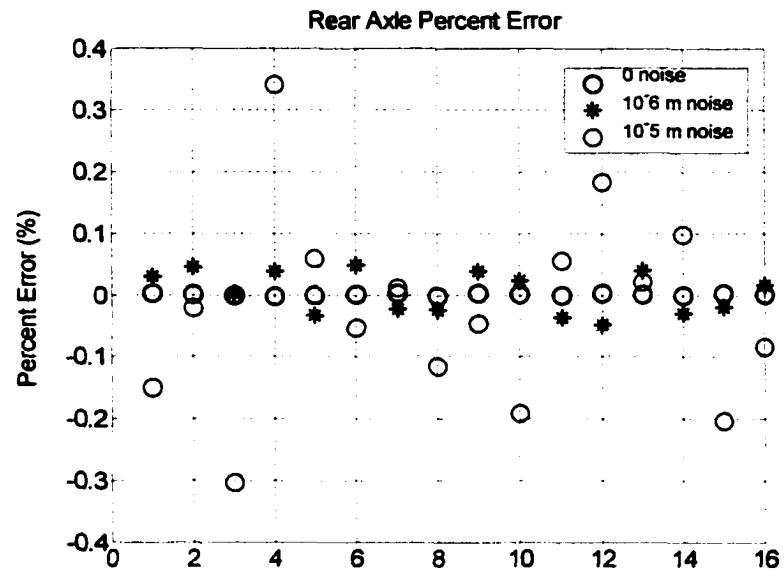


Figure 6.11 Percent Error in Rear Axle Weight

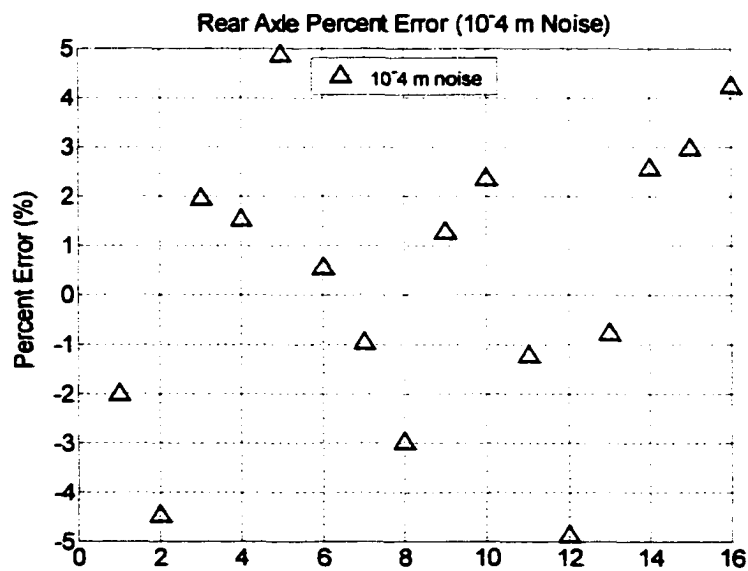


Figure 6.12 Percent Error in Rear Axle Weight Estimates ( $10^{-4}$  m Noise)

Another representation of the percent error data is shown below. The x-axes of Figures 6.13-6.20 represent the truck cases given in Table 3.1. The y-axes give the percent error in the weight estimates.

### Percent Error in Front Axle Weight

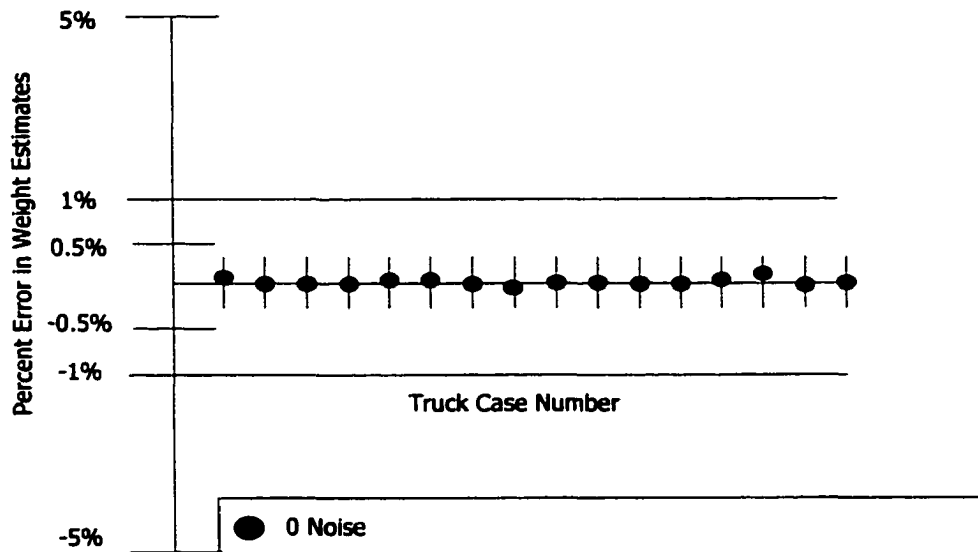


Figure 6.13 Percent Error in Front Axle Weight (a)

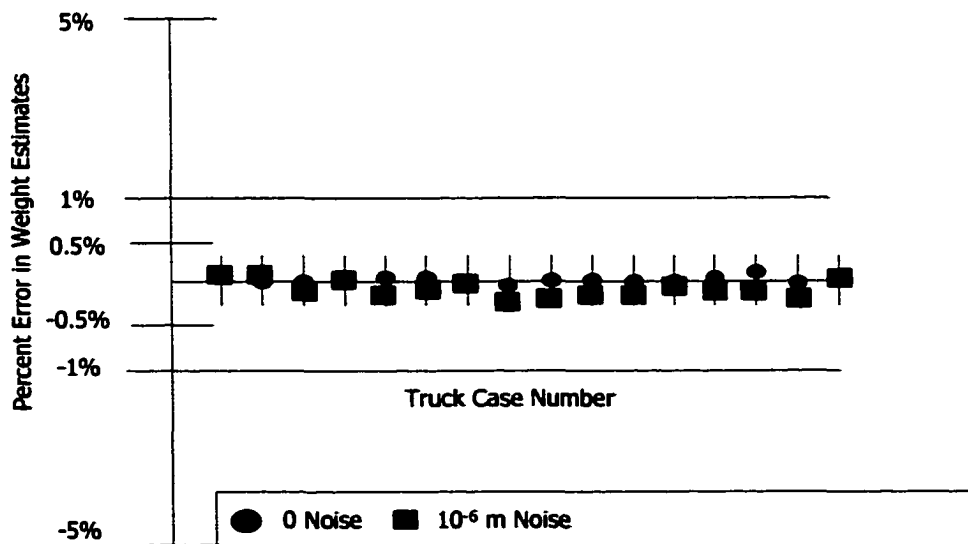


Figure 6.14 Percent Error in Front Axle Weight (b)

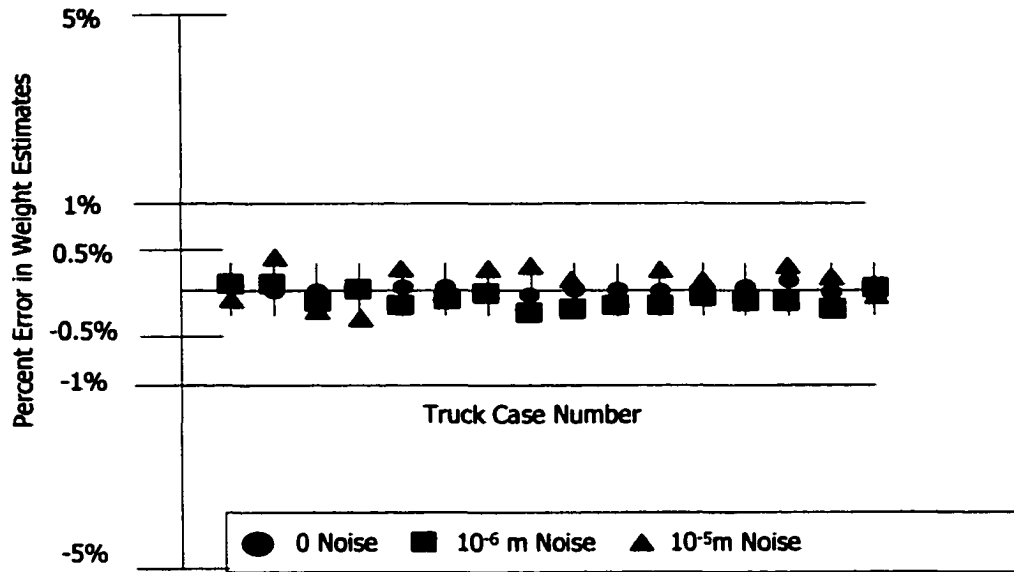


Figure 6.15 Percent Error in Front Axle Weights (c)

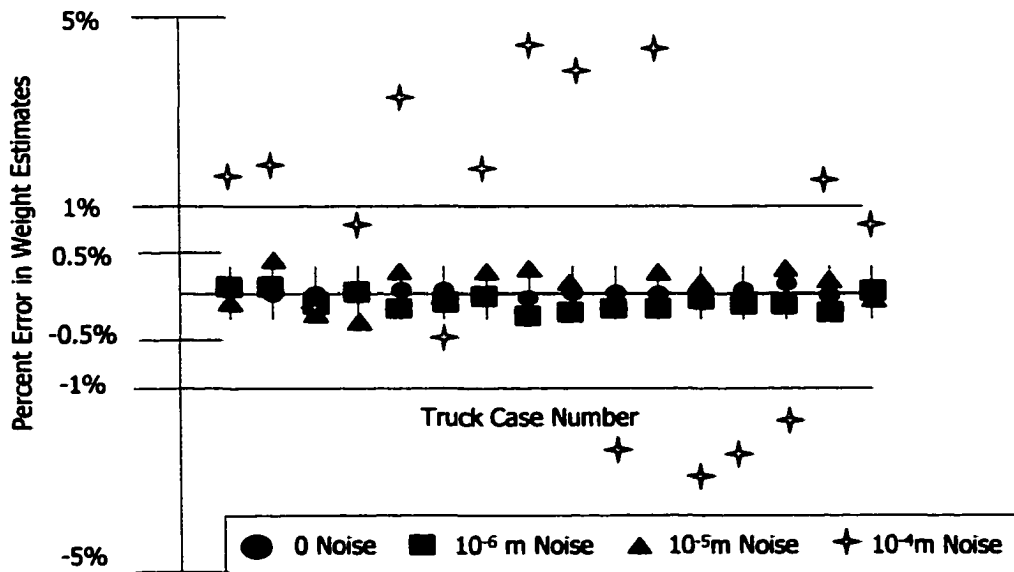


Figure 6.16 Percent Error in Front Axle Weight (d)

# Percent Error in Rear Axle Weight

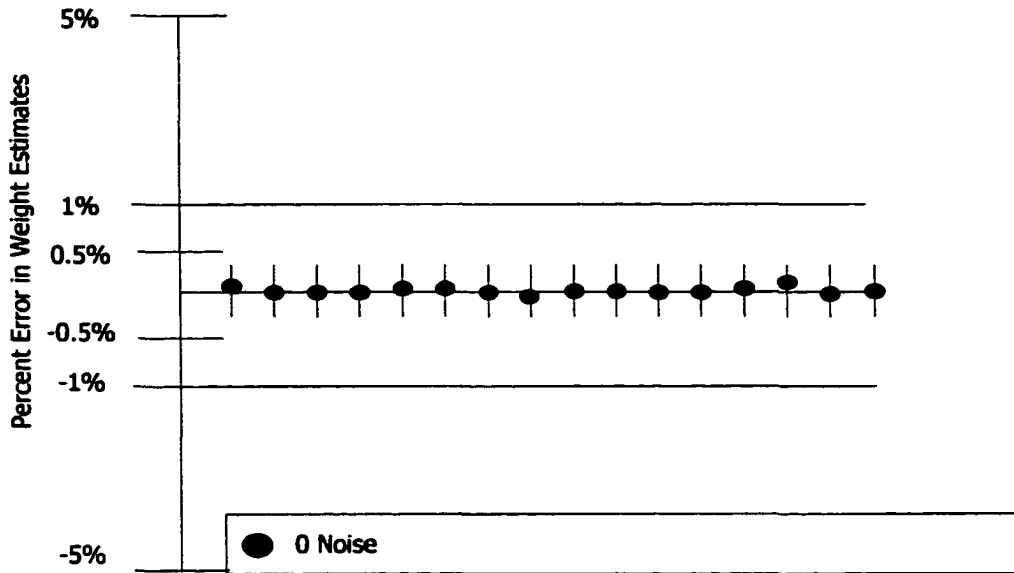


Figure 6.17 Percent Error in Rear Axle Weight (a)

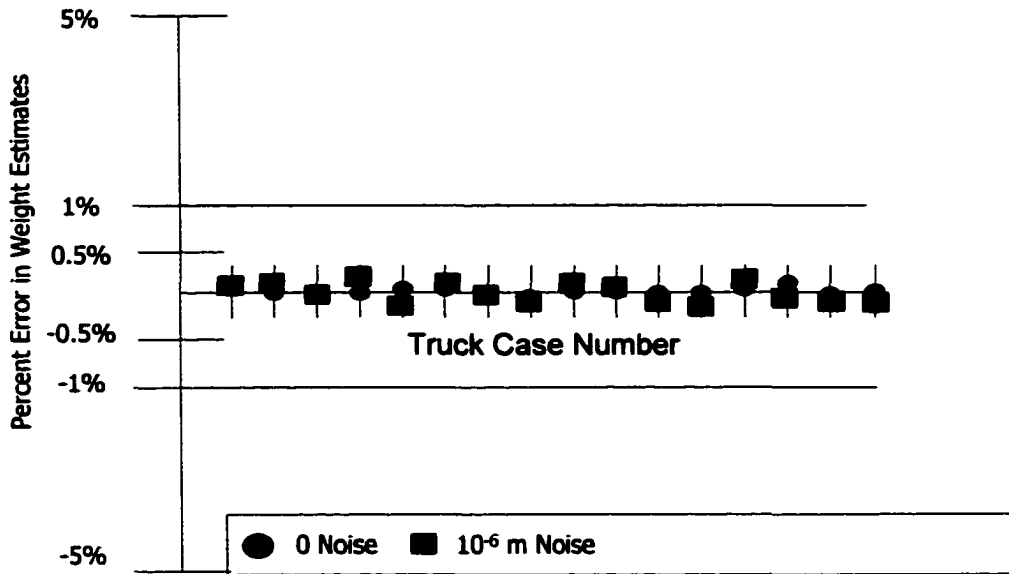


Figure 6.18 Percent Error in Rear Axle Weights (b)

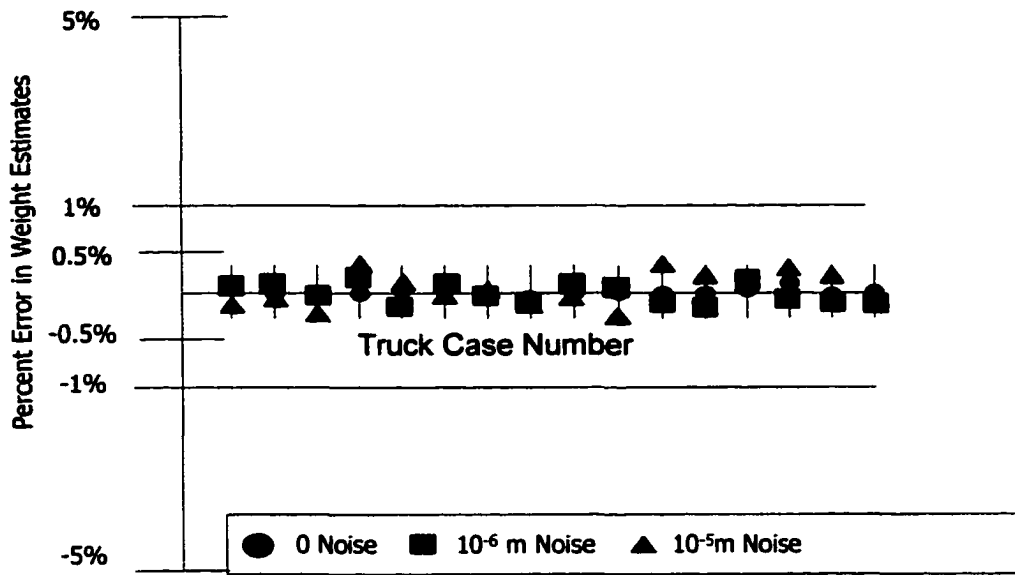


Figure 6.19 Percent Error in Rear Axle Weights (c)

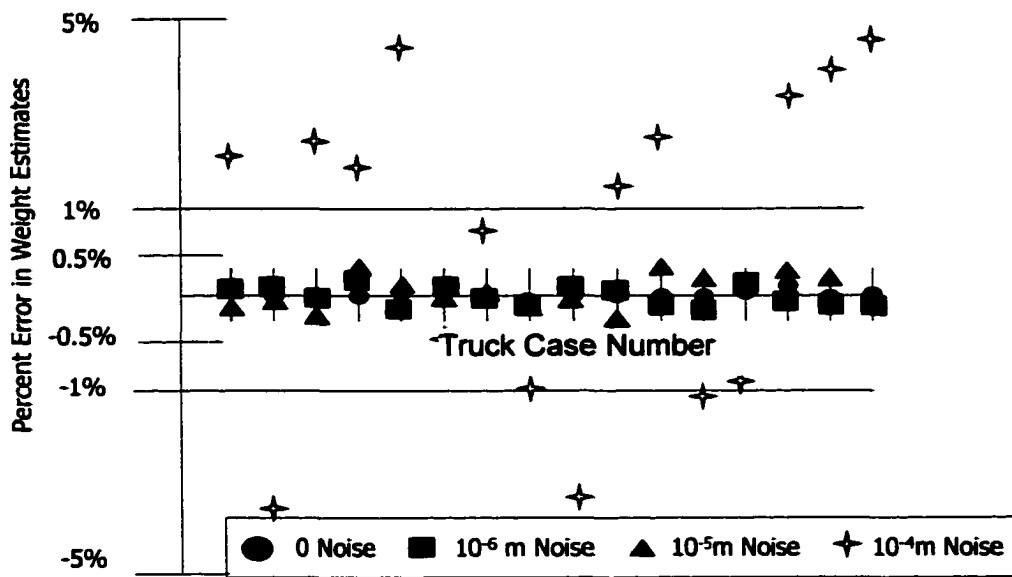


Figure 6.20 Percent Error in Rear Axle Weights (d)

We verified that the noise in the random set of data points that minimized the objective function has the same noise distribution as the noise over the whole data set. The mean amplitude of the noise in the sampled set was always within 7% of the mean of the total noise distribution and sometimes had a larger average value (worse) than that of the total set. The standard deviations of the noise in both the sampled sets and the entire profile are within 1% of each other.

The random sampling method proved very effective in eliminating the convergence problems observed with the uniform sampling method caused by the discontinuities in the derivatives. We found that using six random samples virtually ensured that one of them would not contain points at or near the discontinuities. It gave the optimization a suitable form of the objective function that avoided the discontinuous derivative problem.

## **6.5 Chapter Conclusions and Contributions**

In this chapter, the static bridge finite element model and the moving point force truck model were used to simulate the static bridge/static truck system. An optimization routine was used to minimize the difference between the “measured” deflection profile and the one generated using the approximate truck parameters in order to identify the truck’s axle weights and axle spacing. The relationship between the truck’s total time on the bridge,  $t_f$ , and the speed given in Equation (5.8) was used to obtain a speed estimate based on the axle spacing estimate. Because of the geometric properties of the truck and bridge models, discontinuities in the derivatives of the objective function with respect to the optimization parameter  $a$  existed which prevented the optimization routine from

converging. A random sampling method was employed to reduce the likelihood that a point used in the objective function would be at or near the discontinuities.

The static truck configurations given in Table 3.1 were used to assess the performance of the identification algorithm. Sixteen trucks with front axle weights ranging from  $4.96 \times 10^4 \text{N}$  to  $1.2 \times 10^5 \text{N}$  and rear axle weights from  $1.38 \times 10^5 \text{N}$  to  $2.72 \times 10^5 \text{N}$  were examined. The axle spacings varied from 5-7m and speeds varied from 25-35 m/s.

The average and maximum magnitudes of the percent error in front and rear axle weight estimates are given in Tables 6.2 and 6.3. For zero measurement noise, the average magnitude of the error in the axle weight estimates was  $10^{-3}\%$  with a maximum error of  $4.5 \times 10^{-3}\%$ . Measurement noise was then added to the deflection profiles. For measurement noise of  $\pm 1 \times 10^{-6}$  m, the maximum error in axle weight estimates was 0.062%. For noise of  $\pm 1 \times 10^{-5}$  m, the maximum error was 0.35%, and for measurement noise of  $\pm 1 \times 10^{-4}$  m, the maximum error was 4.9%. Error in the estimates of axle spacing was negligible ( $\sim 10^{-4}\%$ ) for all noise levels used.

# Chapter 7

## Dynamic Bridge/Static Truck

Next, we consider the case of a static truck crossing a dynamic bridge. A method similar to that described in Chapter 6 is used to estimate the truck parameters. An optimization routine is again used to minimize the difference between a measured deflection profile and the estimated one. The bridge model, however, includes the dynamic effects of the bridge. Two different scenarios are compared—one which uses one deflection measurement and assumes that speed and axle spacing are known and one which uses three sensors and assumes that only the truck's total time on the bridge is known. This leaves axle spacing and axle weights to be found by the optimization routine. The performance of the two methods with the addition of noise is also examined.

### 7.1 1<sup>st</sup> Scenario-Speed and Axle Spacing Known

The reduced order dynamic bridge model described in Chapter 2 is used to represent the beam response. This model includes the first four odd numbered modes, which represent 99.5% of the midpoint deflection. One deflection measurement is made at the span midpoint and is used to formulate the objective function.

In the first scenario, it is assumed that the speed and axle spacing are known from an independent sensor. This is a reasonable assumption since both quantities would be easy to measure in a variety of ways. One proposed method of obtaining both speed and

axle spacing is to place sensors at the entrance and exit of the bridge that would be activated by the passage of each axle. These sensors could be tape switches, piezoelectric sensors or any other similar surface-mounted sensor that would be installed in the wheel path of the vehicle. These sensors would record the times at which each axle crossed them, and would allow speed and axle spacing to be easily calculated. Since the length of the bridge is known, the difference in time between the entrance and exit of the front axle would yield the speed. The difference in time between the crossing of subsequent axles combined with the speed would give both the number of axles and their spacing. While the installation and use of such sensors is not the focus of this work, it is relevant to illustrate the ease with which speed and axle spacing could be obtained and can, therefore, be considered known for the remainder of section 7.1.

Because axle spacing and speed are known, only two optimization parameters remain—the two axle weights. The total weight is found from the sum of the axle weights. The midpoint deflection profile is first generated by integrating the full-order model of the bridge with two constantly moving point forces separated by a constant distance  $a$ . This profile is referred to as the “measured” profile throughout this work since it is used to represent the response of the actual bridge. The bridge parameters used are given in Chapter 2. The optimization routine is given upper and lower bounds for the weight estimates. These are given below in Table 7.1. The lower bound for axle weight is set to zero so the algorithm could eventually be expanded to include more axles. Nonexistent axles would, therefore, have an axle weight of zero. The optimization routine is given an initial value of 250,000N (the midpoint of the two bounds) for each axle.

**Table 7.1 Upper and Lower Bounds for Optimization Parameters**

|               | Minimum Value | Maximum Value |
|---------------|---------------|---------------|
| $W_1$ (front) | 0 N           | 500,000 N     |
| $W_2$ (rear)  | 0 N           | 500,000 N     |

An inequality constraint is also used to bound the weights of the axles relative to each other. This constraint is based on standard truck weight distributions and is given below.

$$0.10W_2 \leq W_1 \leq 0.9W_2 \quad (7.1)$$

At each iteration of the optimization routine, the reduced-order model of the bridge described in Chapter 2 is integrated with the estimates of axle weights and the known speed and axle spacing as the input. The reduced-order bridge response is then transformed back into the physical states of deflection and rotation at the nodes. The midpoint deflection as a function of time is then compared to the measured profile in the objective function. The objective function is of the same form as in Chapter 6 and is given below where  $N$  is the total number of measured points,  $\tilde{w}_i$  is the measured midpoint deflection at the  $i^{\text{th}}$  time step,  $w_i(\bar{p})$ , is the estimated midpoint deflection, and  $\bar{p}$  are the optimization parameters,  $W_1$  and  $W_2$ .

$$J = \sum_{i=1}^N (\tilde{w}_i - w_i(\bar{p}))^2 \quad (7.2)$$

With zero measurement noise, the optimization routine is able to estimate both axle weights to within 0.3% of their actual values for a variety of weight distributions. Uniform random noise is then added to the measured profile to examine the algorithm's ability to estimate weights from a noisy signal. Noise to signal ratios of 0.5%, 5%, 50%, and 250% are used (equivalent to errors of  $\pm 10^{-6}\text{m}$ ,  $10^{-5}\text{m}$ ,  $10^{-4}\text{m}$ , and  $0.5 \times 10^{-3}\text{m}$ ). The

maximum midpoint deflection is on the order of 0.3mm. Estimates of the axle weights for the different noise levels are shown below in Figure 7.1 and Figure 7.2. The truck configurations corresponding to the results in Figure 7.1 and Figure 7.2 are given in Table 3.1.

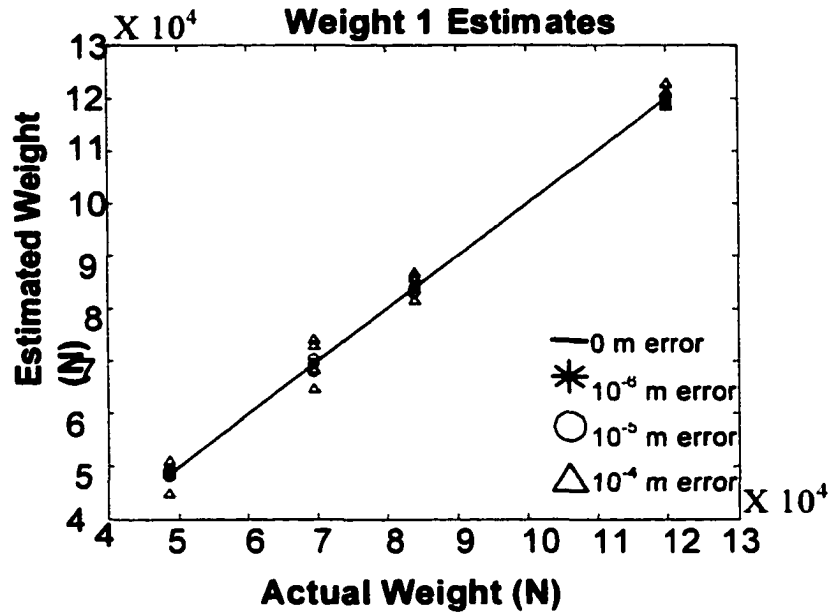


Figure 7.1 Weight 1 (Front) Estimates With Noise Using 1 Measurement

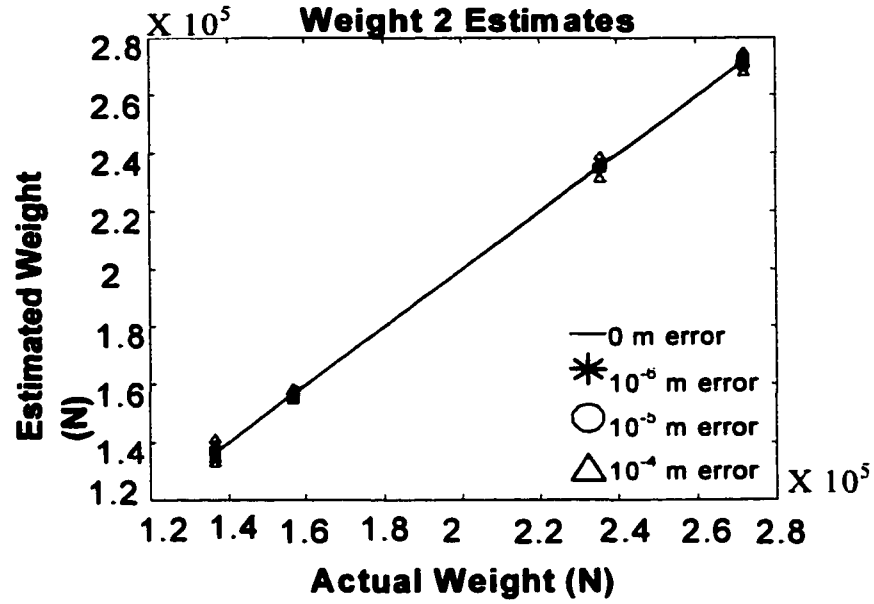


Figure 7.2 Weight 2 (Rear) Estimates With Noise Using 1 Measurement

Another representation of the same results is given below. The percent error in the axle weights and total weights are shown in Figure 7.3 and Figure 7.4 for various noise levels. With larger noise levels, the percent error increases.

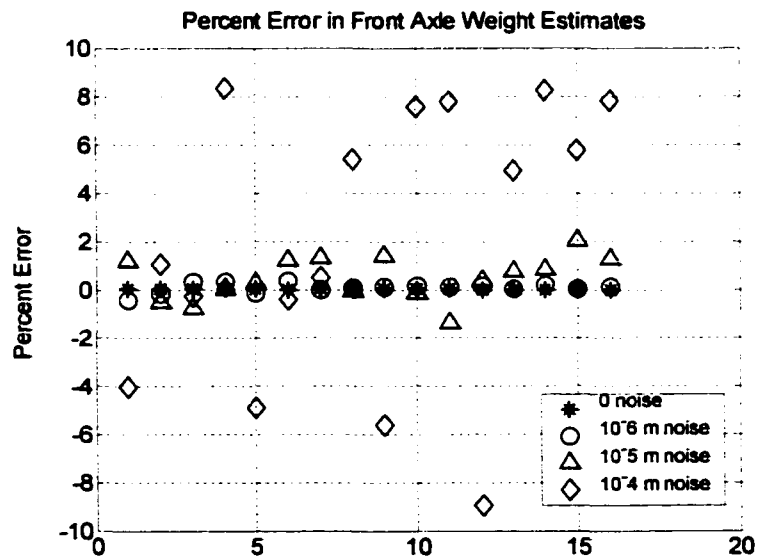
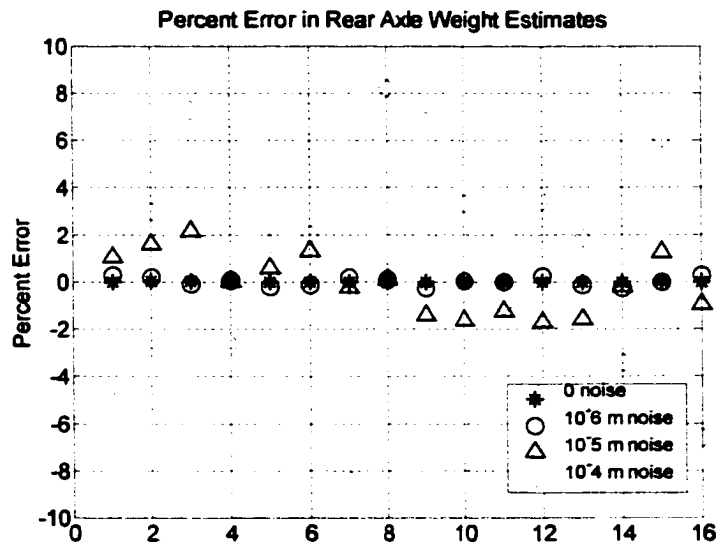


Figure 7.3 Percent Error in Front Axle Weight Estimates Using 1 Sensor



**Figure 7.4 Percent Error in Rear Axle Weight Estimate Using 1 Sensor**

The table below shows the average magnitude of the percent error in axle weight estimates for the noise levels given above. As in Chapter 6, the averages given below are the average magnitudes of the percent error rather than the average of the true error.

**Table 7.2 Average Errors in Axle Weight Estimates With Noise-Axle Spacing and Speed Known**

| Noise to Signal Ratio ( $\pm$ m) | Average Axle Weight Error |
|----------------------------------|---------------------------|
| 0 (0 m)                          | 0.03%                     |
| 0.5% ( $10^{-6}$ m)              | 0.3%                      |
| 5% ( $10^{-5}$ m)                | 1.7%                      |
| 50% ( $10^{-4}$ m)               | 6.1%                      |

### 7.2 2<sup>nd</sup> Scenario-Speed and Axle Spacing Unknown

It was found that by using more deflection measurements, the need for an independent measurement of speed and axle spacing is eliminated, although the assumption that the truck's total time on the bridge  $t_f$  is still made. Three sensor locations are chosen to provide the most information on the deflection based on the static beam

mode shapes. The four mode shapes used in the reduced-order model are shown below in Figure 7.5. It is important to note that the mode shapes depicted in Figure 7.5 are not to scale as to their relative contribution to the beam bending. The mode shapes of a static beam are used because the dominant behavior of the beam for this case is static beam bending. The contribution to the deflection from the inclusion of the dynamics is small in comparison.

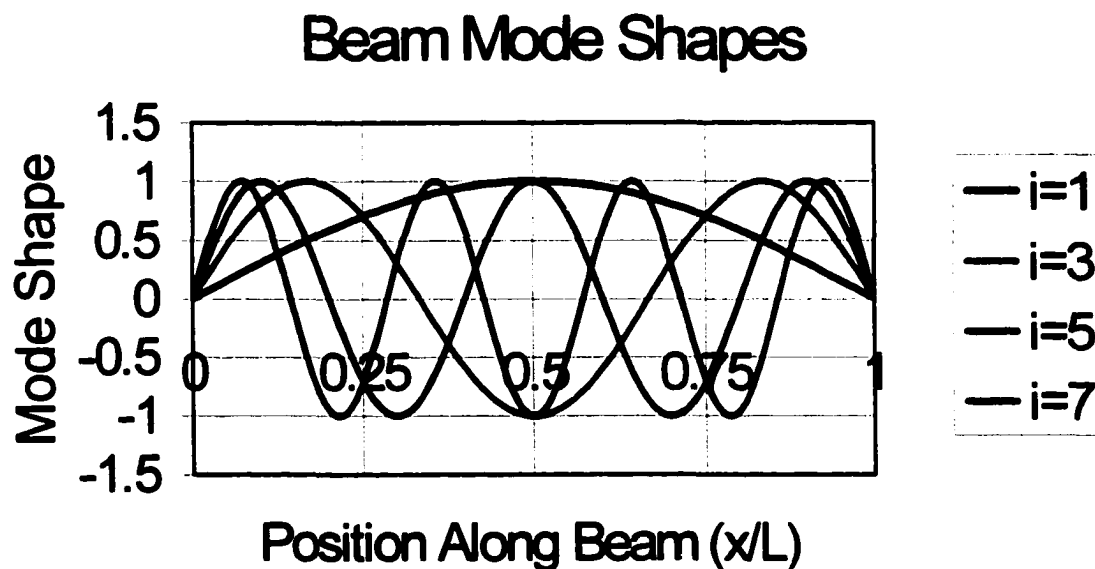


**Figure 7.5 Static Beam Mode Shapes**

The four modes used in the reduced order model were originally chosen because their maximum absolute values occur at the midpoint. There is no other point along the beam at which these four modes have a maximum, but they all have values greater than half of their maximums at the quarter ( $L/4$ ) and three-quarter ( $3L/4$ ) points. As discussed in Section 2.12, these two points are added as sensor locations, bringing the total number of measurement locations to three.

Because axle spacing is unknown in this case, it becomes an optimization parameter. The relationship between axle spacing and speed given in Equation (5.8) is still used to determine an estimate of the speed from an estimate of the axle spacing and the truck's total time on the bridge. The upper and lower bounds for the optimization parameters are given in Table 7.3. The weight inequality constraint given in Equation (7.1) is used in this case as well.

**Table 7.3 Upper and Lower Bounds for Optimization Parameters-  
Speed and Axle Spacing Unknown**

|                        | Minimum Value | Maximum Value |
|------------------------|---------------|---------------|
| a                      | 2 m           | 15 m          |
| W <sub>1</sub> (front) | 0 N           | 500,000 N     |
| W <sub>2</sub> (rear)  | 0 N           | 500,000 N     |

The form of the objective function is also modified slightly to include the three sensor measurements. It contains the same squared differences between measured and approximated profiles as before but for three sensor locations rather than one. The subscripts L/2, L/4, and 3L/4 denote the sensor locations. The weights for each of the sensor measurements were determined iteratively.

$$J = \sum_{i=1}^N 3 \left( \tilde{w}_{\frac{L}{2},i} - w_{\frac{L}{2},i}(\bar{p}) \right)^2 + \left( \tilde{w}_{\frac{L}{4},i} - w_{\frac{L}{4},i}(\bar{p}) \right)^2 + \left( \tilde{w}_{\frac{3L}{4},i} - w_{\frac{3L}{4},i}(\bar{p}) \right)^2 \quad (4)$$

The use of three sensors dramatically improves the truck parameter estimates. With zero measurement noise, estimates of axle weights and axle spacing are essentially zero. The estimates found with the addition of noise are much better than with one measurement as well. Errors of less than 0.1% in axle weight estimates result with noise

levels of  $\pm 10^{-5}$ m (noise to signal ratio of 5%), and errors remain less than 3.5% for noise levels of  $\pm 10^{-4}$ m (noise to signal ratio of 50%). A table outlining the average magnitudes of the error for the multiple measurement case is given below.

**Table 7.4 Average Magnitudes of the Percent Error in Axle Weight Estimates Using Multiple Sensors-Speed and Axle Spacing Unknown**

| Noise to Signal Ratio<br>( $\pm m$ ) | Average Axle Weight Error |
|--------------------------------------|---------------------------|
| 0 (0 m)                              | 0%                        |
| 0.5% ( $10^{-6}$ m)                  | 0.005%                    |
| 5% ( $10^{-5}$ m)                    | 0.04%                     |
| 50% ( $10^{-4}$ m)                   | 1.7%                      |

The maximum error in axle weight estimates is given for each measurement noise level in Table 7.5.

**Table 7.5 Maximum Magnitudes of the Percent Error in Axle Weight Estimates Using Multiple Sensors-Speed and Axle Spacing Unknown**

| Noise to Signal Ratio<br>( $\pm m$ ) | Maximum Axle Weight Error |
|--------------------------------------|---------------------------|
| 0 (0 m)                              | 0.003%                    |
| 0.5% ( $10^{-6}$ m)                  | 0.008%                    |
| 5% ( $10^{-5}$ m)                    | 0.08%                     |
| 50% ( $10^{-4}$ m)                   | 3.1%                      |

Figures displaying the estimates of all parameters using the three measurement locations are shown below. The truck configurations shown are given in Table 3.1.

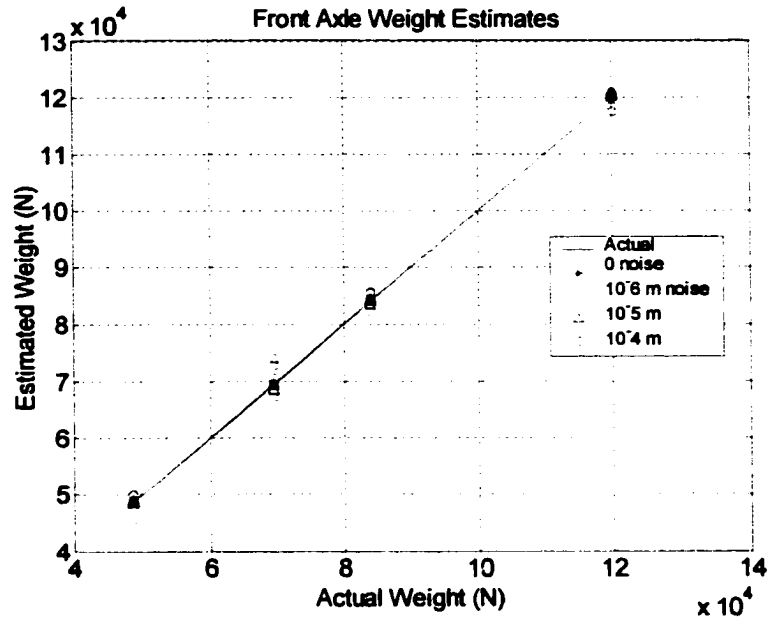


**Figure 7.6 Front Axle Weight Estimates With Noise Using 3 Sensors**

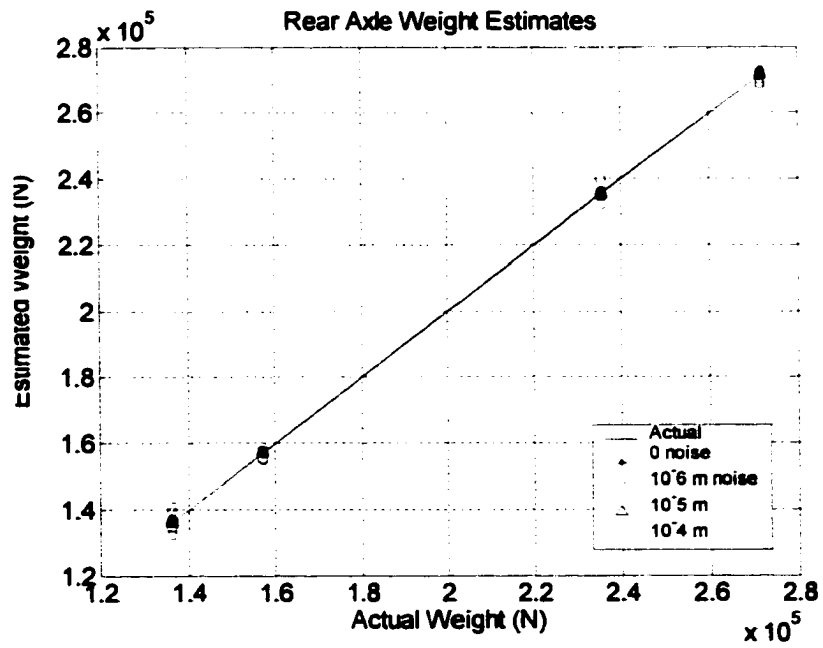


**Figure 7.7 Rear Axle Weight Estimates With Noise Using 3 Measurements**

The percent error in the axle weight and total weight estimates for the different noise levels are shown in Figure 7.8 and Figure 7.9.

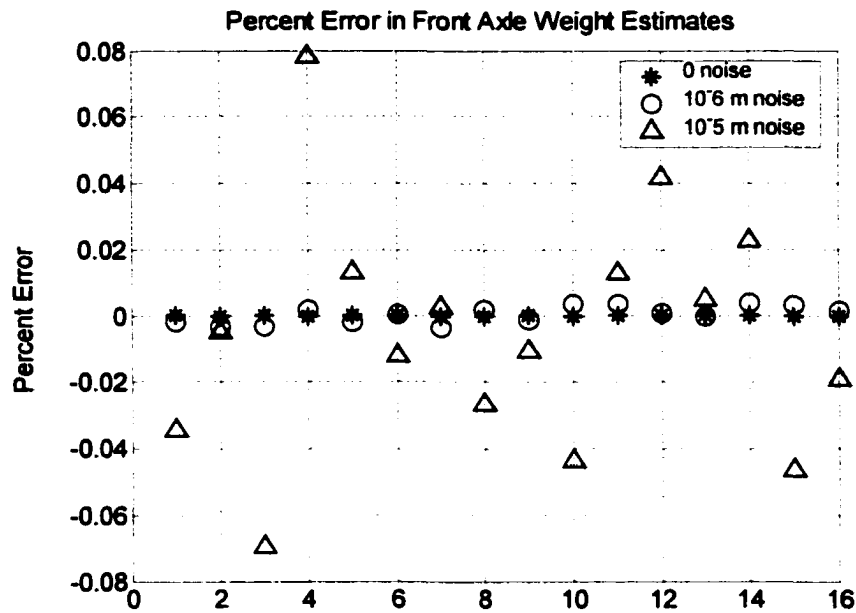


Figure 7.8 Percent Error in the Front Axle Weight Estimates Using 3 Measurements

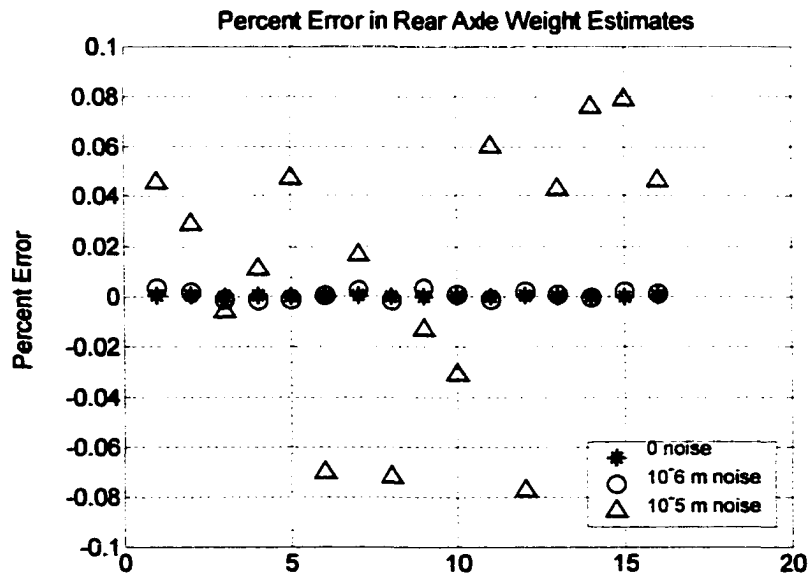


Figure 7.9 Percent Error in the Rear Axle Weight Estimates Using 3 Measurements

Another representation of the percent error in axle weight estimates is shown in the following figures. In Figures 7.10-7.17, the x-axis represents the individual truck cases in Table 3.1. The y-axis is the percent error in axle weight for each truck case.

### Percent Error in Front Axle Weight

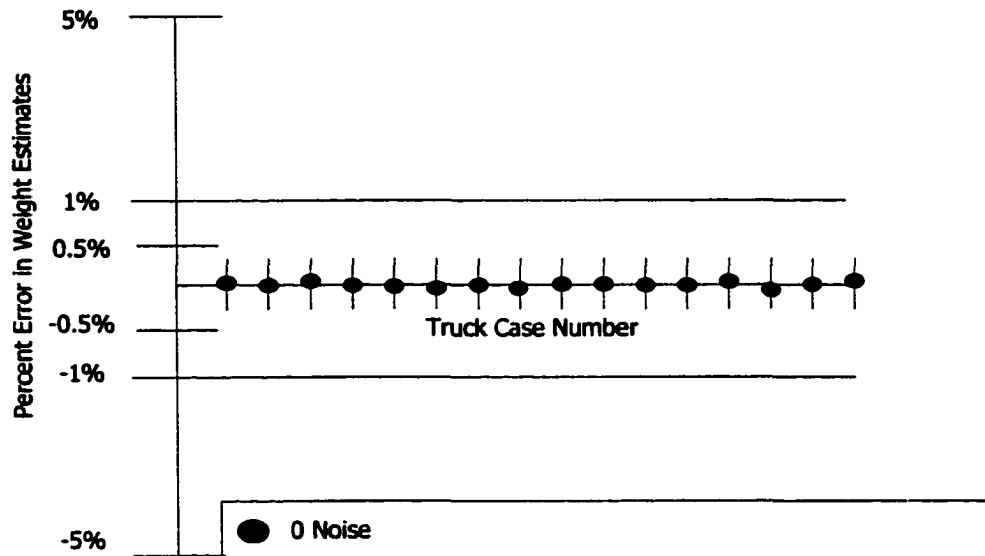


Figure 7.10 Percent Error in Front Axle Weight Estimates (a)

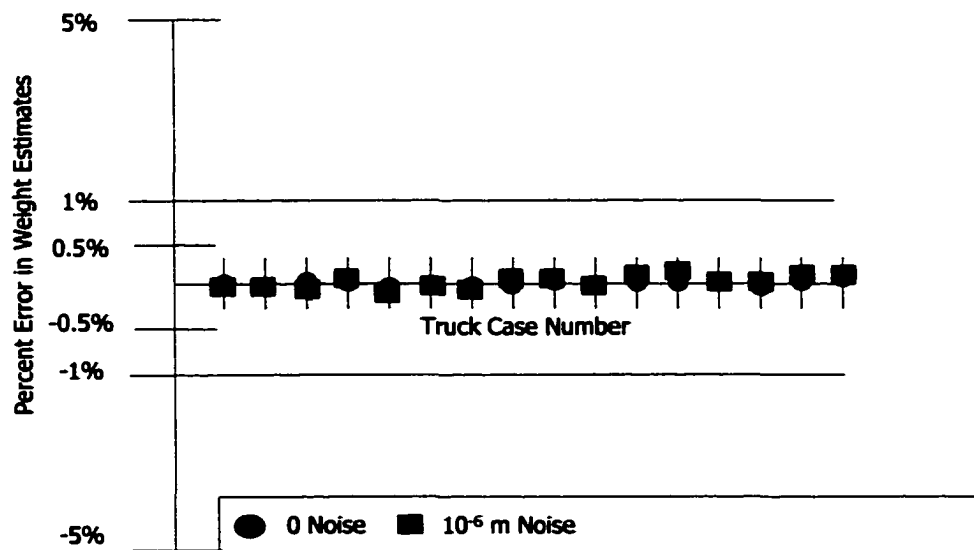


Figure 7.11 Percent Error in Front Axle Weight (b)

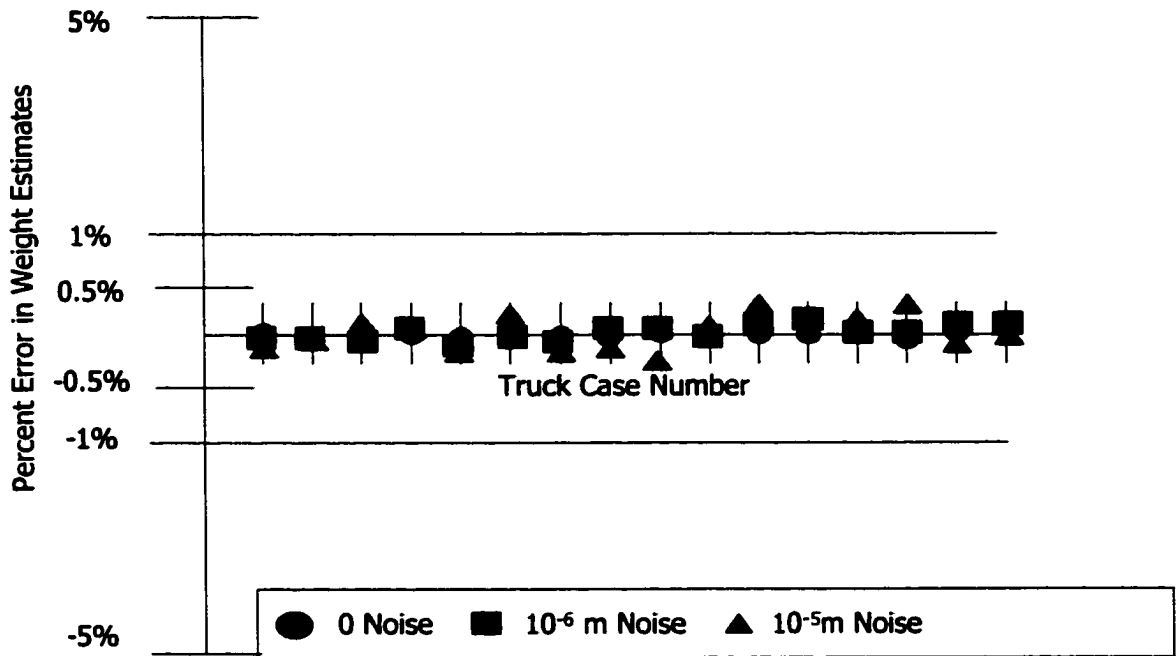


Figure 7.12 Percent Error in Front Axle Weight (c)

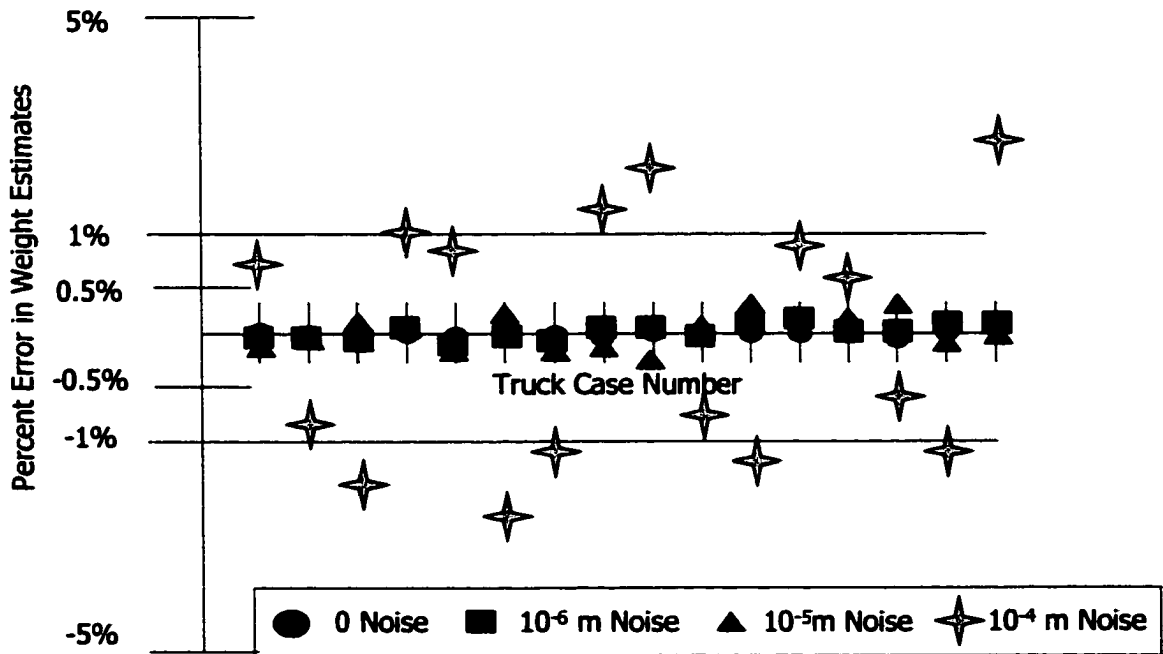


Figure 7.13 Percent Error in Front Axle Weight (d)

### Percent Error in Rear Axle Weight

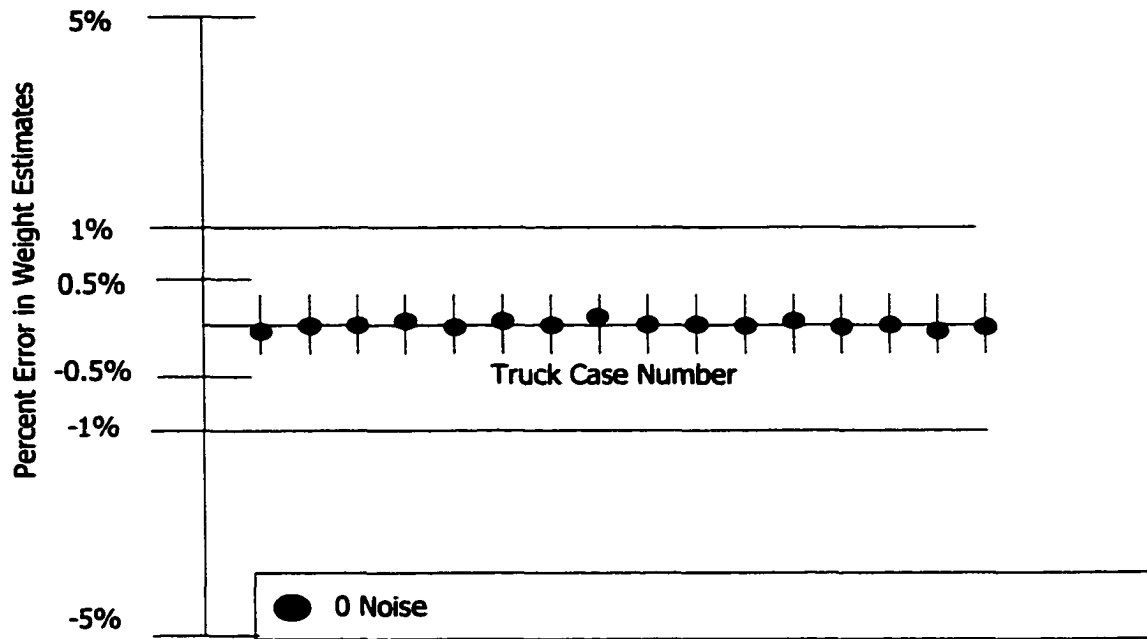


Figure 7.14 Percent Error in Rear Axle Weight (a)

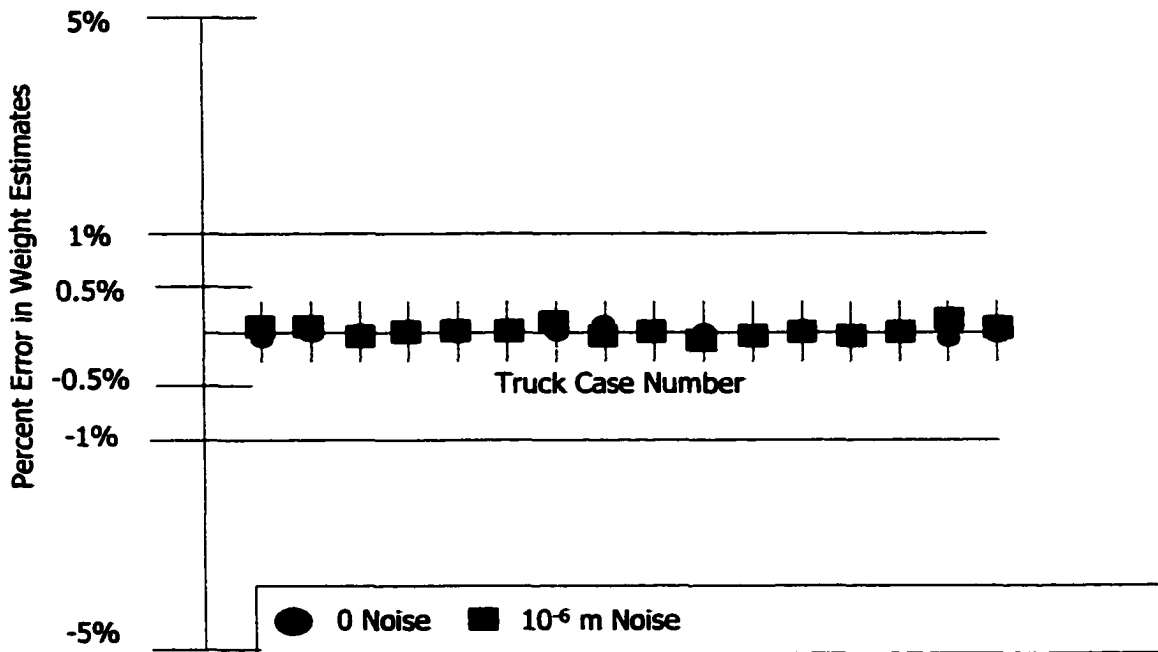


Figure 7.15 Percent Error in Rear Axle Weight (b)

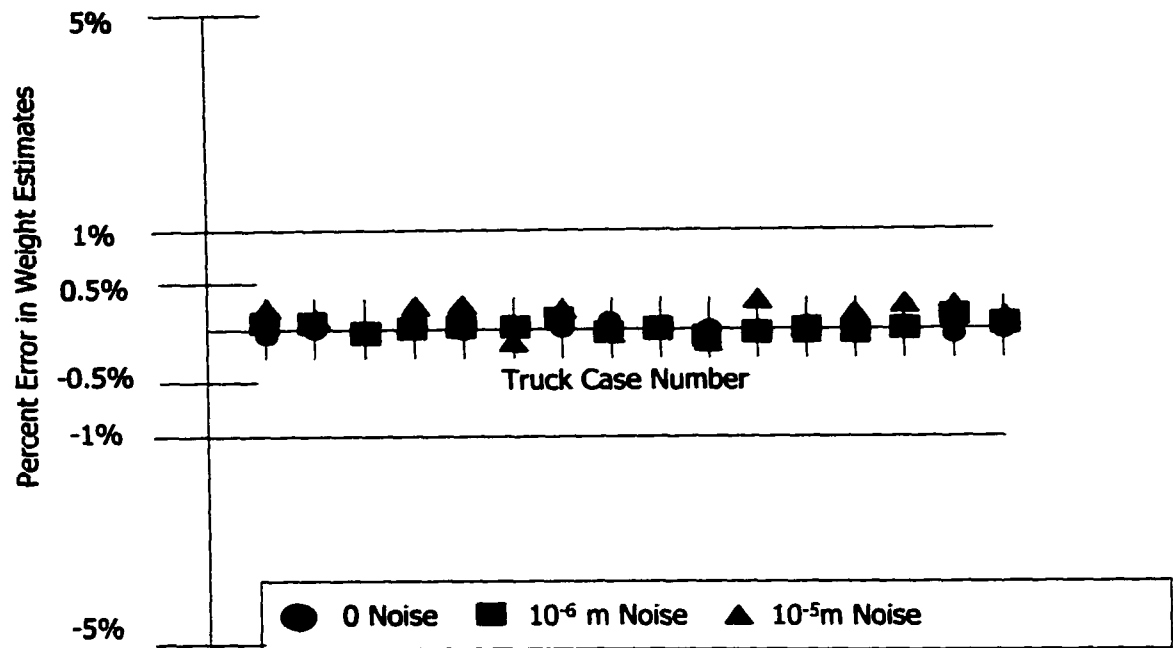


Figure 7.16 Percent Error in Rear Axle Weight (c)

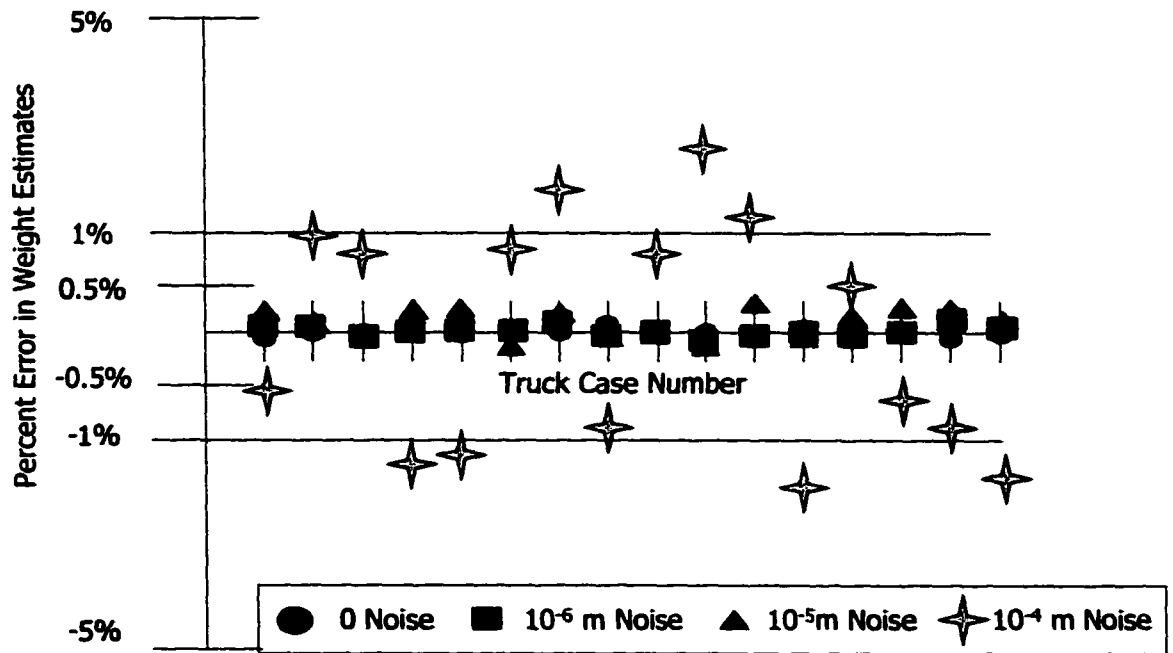


Figure 7.17 Percent Error in Rear Axle Weight (d)

The use of three measurements greatly improved the estimates of axle weights and total weight. Even with noise to signal ratios of 5% ( $\pm 10^{-5}$  m), the magnitude of the percent error in the axle weight estimates remained less than 0.08%. Axle spacing and, therefore, speed could be accurately obtained using either method for all noise levels.

### **7.3 Chapter Conclusions**

In this chapter the use of the dynamic bridge and static truck models to identify the truck's axle weights is examined. The sixteen truck configurations given in Table 3.1 are used to test the identification algorithm. The front axle weights of the trucks varied from  $4.9 \times 10^4$  N to  $1.2 \times 10^5$  N. The rear axle weights ranged from  $1.38 \times 10^5$  N to  $2.72 \times 10^5$  N. The axle spacings varied from 5-7m and speeds varied from 25-35 m/s.

Two scenarios using different numbers of deflection measurement locations are used to formulate the objective function in the optimization routine. In the first scenario, only one deflection measurement is made, and it is assumed that the speed and axle spacing are measured independently and are known precisely. Therefore, front and rear axle weights are the only unknown truck parameters. The percent error in axle weights for different levels of measurement noise is shown in Table 7.2 and Figures 7.3 and 7.4. Using only one deflection measurement and zero measurement noise, the maximum error in axle weight estimates was 0.045%. For measurement noise of  $\pm 1 \times 10^{-6}$  m, the maximum error in axle weight was 0.5%, and for measurement noise of  $\pm 1 \times 10^{-5}$  m, the maximum error was 2.2%. With noise of  $\pm 1 \times 10^{-4}$  m, the maximum error increased to 8.5%.

In the second scenario, the deflection was measured at three locations along the length of the beam, the midpoint, quarter-point, and three-quarter-point. Using multiple

deflection measurement locations eliminated the need to measure axle spacing and speed independently and allowed them to be identified by the optimization routine and the relationship between total time on the bridge and axle spacing in Equation (5.8). The average and maximum magnitudes of the percent error in the axle weight estimates are given in Tables 7.4 and 7.5. For zero measurement noise, the maximum error in axle weight was 0.003%. With measurement noise of  $\pm 1 \times 10^{-6}$  m, the maximum error was 0.008%. With measurement noise of  $\pm 1 \times 10^{-5}$  m, the maximum error in axle weight estimates was 0.08% and for measurement noise of  $\pm 1 \times 10^{-4}$  m, the maximum error was 3.1%. Estimates of axle spacing were also determined for all noise levels with negligible error.

# Chapter 8

## Static Bridge/Dynamic Truck

In this chapter we begin to examine the dynamic truck model and its coupling with the bridge. The dynamic nature of the truck causes a different bridge response than the static truck model and, therefore, requires more parameters to identify it than simply axle weight. To avoid identifying all of the physical parameters individually, it became necessary to develop an approximate model of the force applied to the bridge and optimize the parameters in that model to obtain the best fit to the measured deflection profile. This is done by first determining a homogeneous solution to the differential equations of motion and then adding the effects of the bridge/truck interaction. The assumption that the truck's total time on the bridge is known is again used to relate the axle spacing to the speed.

### 8.1 The Measured Profile

To generate the measured deflection profile, each axle is given a set of initial conditions to represent the truck entering the bridge. A variety of initial conditions are used with a variety of truck configurations that will be described in more detail later in this chapter. The deflection under each axle is calculated and the differential equations of motion for the truck given in Equations (4.11-4.14) (coupled bridge/truck model) are integrated over time to determine the truck's motion. The resulting motion of the unsprung mass,  $x_u$ -which includes the interaction with the bridge-is then used to formulate the force

applied by the truck to the static bridge using the expression given in Chapter 3 which is repeated here for clarity.

$$F_i(t) = -W_i + ku_i(xu_i(t) - y_B(x_i, t)) \quad (8.1)$$

This force is then applied to the finite element model of the bridge described in Chapter 2. The resulting deflection profiles are the “measured” profiles used for comparison inside the optimization routine.

## 8.2 Approximating the Force

To begin to identify the truck, it is necessary to first examine the homogeneous solution of each axle’s differential equations of motion. Referring back to Chapter 3, the differential equations of motion for each axle of the truck are given by

$$\begin{aligned} M_{si} \ddot{x}_{si} + K_{sk\ si} (x_{si} - x_{ui}) + C_{sk\ si} (\dot{x}_{si} - \dot{x}_{ui}) - M_{so} g &= 0 \\ M_{ui} \ddot{x}_{ui} + K_{sk\ ui} (x_{ui} - x_{si}) + C_{sk\ ui} (\dot{x}_{ui} - \dot{x}_{si}) + K_{uk\ ui} (x_{ui} - y_B(\tilde{x}_i, t)) - M_{u} g &= 0 \end{aligned} \quad (8.2)$$

The force applied by the truck has two components. The first, the static weight, is exactly like the static bridge/static truck case in Chapter 6. The second depends on the motion of the unsprung mass  $xu$  and the bridge deflection under each axle  $y_B$ . Since the motion of the unsprung mass is the quantity of interest for the dynamic analysis of the truck, it will be the only degree of freedom considered for the remainder of this section.

Neglecting the bridge interaction term in Equation (8.1), the homogeneous solution of  $xu$  is given by

$$\begin{aligned} xu_1 &= A_{11} e^{-\alpha_{11}(t-t_1)} \sin(\beta_{11}(t-t_1) + \phi_{11}) + A_{12} e^{-\alpha_{12}(t-t_1)} \sin(\beta_{12}(t-t_1) + \phi_{12}) \\ xu_2 &= A_{21} e^{-\alpha_{21}(t-t_2)} \sin(\beta_{21}(t-t_2) + \phi_{21}) + A_{22} e^{-\alpha_{22}(t-t_2)} \sin(\beta_{22}(t-t_2) + \phi_{22}) \end{aligned} \quad (8.3)$$

as shown in Chapter 3. This solution represents two damped oscillatory modes for each axle. Since the force applied by the truck and, hence, the deflection of the bridge, depend on  $xu$ , it is necessary to identify the unknown quantities in this solution. It is assumed that nothing is known about the truck at the time it enters the bridge, so all of the 16 subscripted variables in Equation (8.3) are considered to be unknown and are treated as optimization parameters. The truck's total time on the bridge is considered to be known and used to relate the axle spacing to the speed. Essentially, the static axle weights plus the homogeneous solution for  $xu$  were considered to be unknown in this development.

It should be noted here that, because of the bridge interaction represented by  $\Delta A$  in Equation (4.11) (the time dependent portion of the state matrix for the coupled bridge/truck system in this case), the natural frequencies and damping ratios of the truck change slightly as the truck travels across the bridge due to the change in stiffness of the bridge at the location of each force. It was found that the maximum change in the truck modal frequencies during transit of the span is less than 0.5% of the original values (0.1 Hz maximum) and has little effect on  $xu(t)$ . The damping ratios of the modes are found to change by less than 0.002 from their true values; the true damping ratio values range from 0.07-0.30. Consequently, Equation (8.3) provides a good approximation of the homogeneous solution to Equation (8.2).

Because of the truck's interaction with the bridge, the particular (or driven) solution of  $xu$  varies from the homogeneous one and has to be included in the approximate force model used in the optimization routine. A plot of the homogeneous solution (without bridge interaction) and the total solution (homogeneous plus bridge interaction effects) is shown in Figure 8.1 for the rear axle of one truck. As the truck

moves farther away from the supports towards the middle of the beam, the deflection becomes larger, and the effect of the interaction is more apparent. To accurately identify the force applied by the truck, it is necessary to represent this interaction effect in the approximate force model.

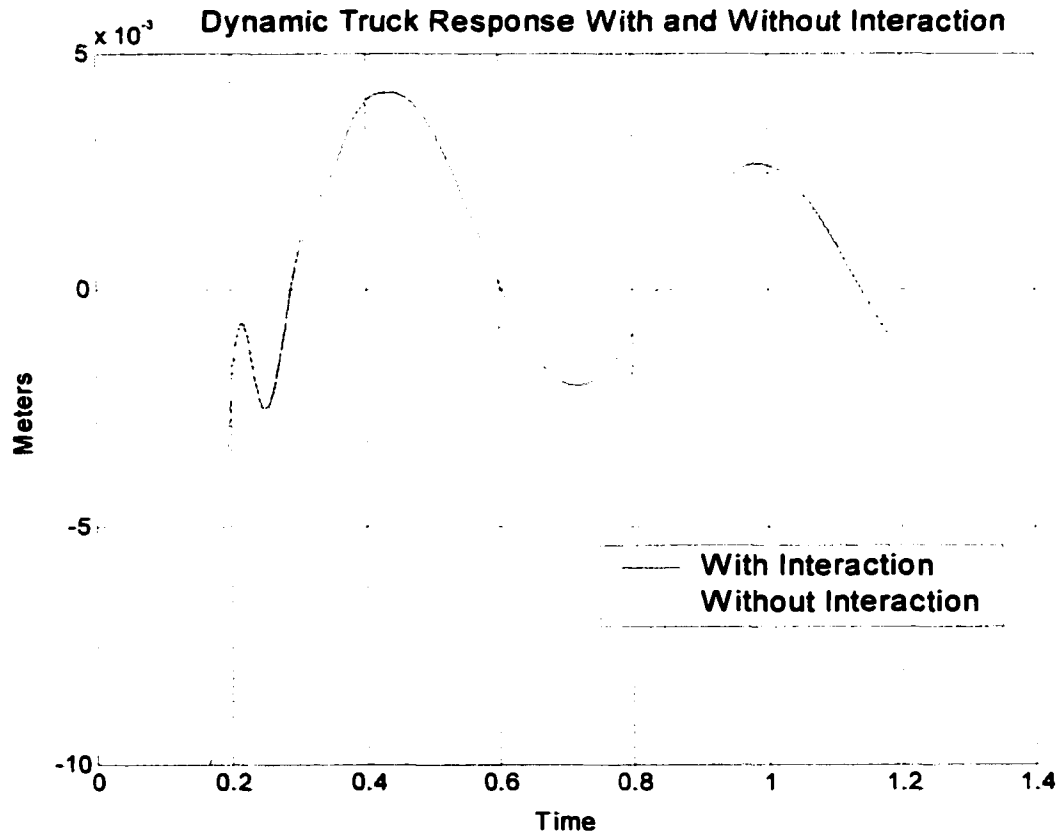


Figure 8.1 Truck Response With and Without Interaction Effects

The “driving effect” of the bridge deflection under each axle is examined to determine an appropriate approximate form to be incorporated into the force approximation. Four terms of the equations of motion of the coupled bridge/truck system given in Equation (4.11) are examined to determine their contribution to  $x_u$ . These terms are  $f_{11}=B(7,1)*W_1$ ,  $f_{12}=B(7,2)*W_2$ ,  $f_{21}=B(8,1)*W_1$ ,  $f_{22}=B(8,1)*W_1$ , where  $B$  is  $B(t)$  in

Equation (4.11). These correspond to the effect on each axle's  $xu$  due to the deflection under that axle. The nomenclature used represents the effect *on* an axle *by* an axle- $f11$  is the effect *of* axle 1 (front) *on* axle 1,  $f12$  is the effect *of* axle 2 (rear) *on* axle 1 (front) and vice versa for axle 2.

It is found that the forcing function produced by each of the terms can be approximated using the solution to the general bending equation for a beam subjected to a moving point load,  $P$ .

$$EI \frac{\partial^4 w(x,t)}{\partial z^4} = \delta(x - \tilde{x}(t))P \quad (8.4)$$

The solution to this differential equation is

$$w(x,t) = \frac{2P}{EIL(\pi/L)^4} \sum_{i=1}^{\infty} \left(\frac{1}{i}\right)^4 \sin \frac{i\pi x}{L} \sin \frac{i\pi \tilde{x}(t)}{L} \quad (8.5)$$

where all constants are defined in Chapter 2.

The forcing functions due to the beam deflection in the  $B(t)W$  term can be approximated using this series representation of the deflection under each axle. It is important to note that these expressions are not the formal solution to the differential equation (Equation (8.4)) for the coupled truck/bridge system, but rather an approximation. It was found, however, that the forcing functions given below in Equation (8.6) are reasonable approximations to the actual interaction effects. The variable  $N_f$  is the number of terms used in the series expansion. Using only two terms in each of these series results in less than 0.1% (approximately 10 N) error in the forcing function estimates.

$$\begin{aligned}
f_{11} &= \frac{ku_1}{mu_1} A \sum_{i=1}^{Nf} \left(\frac{1}{i}\right)^4 F_1(t) \sin^2 \frac{i\pi vt}{L} & f_{22} &= \frac{ku_2}{mu_2} A \sum_{i=1}^{Nf} \left(\frac{1}{i}\right)^4 F_2(t) \sin^2 \frac{i\pi(vt - a)}{L} \\
f_{12} &= \frac{ku_1}{mu_1} A \sum_{i=1}^{Nf} \left(\frac{1}{i}\right)^4 F_2(t) \sin \frac{i\pi vt}{L} \sin \frac{i\pi(vt - a)}{L} \\
f_{21} &= \frac{ku_2}{mu_2} A \sum_{i=1}^{Nf} \left(\frac{1}{i}\right)^4 F_1(t) \sin \frac{i\pi vt}{L} \sin \frac{i\pi(vt - a)}{L} \\
A &= \frac{2}{EIL \left(\frac{\pi}{L}\right)^4}
\end{aligned} \tag{8.6}$$

Determination of the forcing functions due to the bridge interaction allows an approximate model for each axle's unsprung mass motion  $xu$  to be formulated. This expression is the sum of the homogeneous solution for each axle and the effects of the forcing functions given above. The approximate model for  $xu$  of the  $i^{\text{th}}$  axle is given below

$$Xu_i = Xu_{Hi} + A_{ii} Xf_{ii} + A_{ij} Xf_{ij} \tag{8.7}$$

where  $Xf_{ii} = \frac{mu_i}{ku_i} f_{ii}$ ,  $Xf_{ij} = \frac{mu_i}{ku_i} f_{ij}$ ,  $Xu_{Hi}$  is the homogeneous solution of the  $i^{\text{th}}$  axle, and  $A_{ij}$  are unknown amplitudes due to the bridge deflection. The total solution is a superposition of the homogeneous solution and two interaction terms that represent the deflection due to both axles.

Once an expression for the unsprung mass motion  $xu$  is found, the force applied by the truck can be found via Equation (4.8) and given below

$$F = Q(KuXu + W) \text{ where } Q = [I + HKu]^{-1} \tag{8.8}$$

$H$  is the matrix of inverse beam stiffnesses based on the location of each force, and  $Xu$  is the approximate unsprung mass motion given in Equation (8.7).

The above formulation specifically addresses the case when both axles are on the beam. For the times when an axle is not on the beam, its contribution to the force and dynamics is zero.

Once the force from the truck is calculated, three equations are used to calculate the deflection at the three sensor locations,  $x=L/2, L/4, 3L/4$ . These equations are given below.

$$z(x,t) = \begin{bmatrix} H_1(x, b_1(t)) & H_1(x, b_2(t)) \end{bmatrix} \begin{bmatrix} F_1(t) & F_2(t) \end{bmatrix}^T \quad (8.9)$$

where  $x = \frac{L}{2}, \frac{L}{4}, \frac{3L}{4}$

### 8.3 Parameter Identification-Optimization Routine

To identify the unknown truck parameters, the optimization routine discussed in previous chapters is used, although the number of optimization parameters grows significantly. Below is a list of the optimization parameters for each axle and their upper and lower bounds. It is once again assumed that the truck's total time on the bridge is known and is used to calculate speed from axle spacing. The bounds for  $\alpha$  and  $\beta$  are chosen from typical values of the natural frequencies and damping ratios of the two modes. For the lower frequency mode, frequencies typically range from 1.5-4.5 Hz and damping ratios from 1%-30%. For the higher mode, frequencies typically range from 10-20 Hz with damping between 5% and 50%. The bounds for  $\alpha$  and  $\beta$  are determined from these values using the relationships  $\alpha = \xi\omega_n$  and  $\beta = \omega_n \sqrt{1 - \xi^2}$ .

**Table 8.1 Upper and Lower Bounds for Optimization Parameters**

| <b>Parameter</b>                           | <b>Lower</b> | <b>Upper</b> |
|--|--------------|--------------|
| <b>Axle Weight</b>                         | 2.5E3 N      | 10E5N        |
| <b>R<sub>i1</sub>(low mode amplitude)</b>  | -0.1m        | 0.1m         |
| <b>R<sub>i2</sub>(high mode amplitude)</b> | -0.5m        | 0.5m         |
| $\alpha_{i1}$                              | 0.16         | 8.48         |
| $\alpha_{i2}$                              | 3.14         | 62.83        |
| $\beta_{i1}$                               | 5.99         | 28.27        |
| $\beta_{i2}$                               | 54.5         | 125.51       |
| $\varphi_{i1}$                             | 0            | $\pi$        |
| $\varphi_{i2}$                             | 0            | $\pi$        |
| <b>ku</b>                                  | 1E5 N/m      | 5E7 N/m      |
| $A_{ii}$                                   | .1           | 3            |
| $A_{ij}$                                   | .1           | 3            |

There are twelve optimization parameters per axle not including  $a$ , for a total of 25 parameters relating to the truck as a whole.

#### **8.4 Parameter Identification-Force Objective Function**

The optimization routine in MATLAB described previously is used to minimize the objective function  $J$ . For the static bridge/dynamic truck case, the force applied by the truck is a superposition of the static weight, the free vibration solution of the truck's dynamics, and the driven solution. Since this is a more complicated system than the previous static truck cases, two different formulations of the objective function are individually examined to better understand the model. The simpler of these two used the force applied by each axle to formulate the objective function. The objective function is formulated by comparing the difference between the "measured" applied force and the approximate one. This would be equivalent to having a moving force sensor underneath each axle of the truck as it passed across the bridge. Although this has no realistic physical realization, it was found to be a useful tool in perfecting the optimization routine

and approximate truck model. A figure illustrating a sample “measured” force profile is shown below in Figure 8.2. Clearly, the force is a superposition of each axle’s static weight and dynamic behavior. During the times when each axle is not on the beam, the applied force is zero.

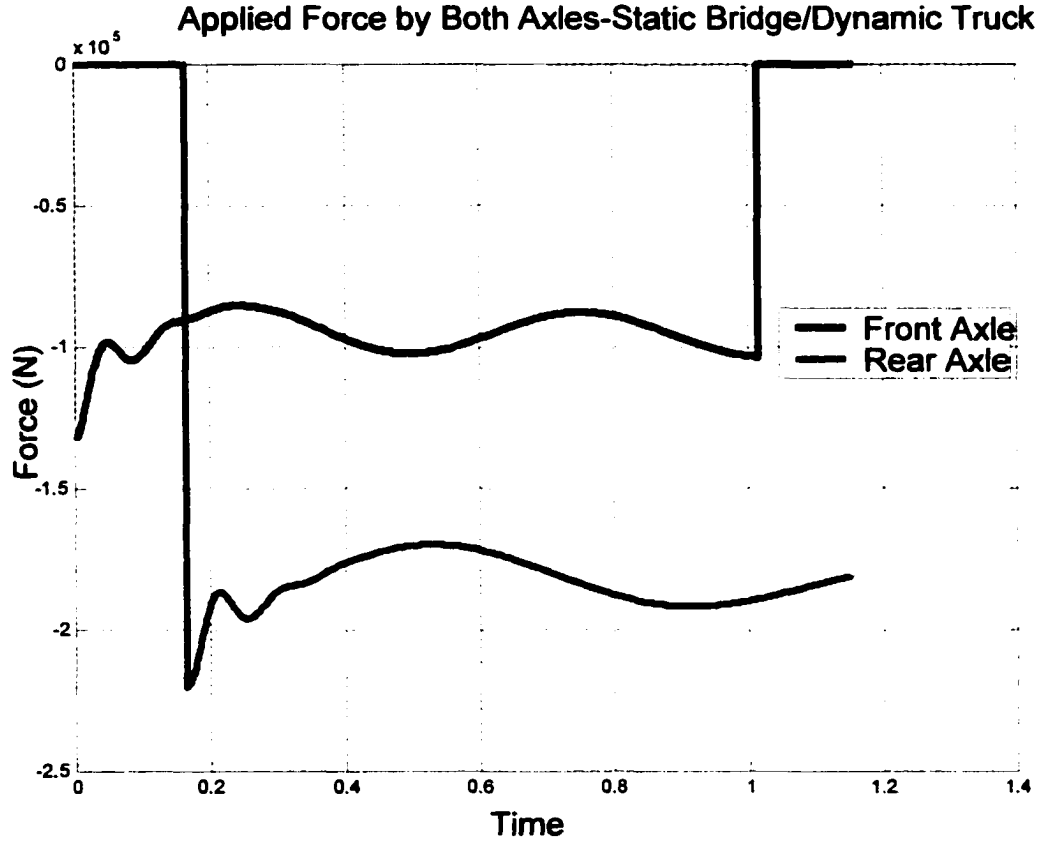


Figure 8.2 Truck Axle Forces

The objective function for this formulation is given below.

$$J_F = \sum_{i=1}^N (\tilde{F}_{1,i} - F_{1,i}(\bar{p}))^2 + (\tilde{F}_{2,i} - F_{2,i}(\bar{p}))^2 \quad (8.10)$$

where  $\tilde{F}_{n,i}$  is the force applied by the  $n^{\text{th}}$  actual axle at the  $i^{\text{th}}$  time step.  $F_{n,i}(\bar{p})$  is the approximate force from the  $n^{\text{th}}$  axle using the optimization parameters  $\bar{p}$ . It is important to note that the vector of truck parameters  $\bar{p}$  does not contain the physical parameters

(stiffness, damping, mass, etc.) given in the original description of the truck model. It contains the variables given in Table 8.1 which are related to the physical parameters but are not them expressly. This objective function is minimized using the optimization routine in Chapter 5.

Estimates of the truck parameters using the force formulation of the objective function are quite accurate. With no noise added to the measured force profile, average errors in axle weight of 0.014% were obtained. Random white noise is then added to the measured force profiles. Noise is added to the force profiles to examine the algorithm's ability to accurately identify the truck parameters from a noisy signal, despite the fact that there is really no realistic counterpart to measuring the tire force underneath each axle. It was suspected that the addition of noise would quickly deteriorate the estimates of the truck's dynamic properties, so the effect on the weight estimates needed to be examined. The noise to signal ratios used were 0.1%, 1%, and 10% (100 N,  $10^3$  N, and  $10^4$  N).

Table 8.2 below shows the average magnitude of the percent error in axle weight estimates for the different noise levels. The results show that the addition of noise to the force profiles did little to degrade the estimates of truck weight, indicating that the method of optimizing the approximate force model was robust to the addition of noise. Estimates of axle spacing are also very accurate using this method with errors less than  $10^{-3}\%$  for all noise levels. Note that the speed is determined using the relationship between axle spacing and total time given in Equation (5.8).

**Table 8.2 Average Magnitude of Percent Error in Axle Weight Estimates Using the Force Objective Function**

| Noise Level     | Average Percent Error in Axle Weights |
|-----------------|---------------------------------------|
| 0               | 0.0088%                               |
| 0.1% (100 N)    | 0.048%                                |
| 1% ( $10^3$ N)  | 0.385%                                |
| 10% ( $10^4$ N) | 0.889%                                |

The figures below show the estimated axle weights using the objective function formulated using the measured force. Negligible error is obtained in axle spacing for all noise levels, so the results will not be given here. The total weight was found from the sum of the two axle weights. The configurations of the trucks shown in the figures below are given in trucks 1, 7, 14, 16, 18 in Table 3.2.

Front Axle Weight Estimates Using the Force Objective Function

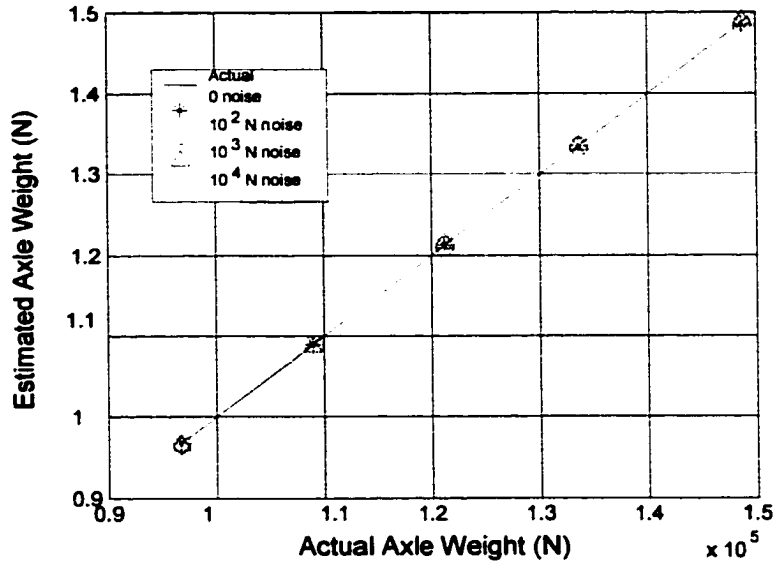


Figure 8.3 Front Axle Weight Estimates Using the Force Objective Function

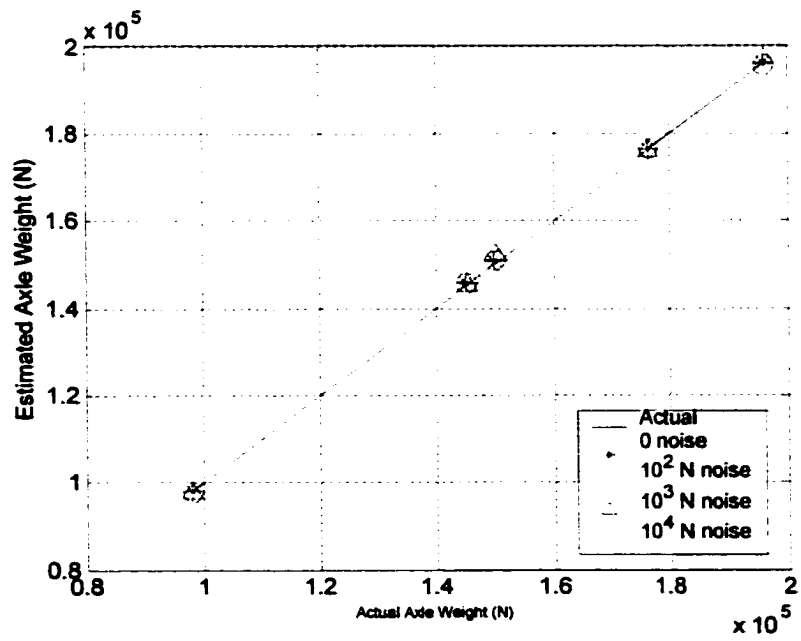


Figure 8.4 Rear Axle Weight Estimates Using Force Objective Function

Estimates of the other optimization parameters relating to the truck's dynamic properties and the bridge/truck interaction are also obtained. Next to axle weights, the natural frequencies and damping ratios of each of the truck's modes are of the greatest interest in this work, so their estimates will be the only ones given here. It is important to note that the actual optimization parameters are  $\alpha$  and  $\beta$  and not frequency and damping, but, for the sake of clarity, the results will be given in terms of  $\omega_n$  and  $\xi$ .

Natural frequencies and damping ratios are estimated quite accurately from the force profile, as well. The tables below show the estimates of frequency and damping ratio for each truck configuration.

**Table 8.3 Front Axle Frequency Estimates (Force Objective Function)**

| <b>Frequency (Hz)<br/>(Low Mode, Front)</b>  | <b>0 m Noise</b> | <b>10<sup>2</sup> N Noise</b> | <b>10<sup>3</sup> N Noise</b> | <b>10<sup>4</sup> N Noise</b> |
|--|------------------|-------------------------------|-------------------------------|-------------------------------|
| 1.91   | 1.93             | 1.86                          | 2.05                          | 2.09                          |
| 1.82   | 1.88             | 1.92                          | 1.62                          | 1.52                          |
| 1.61   | 1.69             | 1.82                          | 2.12                          | 1.51                          |
| 1.66   | 1.59             | 1.72                          | 1.92                          | 1.96                          |
| 1.78   | 1.71             | 1.85                          | 1.97                          | 2.32                          |
| <b>Frequency (Hz)<br/>(High Mode, Front)</b> | <b>0 m Noise</b> | <b>10<sup>2</sup> N Noise</b> | <b>10<sup>3</sup> N Noise</b> | <b>10<sup>4</sup> N Noise</b> |
| 11.27  | 11.39            | 11.52                         | 10.02                         | 13.86                         |
| 12.35  | 12.51            | 12.74                         | 13.78                         | 10.43                         |
| 11.27  | 11.71            | 11.97                         | 10.12                         | 15.35                         |
| 12.06  | 12.91            | 13.56                         | 15.03                         | 16.01                         |
| 11.44  | 11.16            | 10.31                         | 10.22                         | 15.82                         |

**Table 8.4 Front Axle Damping Ratio Estimates (Force Objective Function)**

| <b>Damping (%)<br/>(Low Mode, Front)</b>  | <b>0 m Noise</b> | <b>10<sup>2</sup> N Noise</b> | <b>10<sup>3</sup> N Noise</b> | <b>10<sup>4</sup> N Noise</b> |
|---|------------------|-------------------------------|-------------------------------|-------------------------------|
| 7.2                                       | 6.9              | 7.6                           | 6.2                           | 8.1                           |
| 5.9                                       | 5.8              | 5.2                           | 6.2                           | 7.5                           |
| 6.2                                       | 6.1              | 6.4                           | 5.6                           | 8.1                           |
| 5.9                                       | 5.0              | 5.1                           | 5.0                           | 7.4                           |
| 6.6                                       | 6.9              | 7.3                           | 5.8                           | 7.9                           |
| <b>Damping (%)<br/>(High Mode, Front)</b> | <b>0 m Noise</b> | <b>10<sup>2</sup> N Noise</b> | <b>10<sup>3</sup> N Noise</b> | <b>10<sup>4</sup> N Noise</b> |
| 29.7                                      | 26.1             | 25.7                          | 33.8                          | 34.9                          |
| 37.9                                      | 34.2             | 39.8                          | 45.2                          | 49.6                          |
| 27.1                                      | 25.2             | 21.4                          | 34.8                          | 20.8                          |
| 24.8                                      | 26.9             | 30.1                          | 34.6                          | 36.3                          |
| 27.6                                      | 28.1             | 30.6                          | 21.6                          | 38.1                          |

**Table 8.5 Rear Axle Frequency Estimates (Force Objective Function)**

| <b>Frequency (Hz)<br/>(Low Mode, Rear)</b>  | <b>0 m Noise</b> | <b>10<sup>2</sup> N Noise</b> | <b>10<sup>3</sup> N Noise</b> | <b>10<sup>4</sup> N Noise</b> |
|---|------------------|-------------------------------|-------------------------------|-------------------------------|
| 1.91  | 1.94             | 2.12                          | 1.71                          | 2.10                          |
| 2.04  | 1.92             | 1.80                          | 2.53                          | 1.50                          |
| 1.53  | 1.58             | 1.88                          | 2.62                          | 3.06                          |
| 2.35  | 2.42             | 2.94                          | 1.54                          | 3.02                          |
| 1.87  | 1.79             | 1.89                          | 2.12                          | 2.49                          |
| <b>Frequency (Hz)<br/>(High Mode, Rear)</b> | <b>0 m Noise</b> | <b>10<sup>2</sup> N Noise</b> | <b>10<sup>3</sup> N Noise</b> | <b>10<sup>4</sup> N Noise</b> |
| 11.27                                       | 11.76            | 11.98                         | 12.82                         | 14.98                         |
| 16.72                                       | 16.27            | 15.85                         | 12.34                         | 12.83                         |
| 11.26                                       | 11.41            | 12.16                         | 14.24                         | 15.19                         |
| 18.74                                       | 18.21            | 18.10                         | 15.91                         | 15.02                         |
| 13.34                                       | 13.57            | 13.87                         | 12.02                         | 15.45                         |

**Table 8.6 Rear Axle Damping Ratio Estimates (Force Objective Function)**

| <b>Damping (%)<br/>(Low Mode, Rear)</b>  | <b>0 m Noise</b> | <b>10<sup>2</sup> N Noise</b> | <b>10<sup>3</sup> N Noise</b> | <b>10<sup>4</sup> N Noise</b> |
|--|------------------|-------------------------------|-------------------------------|-------------------------------|
| 7.2                                      | 7.4              | 7.8                           | 5.9                           | 6.0                           |
| 5.9                                      | 5.5              | 5.4                           | 6.6                           | 4.3                           |
| 6.2                                      | 6.2              | 6.8                           | 7.9                           | 3.9                           |
| 5.9                                      | 6.0              | 6.2                           | 6.7                           | 7.8                           |
| 6.6                                      | 6.6              | 6.2                           | 5.1                           | 7.8                           |
| <b>Damping (%)<br/>(High Mode, Rear)</b> | <b>0 m Noise</b> | <b>10<sup>2</sup> N Noise</b> | <b>10<sup>3</sup> N Noise</b> | <b>10<sup>4</sup> N Noise</b> |
| 27.6                                     | 22.1             | 29.8                          | 33.8                          | 37.2                          |
| 16.7                                     | 18.4             | 20.1                          | 21.0                          | 15.0                          |
| 27.1                                     | 28.1             | 24.9                          | 30.2                          | 31.8                          |
| 37.9                                     | 38.7             | 34.9                          | 42.1                          | 45.9                          |
| 29.7                                     | 28.0             | 27.1                          | 22.2                          | 20.4                          |

### **8.5 Parameter Identification-Deflection Objective Function**

The second formulation of the objective function used in this chapter is based on the measured deflection profiles. Sample midpoint deflection profiles of the static beam using both the dynamic and static truck models are shown below in Figure 8.5. The profiles are very similar for the static bridge/static truck case, although the effects of the truck dynamics do result in slight differences between the two.

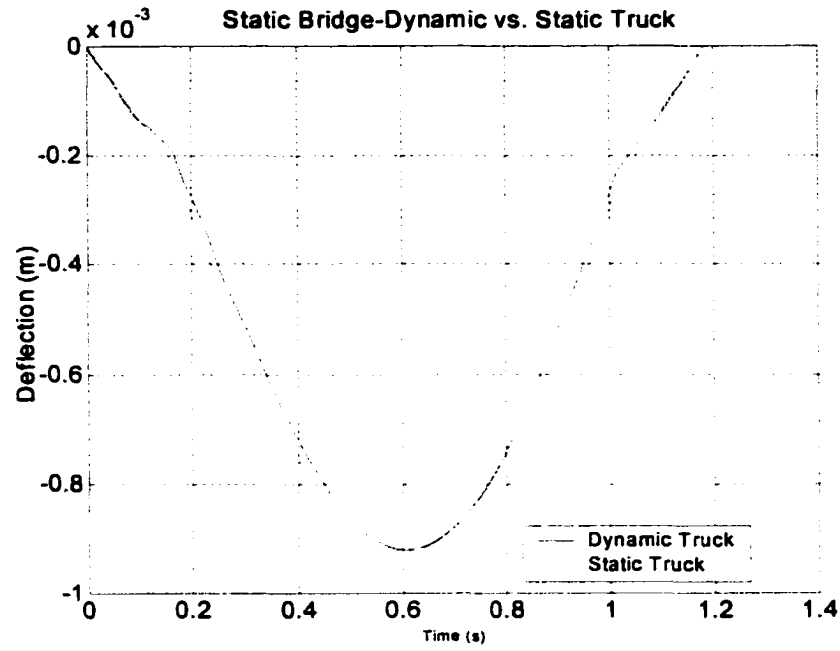


**Figure 8.5 Midpoint Deflection Profile for Static and Dynamic Truck Models**

The objective function used in this section is given below. It is the square of error between the measured deflection profiles and the estimated ones. The subscripts  $L/2$ ,  $L/4$ , and  $3L/4$  in Equation (8.11) below denote the sensor locations. The weights for each of the sensor measurements were determined iteratively.

$$J = \sum_{i=1}^N 3 \left( \tilde{w}_{\frac{L}{2},i} - z_{\frac{L}{2},i}(\bar{p}) \right)^2 + \left( \tilde{w}_{\frac{L}{4},i} - z_{\frac{L}{4},i}(\bar{p}) \right)^2 + \left( \tilde{w}_{\frac{3L}{4},i} - z_{\frac{3L}{4},i}(\bar{p}) \right)^2 \quad (8.11)$$

The optimization routine is first tested using zero measurement error in the data. Deflection profiles are generated by simulating trucks with a range of parameter values to represent the actual truck configurations passing over the bridge. The minimization routine is the used to estimate each truck's parameters. The truck configurations examined are given by truck numbers 1, 7, 14, 16, and 18 in Table 3.2.

With zero measurement noise, the truck weights are determined to within an average magnitude of 0.003%. Axle spacing is determined to within  $10^{-3}\%$ . Uniform random noise is then added to the data to examine its effect on the performance of the algorithm. The amplitude of the noise is expressed as a fraction of the maximum deflection, which was on the order of  $10^{-4}$ m. Noise to signal ratios of 0, 1% and 5% (0,  $1 \times 10^{-6}$ m,  $5 \times 10^{-6}$ m) were examined. For each of them, axle weights could be determined to within 1.3%. Noise had little effect on the estimates of axle spacing and speed, resulting in less than  $10^{-2}\%$  error for all noise levels. The average and maximum magnitudes of the percent error for the different noise levels are given in Table 8.7 and Table 8.8.

**Table 8.7 Average Magnitude of the Percent Error in Axle Weight Using the Deflection Objective Function**

| Noise Level          | Average Percent Error in Axle Weights |
|----------------------|---------------------------------------|
| 0                    | 0.0035%                               |
| $10^{-6}$ m          | 0.11%                                 |
| $5 \times 10^{-6}$ m | 0.63                                  |

**Table 8.8 Maximum Magnitude of the Percent Error in Axle Weights Using the Deflection Objective Function**

| Noise Level          | Maximum Percent Error in Axle Weights |
|----------------------|---------------------------------------|
| 0                    | 0.018%                                |
| $10^{-6}$ m          | 0.25%                                 |
| $5 \times 10^{-6}$ m | 1.3%                                  |

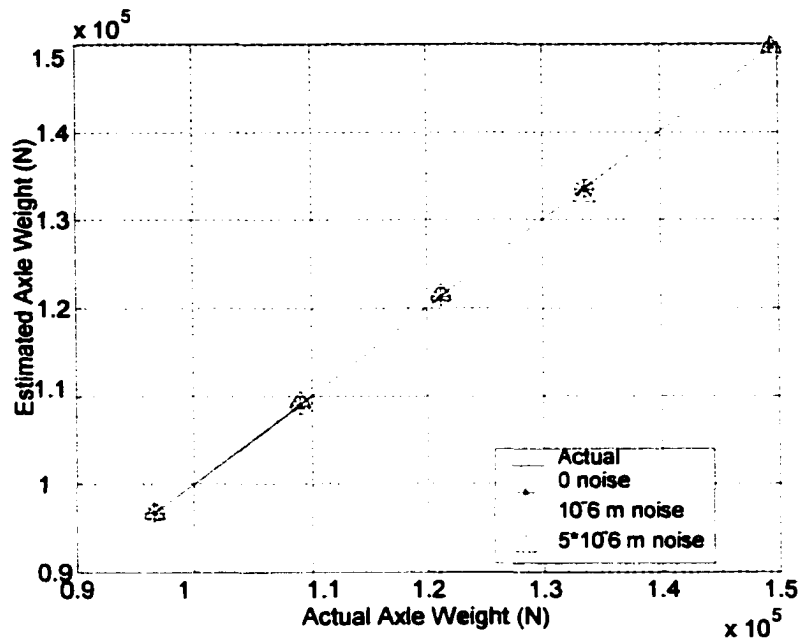


Figure 8.6 Front Axle Weight Estimates Using the Deflection Objective Function

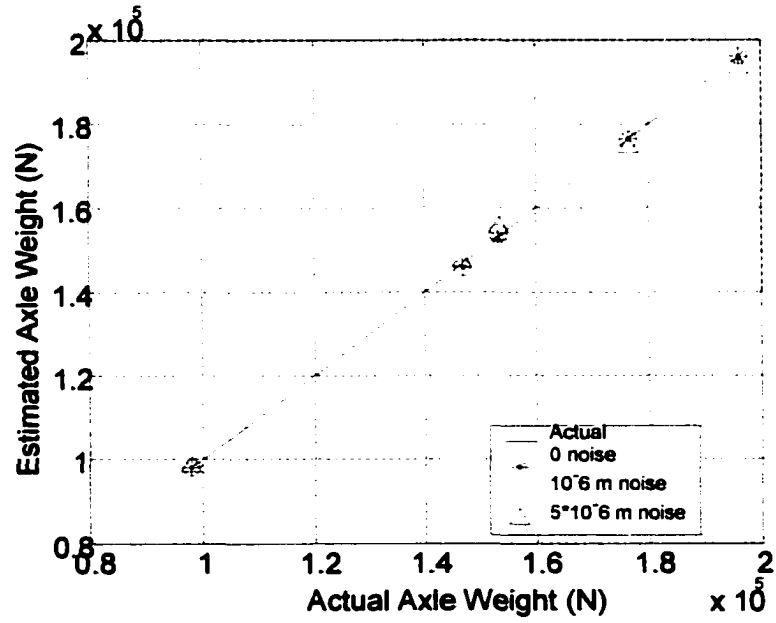


Figure 8.7 Rear Axle Weight Estimates Using the Deflection Objective Function

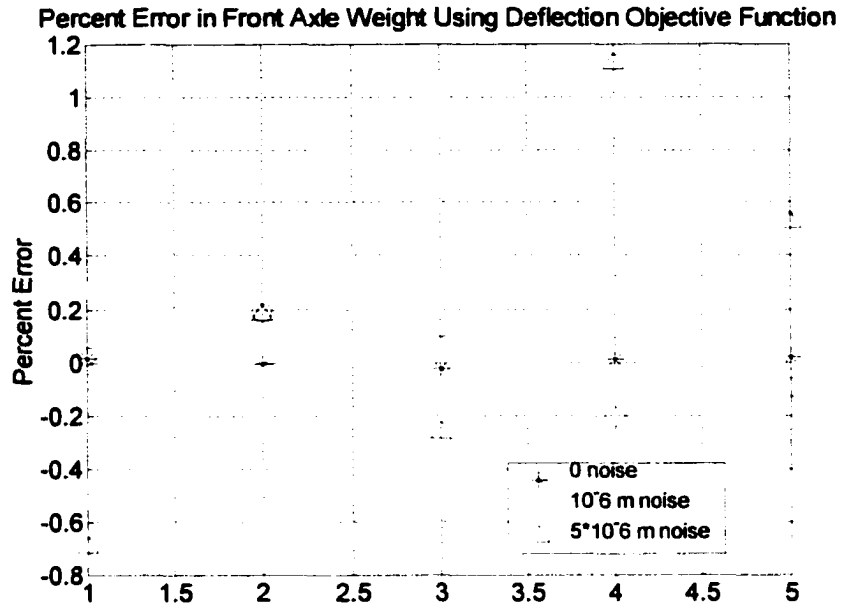


Figure 8.8 Percent Error in Front Axle Weight (Deflection Objective Function)

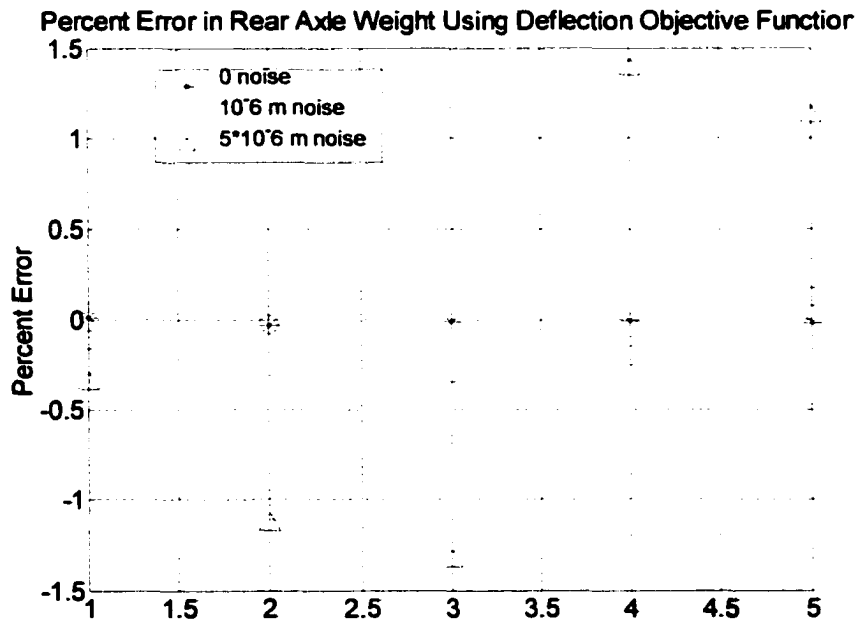


Figure 8.9 Percent Error in Rear Axle Weight (Deflection Objective Function)

Another representation of the axle weight percent error is given in the following figures. In Figures 8.10-8.17, the x-axis is the truck case number corresponding to truck

cases 1, 7, 14, 16, and 18 in Table 3.2. The y-axis is the percent error in axle weight estimates for each truck case.

### Percent Error in Front Axle Weight

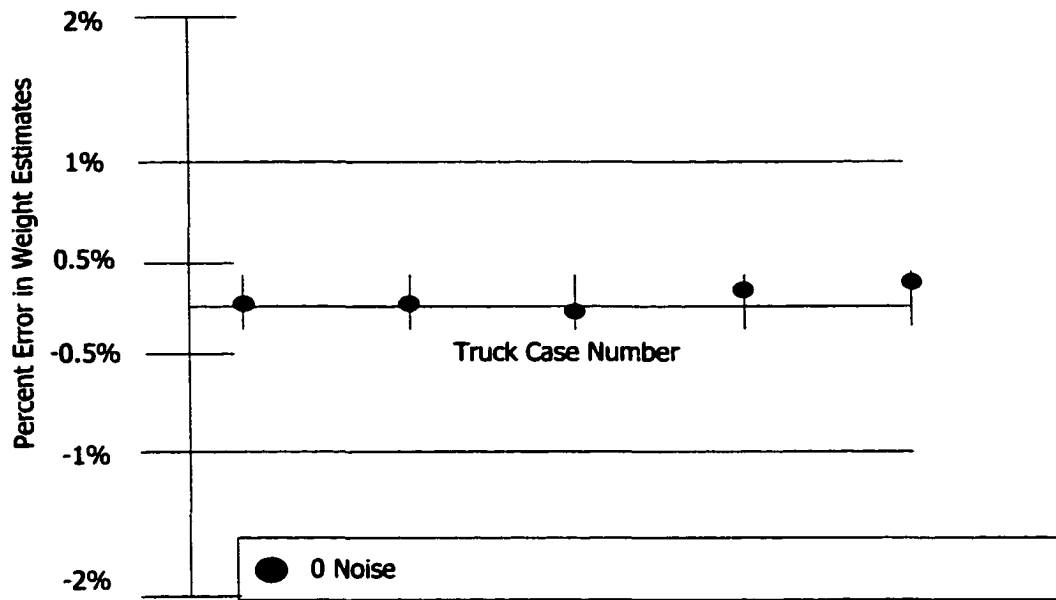


Figure 8.10 Percent Error in Front Axle Weight (a)

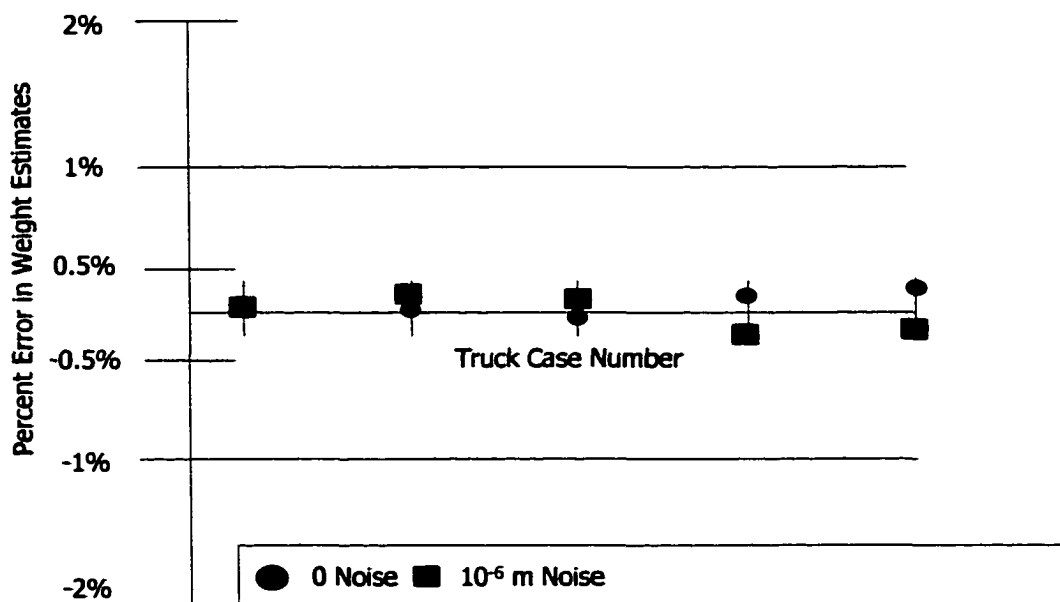


Figure 8.11 Percent Error in Front Axle Weight (b)

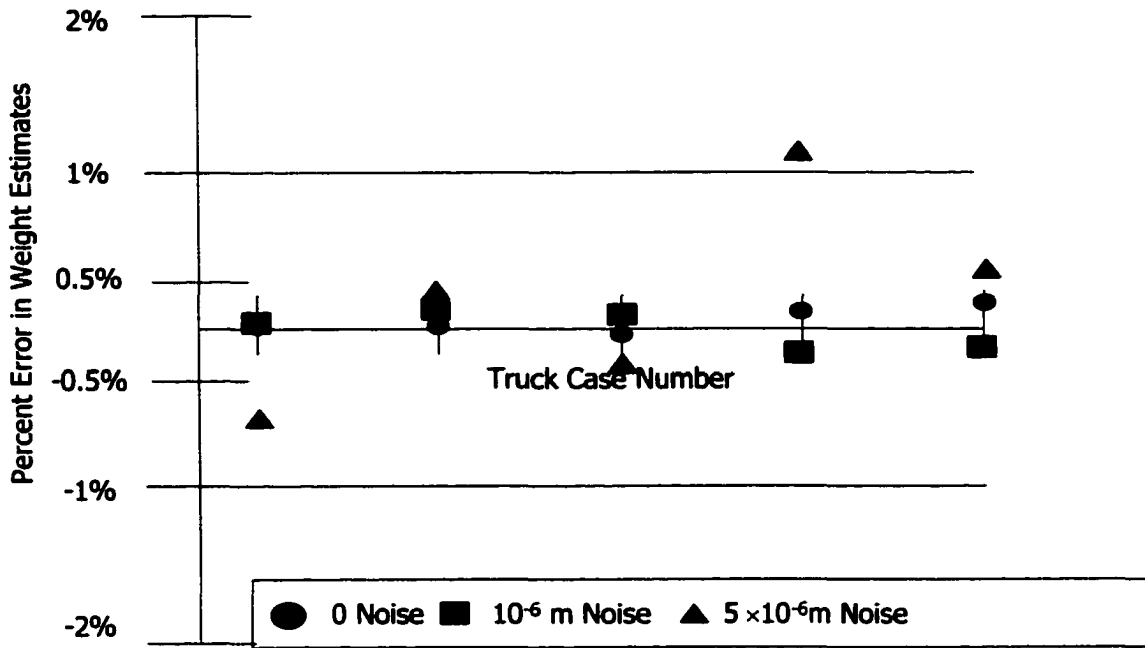


Figure 8.12 Percent Error in Front Axle Weight (c)

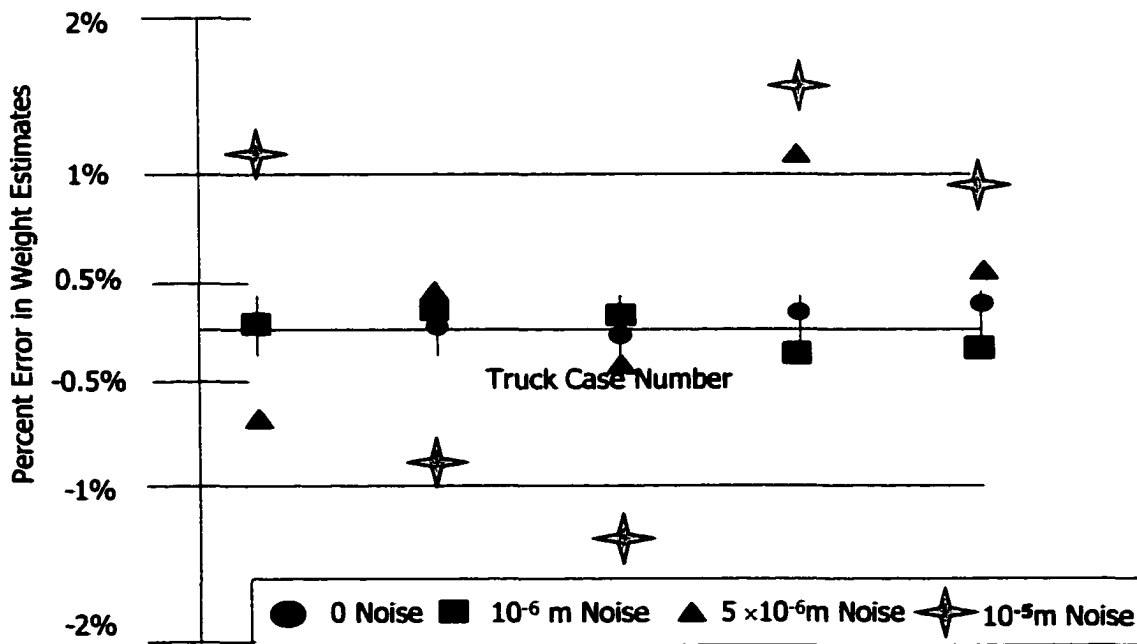


Figure 8.13 Percent Error in Front Axle Weight (d)

### Percent Error in Rear Axle Weights

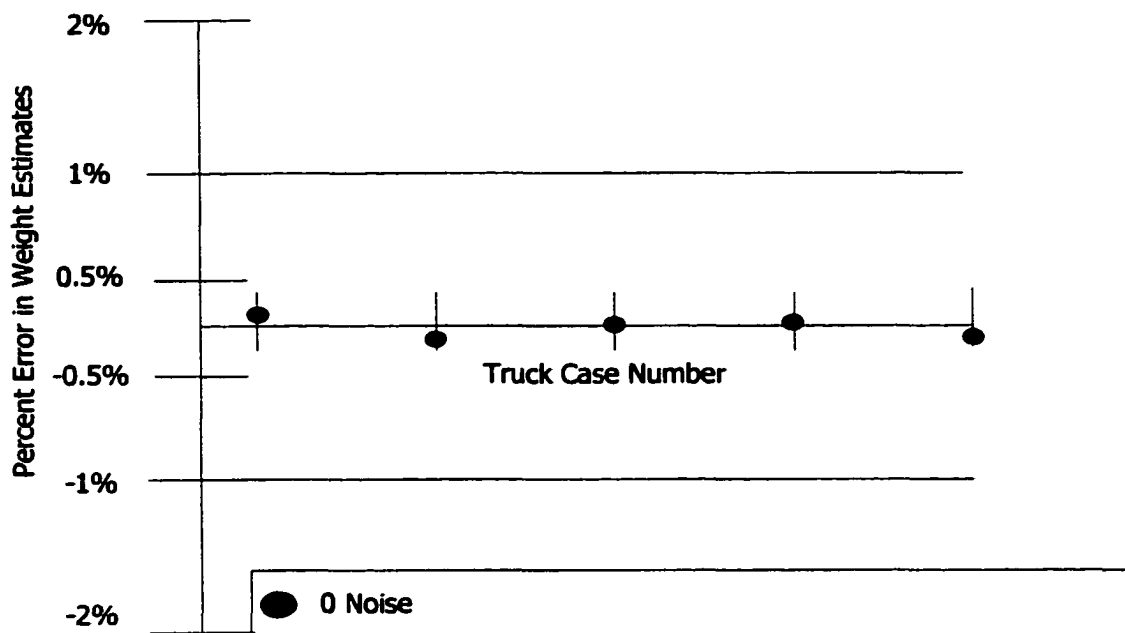


Figure 8.14 Percent Error in Rear Axle Weight (a)

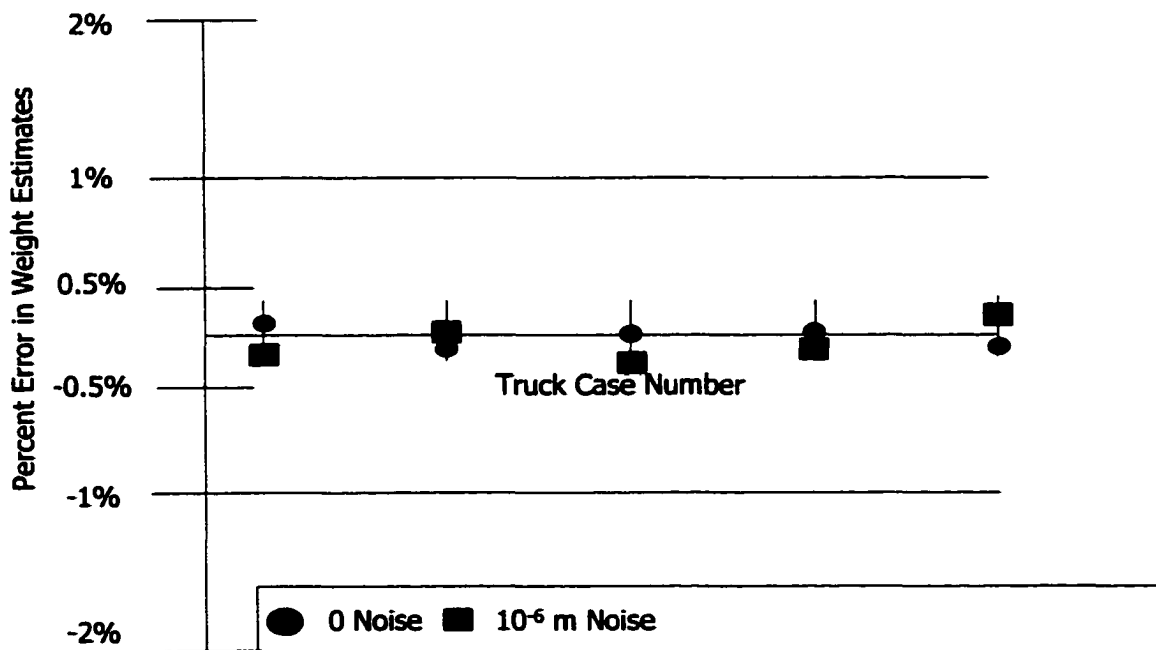


Figure 8.15 Percent Error in Rear Axle Weight (b)

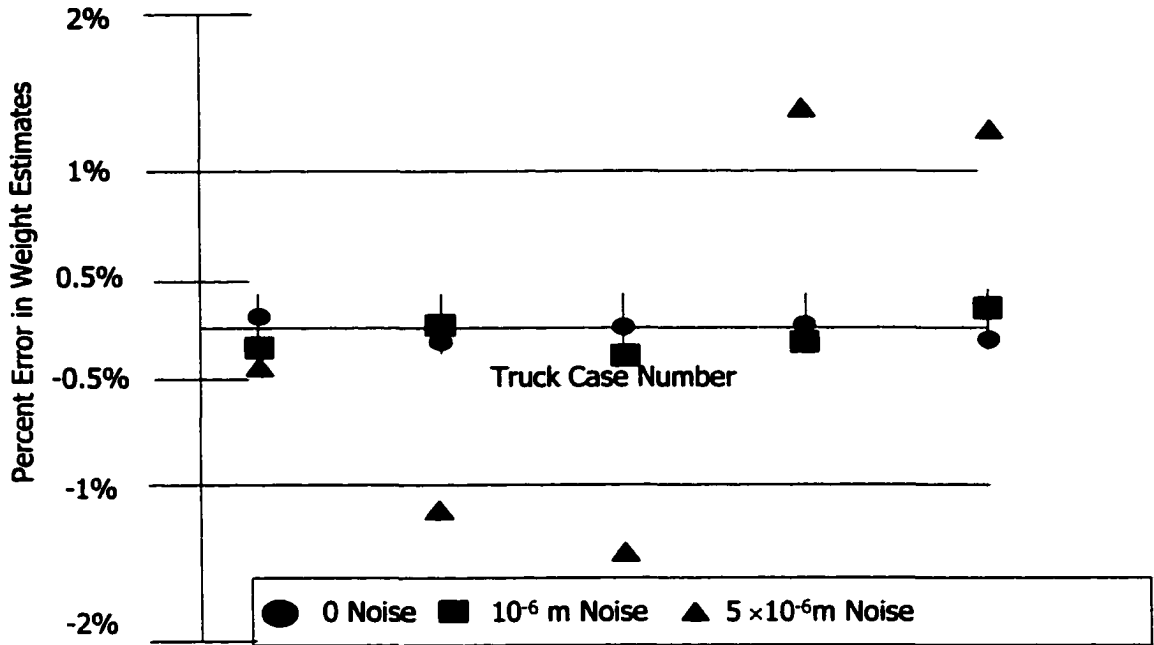


Figure 8.16 Percent Error in Rear Axle Weight (c)

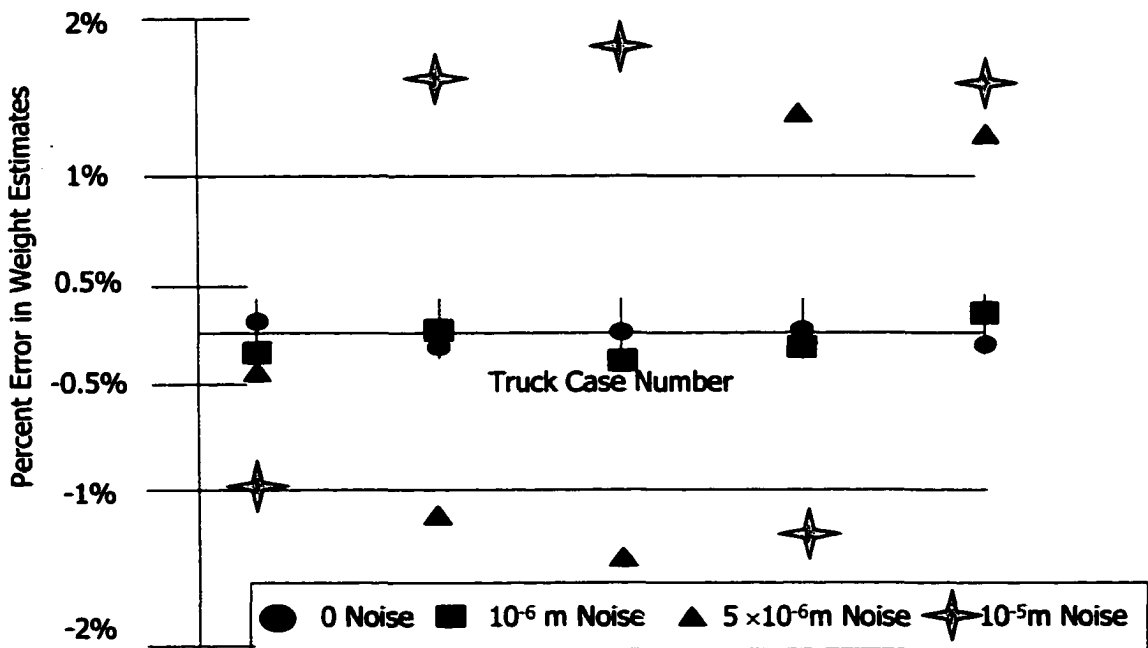


Figure 8.17 Percent Error in Rear Axle Weight (d)

The dynamic properties of each axle are also obtained from the optimization routine. Below are the estimates of natural frequencies and damping ratios obtained from the deflection objective function.

**Table 8.9 Front Axle Frequency Estimates (Deflection Objective Function)**

| <b>Frequency (Hz)<br/>(Low Mode, Front)</b>  | <b>0 m Noise</b> | <b>10<sup>-6</sup> m Noise</b> | <b>5×10<sup>-6</sup> m Noise</b> | <b>10<sup>-5</sup> m Noise</b> |
|--|------------------|--------------------------------|----------------------------------|--------------------------------|
| 1.91   | 1.81             | 2.04                           | 2.22                             | 1.53                           |
| 1.82   | 1.68             | 1.99                           | 2.39                             | 2.42                           |
| 1.61   | 1.58             | 1.91                           | 2.03                             | 1.50                           |
| 1.66   | 1.61             | 1.88                           | 1.95                             | 1.50                           |
| 1.78   | 1.85             | 2.16                           | 2.63                             | 2.81                           |
| <b>Frequency (Hz)<br/>(High Mode, Front)</b> | <b>0 m Noise</b> | <b>10<sup>-6</sup> m Noise</b> | <b>5×10<sup>-6</sup> m Noise</b> | <b>10<sup>-5</sup> m Noise</b> |
| 11.27  | 11.54            | 12.83                          | 13.10                            | 10.12                          |
| 12.35  | 12.92            | 10.20                          | 17.02                            | 16.21                          |
| 11.27  | 11.94            | 12.03                          | 13.61                            | 18.27                          |
| 12.06  | 12.71            | 13.94                          | 14.12                            | 19.16                          |
| 11.44  | 10.92            | 13.17                          | 13.94                            | 16.21                          |

**Table 8.10 Front Axle Damping Ratio Estimates (Deflection Objective Function)**

| <b>Damping (%)<br/>(Low Mode, Front)</b>  | <b>0 m Noise</b> | <b>10<sup>-6</sup> m Noise</b> | <b>5×10<sup>-6</sup> m Noise</b> | <b>10<sup>-5</sup> m Noise</b> |
|---|------------------|--------------------------------|----------------------------------|--------------------------------|
| 7.2                                       | 6.7              | 7.8                            | 5.6                              | 5.0                            |
| 5.9                                       | 6.2              | 5.0                            | 7.8                              | 8.8                            |
| 6.2                                       | 5.7              | 5.4                            | 5.0                              | 7.9                            |
| 5.9                                       | 5.2              | 5.0                            | 6.9                              | 8.3                            |
| 6.6                                       | 5.7              | 6.0                            | 8.4                              | 9.4                            |
| <b>Damping (%)<br/>(High Mode, Front)</b> | <b>0 m Noise</b> | <b>10<sup>-6</sup> m Noise</b> | <b>5×10<sup>-6</sup> m Noise</b> | <b>10<sup>-5</sup> m Noise</b> |
| 29.7                                      | 25.7             | 19.9                           | 36.3                             | 37.3                           |
| 37.9                                      | 35.1             | 40.2                           | 52.8                             | 19.4                           |
| 27.1                                      | 23.8             | 36.1                           | 36.2                             | 40.6                           |
| 24.8                                      | 26.7             | 19.6                           | 33.8                             | 37.7                           |
| 27.6                                      | 29.7             | 38.5                           | 41.0                             | 40.6                           |

**Table 8.11 Rear Axle Frequency Estimates (Deflection Objective Function)**

| <b>Frequency (Hz)<br/>(Low Mode, Rear)</b>  | <b>0 m Noise</b> | <b>10<sup>-6</sup> m Noise</b> | <b>5×10<sup>-6</sup> m Noise</b> | <b>10<sup>-5</sup> m Noise</b> |
|---|------------------|--------------------------------|----------------------------------|--------------------------------|
| 1.91  | 1.72             | 1.51                           | 2.31                             | 2.72                           |
| 2.04  | 1.81             | 1.65                           | 2.89                             | 1.50                           |
| 1.53  | 1.61             | 1.77                           | 1.50                             | 2.62                           |
| 2.35  | 2.01             | 2.83                           | 2.91                             | 1.50                           |
| 1.87  | 1.62             | 1.58                           | 2.24                             | 2.39                           |
| <b>Frequency (Hz)<br/>(High Mode, Rear)</b> | <b>0 m Noise</b> | <b>10<sup>-6</sup> m Noise</b> | <b>5×10<sup>-6</sup> m Noise</b> | <b>10<sup>-5</sup> m Noise</b> |
| 11.27                                       | 13.02            | 14.02                          | 16.10                            | 18.26                          |
| 16.72                                       | 15.87            | 15.29                          | 15.00                            | 12.71                          |
| 11.26                                       | 10.92            | 13.92                          | 17.27                            | 17.01                          |
| 18.74                                       | 18.95            | 16.96                          | 15.20                            | 12.84                          |
| 13.34                                       | 12.15            | 10.07                          | 10.51                            | 22.86                          |

**Table 8.12 Rear Axle Damping Ratio Estimates (Deflection Objective Function)**

| <b>Damping (%)<br/>(Low Mode, Rear)</b>  | <b>0 m Noise</b> | <b>10<sup>-6</sup> m Noise</b> | <b>5×10<sup>-6</sup> m Noise</b> | <b>10<sup>-5</sup> m Noise</b> |
|--|------------------|--------------------------------|----------------------------------|--------------------------------|
| 7.2                                      | 7.7              | 6.1                            | 5.4                              | 9.5                            |
| 5.9                                      | 4.9              | 6.3                            | 7.5                              | 8.1                            |
| 6.2                                      | 6.8              | 7.0                            | 8.3                              | 8.6                            |
| 5.9                                      | 6.1              | 6.8                            | 5.0                              | 5.0                            |
| 6.6                                      | 6.2              | 5.0                            | 7.5                              | 7.7                            |
| <b>Damping (%)<br/>(High Mode, Rear)</b> | <b>0 m Noise</b> | <b>10<sup>-6</sup> m Noise</b> | <b>5×10<sup>-6</sup> m Noise</b> | <b>10<sup>-5</sup> m Noise</b> |
| 27.6                                     | 24.6             | 30.1                           | 34.6                             | 39.5                           |
| 16.7                                     | 17.9             | 19.7                           | 14.2                             | 10.6                           |
| 27.1                                     | 28.7             | 22.6                           | 20.7                             | 38.3                           |
| 37.9                                     | 35.1             | 34.8                           | 45.8                             | 18.6                           |
| 29.7                                     | 28.3             | 18.8                           | 23.7                             | 17.4                           |

## 8.6 Chapter Conclusions

In this chapter, we describe the identification of truck parameters using the dynamic truck and static bridge models. The deflection of the beam under each axle is calculated using the static beam bending expressions and is used as the input into the

system of equations of each quarter-car truck model. The truck equations are then integrated over time to determine the truck's motion and the beam deflection at the sensor locations. Inside the optimization routine, an approximate truck force model is developed that is the superposition of each axle's static weight, homogeneous solution, and the effect of the bridge interaction. The homogeneous solution is a superposition of two damped oscillatory modes for each axle. The amplitudes, phases, damping ratios and natural frequencies of each mode are unknown optimization parameters identified by the algorithm. The interaction term is the truncated series solution of the beam bending equation. Two weighting parameters are used as optimization parameters to determine the magnitude of the interaction effects.

The truck configurations used to test the identification routine are given in truck numbers 1, 7, 14, 16, and 18 in Table 3.2. They had front axle weights ranging from  $9.8 \times 10^4 \text{N}$  to  $1.5 \times 10^5 \text{N}$  and rear axle weights from  $9.8 \times 10^4 \text{N}$  to  $1.93 \times 10^5 \text{N}$ . The front and rear axles were given independent suspension properties as shown in Table 3.2. The lower modes of the axles had natural frequencies ranging from 1.6 Hz to 2.35 Hz and damping ratios from 5.1% to 12.1% of their critical damping. The high modes ranged in frequency from 11.2 Hz to 18.7 Hz and from 16.7% to 27.6% in damping ratio. A variety of initial conditions for each axle were also used.

The average and maximum magnitudes of the percent error in axle weights are given in Tables 8.7 and 8.8. For zero measurement noise, the error in axle weight estimates remained below 0.018%. With measurement noise of  $\pm 1 \times 10^{-6} \text{m}$ , the error in axle weight remained below 0.25%, and for noise of  $\pm 5 \times 10^{-6} \text{m}$ , error was less than 1.3%.

Estimates of the natural frequencies and damping ratios of each axle were also made using the optimization routine. Tables 8.9-8.12 give the estimates of the high and low mode frequencies and damping ratio estimates for each truck examined. For zero measurement noise, the natural frequency of the low mode could be determined within 0.35 Hz, and the damping ratio could be determined within 0.9% of critical. The natural frequency of the high mode could be determined within 1.75 Hz and the damping ratio within 4% of critical. For measurement noise of  $\pm 5 \times 10^{-6}$  m, the natural frequency and damping ratio of the low mode could be determined with 0.5 Hz and 3% of critical. For the same noise level, the frequency of the high mode could be determined within 9.5 Hz and the damping ratio within 11%. With measurement noise of  $\pm 1 \times 10^{-5}$  m, the natural frequency and damping ratio of the low mode could be determined within 1.15 Hz and 10% of critical. The frequency of the high mode could be determined within 9.5 Hz and the damping ratio within 20%. Axle spacing was again determined very accurately for all noise levels.

# Chapter 9

## Dynamic Bridge/Dynamic Truck

Finally, we treat the main problem of this dissertation. In this chapter, the use of the dynamic bridge and dynamic truck models to simulate and identify the truck is discussed. The identification procedure uses the same optimization routine described in previous chapters, but the models are both dynamic. The dynamic beam model described in Chapter 2 is used to model the bridge, and the quarter-car model described in Chapter 3 is used to represent the truck. The interaction between the two models is included in both the initial simulation of the system and in the method to identify the truck parameters. The assumption that the truck's total time on the bridge is known still applies and is used to calculate speed from the axle spacing.

### 9.1 Simulating the Truck and Bridge-Full Model

In this chapter, the bridge is modeled using the finite element model, including inertial effects, described in Chapter 2. Each axle of the truck is modeled as a quarter-car as described in Chapter 3. The interaction due to each axle's contact with the bridge is included in the simulation. The equations of motion for the coupled bridge/truck system are derived in Chapter 4 and are restated here for clarity. All quantities are defined in section 4.8 of this work.

$$\begin{bmatrix} \dot{\bar{x}}_B \\ \dot{\bar{x}}_T \end{bmatrix} = \begin{bmatrix} \mathbf{A}_B - \mathbf{B}_B(t)\mathbf{K}_u\mathbf{C}(\mathbf{x}_1, \mathbf{x}_2) & \mathbf{B}_B(t)\mathbf{K}_u\mathbf{B}_u \\ \mathbf{B}_T\mathbf{C}(\mathbf{x}_1, \mathbf{x}_2) & \mathbf{A}_T \end{bmatrix} \begin{bmatrix} \bar{x}_B \\ \bar{x}_T \end{bmatrix} + \begin{bmatrix} \mathbf{B}_B(t) \\ \mathbf{0}_{8 \times 2} \end{bmatrix} \overline{W} \quad (9.1)$$

These equations of motion include the interaction between the truck and the bridge and are integrated in three time intervals to yield the deflection profiles of the bridge. The three time intervals result from the three force conditions due to the entrance and exit of each axle. The truck is given some initial conditions to represent the roughness at the entrance to the bridge. Different sets of initial conditions are used to test the optimization routine's ability to determine them. Three deflection measurement locations are selected on the beam. They are located at the midpoint, quarter-point, and three-quarter-point ( $x=L/2, L/4, 3L/4$ ).

A sample midpoint deflection profile of the dynamic bridge/dynamic truck coupled system is shown below in Figure 9.1. It is compared to a static bridge/static truck profile due to a truck of the same axle weights. From the figure, it is obvious that the static beam bending due to the static weight of the truck is the primary component of the deflection profile, but the bridge and truck dynamics contribute a great deal as well. The first natural frequency of the beam is approximately 2.5 Hz. The axles used in Figure 9.1 both have their first mode at 1.9 Hz.

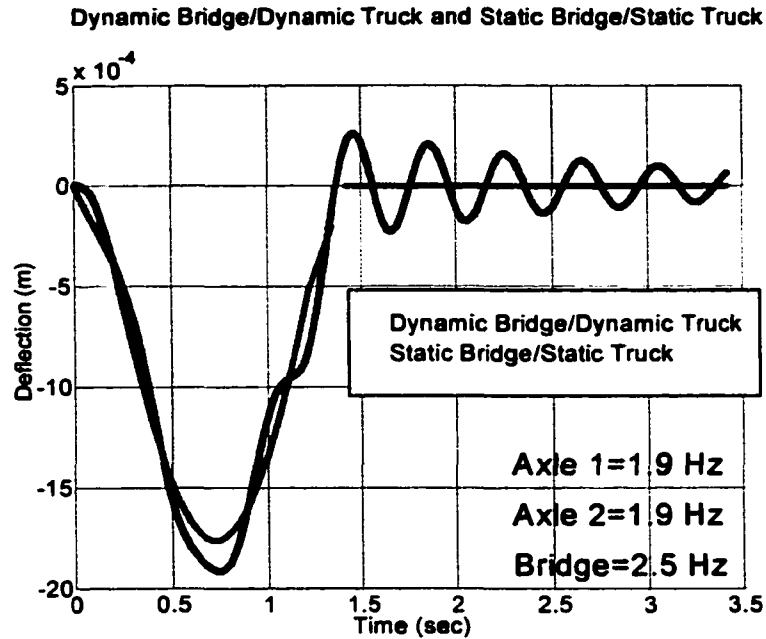


**Figure 9.1 Dynamic Bridge/Dynamic Truck and Static Bridge/Static Truck Deflection Profiles  
(different bridge and truck frequencies)**

Another sample midpoint deflection profile is shown in Figure 9.2. This one also shows a dynamic bridge/dynamic truck profile and a static bridge/static truck profile for a truck of the same static weight, but the natural frequencies of the axles are different than in Figure 9.1. In Figure 9.1, the natural frequencies of the axles are relatively far from the natural frequency of the bridge. In Figure 9.2, the natural frequency of the rear axle is 2.5 Hz, which is equal to the first mode of the bridge. Since the driving force of the rear axle is near the first mode of the bridge, the dynamic response of the beam is greater than in Figure 9.1, where the bridge and truck frequencies are not as close together. These two figures are shown to illustrate the effect of the dynamic coupling between the bridge and the truck and its influence on the deflection profiles. It should be noted that the natural decay of the free vibration of the bridge is not included in the deflection profiles used in

the optimization routine. The times at which the free vibration begins correspond to the times at which the truck exits the bridge.

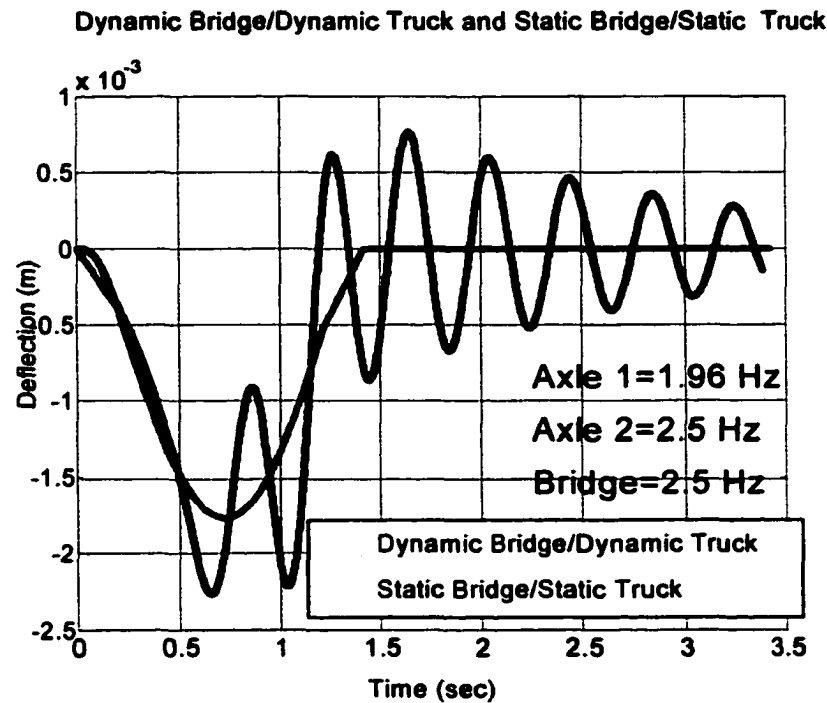


**Figure 9.2 Dynamic Bridge/Dynamic Truck and Static Bridge/Static Truck Deflection Profiles  
(truck and bridge frequencies close together)**

## 9.2 Approximate Force Model

As in the static bridge/dynamic truck case described in Chapter 8, we develop an approximate model for the force due to the truck. In the case of the static beam, the solution of the differential equation of motion is found easily and used to approximate the effect of the interaction. Such a solution is not apparent for the dynamic bridge/dynamic truck case. Like the static bridge case, the solution for the dynamic bridge subject to a moving point force can be found, but it does not include the coupling between the bridge and the truck. In the static bridge case, an approximation of the interaction force is accurate enough to approximate the force, but this is not the case for the dynamic bridge.

As shown in Figure 9.1 and Figure 9.2, because the truck and the bridge can have similar natural frequencies, the interaction is quite important. Therefore, the force due to the truck has to be found using a more direct method.

In the dynamic bridge/dynamic truck case, it is assumed that the truck has a homogeneous solution with two damped oscillatory modes as discussed previously. Since no approximate solution for the dynamic bridge deflection can be obtained, it is necessary to integrate the differential equations of motion for the bridge to obtain the deflection profiles inside the optimization routine. The driving force due to the bridge deflection is found directly during the integration of the differential equations through the direct integration of the truck differential equations as well.

The need to directly integrate the differential equations of motion of the truck presents a new problem. It is desirable to keep the number of optimization parameters as small as possible, and the truck system has many unknowns. The stiffnesses, damping ratios, and masses in the quarter-car model are all unknown, as are the initial conditions of the truck as it entered the bridge. Having had good success with the assumption of a homogeneous solution to the truck equations, we decide to stay with this method. The homogeneous solution of the unsprung mass motion of each axle is given in Chapter 3 and is repeated here.

$$\begin{aligned}Xu_1 &= A_{11}e^{-\alpha_{11}(t-t_1)}\sin(\beta_{11}(t-t_1)+\phi_{11})+A_{12}e^{-\alpha_{12}(t-t_1)}\sin(\beta_{12}(t-t_1)+\phi_{12}) \\Xu_2 &= A_{21}e^{-\alpha_{21}(t-t_2)}\sin(\beta_{21}(t-t_2)+\phi_{21})+A_{22}e^{-\alpha_{22}(t-t_2)}\sin(\beta_{22}(t-t_2)+\phi_{22})\end{aligned}\tag{9.2}$$

Although they are expressed in terms of different parameters, the homogeneous solution in Equation (9.2) and the state matrices given in Equations (3.5-3.6e), which are

in terms of the stiffness, damping, and mass of the quarter-car model, describe the same system. The parameters in Equation (9.2) are found in the optimization routine, but the physical parameters of the truck are not. Thus, to write the truck's system of equations, a transformation of the differential equations in terms of the parameters in Equation (9.2) is needed. The state matrices resulting from this transformation are discussed in Chapter 3, but are given again here.

$$\mathbf{A}_T = \begin{bmatrix} \mathbf{0}_{2 \times 2} & \mathbf{I}_{2 \times 2} \\ -\theta_1^2 & \theta_1^2 & -2\sigma_1 & 2\sigma_1 \\ \theta_1^2 \frac{\sigma_2}{\sigma_1} & -\theta_2^2 & 2\sigma_2 & -2\sigma_2 \end{bmatrix} \text{ and } \mathbf{B}_T = \begin{bmatrix} \mathbf{0}_{3 \times 1} \\ \theta_2^2 & -\theta_1^2 \frac{\sigma_2}{\sigma_1} \end{bmatrix} \quad (9.3)$$

The variables  $\theta$  and  $\sigma$  are defined in Chapter 3, but are all given in terms of the  $\alpha$ 's and  $\beta$ 's in Equation (9.2). This transformation allows the assumption of the homogeneous solution in Equation (9.2), but still allows the state matrices of the truck to be formed and used in the integration routine.

The coupled differential equations of the bridge/truck system are stated below. Their derivation is given in Chapter 4. The state matrices of the truck  $A_T$  and  $B_T$  are in the transformed form in Equation (9.3).

$$\begin{bmatrix} \dot{\bar{x}}_B \\ \dot{\bar{x}}_T \end{bmatrix} = \begin{bmatrix} \mathbf{A}_B - \mathbf{B}_B(t)\mathbf{K}\mathbf{u}\mathbf{C}(x_1, x_2) & \mathbf{B}_B(t)\mathbf{K}\mathbf{u}\mathbf{B}_u \\ \mathbf{B}_T\mathbf{C}(x_1, x_2) & \mathbf{A}_T \end{bmatrix} \begin{bmatrix} \bar{x}_B \\ \bar{x}_T \end{bmatrix} + \begin{bmatrix} \mathbf{B}_B(t) \\ \mathbf{0}_{8 \times 2} \end{bmatrix} \bar{F}(t) \quad (9.4)$$

The term  $\bar{F}(t)$  is the sum of the total axle weight and the homogeneous solution given in Equation (9.2). This expression is given below.

$$\bar{F}(t) = \begin{bmatrix} -W_1 \\ -W_2 \end{bmatrix} + \mathbf{K}\mathbf{u} \begin{bmatrix} xu_1(t) \\ xu_2(t) \end{bmatrix} \quad (9.5)$$

The truck is given zero initial conditions in this integration routine since the initial conditions are incorporated into the homogeneous solution  $xu(t)$ . The coupled system of equations is then integrated over time to obtain the deflection profiles to be used in the optimization routine.

### **9.3 WIM Algorithm**

The bridge WIM algorithm consists of three parts. First, an initial estimate of each of the optimization parameters is made. The midpoint between the upper and lower bounds of each of the optimization parameters given in Table 8.1 are used as the starting point. These parameters are the unknowns in approximate truck force model, which is the superposition of the static axle weights and the homogeneous solution given in Equation (9.2). The transformed truck system in Equation (3.11) is made up of these estimated values of the unknowns and is combined with the bridge system in Equation (9.4) and integrated over time. From this integration, the deflection profiles at each sensor location are found and compared to the measured profiles. The objective function is made up of the sum of the differences in the estimated and measured profiles. At each iteration of the optimization routine, the optimization parameters are varied to obtain the smallest value of the objective function. Each truck case requires approximately 7,000 iterations, and each iteration requires approximately five seconds to integrate the bridge/truck equations.

### **9.4 Parameter Identification**

To identify the truck parameters, the optimization routine discussed previously is again used to minimize the difference between the measured and estimated deflection

profiles. Three measurements are made at the midpoint, quarter-point, and three-quarter-point of the beam and used to formulate the objective function. The optimization parameters and their upper and lower bounds are given in Table 8.1 of Chapter 8 with a few omissions. The parameters  $A_{ij}$  and  $A_{ji}$  are not needed since they referred only to the approximation of the interaction between the truck and the bridge. Since this interaction is calculated directly, there is no need for these parameters. We determined through the course of this work that an expression for  $ku$  could be found in terms of existing optimization parameters, which would reduce the number per axle by one more. This expression comes from the manipulation of the transformation discussed in Chapter 4 and is given by

$$ku_i = W_i \left( \theta_1^2 - \theta_2^2 \frac{\sigma_2}{\sigma_1} \right) \quad (9.6)$$

The relationship between speed and axle spacing discussed in previous chapters and given in Equation (5.8) is also used to eliminate speed as an optimization parameter. Therefore, the total number of optimization parameters for both axles, including axle spacing is 19. The objective function is the least-squares difference between the three measured and estimated deflection profiles described in Chapter 8.

The optimization routine is tested using the various truck configurations given in Chapter 3. These configurations are chosen to cover a wide range of truck types. The upper limit on the number of iterations performed by the optimization routine is set high enough that the routine is certain to converge before it performs the maximum number of iterations. It is found that the optimization routine typically converges after approximately 1,000 iterations, so the maximum number of iterations was set at 5,000.

The optimization procedure is repeated for three levels of measurement noise of  $\pm 10^{-6}m$ ,  $10^{-5}m$ , and  $10^{-4}m$  for each truck configuration.

### 9.5 Optimization Results

The error found in the optimization parameters is very small ( $\sim 10^{-2}\%$  for all parameters) for zero measurement noise. The average magnitude of the percent error in axle weight estimates for each of the noise levels is given below in Table 9.1. As in the previous chapters, this average is the average of the magnitude of the percent error.

**Table 9.1 Average Error in Axle Weights Using Unlimited Optimization Iterations**

| Parameter         | 0 Noise | $10^{-6} m$ Noise | $10^{-5} m$ Noise | $10^{-4} m$ Noise |
|-------------------|---------|-------------------|-------------------|-------------------|
| Front Axle Weight | 0.007%  | 0.029%            | 0.391%            | 1.144%            |
| Rear Axle Weight  | 0.005%  | 0.024%            | 0.604%            | 1.146%            |

The figures below show estimates of the axle weights for trucks 1-10 in Table 3.2.

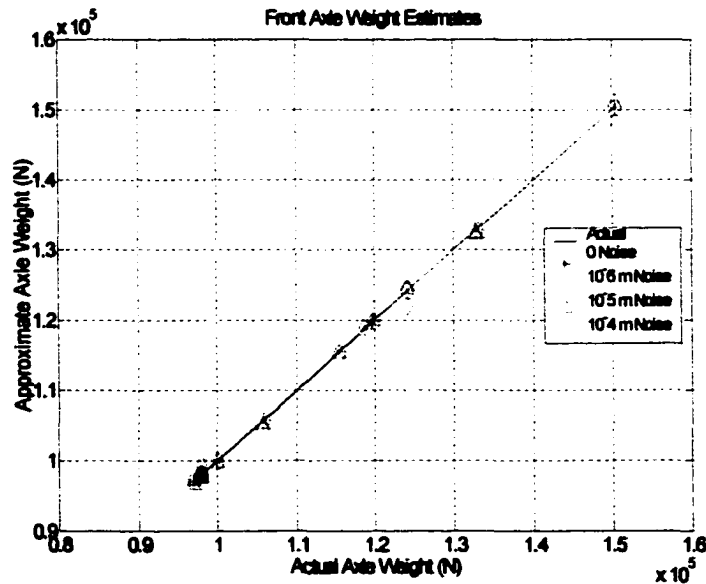


**Figure 9.3 Front Axle Weight Estimates With Noise (Trucks 1-20)**

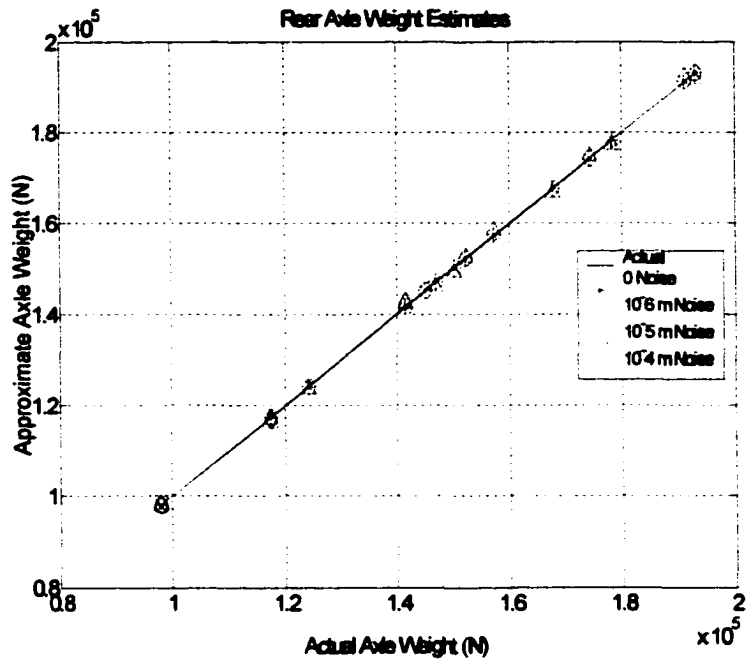


Figure 9.4 Rear Axle Weight Estimates With Noise (Trucks 1-20)

The percent error in each of the axle weight estimates are shown in the figures below. In Figures 9.5-9.12, the x-axis is the truck case number of the twenty trucks given in Table 3.2. The y-axis is the percent error in axle weight estimates of each of the trucks.

### Percent Error in Front Axle Weights

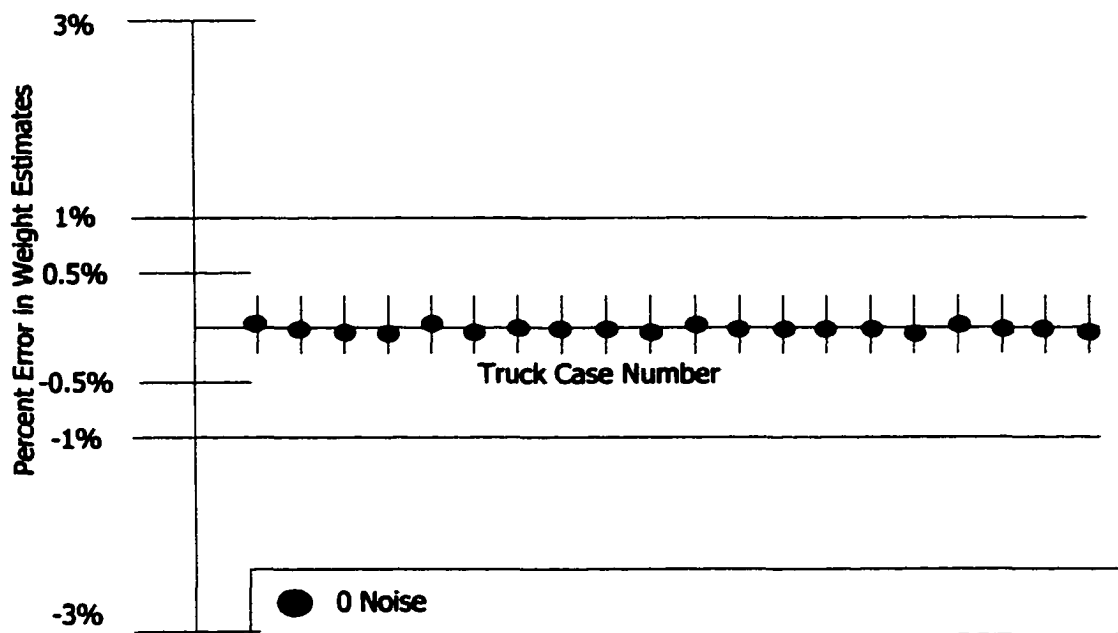


Figure 9.5 Percent Error in Front Axle Weight (a)

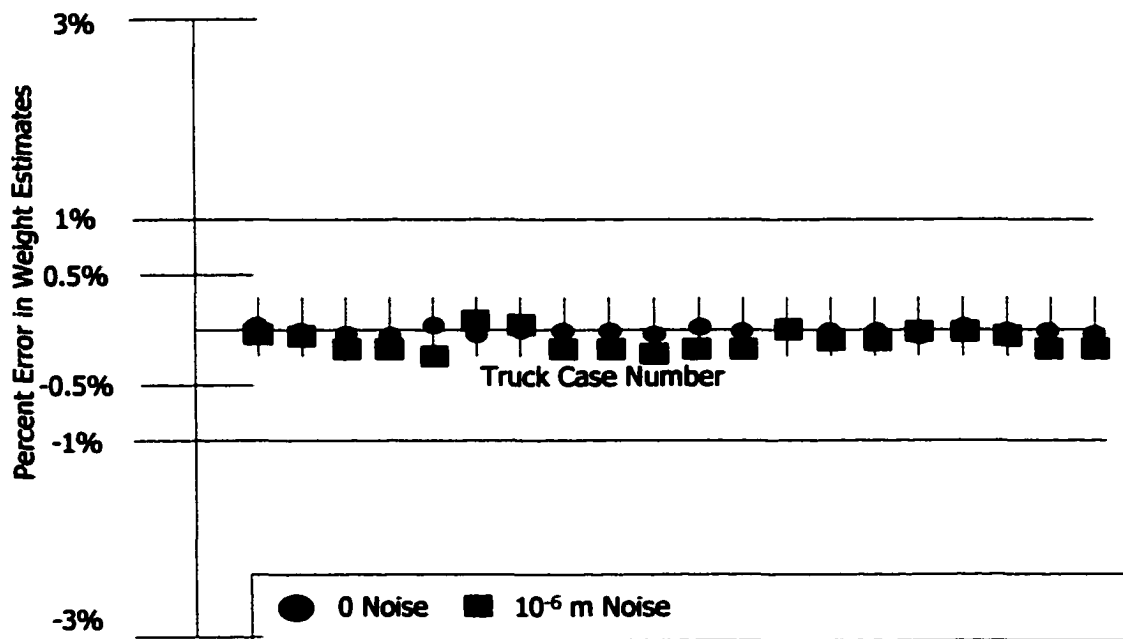


Figure 9.6 Percent Error in Front Axle Weight (b)

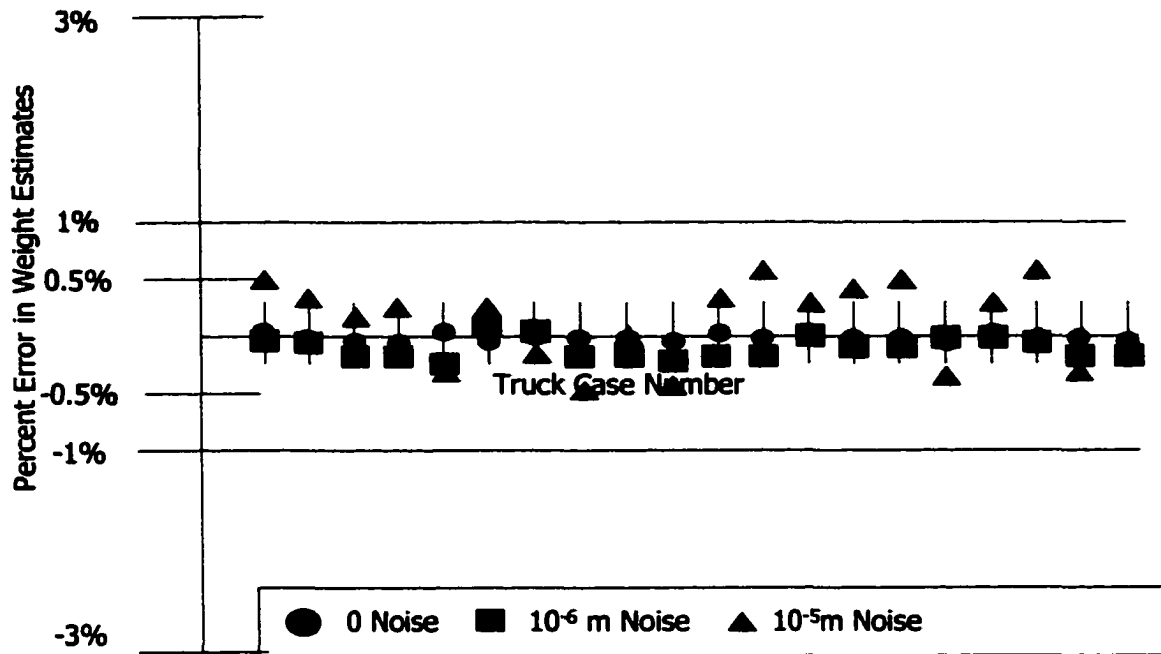


Figure 9.7 Percent Error in Front Axle Weight (c)

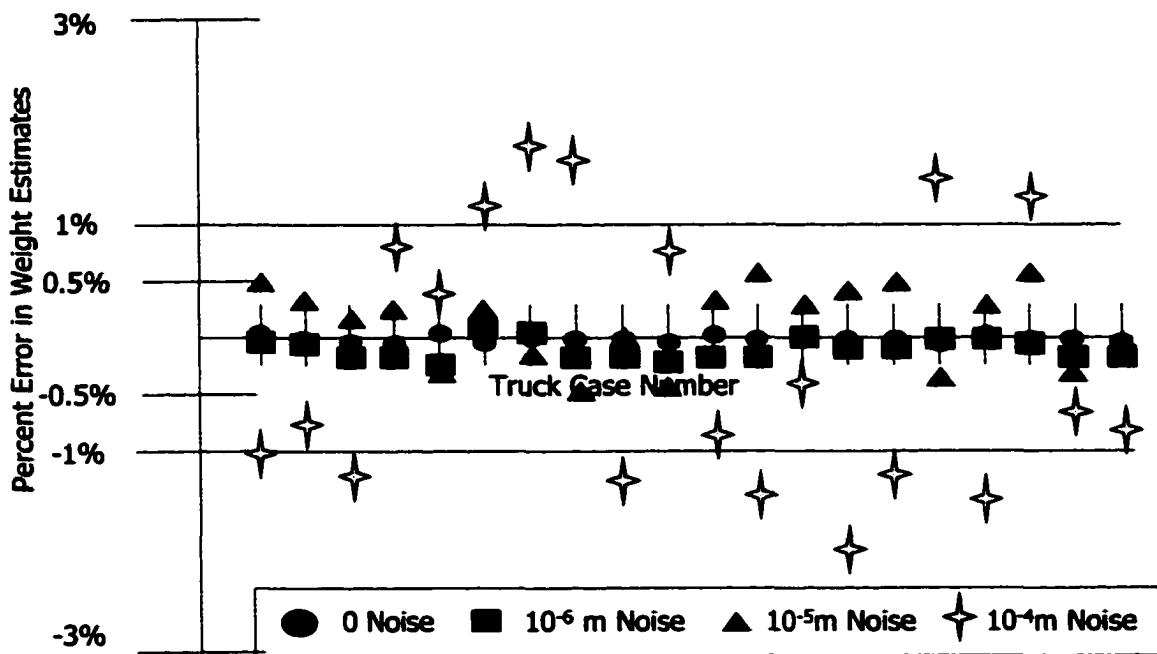


Figure 9.8 Percent Error in Front Axle Weight (d)

### Percent Error in Rear Axle Weight

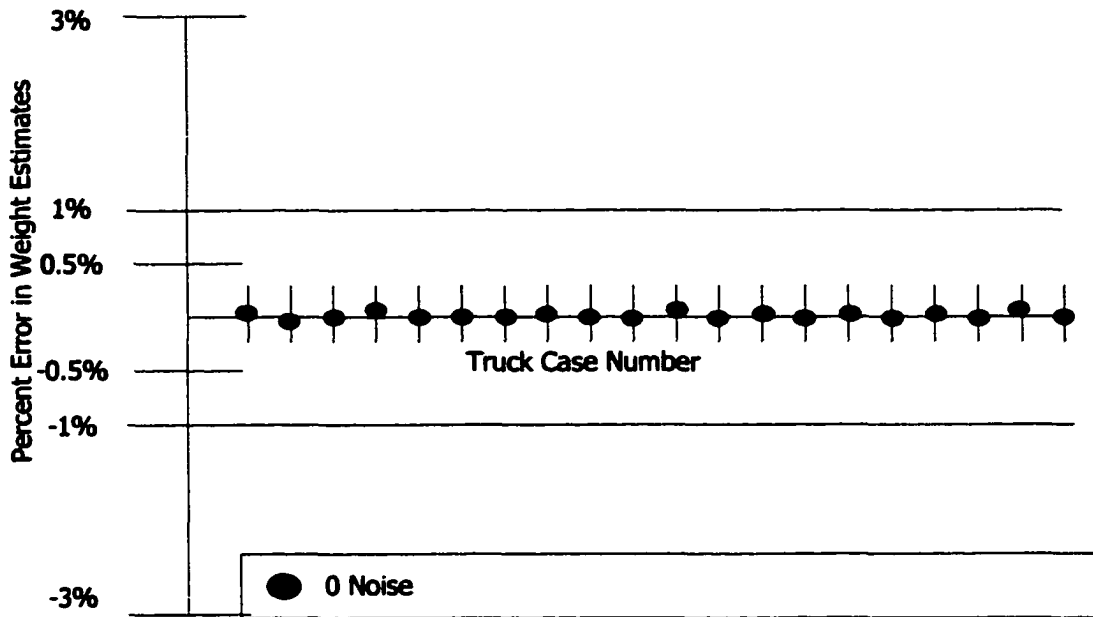


Figure 9.9 Percent Error in Rear Axle Weight (a)

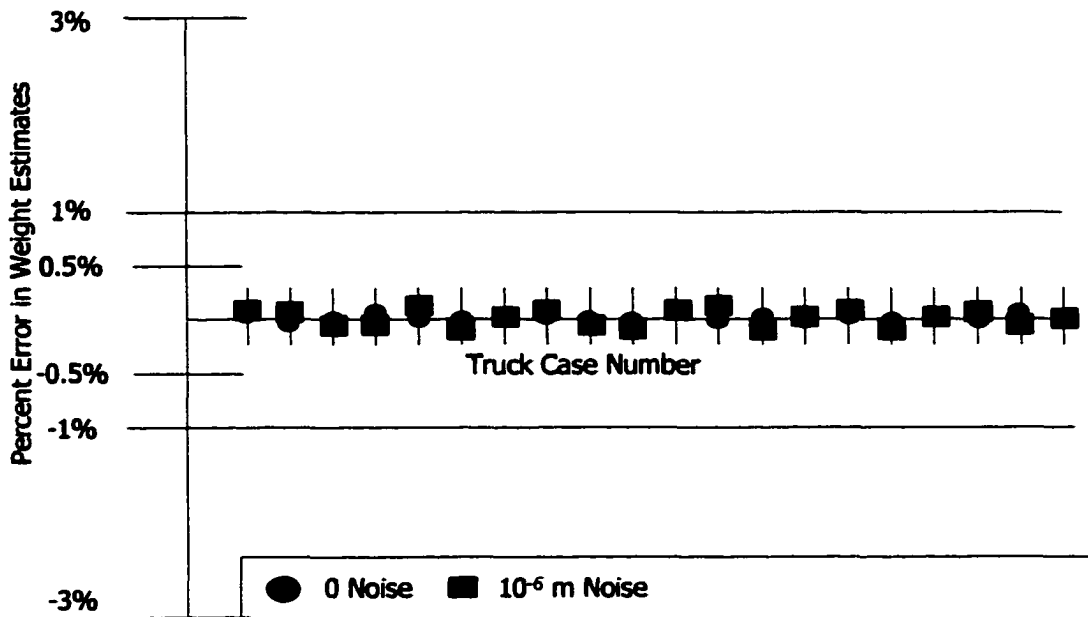


Figure 9.10 Percent Error in Rear Axle Weight (b)

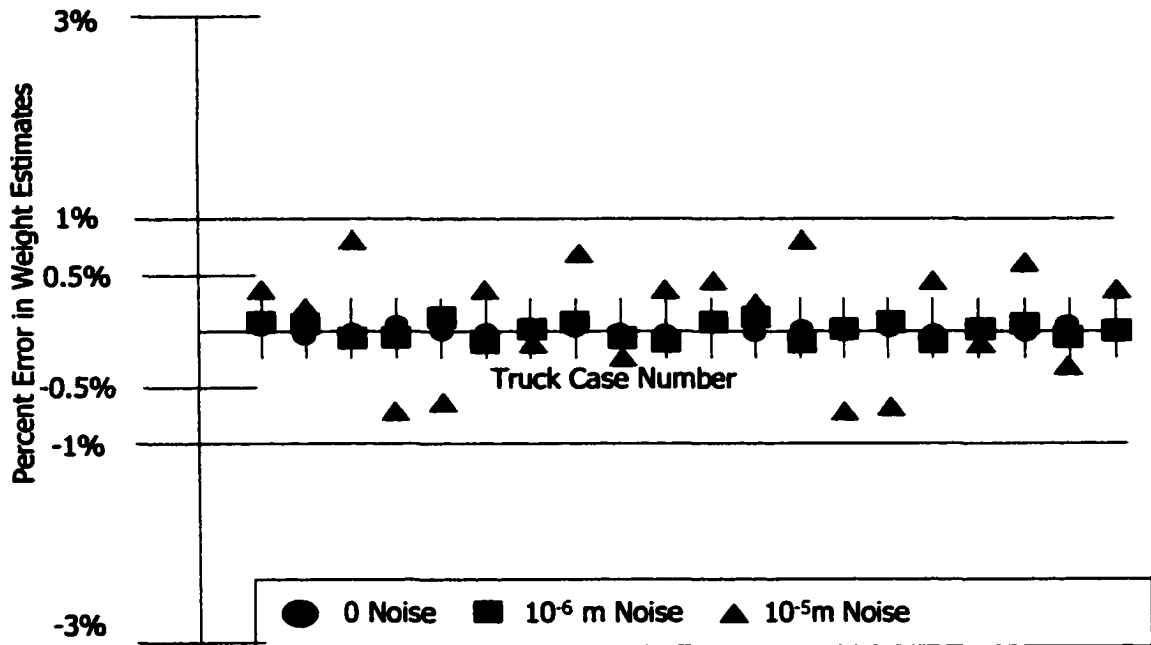


Figure 9.11 Percent Error in Rear Axle Weight (c)

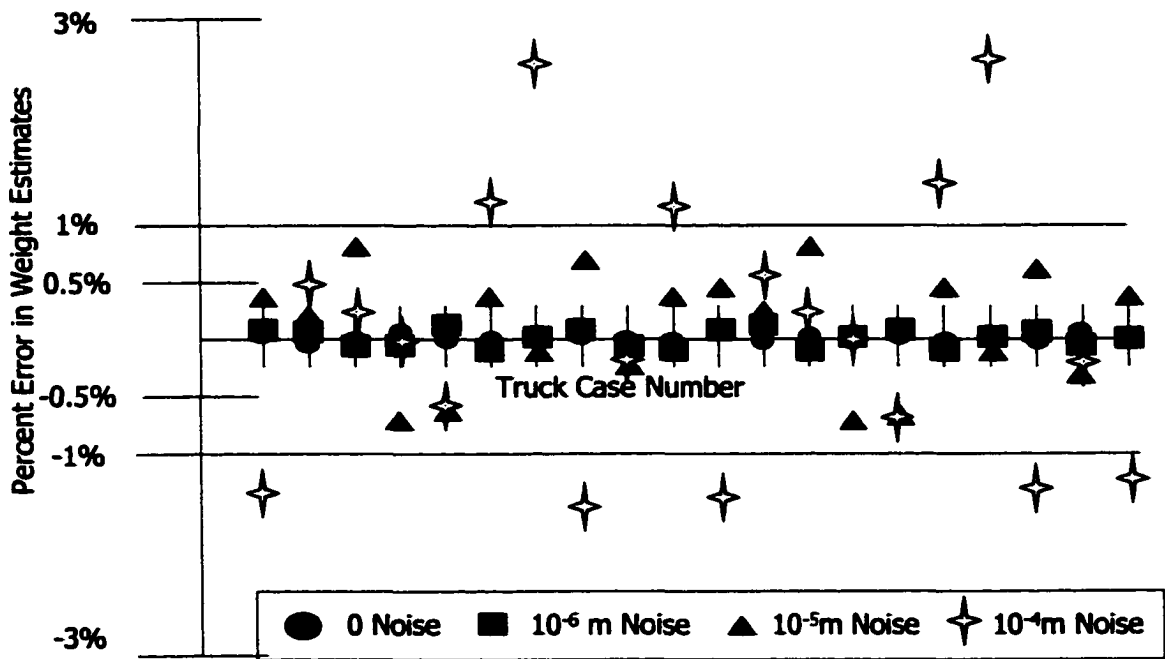


Figure 9.12 Percent Error in Rear Axle Weight (d)

Although they are not the primary focus of this work, the other parameters relating to the dynamic properties of the truck are also estimated very accurately. In the following section, the parameter estimates for the different truck configurations with varying noise levels are given. Figures showing the true and estimated values of the natural frequency and damping ratio for each mode of each axle are given below. In each of the figures, the x-axis represents the first ten truck case numbers in Table 3.2. The y-axis represents the frequency or damping ratio estimate of each truck. True values of these parameters are given in truck cases 1-10 in Table 3.2. Tables of the estimated truck parameters are then given to more clearly illustrate the numerical precision of this routine.

### Front Axle, Low Mode, Frequency Estimates

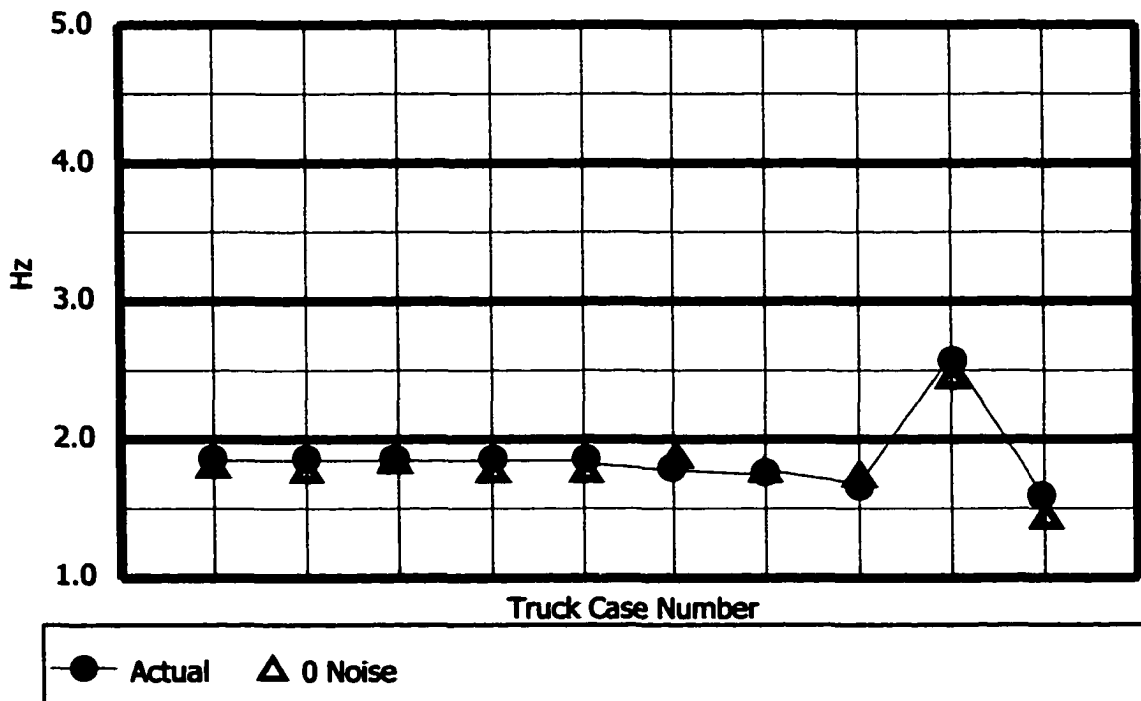


Figure 9.13 Front Axle, Low Mode, Frequency Estimate (a)

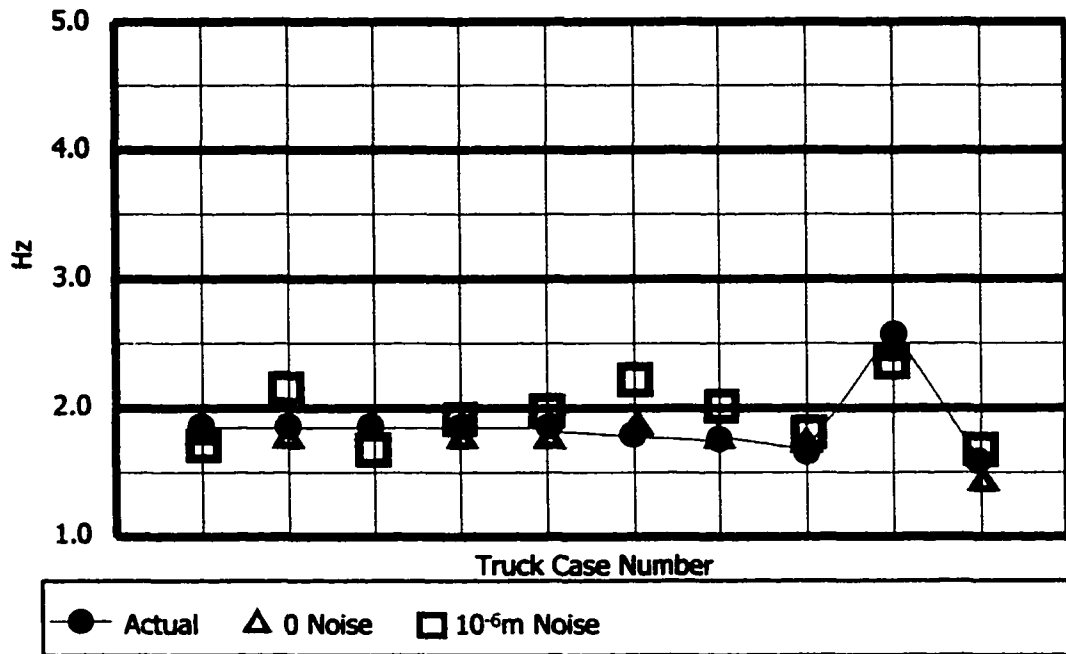


Figure 9.14 Front Axle, Low Mode, Frequency Estimate (b)

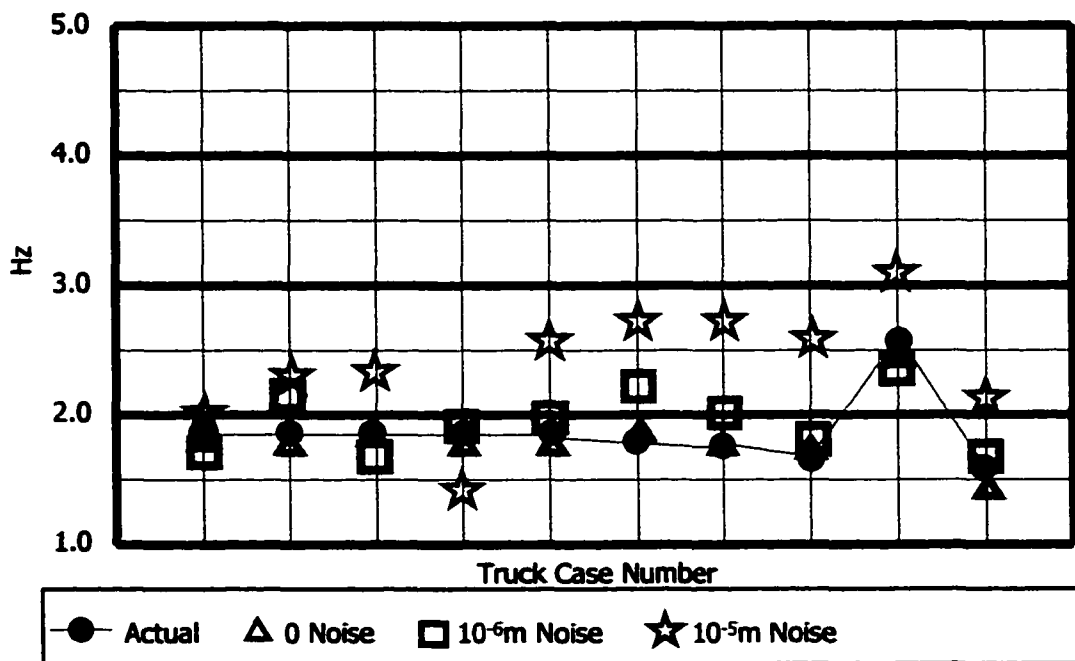


Figure 9.15 Front Axle, Low Mode, Frequency Estimate (c)

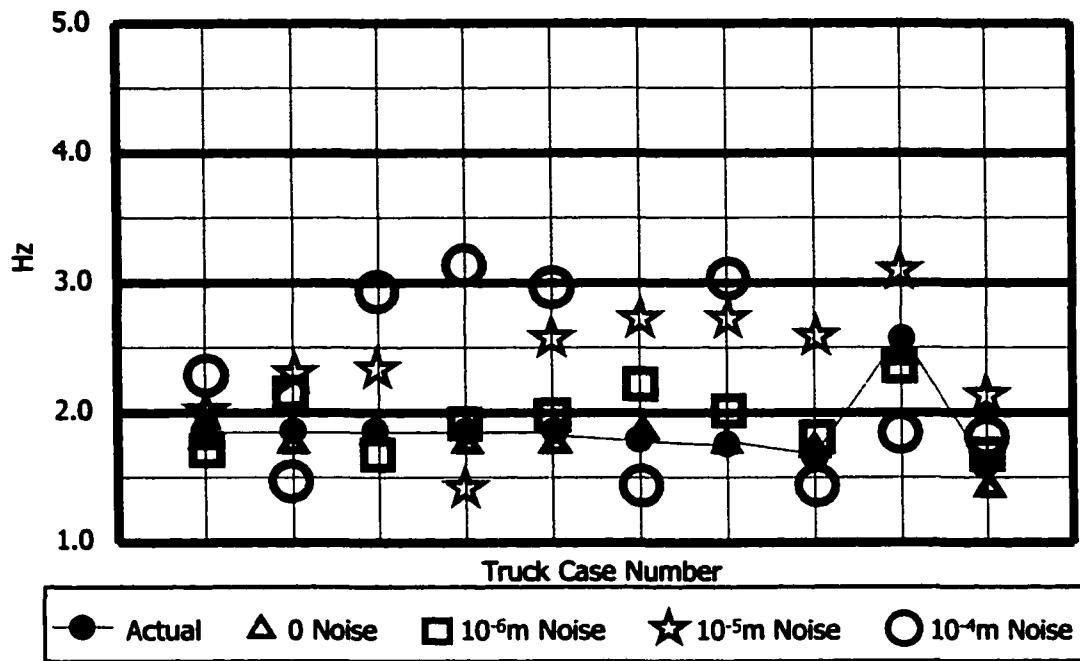


Figure 9.16 Front Axle, Low Mode, Frequency Estimate (d)

### Front Axle, Low Mode, Damping Ratio

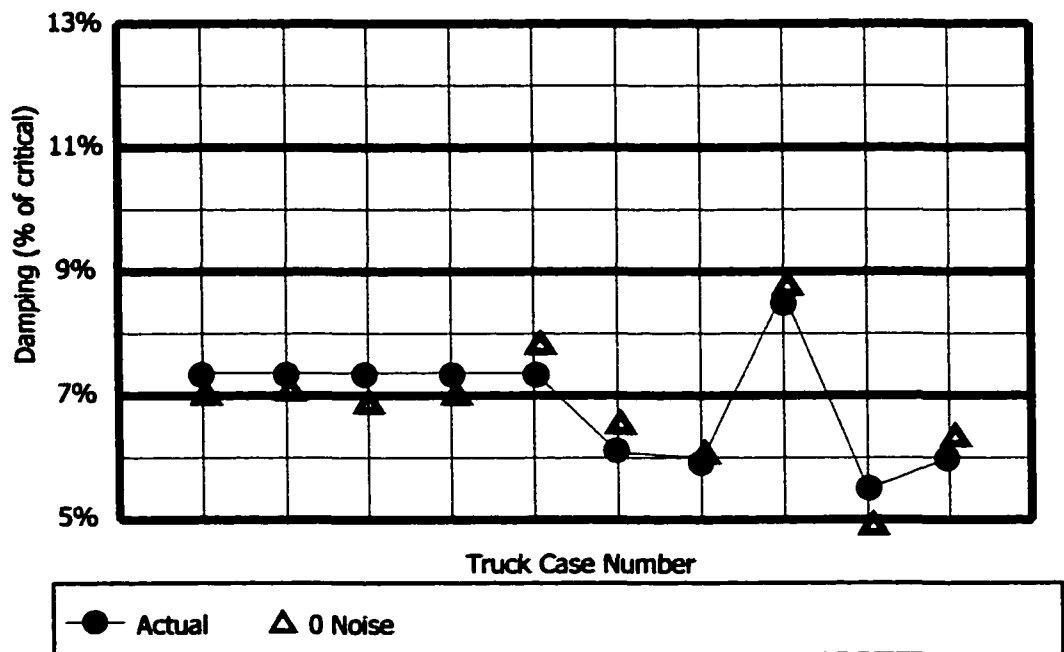


Figure 9.17 Front Axle, Low Mode, Damping Ratio Estimate (a)

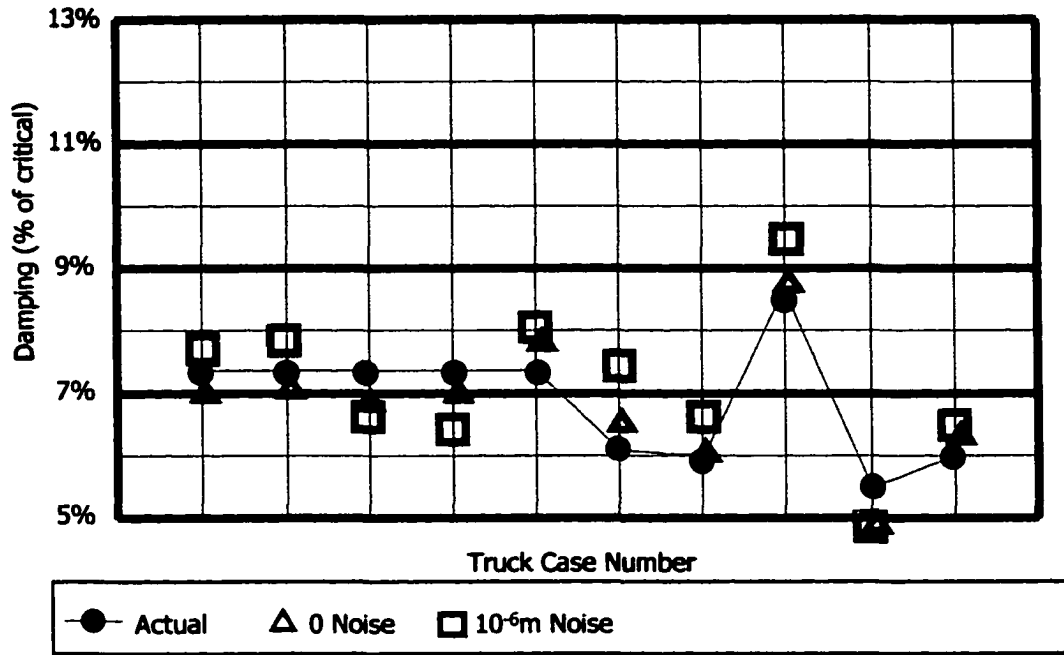


Figure 9.18 Front Axle, Low Mode, Damping Ratio Estimate (b)

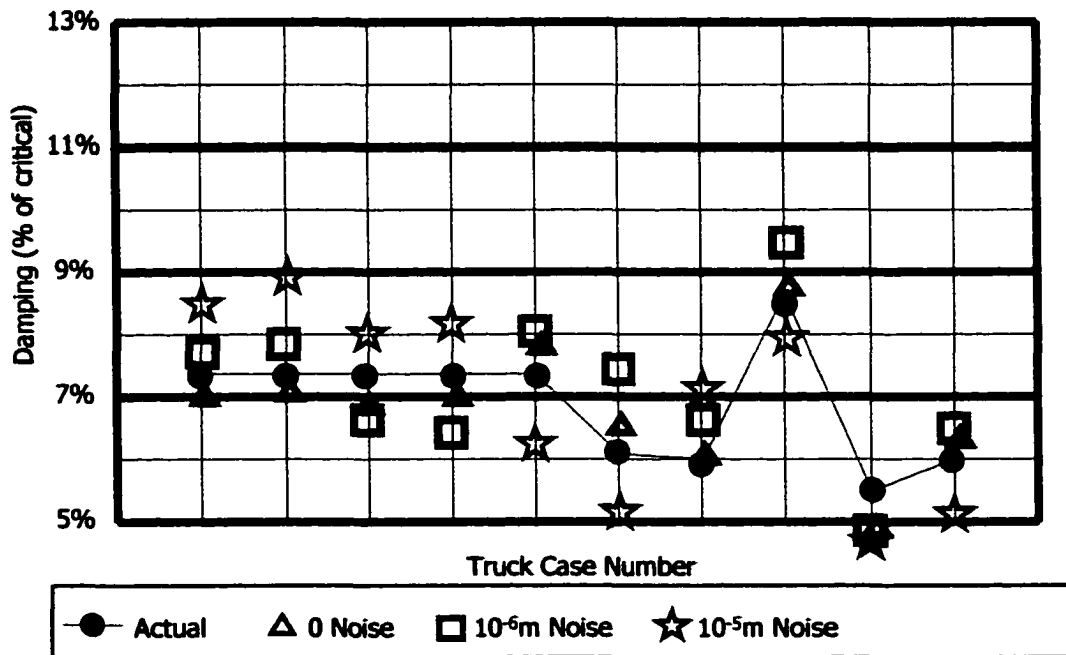


Figure 9.19 Front Axle, Low Mode, Damping Ratio Estimate (c)

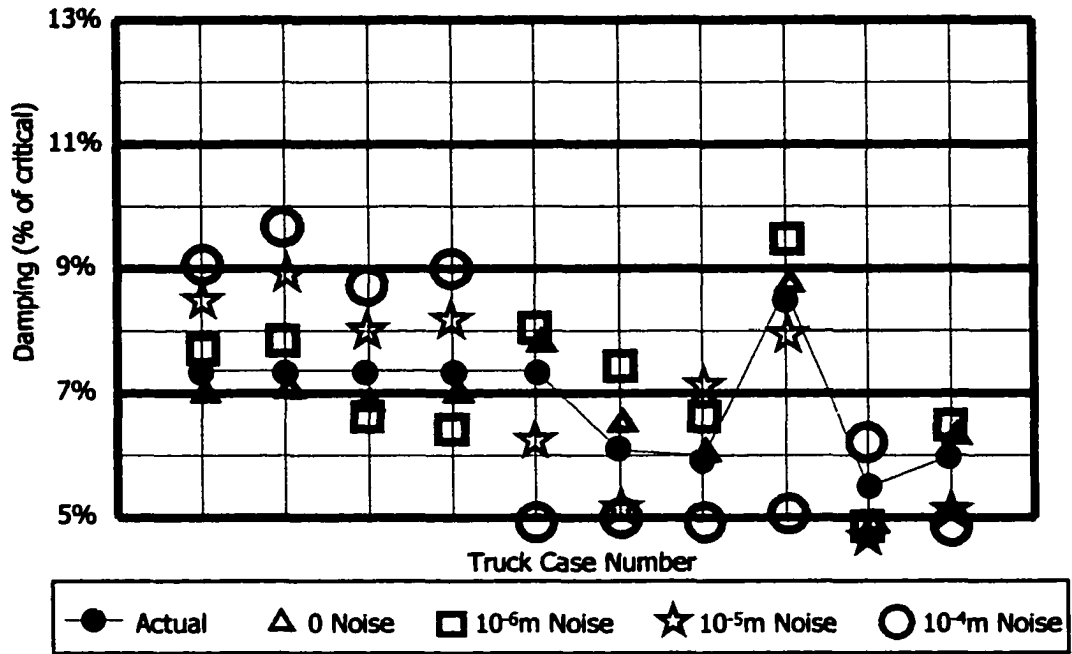


Figure 9.20 Front Axle, Low Mode, Damping Ratio Estimate (d)

### Front Axle, High Mode, Frequency Estimates

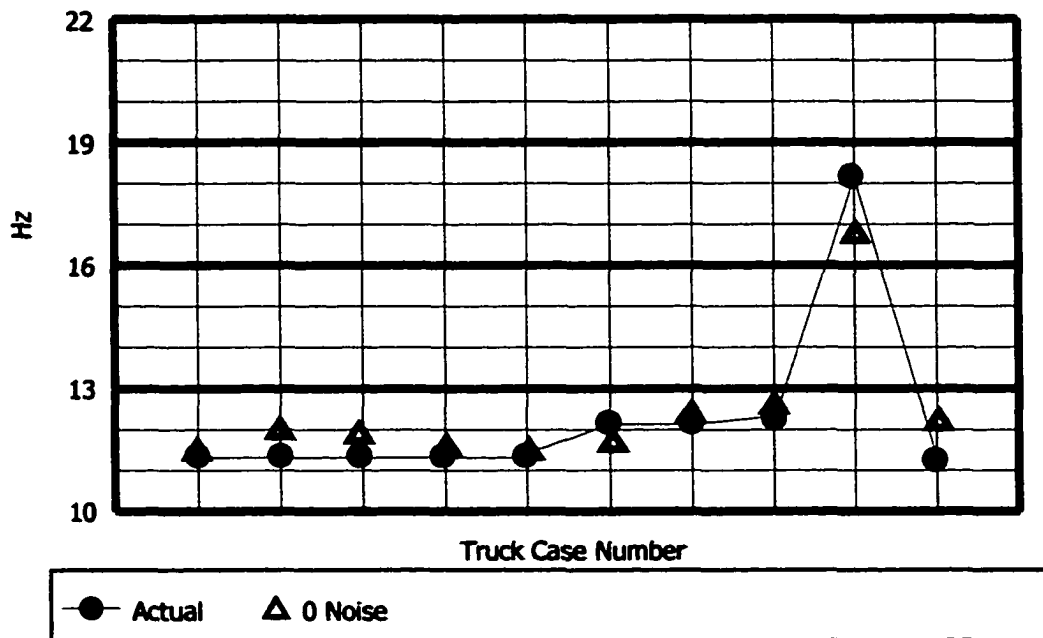


Figure 9.21 Front Axle, High Mode, Frequency Estimate (a)

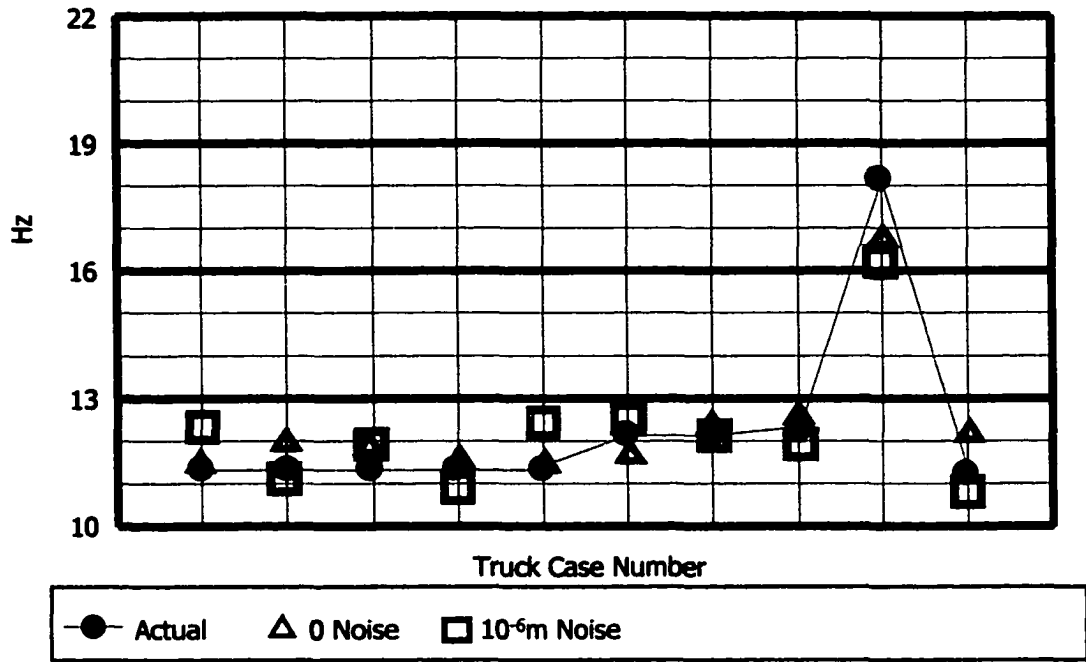


Figure 9.22 Front Axle, High Mode, Frequency Estimate (b)

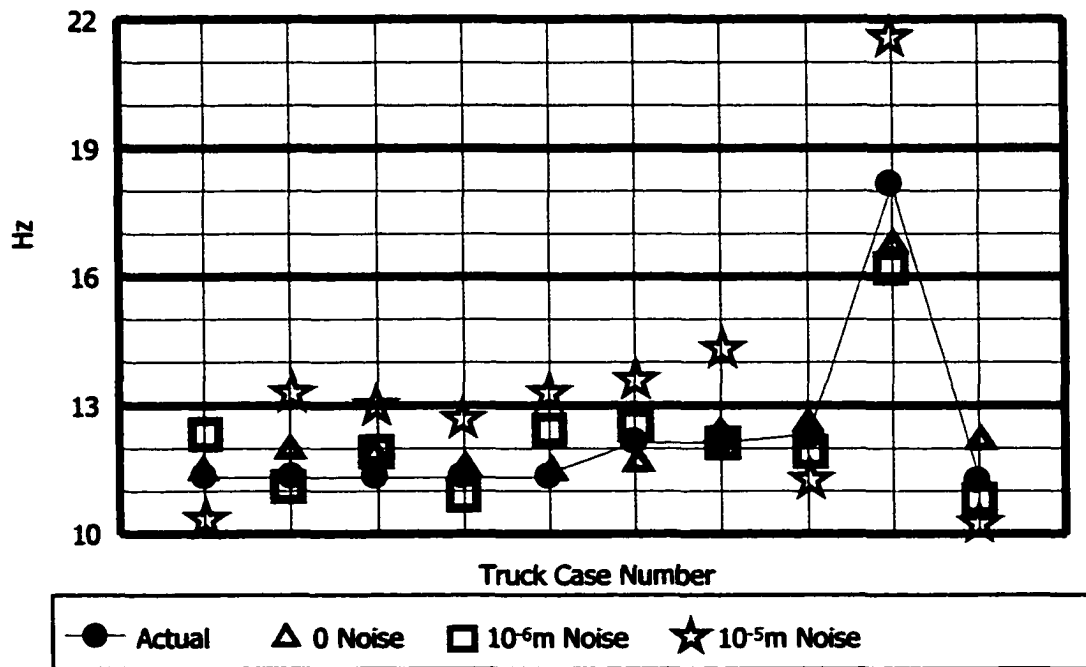


Figure 9.23 Front Axle, High Mode, Frequency Estimate (c)

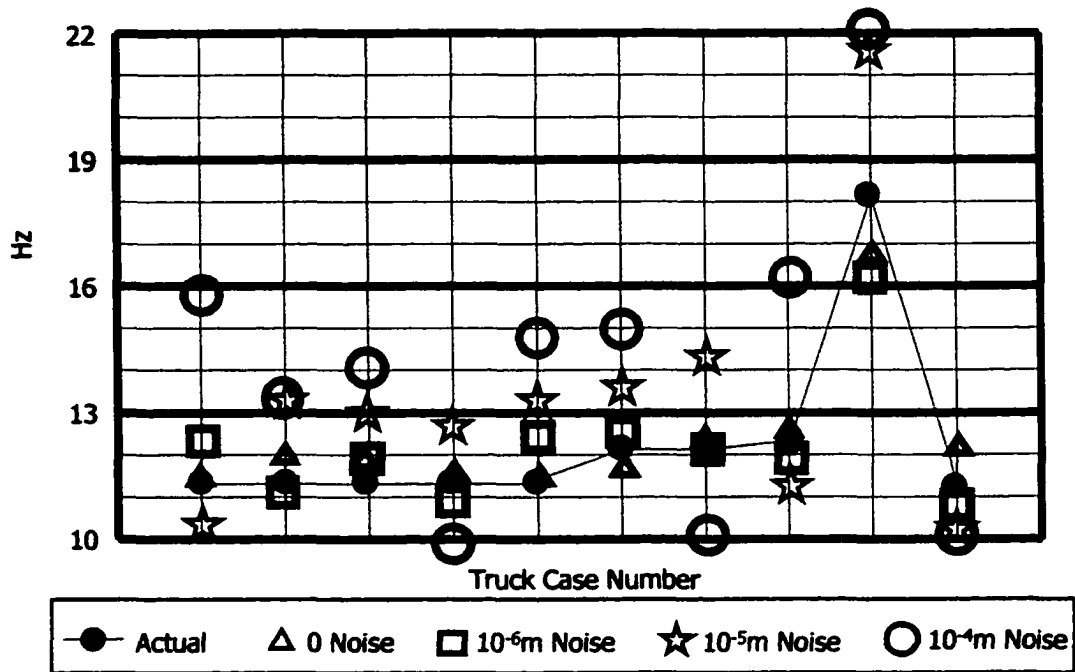


Figure 9.24 Front Axle, High Mode, Frequency Estimate (d)

### Front Axle, High Mode, Damping Ratios

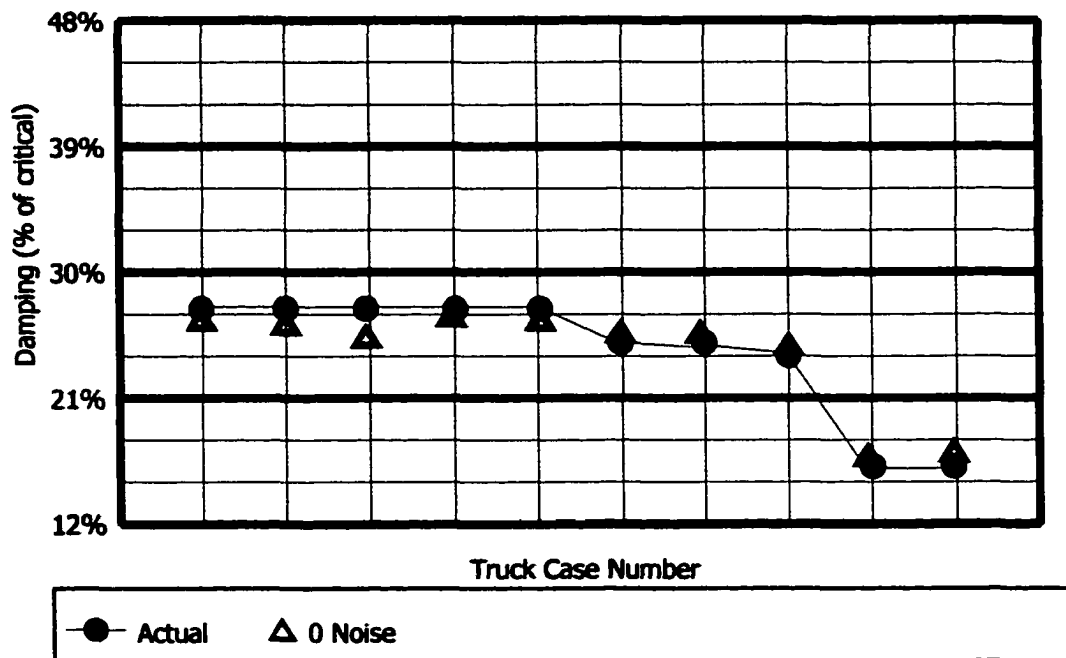


Figure 9.25 Front Axle, High Mode, Damping Ratio Estimate (a)

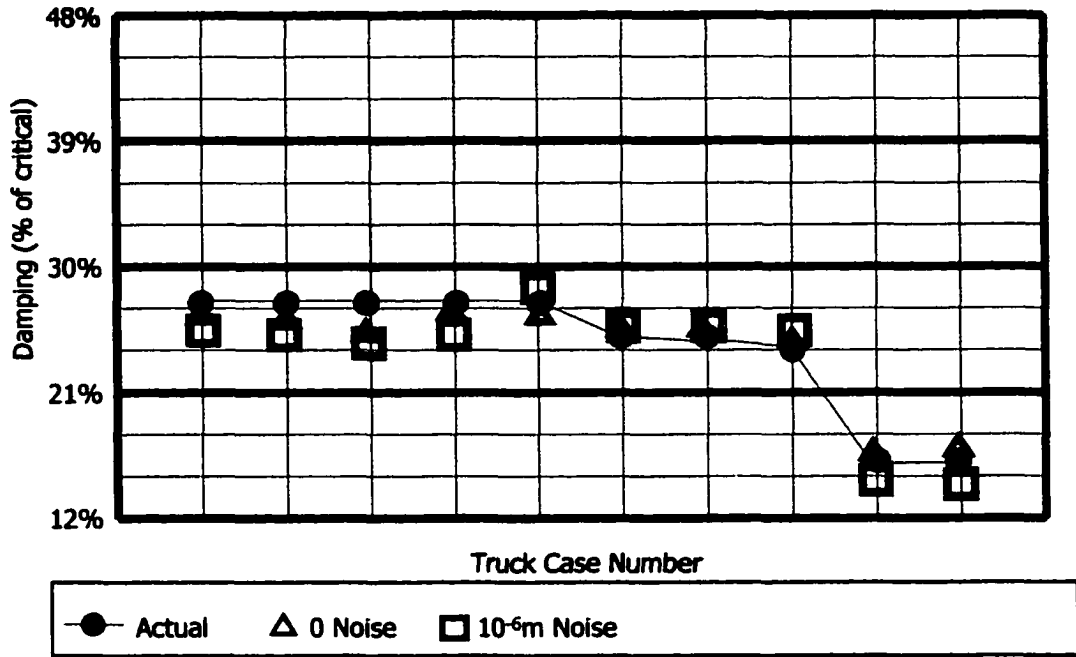


Figure 9.26 Front Axle, High Mode, Damping Ratio Estimate (b)

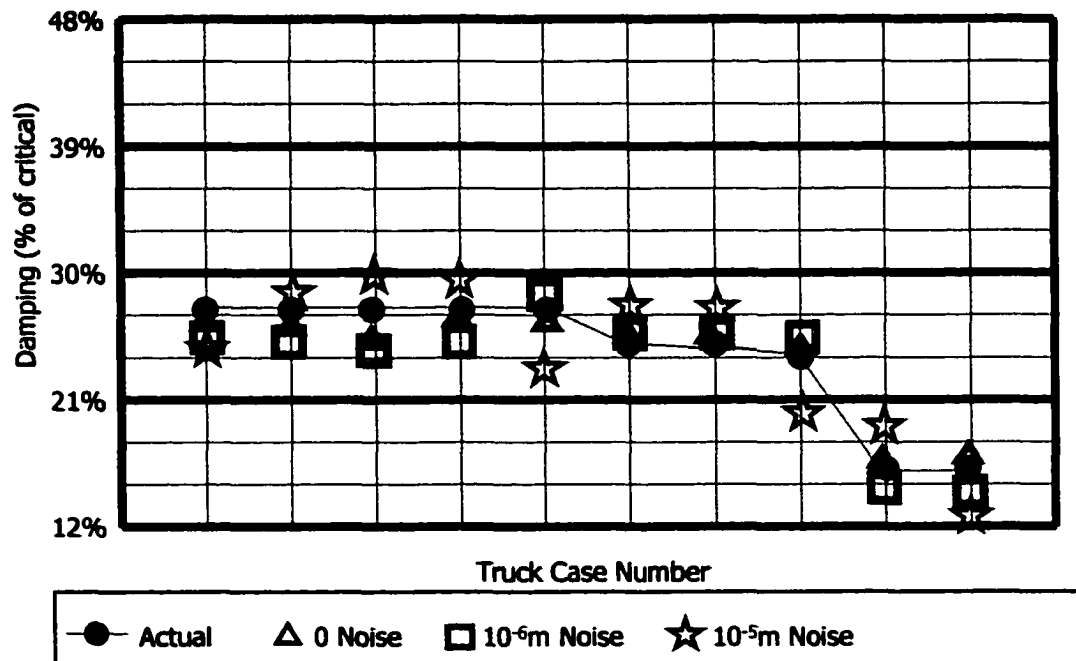


Figure 9.27 Front Axle, High Mode, Damping Ratio Estimate (c)

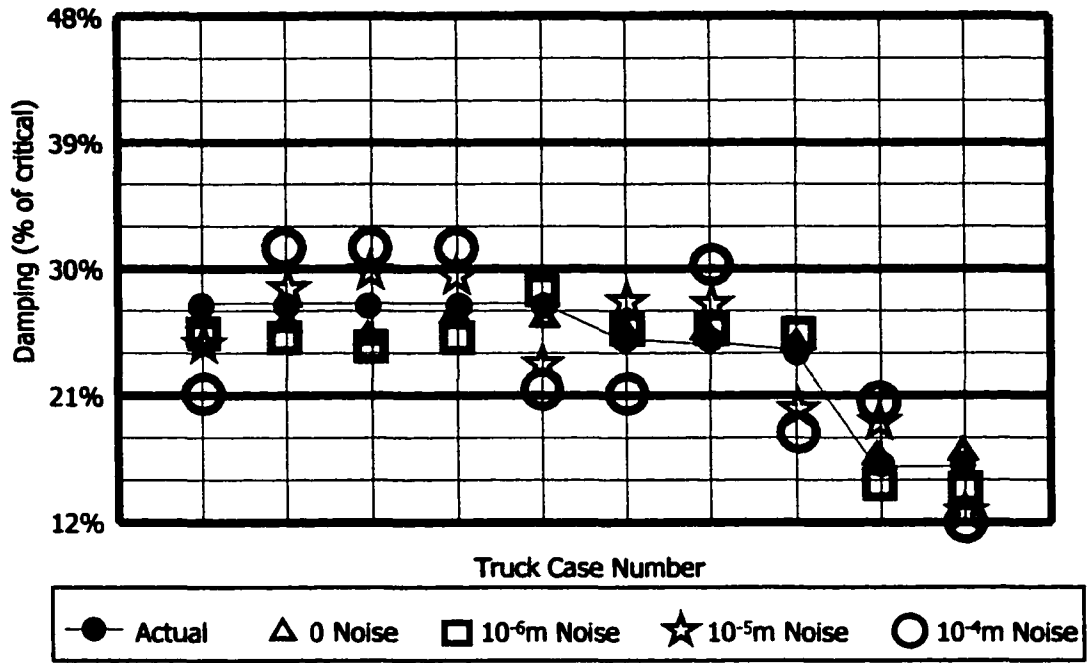


Figure 9.28 Front Axle, High Mode, Damping Ratio Estimate (d)

**Rear Axle, Low Mode, Frequency Estimates**

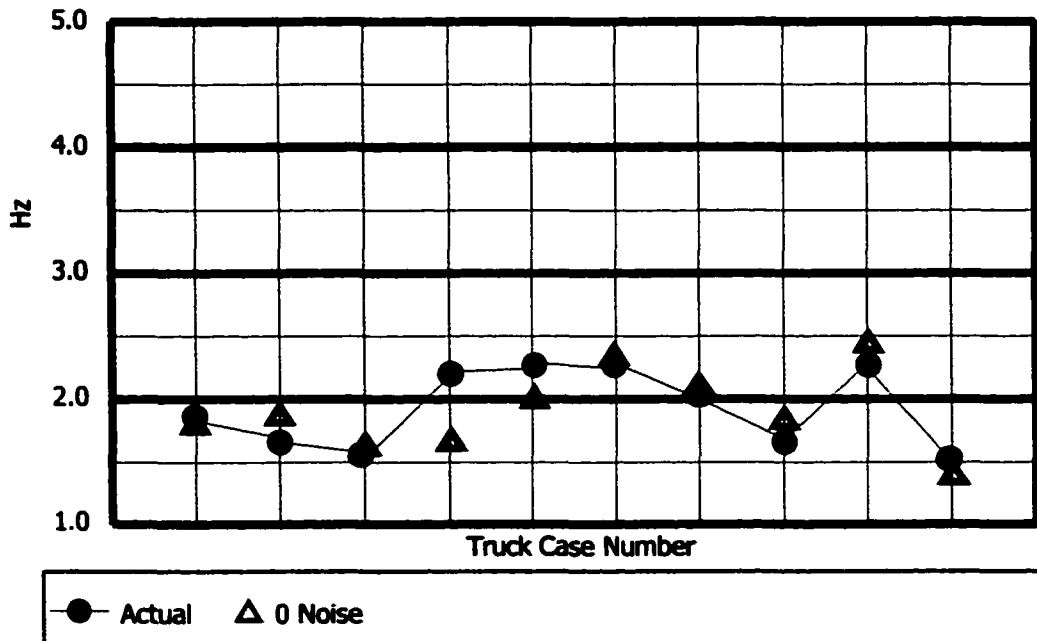


Figure 9.29 Rear Axle, Low Mode, Frequency Estimate (a)

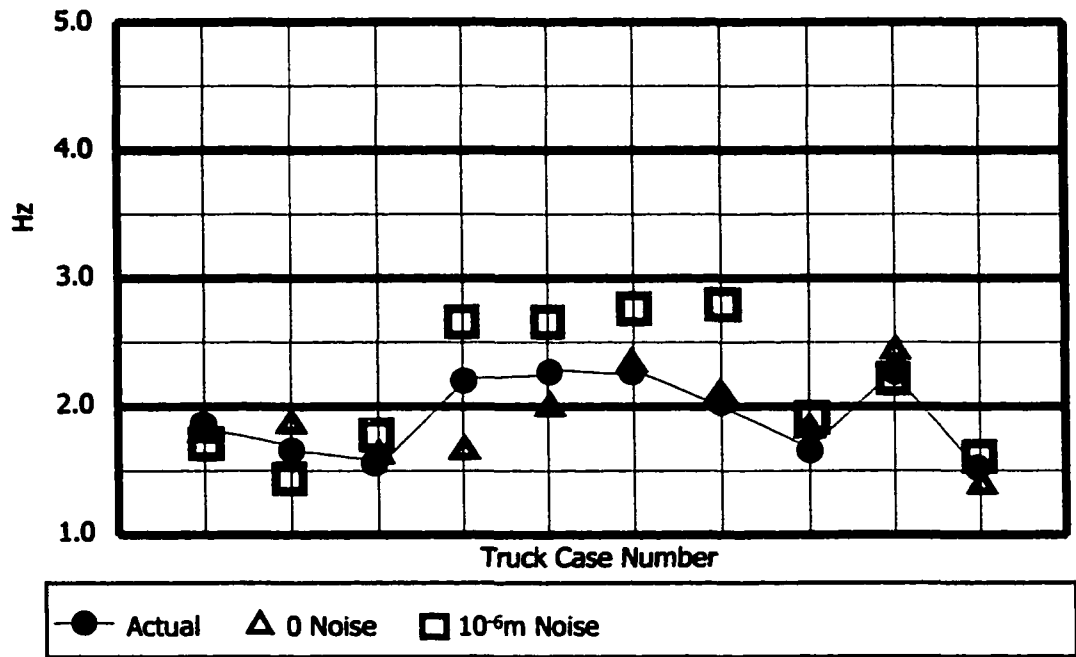


Figure 9.30 Rear Axle, Low Mode, Frequency Estimate (b)

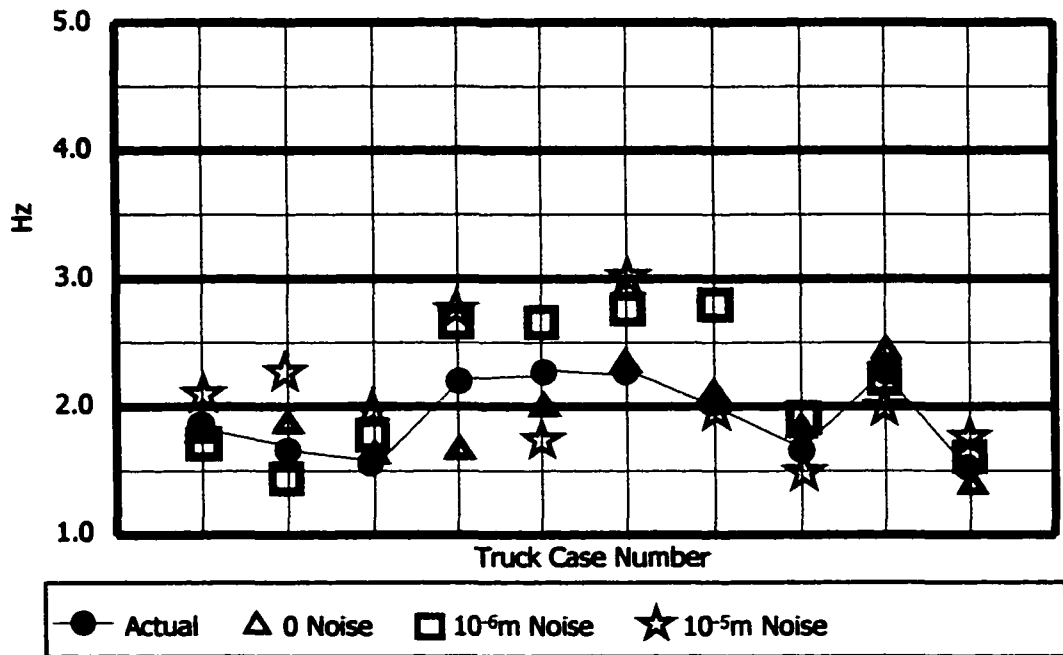


Figure 9.31 Rear Axle, Low Mode, Frequency Estimate (c)

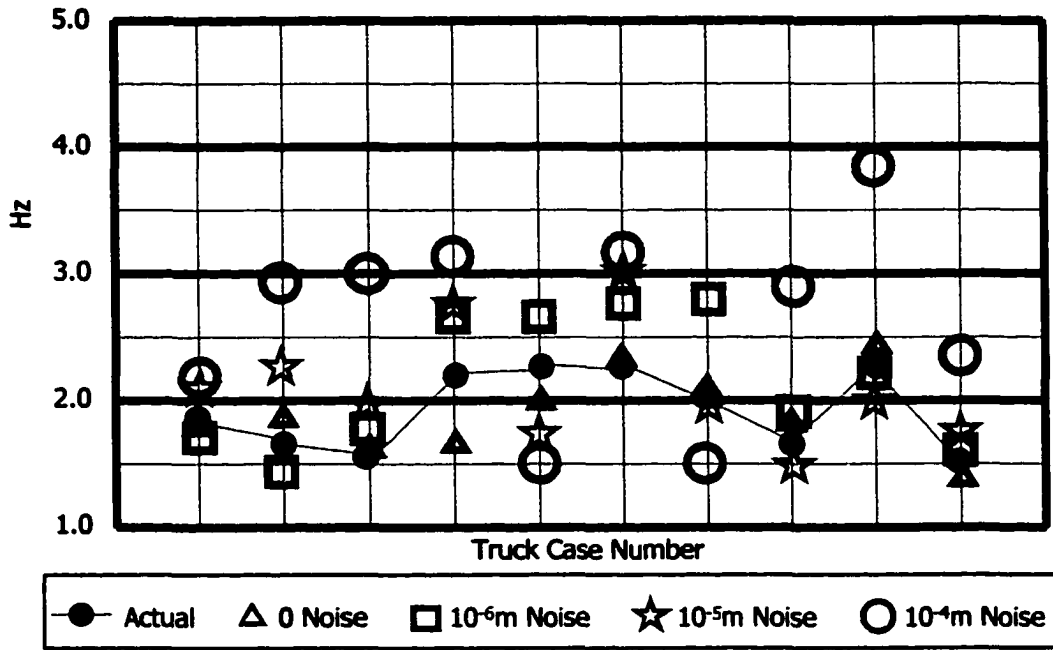


Figure 9.32 Rear Axle, Low Mode, Frequency Estimate (d)

### Rear Axle, Low Mode, Damping Ratios

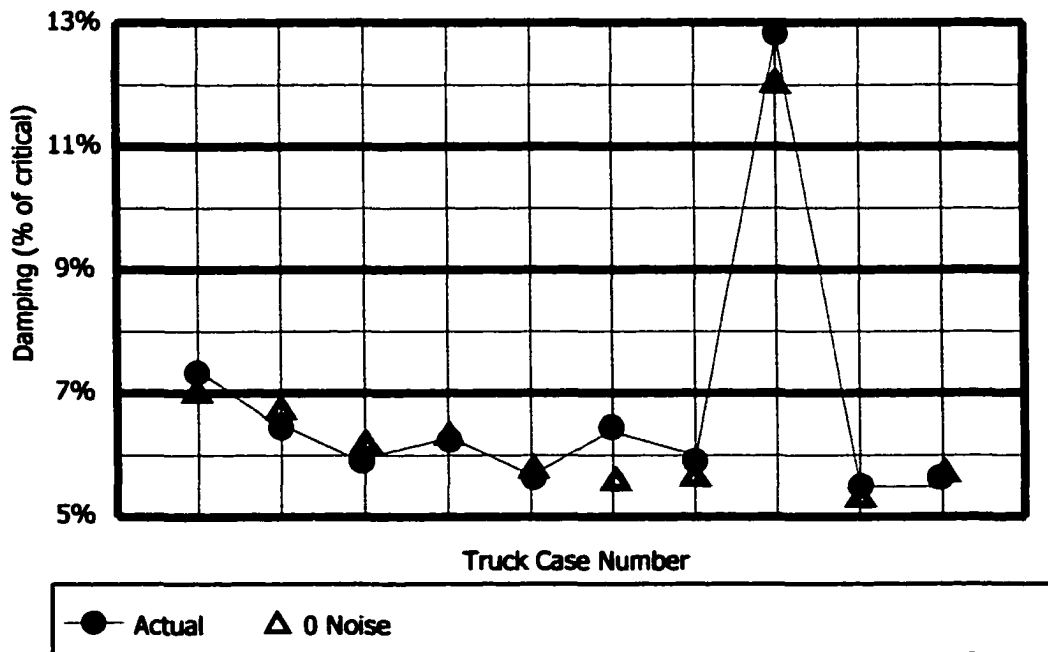


Figure 9.33 Rear Axle, Low Mode, Damping Ratio Estimate (a)

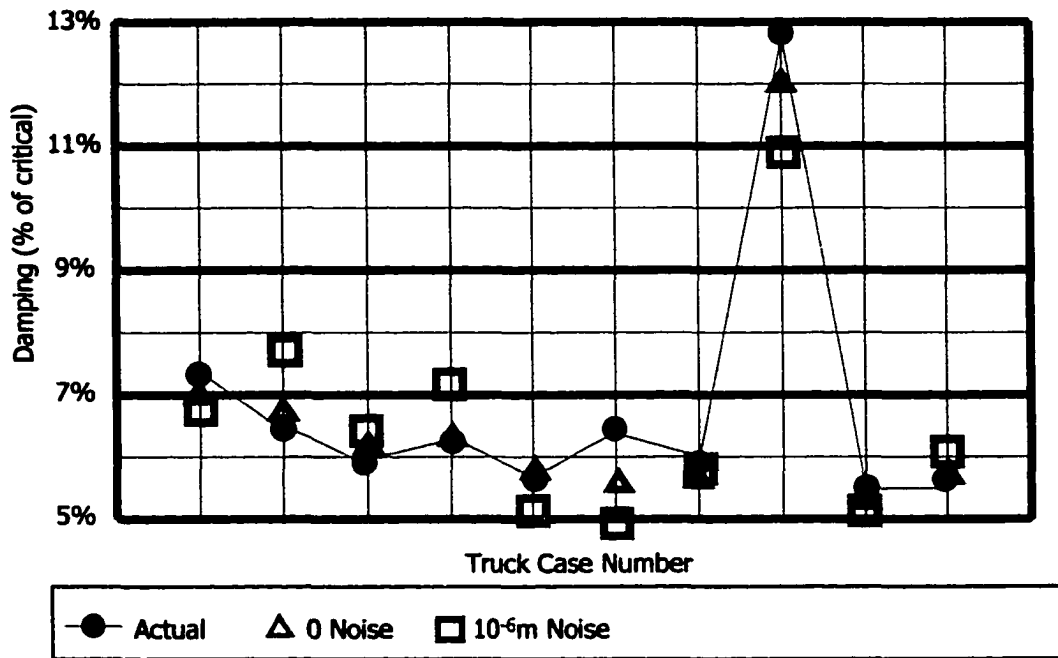


Figure 9.34 Rear Axle, Low Mode, Damping Ratio Estimate (b)

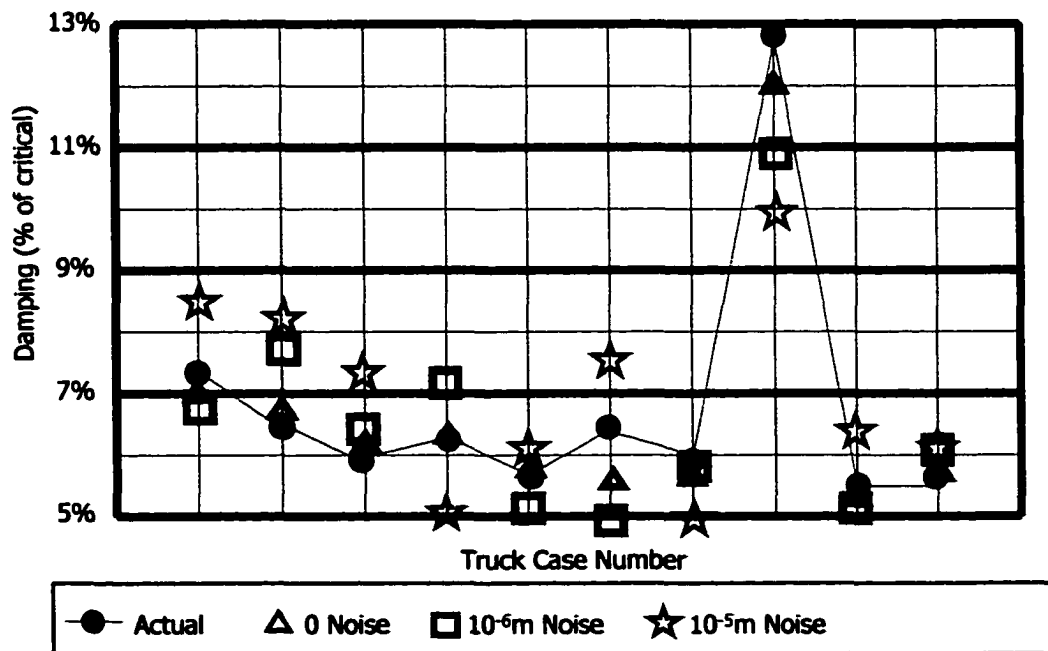


Figure 9.35 Rear Axle, Low Mode, Damping Ratio Estimate (c)

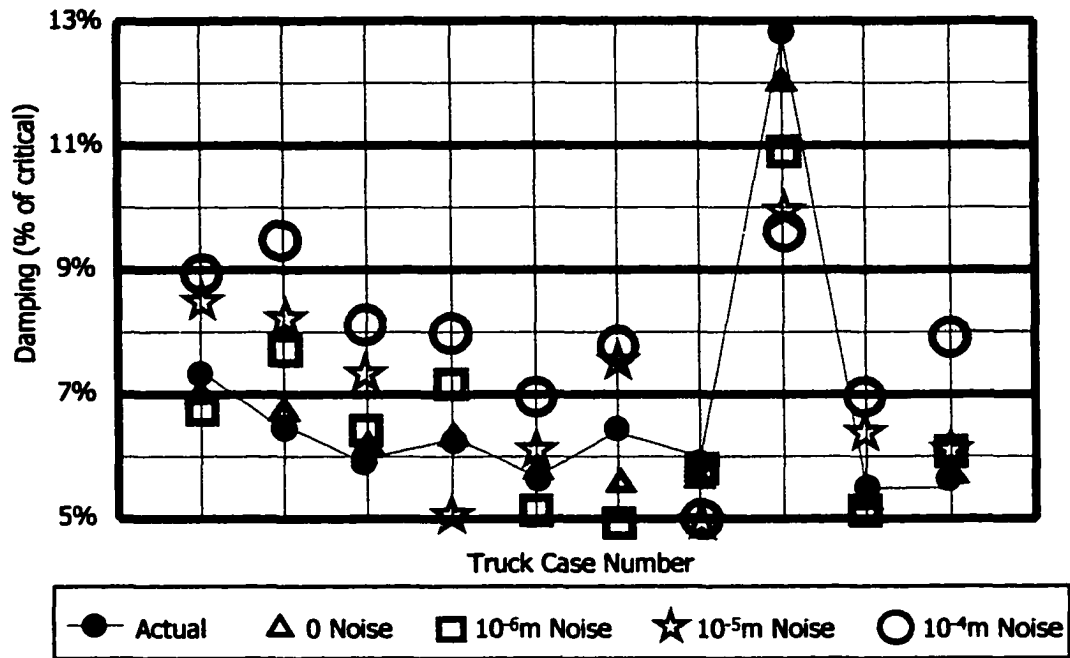


Figure 9.36 Rear Axle, Low Mode, Damping Ratio Estimate (d)

### Rear Axle, High Mode, Frequency Estimates

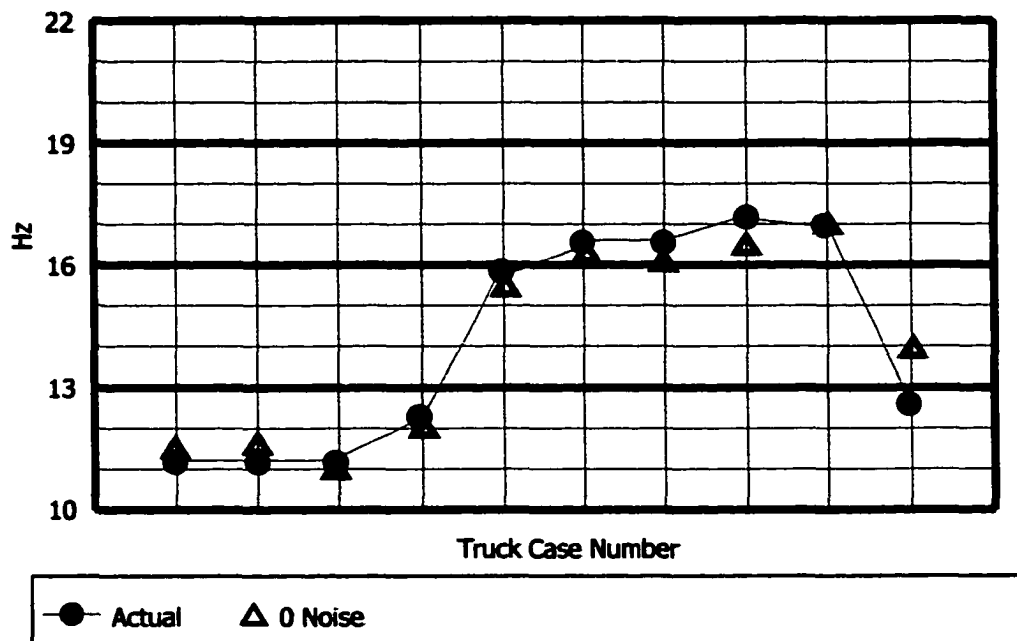


Figure 9.37 Rear Axle, High Mode, Frequency Estimate (a)

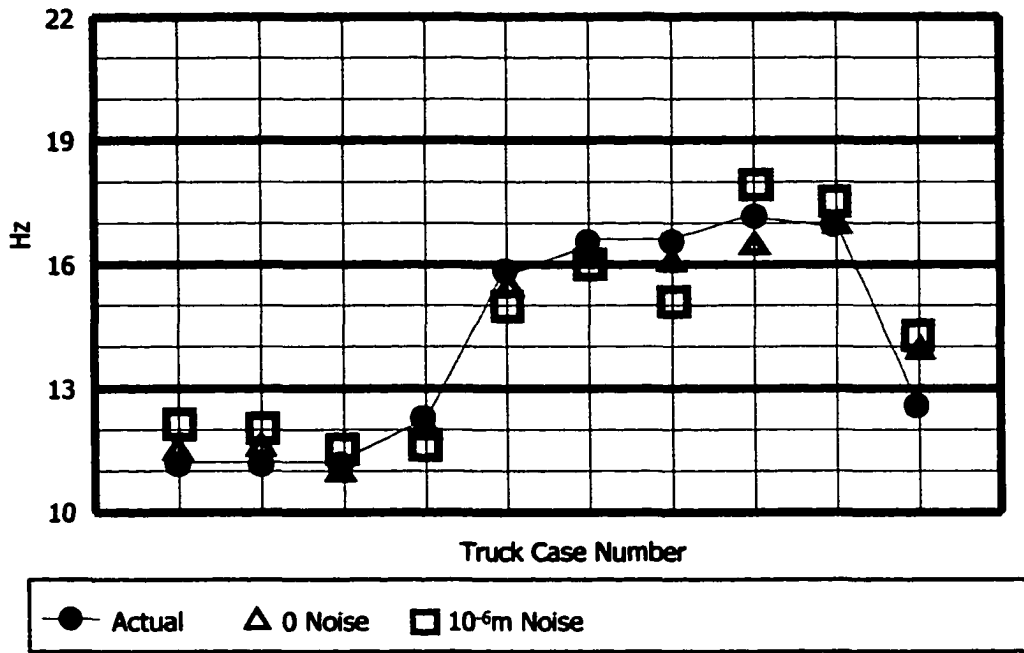


Figure 9.38 Rear Axle, High Mode, Frequency Estimate (b)

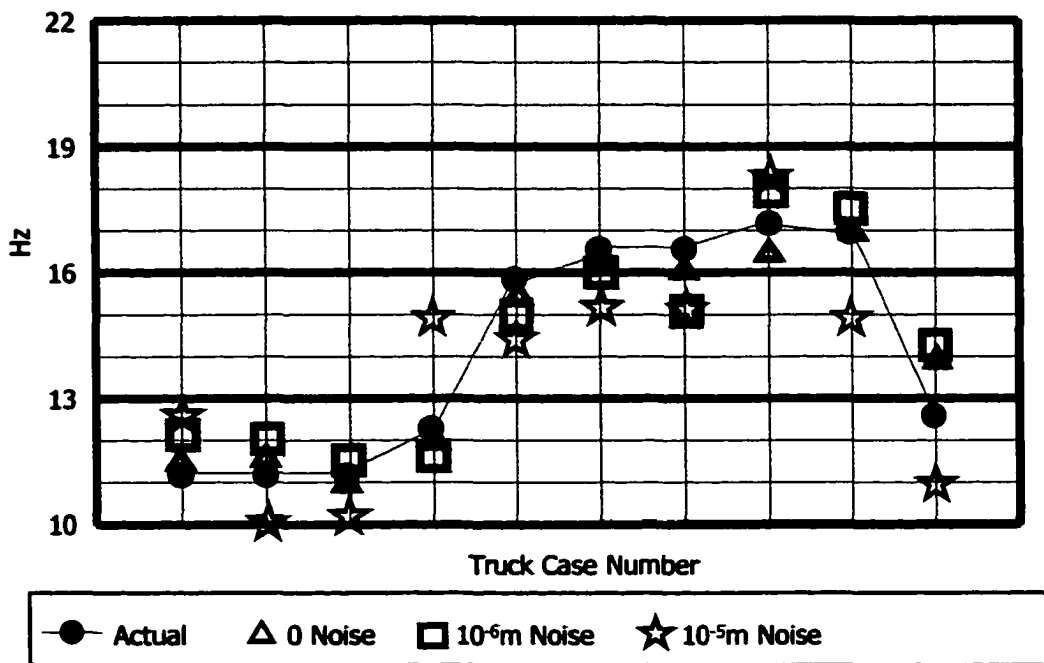


Figure 9.39 Rear Axle, High Mode, Frequency Estimate (c)

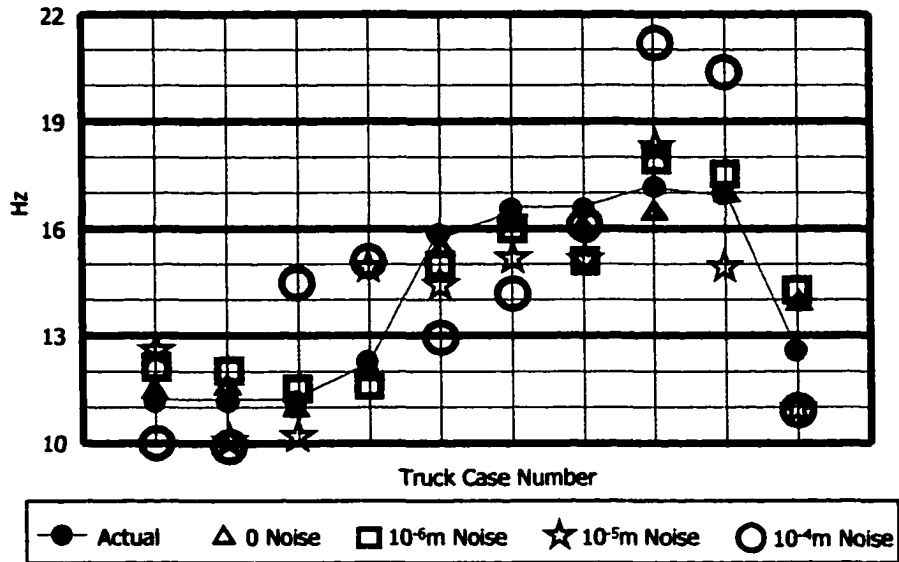


Figure 9.40 Rear Axle, High Mode, Frequency Estimate (d)

### Rear Axle, High Mode, Damping Ratios

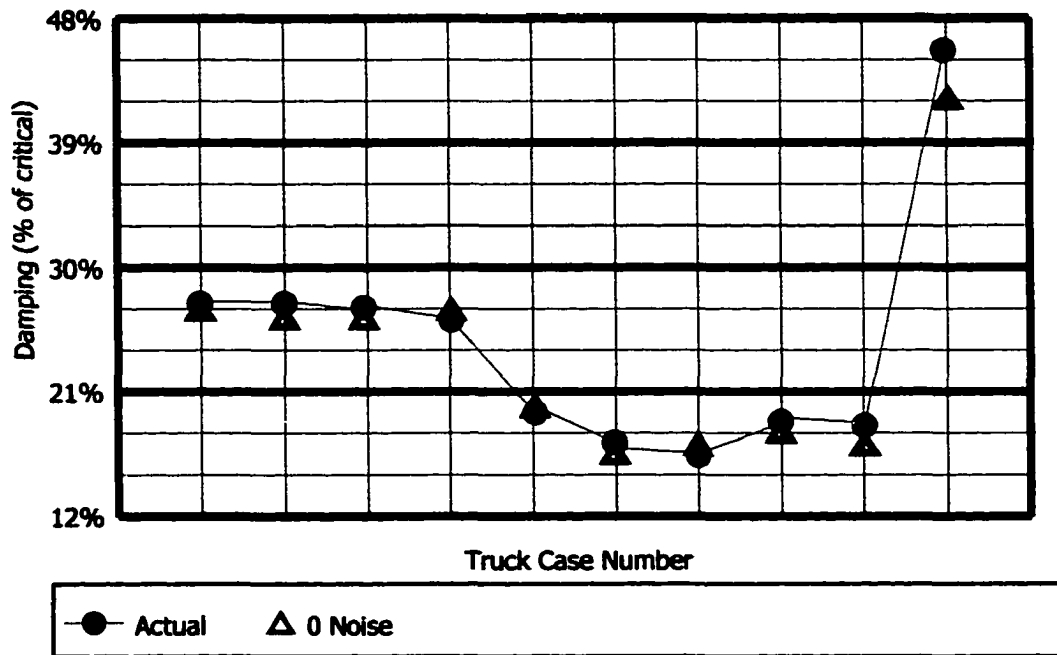


Figure 9.41 Rear Axle, High Mode, Damping Ratio Estimates (a)

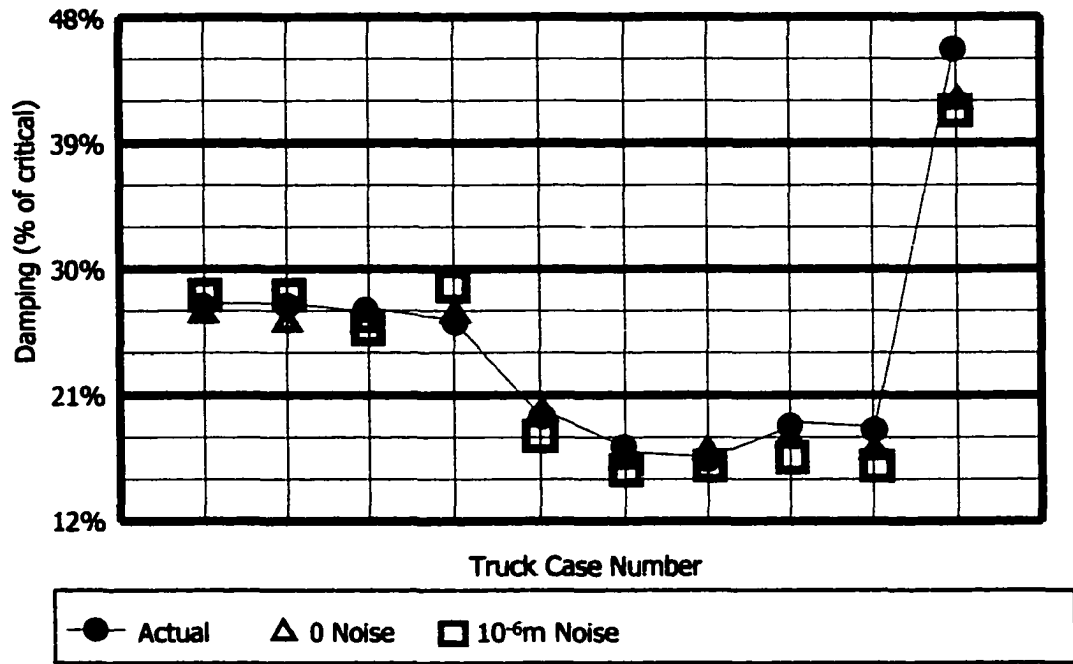


Figure 9.42 Rear Axle, High Mode, Damping Ratio Estimates (b)

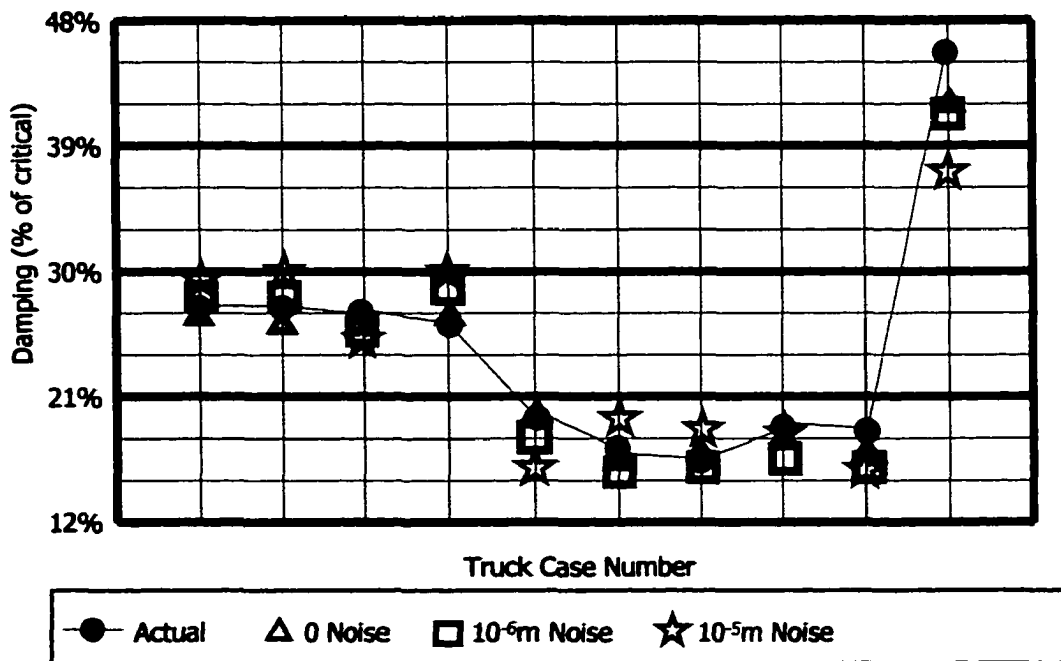


Figure 9.43 Rear Axle, High Mode, Damping Ratio Estimates (c)

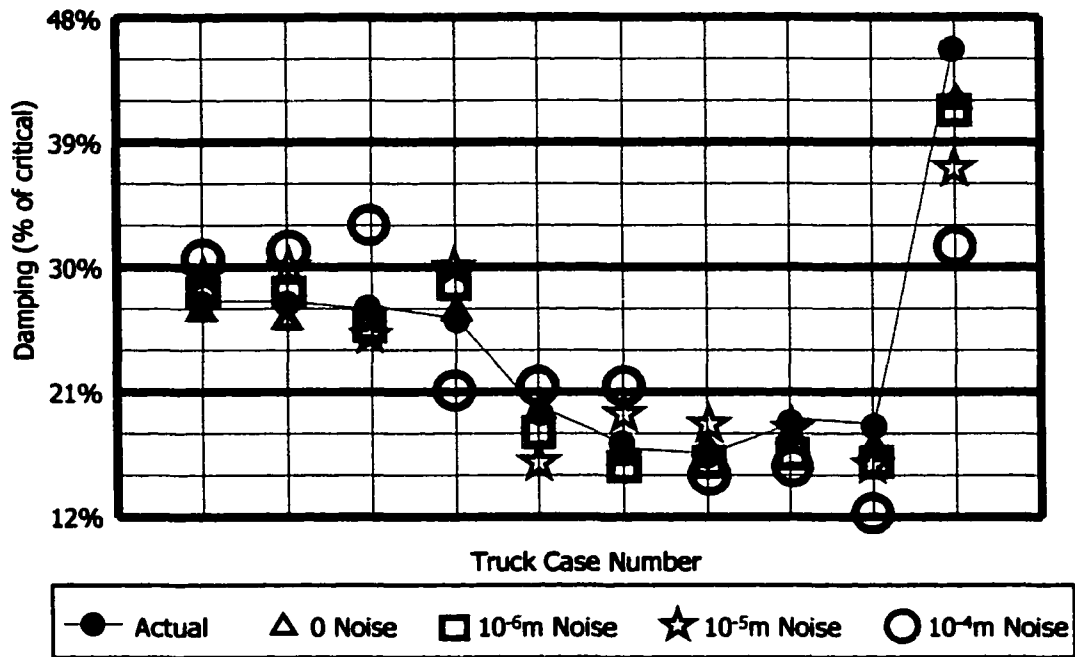


Figure 9.44 Rear Axle, High Mode, Damping Ratio Estimate (d)

In the following section, numerical results for the optimization parameters associated with each of the twenty sample trucks are given.

## 9.6 Numerical Results

Table 9.2 Truck 1 Estimates

| Parameter  | True Value                 | 0 Noise                    | 10 <sup>-6</sup> m Noise   | 10 <sup>-5</sup> m Noise   | 10 <sup>-4</sup> m Noise   |
|--|----------------------------|----------------------------|----------------------------|----------------------------|----------------------------|
| Front Axle Weight                                  | 98,000 N                   | 97,999 N                   | 98,002 N                   | 97,527 N                   | 99,020 N                   |
| Rear Axle Weight                                   | 98,000N                    | 97,999 N                   | 97,529 N                   | 98,602 N                   | 97,831 N                   |
| Speed  | 25 m/s                     | 25 m/s                     | 24.9 m/s                   | 24.9 m/s                   | 25.2 m/s                   |
| Axle Spacing                                       | 5 m                        | 5 m                        | 5 m                        | 5.1 m                      | 4.8 m                      |
| R <sub>11</sub><br>(low mode<br>amplitude, front)  | 2.36×10 <sup>-3</sup><br>m | 2.42×10 <sup>-3</sup><br>m | 2.01×10 <sup>-3</sup><br>m | 3.63×10 <sup>-3</sup><br>m | 1.87×10 <sup>-3</sup><br>m |
| R <sub>12</sub><br>(high mode<br>amplitude, front) | 1.01×10 <sup>-2</sup><br>m | 1.12×10 <sup>-3</sup><br>m | 1.31×10 <sup>-3</sup><br>m | 1.81×10 <sup>-3</sup><br>m | 2.11×10 <sup>-3</sup><br>m |
| ω <sub>11</sub> (low mode,<br>front)               | 1.91 Hz                    | 1.90 Hz                    | 1.81 Hz                    | 2.09 Hz                    | 2.41 Hz                    |
| ξ <sub>11</sub> (low mode,<br>front)               | 7.2%                       | 7.0%                       | 7.6%                       | 8.3%                       | 9.1%                       |
| ω <sub>12</sub> (high mode,<br>front)              | 11.27 Hz                   | 11.15 Hz                   | 12.04 Hz                   | 10.04 Hz                   | 15.92 Hz                   |
| ξ <sub>12</sub> (high mode,<br>front)              | 27.6%                      | 27.4%                      | 26.7%                      | 25.4%                      | 21.9%                      |
| R <sub>21</sub><br>(low mode<br>amplitude, rear)   | 2.36×10 <sup>-3</sup><br>m | 2.48×10 <sup>-3</sup><br>m | 1.94×10 <sup>-3</sup><br>m | 3.83×10 <sup>-3</sup><br>m | 1.65×10 <sup>-3</sup><br>m |
| R <sub>22</sub><br>(high mode<br>amplitude, rear)  | 1.01×10 <sup>-2</sup><br>m | 1.31×10 <sup>-2</sup><br>m | 1.43×10 <sup>-2</sup><br>m | 1.91×10 <sup>-2</sup><br>m | 2.95×10 <sup>-2</sup><br>m |
| ω <sub>21</sub> (low mode, rear)                   | 1.91 Hz                    | 1.89 Hz                    | 1.83 Hz                    | 2.14 Hz                    | 2.16 Hz                    |
| ξ <sub>21</sub> (low mode, rear)                   | 7.2%                       | 7.0%                       | 6.7%                       | 8.5%                       | 8.9%                       |
| ω <sub>22</sub> (high mode,<br>rear)               | 11.27 Hz                   | 11.43 Hz                   | 11.59 Hz                   | 12.12 Hz                   | 10.03 Hz                   |
| ξ <sub>22</sub> (high mode, rear)                  | 27.6%                      | 27.1%                      | 28.4%                      | 29.2%                      | 29.6%                      |

**Table 9.3 Truck 2 Estimates**

| <b>Parameter</b>                                | <b>True Value</b>       | <b>0 Noise</b>          | <b>10<sup>-6</sup> m Noise</b> | <b>10<sup>-5</sup> m Noise</b> | <b>10<sup>-4</sup> m Noise</b> |
|---|-------------------------|-------------------------|--------------------------------|--------------------------------|--------------------------------|
| Front Axle Weight                               | 98,000 N                | 97,997 N                | 98,012 N                       | 97,654 N                       | 98,662 N                       |
| Rear Axle Weight                                | 124,160N                | 124,174 N               | 124,104 N                      | 125,143 N                      | 126,738 N                      |
| Speed   | 25 m/s                  | 25 m/s                  | 25.2 m/s                       | 24.8 m/s                       | 25.1 m/s                       |
| Axle Spacing                                    | 5 m                     | 4.9 m                   | 4.9 m                          | 5 m                            | 4.9 m                          |
| R <sub>11</sub><br>(low mode amplitude, front)  | 2.36×10 <sup>-3</sup> m | 2.12×10 <sup>-3</sup> m | 2.61×10 <sup>-3</sup> m        | 3.53×10 <sup>-3</sup> m        | 3.97×10 <sup>-3</sup> m        |
| R <sub>12</sub><br>(high mode amplitude, front) | 1.01×10 <sup>-2</sup> m | 1.09×10 <sup>-2</sup> m | 1.14×10 <sup>-2</sup> m        | 1.97×10 <sup>-2</sup> m        | 2.22×10 <sup>-2</sup> m        |
| ω <sub>11</sub> (low mode, front)               | 1.91 Hz                 | 1.89 Hz                 | 1.77 Hz                        | 2.29 Hz                        | 1.56 Hz                        |
| ξ <sub>11</sub> (low mode, front)               | 7.2%                    | 7.1%                    | 7.8%                           | 8.8%                           | 9.6%                           |
| ω <sub>12</sub> (high mode, front)              | 11.27 Hz                | 11.39 Hz                | 11.01 Hz                       | 13.03 Hz                       | 12.97 Hz                       |
| ξ <sub>12</sub> (high mode, front)              | 27.6%                   | 27.3%                   | 25.7%                          | 25.3%                          | 30.6%                          |
| R <sub>21</sub><br>(low mode amplitude, rear)   | 2.45×10 <sup>-3</sup> m | 2.49×10 <sup>-3</sup> m | 2.94×10 <sup>-3</sup> m        | 1.52×10 <sup>-3</sup> m        | 1.15×10 <sup>-3</sup> m        |
| R <sub>22</sub><br>(high mode amplitude, rear)  | 1.08×10 <sup>-2</sup> m | 1.28×10 <sup>-2</sup> m | 1.66×10 <sup>-2</sup> m        | 0.61×10 <sup>-2</sup> m        | 1.99×10 <sup>-2</sup> m        |
| ω <sub>21</sub> (low mode, rear)                | 1.67 Hz                 | 1.80 Hz                 | 1.46 Hz                        | 2.24 Hz                        | 2.82 Hz                        |
| ξ <sub>21</sub> (low mode, rear)                | 6.5%                    | 6.8%                    | 7.7%                           | 8.2%                           | 9.4%                           |
| ω <sub>22</sub> (high mode, rear)               | 11.27 Hz                | 11.36 Hz                | 12.02 Hz                       | 10.02 Hz                       | 10.01 Hz                       |
| ξ <sub>22</sub> (high mode, rear)               | 27.1%                   | 26.8%                   | 28.5%                          | 30.0%                          | 30.6%                          |

**Table 9.4 Truck 3 Estimates**

| <b>Parameter</b>                                | <b>True Value</b>       | <b>0 Noise</b>          | <b>10<sup>-6</sup> m Noise</b> | <b>10<sup>-5</sup> m Noise</b> | <b>10<sup>-4</sup> m Noise</b> |
|---|-------------------------|-------------------------|--------------------------------|--------------------------------|--------------------------------|
| Front Axle Weight                               | 98,000 N                | 98,011 N                | 98,027 N                       | 97,866 N                       | 99,546 N                       |
| Rear Axle Weight                                | 150,332N                | 150,343 N               | 150,264 N                      | 149,249 N                      | 148,291 N                      |
| Speed   | 30 m/s                  | 30 m/s                  | 30.1 m/s                       | 29.8 m/s                       | 29.7 m/s                       |
| Axle Spacing                                    | 5 m                     | 5 m                     | 4.9 m                          | 5 m                            | 5.3 m                          |
| R <sub>11</sub><br>(low mode amplitude, front)  | 2.36×10 <sup>-3</sup> m | 2.16×10 <sup>-3</sup> m | 2.11×10 <sup>-3</sup> m        | 2.98×10 <sup>-3</sup> m        | 3.17×10 <sup>-3</sup> m        |
| R <sub>12</sub><br>(high mode amplitude, front) | 1.01×10 <sup>-2</sup> m | 1.14×10 <sup>-2</sup> m | 1.16×10 <sup>-2</sup> m        | 2.07×10 <sup>-2</sup> m        | 2.92×10 <sup>-2</sup> m        |
| ω <sub>11</sub> (low mode, front)               | 1.91 Hz                 | 1.90 Hz                 | 1.88 Hz                        | 2.30 Hz                        | 3.01 Hz                        |
| ξ <sub>11</sub> (low mode, front)               | 7.2%                    | 6.9%                    | 6.8%                           | 7.9%                           | 8.7%                           |
| ω <sub>12</sub> (high mode, front)              | 11.27 Hz                | 11.34 Hz                | 11.41 Hz                       | 12.93 Hz                       | 14.09 Hz                       |
| ξ <sub>12</sub> (high mode, front)              | 27.6%                   | 26.9%                   | 26.3%                          | 28.9%                          | 31.0%                          |
| R <sub>21</sub><br>(low mode amplitude, rear)   | 2.64×10 <sup>-3</sup> m | 2.69×10 <sup>-3</sup> m | 2.78×10 <sup>-3</sup> m        | 3.02×10 <sup>-3</sup> m        | 3.32×10 <sup>-3</sup> m        |
| R <sub>22</sub><br>(high mode amplitude, rear)  | 1.15×10 <sup>-2</sup> m | 1.11×10 <sup>-2</sup> m | 1.06×10 <sup>-2</sup> m        | 2.01×10 <sup>-2</sup> m        | 2.69×10 <sup>-2</sup> m        |
| ω <sub>21</sub> (low mode, rear)                | 1.51 Hz                 | 1.54 Hz                 | 1.58 Hz                        | 1.99 Hz                        | 3.01 Hz                        |
| ξ <sub>21</sub> (low mode, rear)                | 5.9%                    | 6.3%                    | 6.5%                           | 7.3%                           | 8.2%                           |
| ω <sub>22</sub> (high mode, rear)               | 11.26 Hz                | 11.36 Hz                | 11.51 Hz                       | 10.11 Hz                       | 14.21 Hz                       |
| ξ <sub>22</sub> (high mode, rear)               | 26.9%                   | 26.1%                   | 25.9%                          | 25.2%                          | 32.2%                          |

**Table 9.5 Truck 4 Estimates**

| <b>Parameter</b>                                | <b>True Value</b>       | <b>0 Noise</b>          | <b>10<sup>-6</sup> m Noise</b> | <b>10<sup>-5</sup> m Noise</b> | <b>10<sup>-4</sup> m Noise</b> |
|---|-------------------------|-------------------------|--------------------------------|--------------------------------|--------------------------------|
| Front Axle Weight                               | 98,000 N                | 98,012 N                | 98,029 N                       | 97,758 N                       | 97,088 N                       |
| Rear Axle Weight                                | 98,000 N                | 97,999 N                | 97,954 N                       | 98,583 N                       | 97,771 N                       |
| Speed   | 30 m/s                  | 29.9 m/s                | 30 m/s                         | 29.9 m/s                       | 30.4 m/s                       |
| Axle Spacing                                    | 5 m                     | 5 m                     | 4.9 m                          | 5.1 m                          | 4.9 m                          |
| R <sub>11</sub><br>(low mode amplitude, front)  | 2.36×10 <sup>-3</sup> m | 2.46×10 <sup>-3</sup> m | 2.01×10 <sup>-3</sup> m        | 2.76×10 <sup>-3</sup> m        | 3.23×10 <sup>-3</sup> m        |
| R <sub>12</sub><br>(high mode amplitude, front) | 1.01×10 <sup>-2</sup> m | 1.20×10 <sup>-2</sup> m | 0.91×10 <sup>-2</sup> m        | 2.13×10 <sup>-2</sup> m        | 2.55×10 <sup>-2</sup> m        |
| ω <sub>11</sub> (low mode, front)               | 1.91 Hz                 | 1.83 Hz                 | 1.98 Hz                        | 1.48 Hz                        | 3.21 Hz                        |
| ξ <sub>11</sub> (low mode, front)               | 7.2%                    | 7.0%                    | 6.6%                           | 8.1%                           | 9.0%                           |
| ω <sub>12</sub> (high mode, front)              | 11.27 Hz                | 11.11 Hz                | 10.91 Hz                       | 12.45 Hz                       | 10.02 Hz                       |
| ξ <sub>12</sub> (high mode, front)              | 27.6%                   | 27.0%                   | 25.6%                          | 29.5%                          | 30.7%                          |
| R <sub>21</sub><br>(low mode amplitude, rear)   | 2.71×10 <sup>-3</sup> m | 2.69×10 <sup>-3</sup> m | 2.78×10 <sup>-3</sup> m        | 3.02×10 <sup>-3</sup> m        | 3.32×10 <sup>-3</sup> m        |
| R <sub>22</sub><br>(high mode amplitude, rear)  | 1.10×10 <sup>-2</sup> m | 1.11×10 <sup>-2</sup> m | 1.06×10 <sup>-2</sup> m        | 2.01×10 <sup>-2</sup> m        | 2.69×10 <sup>-2</sup> m        |
| ω <sub>21</sub> (low mode, rear)                | 2.12 Hz                 | 2.53 Hz                 | 1.78 Hz                        | 2.68 Hz                        | 3.11 Hz                        |
| ξ <sub>21</sub> (low mode, rear)                | 6.2%                    | 6.5%                    | 7.2%                           | 5.1%                           | 8.0%                           |
| ω <sub>22</sub> (high mode, rear)               | 12.35 Hz                | 12.02 Hz                | 11.72 Hz                       | 14.83 Hz                       | 14.98 Hz                       |
| ξ <sub>22</sub> (high mode, rear)               | 25.9%                   | 26.6%                   | 28.1%                          | 30.2%                          | 20.5%                          |

**Table 9.6 Truck 5 Estimates**

| <b>Parameter</b>                                | <b>True Value</b>       | <b>0 Noise</b>          | <b>10<sup>-6</sup> m Noise</b> | <b>10<sup>-5</sup> m Noise</b> | <b>10<sup>-4</sup> m Noise</b> |
|---|-------------------------|-------------------------|--------------------------------|--------------------------------|--------------------------------|
| Front Axle Weight                               | 98,000 N                | 97,999 N                | 98,043 N                       | 97,312 N                       | 97,681 N                       |
| Rear Axle Weight                                | 141,610 N               | 141,615 N               | 141,574 N                      | 142,700 N                      | 142,727 N                      |
| Speed   | 25 m/s                  | 25 m/s                  | 24.9 m/s                       | 24.8 m/s                       | 25.3 m/s                       |
| Axle Spacing                                    | 6 m                     | 6 m                     | 6 m                            | 6.1 m                          | 5.8 m                          |
| R <sub>11</sub><br>(low mode amplitude, front)  | 2.36×10 <sup>-3</sup> m | 2.12×10 <sup>-3</sup> m | 2.70×10 <sup>-3</sup> m        | 2.00×10 <sup>-3</sup> m        | 1.63×10 <sup>-3</sup> m        |
| R <sub>12</sub><br>(high mode amplitude, front) | 1.01×10 <sup>-2</sup> m | 1.08×10 <sup>-2</sup> m | 0.95×10 <sup>-2</sup> m        | 2.83×10 <sup>-2</sup> m        | 3.05×10 <sup>-2</sup> m        |
| ω <sub>11</sub> (low mode, front)               | 1.91 Hz                 | 1.92 Hz                 | 2.02 Hz                        | 2.69 Hz                        | 2.98 Hz                        |
| ξ <sub>11</sub> (low mode, front)               | 7.2%                    | 7.4%                    | 7.9%                           | 6.2%                           | 4.9%                           |
| ω <sub>12</sub> (high mode, front)              | 11.27 Hz                | 11.12 Hz                | 12.31 Hz                       | 13.05 Hz                       | 13.92 Hz                       |
| ξ <sub>12</sub> (high mode, front)              | 27.6%                   | 27.2%                   | 28.2%                          | 28.9%                          | 21.4%                          |
| R <sub>21</sub><br>(low mode amplitude, rear)   | 2.75×10 <sup>-3</sup> m | 2.91×10 <sup>-3</sup> m | 3.07×10 <sup>-3</sup> m        | 3.09×10 <sup>-3</sup> m        | 1.52×10 <sup>-3</sup> m        |
| R <sub>22</sub><br>(high mode amplitude, rear)  | 1.13×10 <sup>-2</sup> m | 1.26×10 <sup>-2</sup> m | 1.64×10 <sup>-2</sup> m        | 2.02×10 <sup>-2</sup> m        | 3.01×10 <sup>-2</sup> m        |
| ω <sub>21</sub> (low mode, rear)                | 2.19 Hz                 | 2.03 Hz                 | 2.64 Hz                        | 1.75 Hz                        | 1.53 Hz                        |
| ξ <sub>21</sub> (low mode, rear)                | 5.6%                    | 5.8%                    | 5.2%                           | 6.1%                           | 6.9%                           |
| ω <sub>22</sub> (high mode, rear)               | 15.95 Hz                | 15.36 Hz                | 15.01 Hz                       | 14.22 Hz                       | 12.98 Hz                       |
| ξ <sub>22</sub> (high mode, rear)               | 19.2%                   | 19.5%                   | 18.0%                          | 16.7%                          | 20.5%                          |

Table 9.7 Truck 6 Estimates

| Parameter                                       | True Value             | 0 Noise                 | 10 <sup>-6</sup> m Noise | 10 <sup>-5</sup> m Noise | 10 <sup>-4</sup> m Noise |
|---|------------------------|-------------------------|--------------------------|--------------------------|--------------------------|
| Front Axle Weight                               | 115,415 N              | 115,467 N               | 115,396 N                | 115,218 N                | 114,105 N                |
| Rear Axle Weight                                | 167,890 N              | 167,814 N               | 167,815 N                | 166,729 N                | 171,090 N                |
| Speed   | 25 m/s                 | 25 m/s                  | 25 m/s                   | 24.7 m/s                 | 25.1 m/s                 |
| Axle Spacing                                    | 6 m                    | 6 m                     | 6 m                      | 6.2 m                    | 6 m                      |
| R <sub>11</sub><br>(low mode amplitude, front)  | 5.0×10 <sup>-3</sup> m | 5.72×10 <sup>-3</sup> m | 5.97×10 <sup>-3</sup> m  | 4.02×10 <sup>-3</sup> m  | 3.43×10 <sup>-3</sup> m  |
| R <sub>12</sub><br>(high mode amplitude, front) | 15×10 <sup>-2</sup> m  | 14.5×10 <sup>-2</sup> m | 14.2×10 <sup>-2</sup> m  | 12.8×10 <sup>-2</sup> m  | 11.9×10 <sup>-2</sup> m  |
| ω <sub>11</sub> (low mode, front)               | 1.89 Hz                | 1.94 Hz                 | 2.21 Hz                  | 2.86 Hz                  | 1.51 Hz                  |
| ξ <sub>11</sub> (low mode, front)               | 6.1%                   | 6.4%                    | 7.3%                     | 5.1%                     | 5.0%                     |
| ω <sub>12</sub> (high mode, front)              | 12.35 Hz               | 11.12 Hz                | 12.31 Hz                 | 13.05 Hz                 | 15.05 Hz                 |
| ξ <sub>12</sub> (high mode, front)              | 24.9%                  | 25.2%                   | 25.0%                    | 22.6%                    | 21.0%                    |
| R <sub>21</sub><br>(low mode amplitude, rear)   | 5.2×10 <sup>-3</sup> m | 5.63×10 <sup>-3</sup> m | 5.88×10 <sup>-3</sup> m  | 3.78×10 <sup>-3</sup> m  | 3.66×10 <sup>-3</sup> m  |
| R <sub>22</sub><br>(high mode amplitude, rear)  | 15×10 <sup>-2</sup> m  | 13.8×10 <sup>-2</sup> m | 12.9×10 <sup>-2</sup> m  | 17.2×10 <sup>-2</sup> m  | 17.9×10 <sup>-2</sup> m  |
| ω <sub>21</sub> (low mode, rear)                | 2.19 Hz                | 2.23 Hz                 | 2.75 Hz                  | 3.01 Hz                  | 3.14 Hz                  |
| ξ <sub>21</sub> (low mode, rear)                | 6.4%                   | 5.7%                    | 4.9%                     | 7.5%                     | 7.7%                     |
| ω <sub>22</sub> (high mode, rear)               | 16.72 Hz               | 16.26 Hz                | 16.12 Hz                 | 15.18 Hz                 | 14.28 Hz                 |
| ξ <sub>22</sub> (high mode, rear)               | 17.5%                  | 17.0%                   | 16.2%                    | 20.1%                    | 21.0%                    |

**Table 9.8 Truck 7 Estimates**

| <b>Parameter</b>                                | <b>True Value</b>      | <b>0 Noise</b>          | <b>10<sup>-6</sup> m Noise</b> | <b>10<sup>-5</sup> m Noise</b> | <b>10<sup>-4</sup> m Noise</b> |
|---|------------------------|-------------------------|--------------------------------|--------------------------------|--------------------------------|
| Front Axle Weight                               | 124,178 N              | 124,186 N               | 124,156 N                      | 124,379 N                      | 121,811 N                      |
| Rear Axle Weight                                | 193,184 N              | 193,195 N               | 193,187 N                      | 191,815 N                      | 193,070 N                      |
| Speed   | 35 m/s                 | 35 m/s                  | 34.5 m/s                       | 34.6 m/s                       | 35.5 m/s                       |
| Axle Spacing                                    | 6 m                    | 6 m                     | 6.2 m                          | 6.2 m                          | 5.9 m                          |
| R <sub>11</sub><br>(low mode amplitude, front)  | 5.0×10 <sup>-3</sup> m | 5.21×10 <sup>-3</sup> m | 5.82×10 <sup>-3</sup> m        | 6.10×10 <sup>-3</sup> m        | 6.63×10 <sup>-3</sup> m        |
| R <sub>12</sub><br>(high mode amplitude, front) | 15×10 <sup>-2</sup> m  | 15.8×10 <sup>-2</sup> m | 16.1×10 <sup>-2</sup> m        | 16.9×10 <sup>-2</sup> m        | 12.3×10 <sup>-2</sup> m        |
| ω <sub>11</sub> (low mode, front)               | 1.82 Hz                | 1.87 Hz                 | 2.04 Hz                        | 2.75 Hz                        | 3.05 Hz                        |
| ξ <sub>11</sub> (low mode, front)               | 5.9%                   | 6.0%                    | 6.6%                           | 7.0%                           | 4.7%                           |
| ω <sub>12</sub> (high mode, front)              | 12.35 Hz               | 12.19 Hz                | 12.01 Hz                       | 14.03 Hz                       | 10.87 Hz                       |
| ξ <sub>12</sub> (high mode, front)              | 24.8%                  | 25.0%                   | 25.4%                          | 26.9%                          | 29.2%                          |
| R <sub>21</sub><br>(low mode amplitude, rear)   | 5.2×10 <sup>-3</sup> m | 5.08×10 <sup>-3</sup> m | 5.64×10 <sup>-3</sup> m        | 6.38×10 <sup>-3</sup> m        | 3.71×10 <sup>-3</sup> m        |
| R <sub>22</sub><br>(high mode amplitude, rear)  | 15×10 <sup>-2</sup> m  | 16.3×10 <sup>-2</sup> m | 15.9×10 <sup>-2</sup> m        | 16.9×10 <sup>-2</sup> m        | 18.2×10 <sup>-2</sup> m        |
| ω <sub>21</sub> (low mode, rear)                | 2.04 Hz                | 2.12 Hz                 | 2.83 Hz                        | 1.90 Hz                        | 1.50 Hz                        |
| ξ <sub>21</sub> (low mode, rear)                | 5.9%                   | 5.6%                    | 5.8%                           | 5.0%                           | 3.7%                           |
| ω <sub>22</sub> (high mode, rear)               | 16.72 Hz               | 16.02 Hz                | 15.23 Hz                       | 15.28 Hz                       | 15.99 Hz                       |
| ξ <sub>22</sub> (high mode, rear)               | 16.7%                  | 17.4%                   | 16.9%                          | 18.3%                          | 14.5%                          |

**Table 9.9 Truck 8 Estimates**

| <b>Parameter</b>                                | <b>True Value</b>       | <b>0 Noise</b>          | <b>10<sup>-6</sup> m Noise</b> | <b>10<sup>-5</sup> m Noise</b> | <b>10<sup>-4</sup> m Noise</b> |
|---|-------------------------|-------------------------|--------------------------------|--------------------------------|--------------------------------|
| Front Axle Weight                               | 124,178 N               | 124,184 N               | 124,216 N                      | 124,871 N                      | 122,045 N                      |
| Rear Axle Weight                                | 191,222 N               | 191,129 N               | 191,260 N                      | 192,176 N                      | 195,937 N                      |
| Speed   | 35 m/s                  | 35 m/s                  | 36.0 m/s                       | 35.2 m/s                       | 36.3 m/s                       |
| Axle Spacing                                    | 4 m                     | 4.1 m                   | 4.3 m                          | 4 m                            | 4.6 m                          |
| R <sub>11</sub><br>(low mode amplitude, front)  | 5.0×10 <sup>-3</sup> m  | 5.54×10 <sup>-3</sup> m | 6.01×10 <sup>-3</sup> m        | 4.15×10 <sup>-3</sup> m        | 7.33×10 <sup>-3</sup> m        |
| R <sub>12</sub><br>(high mode amplitude, front) | 15.6×10 <sup>-2</sup> m | 15.0×10 <sup>-2</sup> m | 14.7×10 <sup>-2</sup> m        | 13.9×10 <sup>-2</sup> m        | 11.7×10 <sup>-2</sup> m        |
| ω <sub>11</sub> (low mode, front)               | 1.70 Hz                 | 1.81 Hz                 | 1.83 Hz                        | 2.63 Hz                        | 1.50 Hz                        |
| ξ <sub>11</sub> (low mode, front)               | 8.5%                    | 8.8%                    | 9.4%                           | 8.0%                           | 5.2%                           |
| ω <sub>12</sub> (high mode, front)              | 12.39 Hz                | 12.22 Hz                | 11.81 Hz                       | 11.26 Hz                       | 16.21 Hz                       |
| ξ <sub>12</sub> (high mode, front)              | 24.4%                   | 24.9%                   | 25.3%                          | 20.8%                          | 18.6%                          |
| R <sub>21</sub><br>(low mode amplitude, rear)   | 5.70×10 <sup>-3</sup> m | 5.32×10 <sup>-3</sup> m | 5.74×10 <sup>-3</sup> m        | 4.67×10 <sup>-3</sup> m        | 4.21×10 <sup>-3</sup> m        |
| R <sub>22</sub><br>(high mode amplitude, rear)  | 15.9×10 <sup>-2</sup> m | 15.0×10 <sup>-2</sup> m | 14.1×10 <sup>-2</sup> m        | 13.7×10 <sup>-2</sup> m        | 19.8×10 <sup>-2</sup> m        |
| ω <sub>21</sub> (low mode, rear)                | 1.60 Hz                 | 1.72 Hz                 | 1.89 Hz                        | 1.50 Hz                        | 2.83 Hz                        |
| ξ <sub>21</sub> (low mode, rear)                | 12.9%                   | 12.0%                   | 10.8%                          | 9.9%                           | 9.7%                           |
| ω <sub>22</sub> (high mode, rear)               | 17.12 Hz                | 16.42 Hz                | 17.92 Hz                       | 18.21 Hz                       | 21.04 Hz                       |
| ξ <sub>22</sub> (high mode, rear)               | 19.1%                   | 17.9%                   | 16.7%                          | 17.8%                          | 15.8%                          |

**Table 9.10 Truck 9 Estimates**

| <b>Parameter</b>                                | <b>True Value</b>       | <b>0 Noise</b>          | <b>10<sup>-6</sup> m Noise</b> | <b>10<sup>-5</sup> m Noise</b> | <b>10<sup>-4</sup> m Noise</b> |
|---|-------------------------|-------------------------|--------------------------------|--------------------------------|--------------------------------|
| Front Axle Weight                               | 119,810 N               | 119,819 N               | 119,791 N                      | 119,829 N                      | 121,542 N                      |
| Rear Axle Weight                                | 141,610 N               | 141,617 N               | 141,624 N                      | 142,206 N                      | 140,716 N                      |
| Speed   | 30 m/s                  | 30 m/s                  | 29.9 m/s                       | 31.0 m/s                       | 29.1 m/s                       |
| Axle Spacing                                    | 4 m                     | 4 m                     | 3.8 m                          | 4.3 m                          | 4.5 m                          |
| R <sub>11</sub><br>(low mode amplitude, front)  | 5.66×10 <sup>-3</sup> m | 5.60×10 <sup>-3</sup> m | 5.10×10 <sup>-3</sup> m        | 4.55×10 <sup>-3</sup> m        | 6.13×10 <sup>-3</sup> m        |
| R <sub>12</sub><br>(high mode amplitude, front) | 16.0×10 <sup>-2</sup> m | 15.1×10 <sup>-2</sup> m | 14.9×10 <sup>-2</sup> m        | 18.2×10 <sup>-2</sup> m        | 17.8×10 <sup>-2</sup> m        |
| ω <sub>11</sub> (low mode, front)               | 2.59 Hz                 | 2.50 Hz                 | 2.41 Hz                        | 3.24 Hz                        | 1.97 Hz                        |
| ξ <sub>11</sub> (low mode, front)               | 5.4%                    | 4.8%                    | 4.6%                           | 3.9%                           | 6.4%                           |
| ω <sub>12</sub> (high mode, front)              | 18.20 Hz                | 16.14 Hz                | 16.05 Hz                       | 21.83 Hz                       | 22.51 Hz                       |
| ξ <sub>12</sub> (high mode, front)              | 16.69%                  | 17.0%                   | 15.2%                          | 18.5%                          | 18.4%                          |
| R <sub>21</sub><br>(low mode amplitude, rear)   | 5.73×10 <sup>-3</sup> m | 5.12×10 <sup>-3</sup> m | 5.10×10 <sup>-3</sup> m        | 6.97×10 <sup>-3</sup> m        | 7.09×10 <sup>-3</sup> m        |
| R <sub>22</sub><br>(high mode amplitude, rear)  | 15.4×10 <sup>-2</sup> m | 15.9×10 <sup>-2</sup> m | 16.2×10 <sup>-2</sup> m        | 11.8×10 <sup>-2</sup> m        | 12.0×10 <sup>-2</sup> m        |
| ω <sub>21</sub> (low mode, rear)                | 2.36 Hz                 | 2.45 Hz                 | 2.31 Hz                        | 2.00 Hz                        | 3.72 Hz                        |
| ξ <sub>21</sub> (low mode, rear)                | 5.6%                    | 5.4%                    | 5.3%                           | 6.4%                           | 6.9%                           |
| ω <sub>22</sub> (high mode, rear)               | 16.79 Hz                | 16.81 Hz                | 17.04 Hz                       | 14.92 Hz                       | 20.63 Hz                       |
| ξ <sub>22</sub> (high mode, rear)               | 18.4%                   | 17.8%                   | 17.1%                          | 16.8%                          | 12.0%                          |

**Table 9.11 Truck 10 Estimates**

| <b>Parameter</b>                                | <b>True Value</b>       | <b>0 Noise</b>          | <b>10<sup>-6</sup> m Noise</b> | <b>10<sup>-5</sup> m Noise</b> | <b>10<sup>-4</sup> m Noise</b> |
|---|-------------------------|-------------------------|--------------------------------|--------------------------------|--------------------------------|
| Front Axle Weight                               | 118,835 N               | 118,846 N               | 118,890 N                      | 119,459 N                      | 118,060 N                      |
| Rear Axle Weight                                | 174,326 N               | 174,314 N               | 174,338 N                      | 174,820 N                      | 174,601 N                      |
| Speed   | 25 m/s                  | 25 m/s                  | 25 m/s                         | 24.9 m/s                       | 24.9 m/s                       |
| Axle Spacing                                    | 4 m                     | 4 m                     | 3.8 m                          | 4.3 m                          | 4.5 m                          |
| R <sub>11</sub><br>(low mode amplitude, front)  | 2.16×10 <sup>-3</sup> m | 2.76×10 <sup>-3</sup> m | 3.02×10 <sup>-3</sup> m        | 3.04×10 <sup>-3</sup> m        | 3.43×10 <sup>-3</sup> m        |
| R <sub>12</sub><br>(high mode amplitude, front) | 5.1×10 <sup>-2</sup> m  | 5.6×10 <sup>-2</sup> m  | 6.3×10 <sup>-2</sup> m         | 7.1×10 <sup>-2</sup> m         | 7.3×10 <sup>-2</sup> m         |
| ω <sub>11</sub> (low mode, front)               | 1.62 Hz                 | 1.54 Hz                 | 1.83 Hz                        | 2.20 Hz                        | 1.98 Hz                        |
| ξ <sub>11</sub> (low mode, front)               | 6.0%                    | 6.3%                    | 6.4%                           | 5.2%                           | 3.2%                           |
| ω <sub>12</sub> (high mode, front)              | 11.09 Hz                | 11.92 Hz                | 10.91 Hz                       | 10.26 Hz                       | 10.19 Hz                       |
| ξ <sub>12</sub> (high mode, front)              | 16.67%                  | 16.8%                   | 14.7%                          | 14.6%                          | 12.1%                          |
| R <sub>21</sub><br>(low mode amplitude, rear)   | 2.01×10 <sup>-3</sup> m | 2.15×10 <sup>-3</sup> m | 2.21×10 <sup>-3</sup> m        | 2.85×10 <sup>-3</sup> m        | 3.29×10 <sup>-3</sup> m        |
| R <sub>22</sub><br>(high mode amplitude, rear)  | 5.2×10 <sup>-2</sup> m  | 6.1×10 <sup>-2</sup> m  | 6.6×10 <sup>-2</sup> m         | 6.7×10 <sup>-2</sup> m         | 8.2×10 <sup>-2</sup> m         |
| ω <sub>21</sub> (low mode, rear)                | 1.58 Hz                 | 1.46 Hz                 | 1.62 Hz                        | 2.12 Hz                        | 2.24 Hz                        |
| ξ <sub>21</sub> (low mode, rear)                | 5.8%                    | 5.9%                    | 6.1%                           | 6.1%                           | 7.9%                           |
| ω <sub>22</sub> (high mode, rear)               | 12.76 Hz                | 13.82 Hz                | 14.14 Hz                       | 11.27 Hz                       | 11.04 Hz                       |
| ξ <sub>22</sub> (high mode, rear)               | 46.8%                   | 42.7%                   | 42.6%                          | 36.9%                          | 31.1%                          |

**Table 9.12 Truck 11 Estimates**

| <b>Parameter</b>                                | <b>True Value</b>       | <b>0 Noise</b>          | <b>10<sup>-6</sup> m Noise</b> | <b>10<sup>-5</sup> m Noise</b> | <b>10<sup>-4</sup> m Noise</b> |
|---|-------------------------|-------------------------|--------------------------------|--------------------------------|--------------------------------|
| Front Axle Weight                               | 97,900 N                | 97,013 N                | 97,064 N                       | 96,617N                        | 97,650 N                       |
| Rear Axle Weight                                | 98,000 N                | 97,991 N                | 97,982 N                       | 97,590 N                       | 99,338 N                       |
| Speed   | 25 m/s                  | 25 m/s                  | 25 m/s                         | 25.1 m/s                       | 25 m/s                         |
| Axle Spacing                                    | 4 m                     | 4 m                     | 4 m                            | 4 m                            | 3.9 m                          |
| R <sub>11</sub><br>(low mode amplitude, front)  | 1.90×10 <sup>-3</sup> m | 1.92×10 <sup>-3</sup> m | 3.15×10 <sup>-3</sup> m        | 3.34×10 <sup>-3</sup> m        | 4.01×10 <sup>-3</sup> m        |
| R <sub>12</sub><br>(high mode amplitude, front) | 5.1×10 <sup>-2</sup> m  | 4.3×10 <sup>-2</sup> m  | 4.0×10 <sup>-2</sup> m         | 2.8×10 <sup>-2</sup> m         | 2.7×10 <sup>-2</sup> m         |
| ω <sub>11</sub> (low mode, front)               | 2.18 Hz                 | 2.02 Hz                 | 1.75 Hz                        | 3.27 Hz                        | 3.71 Hz                        |
| ξ <sub>11</sub> (low mode, front)               | 9.6%                    | 9.1%                    | 7.2%                           | 6.7%                           | 6.2%                           |
| ω <sub>12</sub> (high mode, front)              | 13.39 Hz                | 12.04 Hz                | 11.41 Hz                       | 18.92 Hz                       | 19.31 Hz                       |
| ξ <sub>12</sub> (high mode, front)              | 38.0%                   | 34.25%                  | 46.6%                          | 21.2%                          | 19.6%                          |
| R <sub>21</sub><br>(low mode amplitude, rear)   | 1.87×10 <sup>-3</sup> m | 2.12×10 <sup>-3</sup> m | 1.40×10 <sup>-3</sup> m        | 3.02×10 <sup>-3</sup> m        | 3.14×10 <sup>-3</sup> m        |
| R <sub>22</sub><br>(high mode amplitude, rear)  | 6.3×10 <sup>-2</sup> m  | 5.4×10 <sup>-2</sup> m  | 7.9×10 <sup>-2</sup> m         | 8.4×10 <sup>-2</sup> m         | 8.9×10 <sup>-2</sup> m         |
| ω <sub>21</sub> (low mode, rear)                | 1.95 Hz                 | 2.15 Hz                 | 2.31 Hz                        | 1.50 Hz                        | 1.50 Hz                        |
| ξ <sub>21</sub> (low mode, rear)                | 10.7%                   | 9.8%                    | 12.1%                          | 8.4%                           | 13.5%                          |
| ω <sub>22</sub> (high mode, rear)               | 11.39 Hz                | 11.85 Hz                | 10.23 Hz                       | 15.71 Hz                       | 17.85 Hz                       |
| ξ <sub>22</sub> (high mode, rear)               | 40.9%                   | 45.0%                   | 32.1%                          | 48.8%                          | 27.2%                          |

**Table 9.13 Truck 12 Estimates**

| <b>Parameter</b>                                | <b>True Value</b>       | <b>0 Noise</b>          | <b>10<sup>-6</sup> m Noise</b> | <b>10<sup>-5</sup> m Noise</b> | <b>10<sup>-4</sup> m Noise</b> |
|---|-------------------------|-------------------------|--------------------------------|--------------------------------|--------------------------------|
| Front Axle Weight                               | 98,000 N                | 98,002 N                | 98,052 N                       | 98,052 N                       | 97,463 N                       |
| Rear Axle Weight                                | 117,400 N               | 117,413 N               | 117,385 N                      | 117,113 N                      | 116,708 N                      |
| Speed   | 25 m/s                  | 25 m/s                  | 24.9 m/s                       | 25 m/s                         | 24.9 m/s                       |
| Axle Spacing                                    | 6 m                     | 6 m                     | 6 m                            | 6.1 m                          | 6.1 m                          |
| R <sub>11</sub><br>(low mode amplitude, front)  | 2.72×10 <sup>-3</sup> m | 2.48×10 <sup>-3</sup> m | 3.72×10 <sup>-3</sup> m        | 1.94×10 <sup>-3</sup> m        | 1.72×10 <sup>-3</sup> m        |
| R <sub>12</sub><br>(high mode amplitude, front) | 6.8×10 <sup>-2</sup> m  | 5.9×10 <sup>-2</sup> m  | 5.1×10 <sup>-2</sup> m         | 8.7×10 <sup>-2</sup> m         | 4.0×10 <sup>-2</sup> m         |
| ω <sub>11</sub> (low mode, front)               | 2.18 Hz                 | 2.35 Hz                 | 1.95 Hz                        | 1.52 Hz                        | 4.47 Hz                        |
| ξ <sub>11</sub> (low mode, front)               | 9.5%                    | 9.9%                    | 7.9%                           | 6.8%                           | 5.8%                           |
| ω <sub>12</sub> (high mode, front)              | 12.78 Hz                | 13.23 Hz                | 10.87 Hz                       | 10.06 Hz                       | 18.83 Hz                       |
| ξ <sub>12</sub> (high mode, front)              | 36.5%                   | 37.4%                   | 25.5%                          | 22.7%                          | 48.4%                          |
| R <sub>21</sub><br>(low mode amplitude, rear)   | 3.02×10 <sup>-3</sup> m | 3.93×10 <sup>-3</sup> m | 3.89×10 <sup>-3</sup> m        | 1.20×10 <sup>-3</sup> m        | 4.34×10 <sup>-3</sup> m        |
| R <sub>22</sub><br>(high mode amplitude, rear)  | 7.0×10 <sup>-2</sup> m  | 7.6×10 <sup>-2</sup> m  | 6.4×10 <sup>-2</sup> m         | 6.0×10 <sup>-2</sup> m         | 4.2×10 <sup>-2</sup> m         |
| ω <sub>21</sub> (low mode, rear)                | 1.78 Hz                 | 1.64 Hz                 | 1.54 Hz                        | 2.86 Hz                        | 2.91 Hz                        |
| ξ <sub>21</sub> (low mode, rear)                | 9.7%                    | 10.4%                   | 10.5%                          | 11.1%                          | 11.8%                          |
| ω <sub>22</sub> (high mode, rear)               | 10.51 Hz                | 10.00 Hz                | 11.71 Hz                       | 14.17 Hz                       | 14.91 Hz                       |
| ξ <sub>22</sub> (high mode, rear)               | 37.5%                   | 41.1%                   | 34.7%                          | 46.2%                          | 20.1%                          |

**Table 9.14 Truck 13 Estimates**

| <b>Parameter</b>                                | <b>True Value</b>       | <b>0 Noise</b>          | <b>10<sup>-6</sup> m Noise</b> | <b>10<sup>-5</sup> m Noise</b> | <b>10<sup>-4</sup> m Noise</b> |
|---|-------------------------|-------------------------|--------------------------------|--------------------------------|--------------------------------|
| Front Axle Weight                               | 99,900 N                | 99,962 N                | 99,943 N                       | 99,691 N                       | 100,243 N                      |
| Rear Axle Weight                                | 117,400 N               | 117,394 N               | 117,453 N                      | 116,338 N                      | 117,064 N                      |
| Speed   | 25 m/s                  | 25 m/s                  | 25 m/s                         | 25.1 m/s                       | 25.1 m/s                       |
| Axle Spacing                                    | 8 m                     | 8 m                     | 8 m                            | 8 m                            | 8.1 m                          |
| R <sub>11</sub><br>(low mode amplitude, front)  | 2.95×10 <sup>-3</sup> m | 2.51×10 <sup>-3</sup> m | 3.52×10 <sup>-3</sup> m        | 3.86×10 <sup>-3</sup> m        | 4.59×10 <sup>-3</sup> m        |
| R <sub>12</sub><br>(high mode amplitude, front) | 7.3×10 <sup>-2</sup> m  | 7.8×10 <sup>-2</sup> m  | 6.2×10 <sup>-2</sup> m         | 9.4×10 <sup>-2</sup> m         | 9.9×10 <sup>-2</sup> m         |
| ω <sub>11</sub> (low mode, front)               | 1.89 Hz                 | 1.65 Hz                 | 1.51 Hz                        | 3.16 Hz                        | 3.85 Hz                        |
| ξ <sub>11</sub> (low mode, front)               | 5.4%                    | 5.2%                    | 4.4%                           | 5.0%                           | 5.6%                           |
| ω <sub>12</sub> (high mode, front)              | 10.41 Hz                | 10.10 Hz                | 11.24 Hz                       | 12.46 Hz                       | 12.87 Hz                       |
| ξ <sub>12</sub> (high mode, front)              | 19.2%                   | 19.9%                   | 18.0%                          | 21.2%                          | 24.6%                          |
| R <sub>21</sub><br>(low mode amplitude, rear)   | 3.64×10 <sup>-3</sup> m | 3.19×10 <sup>-3</sup> m | 2.74×10 <sup>-3</sup> m        | 4.83×10 <sup>-3</sup> m        | 1.72×10 <sup>-3</sup> m        |
| R <sub>22</sub><br>(high mode amplitude, rear)  | 7.7×10 <sup>-2</sup> m  | 8.4×10 <sup>-2</sup> m  | 9.0×10 <sup>-2</sup> m         | 10.2×10 <sup>-2</sup> m        | 3.7×10 <sup>-2</sup> m         |
| ω <sub>21</sub> (low mode, rear)                | 1.72 Hz                 | 1.85 Hz                 | 1.91 Hz                        | 1.51 Hz                        | 1.50 Hz                        |
| ξ <sub>21</sub> (low mode, rear)                | 5.5%                    | 4.9%                    | 4.2%                           | 4.8%                           | 3.1%                           |
| ω <sub>22</sub> (high mode, rear)               | 10.40 Hz                | 10.27 Hz                | 10.05 Hz                       | 14.78 Hz                       | 17.07 Hz                       |
| ξ <sub>22</sub> (high mode, rear)               | 19.0%                   | 20.3%                   | 23.6%                          | 23.8%                          | 12.8%                          |

**Table 9.15 Truck 14 Estimates**

| <b>Parameter</b>                                | <b>True Value</b>       | <b>0 Noise</b>          | <b>10<sup>-6</sup> m Noise</b> | <b>10<sup>-5</sup> m Noise</b> | <b>10<sup>-4</sup> m Noise</b> |
|---|-------------------------|-------------------------|--------------------------------|--------------------------------|--------------------------------|
| Front Axle Weight                               | 132,900 N               | 132,891 N               | 132,885 N                      | 132,221 N                      | 134,472 N                      |
| Rear Axle Weight                                | 145,100 N               | 145,111 N               | 145,130 N                      | 146,172 N                      | 144,982 N                      |
| Speed   | 30 m/s                  | 30 m/s                  | 30.1 m/s                       | 30 m/s                         | 29.8 m/s                       |
| Axle Spacing                                    | 10 m                    | 10 m                    | 10 m                           | 9.9 m                          | 10.1 m                         |
| R <sub>11</sub><br>(low mode amplitude, front)  | 3.02×10 <sup>-3</sup> m | 3.26×10 <sup>-3</sup> m | 2.28×10 <sup>-3</sup> m        | 4.01×10 <sup>-3</sup> m        | 4.74×10 <sup>-3</sup> m        |
| R <sub>12</sub><br>(high mode amplitude, front) | 7.8×10 <sup>-2</sup> m  | 7.1×10 <sup>-2</sup> m  | 8.9×10 <sup>-2</sup> m         | 9.0×10 <sup>-2</sup> m         | 5.1×10 <sup>-2</sup> m         |
| ω <sub>11</sub> (low mode, front)               | 1.61 Hz                 | 1.67 Hz                 | 1.75 Hz                        | 1.50 Hz                        | 2.48 Hz                        |
| ξ <sub>11</sub> (low mode, front)               | 6.2%                    | 6.6%                    | 5.7%                           | 5.3%                           | 3.2%                           |
| ω <sub>12</sub> (high mode, front)              | 11.27 Hz                | 12.12 Hz                | 10.58 Hz                       | 14.03 Hz                       | 10.00 Hz                       |
| ξ <sub>12</sub> (high mode, front)              | 27.1%                   | 26.3%                   | 29.2%                          | 29.8%                          | 32.1%                          |
| R <sub>21</sub><br>(low mode amplitude, rear)   | 3.91×10 <sup>-3</sup> m | 3.28×10 <sup>-3</sup> m | 4.51×10 <sup>-3</sup> m        | 2.50×10 <sup>-3</sup> m        | 2.17×10 <sup>-3</sup> m        |
| R <sub>22</sub><br>(high mode amplitude, rear)  | 8.1×10 <sup>-2</sup> m  | 8.9×10 <sup>-2</sup> m  | 7.2×10 <sup>-2</sup> m         | 6.8×10 <sup>-2</sup> m         | 5.8×10 <sup>-2</sup> m         |
| ω <sub>21</sub> (low mode, rear)                | 1.53 Hz                 | 1.68 Hz                 | 1.89 Hz                        | 2.01 Hz                        | 2.37 Hz                        |
| ξ <sub>21</sub> (low mode, rear)                | 5.9%                    | 5.2%                    | 5.0%                           | 4.7%                           | 8.2%                           |
| ω <sub>22</sub> (high mode, rear)               | 11.26 Hz                | 11.60 Hz                | 12.28 Hz                       | 12.64 Hz                       | 14.86 Hz                       |
| ξ <sub>22</sub> (high mode, rear)               | 26.9%                   | 28.0%                   | 30.1%                          | 21.4%                          | 19.3%                          |

**Table 9.16 Truck 15 Estimates**

| <b>Parameter</b>                                | <b>True Value</b>       | <b>0 Noise</b>          | <b>10<sup>-6</sup> m Noise</b> | <b>10<sup>-5</sup> m Noise</b> | <b>10<sup>-4</sup> m Noise</b> |
|---|-------------------------|-------------------------|--------------------------------|--------------------------------|--------------------------------|
| Front Axle Weight                               | 132,900 N               | 132,897 N               | 132,878 N                      | 132,294 N                      | 135,501 N                      |
| Rear Axle Weight                                | 157,200 N               | 157,308 N               | 157,271 N                      | 158,403 N                      | 158,173 N                      |
| Speed   | 25 m/s                  | 25 m/s                  | 25 m/s                         | 25 m/s                         | 25.1 m/s                       |
| Axle Spacing                                    | 10 m                    | 10 m                    | 9.9 m                          | 10 m                           | 10 m                           |
| R <sub>11</sub><br>(low mode amplitude, front)  | 3.16×10 <sup>-3</sup> m | 3.51×10 <sup>-3</sup> m | 3.88×10 <sup>-3</sup> m        | 4.15×10 <sup>-3</sup> m        | 2.14×10 <sup>-3</sup> m        |
| R <sub>12</sub><br>(high mode amplitude, front) | 7.9×10 <sup>-2</sup> m  | 7.6×10 <sup>-2</sup> m  | 6.9×10 <sup>-2</sup> m         | 6.2×10 <sup>-2</sup> m         | 10.4×10 <sup>-2</sup> m        |
| ω <sub>11</sub> (low mode, front)               | 1.61 Hz                 | 1.66 Hz                 | 1.71 Hz                        | 2.11 Hz                        | 2.56 Hz                        |
| ξ <sub>11</sub> (low mode, front)               | 6.2%                    | 6.4%                    | 6.7%                           | 7.2%                           | 7.9%                           |
| ω <sub>12</sub> (high mode, front)              | 11.27 Hz                | 11.76 Hz                | 12.26 Hz                       | 10.02 Hz                       | 13.71 Hz                       |
| ξ <sub>12</sub> (high mode, front)              | 27.1%                   | 26.6%                   | 25.9%                          | 29.2%                          | 30.6%                          |
| R <sub>21</sub><br>(low mode amplitude, rear)   | 3.97×10 <sup>-3</sup> m | 4.16×10 <sup>-3</sup> m | 3.08×10 <sup>-3</sup> m        | 4.95×10 <sup>-3</sup> m        | 5.61×10 <sup>-3</sup> m        |
| R <sub>22</sub><br>(high mode amplitude, rear)  | 8.4×10 <sup>-2</sup> m  | 9.0×10 <sup>-2</sup> m  | 9.6×10 <sup>-2</sup> m         | 7.0×10 <sup>-2</sup> m         | 10.4×10 <sup>-2</sup> m        |
| ω <sub>21</sub> (low mode, rear)                | 2.64 Hz                 | 2.85 Hz                 | 2.16 Hz                        | 1.72 Hz                        | 3.91 Hz                        |
| ξ <sub>21</sub> (low mode, rear)                | 6.6%                    | 6.9%                    | 6.0%                           | 5.6%                           | 4.9%                           |
| ω <sub>22</sub> (high mode, rear)               | 19.75 Hz                | 19.03 Hz                | 17.85 Hz                       | 22.45 Hz                       | 23.65 Hz                       |
| ξ <sub>22</sub> (high mode, rear)               | 16.0%                   | 16.9%                   | 17.2%                          | 19.1%                          | 12.7%                          |

**Table 9.17 Truck 16 Estimates**

| <b>Parameter</b>                                | <b>True Value</b>       | <b>0 Noise</b>          | <b>10<sup>-6</sup> m Noise</b> | <b>10<sup>-5</sup> m Noise</b> | <b>10<sup>-4</sup> m Noise</b> |
|---|-------------------------|-------------------------|--------------------------------|--------------------------------|--------------------------------|
| Front Axle Weight                               | 150,100 N               | 150,356 N               | 150,276 N                      | 150,943 N                      | 148,192 N                      |
| Rear Axle Weight                                | 178,174 N               | 178,252 N               | 173,344 N                      | 177,429 N                      | 175,367 N                      |
| Speed   | 35 m/s                  | 35 m/s                  | 34.9 m/s                       | 34.9 m/s                       | 34.9 m/s                       |
| Axle Spacing                                    | 8 m                     | 8 m                     | 8.1 m                          | 8 m                            | 8.2 m                          |
| R <sub>11</sub><br>(low mode amplitude, front)  | 1.03×10 <sup>-3</sup> m | 1.94×10 <sup>-3</sup> m | 0.69×10 <sup>-3</sup> m        | 2.38×10 <sup>-3</sup> m        | 3.21×10 <sup>-3</sup> m        |
| R <sub>12</sub><br>(high mode amplitude, front) | 5.4×10 <sup>-2</sup> m  | 6.2×10 <sup>-2</sup> m  | 3.1×10 <sup>-2</sup> m         | 3.0×10 <sup>-2</sup> m         | 8.9×10 <sup>-2</sup> m         |
| ω <sub>11</sub> (low mode, front)               | 1.66 Hz                 | 1.84 Hz                 | 2.20 Hz                        | 1.50 Hz                        | 2.41 Hz                        |
| ξ <sub>11</sub> (low mode, front)               | 5.9%                    | 6.2%                    | 4.5%                           | 7.1%                           | 7.9%                           |
| ω <sub>12</sub> (high mode, front)              | 12.06 Hz                | 12.89 Hz                | 11.04 Hz                       | 13.51 Hz                       | 15.26 Hz                       |
| ξ <sub>12</sub> (high mode, front)              | 37.9%                   | 34.8%                   | 30.5%                          | 29.1%                          | 29.0%                          |
| R <sub>21</sub><br>(low mode amplitude, rear)   | 1.28×10 <sup>-3</sup> m | 2.12×10 <sup>-3</sup> m | 2.86×10 <sup>-3</sup> m        | 0.68×10 <sup>-3</sup> m        | 0.53×10 <sup>-3</sup> m        |
| R <sub>22</sub><br>(high mode amplitude, rear)  | 6.0×10 <sup>-2</sup> m  | 4.7×10 <sup>-2</sup> m  | 4.2×10 <sup>-2</sup> m         | 8.5×10 <sup>-2</sup> m         | 9.7×10 <sup>-2</sup> m         |
| ω <sub>21</sub> (low mode, rear)                | 2.35 Hz                 | 2.59 Hz                 | 1.97 Hz                        | 3.05 Hz                        | 3.83 Hz                        |
| ξ <sub>21</sub> (low mode, rear)                | 7.7%                    | 8.1%                    | 8.3%                           | 6.2%                           | 5.8%                           |
| ω <sub>22</sub> (high mode, rear)               | 18.74 Hz                | 19.15 Hz                | 20.19 Hz                       | 20.62 Hz                       | 15.18 Hz                       |
| ξ <sub>22</sub> (high mode, rear)               | 25.1%                   | 23.7%                   | 22.9%                          | 28.7%                          | 30.0%                          |

**Table 9.18 Truck 17 Estimates**

| <b>Parameter</b>                                | <b>True Value</b>       | <b>0 Noise</b>          | <b>10<sup>-6</sup> m Noise</b> | <b>10<sup>-5</sup> m Noise</b> | <b>10<sup>-4</sup> m Noise</b> |
|---|-------------------------|-------------------------|--------------------------------|--------------------------------|--------------------------------|
| Front Axle Weight                               | 98,000 N                | 97,990 N                | 97,965 N                       | 97,647 N                       | 99,343 N                       |
| Rear Axle Weight                                | 98,000 N                | 97,994 N                | 98,026 N                       | 98,135 N                       | 95,562 N                       |
| Speed   | 25 m/s                  | 25 m/s                  | 25 m/s                         | 25 m/s                         | 24.9 m/s                       |
| Axle Spacing                                    | 6 m                     | 6 m                     | 6 m                            | 6.1 m                          | 6.1 m                          |
| R <sub>11</sub><br>(low mode amplitude, front)  | 2.47×10 <sup>-3</sup> m | 2.89×10 <sup>-3</sup> m | 1.91×10 <sup>-3</sup> m        | 1.48×10 <sup>-3</sup> m        | 4.05×10 <sup>-3</sup> m        |
| R <sub>12</sub><br>(high mode amplitude, front) | 1.26×10 <sup>-2</sup> m | 2.0×10 <sup>-2</sup> m  | 2.2×10 <sup>-2</sup> m         | 0.8×10 <sup>-2</sup> m         | 3.1×10 <sup>-2</sup> m         |
| ω <sub>11</sub> (low mode, front)               | 1.91 Hz                 | 1.79 Hz                 | 1.62 Hz                        | 2.38 Hz                        | 2.89 Hz                        |
| ξ <sub>11</sub> (low mode, front)               | 10.9%                   | 11.3%                   | 11.6%                          | 8.7%                           | 12.8%                          |
| ω <sub>12</sub> (high mode, front)              | 11.16 Hz                | 11.80 Hz                | 10.27 Hz                       | 13.34 Hz                       | 10.02 Hz                       |
| ξ <sub>12</sub> (high mode, front)              | 41.8%                   | 43.1%                   | 39.6%                          | 37.4%                          | 48.2%                          |
| R <sub>21</sub><br>(low mode amplitude, rear)   | 2.62×10 <sup>-3</sup> m | 2.22×10 <sup>-3</sup> m | 3.17×10 <sup>-3</sup> m        | 3.54×10 <sup>-3</sup> m        | 1.07×10 <sup>-3</sup> m        |
| R <sub>22</sub><br>(high mode amplitude, rear)  | 1.64×10 <sup>-2</sup> m | 2.6×10 <sup>-2</sup> m  | 0.8×10 <sup>-2</sup> m         | 3.1×10 <sup>-2</sup> m         | 0.6×10 <sup>-2</sup> m         |
| ω <sub>21</sub> (low mode, rear)                | 2.50 Hz                 | 2.82 Hz                 | 2.04 Hz                        | 1.82 Hz                        | 3.65 Hz                        |
| ξ <sub>21</sub> (low mode, rear)                | 9.8%                    | 9.2%                    | 10.4%                          | 10.7%                          | 6.9%                           |
| ω <sub>22</sub> (high mode, rear)               | 15.27 Hz                | 14.35 Hz                | 13.96 Hz                       | 19.26 Hz                       | 10.16 Hz                       |
| ξ <sub>22</sub> (high mode, rear)               | 30.3%                   | 31.0%                   | 31.7%                          | 32.8%                          | 25.7%                          |

**Table 9.19 Truck 18 Estimates**

| <b>Parameter</b>                                | <b>True Value</b>       | <b>0 Noise</b>          | <b>10<sup>-6</sup> m Noise</b> | <b>10<sup>-5</sup> m Noise</b> | <b>10<sup>-4</sup> m Noise</b> |
|---|-------------------------|-------------------------|--------------------------------|--------------------------------|--------------------------------|
| Front Axle Weight                               | 106,064 N               | 105,734 N               | 105,753 N                      | 105,173 N                      | 104,410 N                      |
| Rear Axle Weight                                | 147,100 N               | 147,089 N               | 147,023 N                      | 146,123 N                      | 149,208 N                      |
| Speed   | 25 m/s                  | 25 m/s                  | 25 m/s                         | 24.9 m/s                       | 25 m/s                         |
| Axle Spacing                                    | 6 m                     | 6 m                     | 6 m                            | 6.1 m                          | 5.9 m                          |
| R <sub>11</sub><br>(low mode amplitude, front)  | 2.28×10 <sup>-3</sup> m | 2.71×10 <sup>-3</sup> m | 2.82×10 <sup>-3</sup> m        | 3.14×10 <sup>-3</sup> m        | 3.89×10 <sup>-3</sup> m        |
| R <sub>12</sub><br>(high mode amplitude, front) | 1.62×10 <sup>-2</sup> m | 2.1×10 <sup>-2</sup> m  | 1.2×10 <sup>-2</sup> m         | 2.9×10 <sup>-2</sup> m         | 3.8×10 <sup>-2</sup> m         |
| ω <sub>11</sub> (low mode, front)               | 1.78 Hz                 | 1.64 Hz                 | 1.91 Hz                        | 1.50 Hz                        | 3.20 Hz                        |
| ξ <sub>11</sub> (low mode, front)               | 6.6%                    | 6.9%                    | 7.4%                           | 7.8%                           | 8.8%                           |
| ω <sub>12</sub> (high mode, front)              | 11.44 Hz                | 10.94 Hz                | 12.10 Hz                       | 12.82 Hz                       | 14.17 Hz                       |
| ξ <sub>12</sub> (high mode, front)              | 29.7%                   | 30.3%                   | 28.2%                          | 28.3%                          | 34.0%                          |
| R <sub>21</sub><br>(low mode amplitude, rear)   | 2.81×10 <sup>-3</sup> m | 2.42×10 <sup>-3</sup> m | 1.86×10 <sup>-3</sup> m        | 1.72×10 <sup>-3</sup> m        | 4.37×10 <sup>-3</sup> m        |
| R <sub>22</sub><br>(high mode amplitude, rear)  | 1.52×10 <sup>-2</sup> m | 2.0×10 <sup>-2</sup> m  | 2.4×10 <sup>-2</sup> m         | 0.7×10 <sup>-2</sup> m         | 3.8×10 <sup>-2</sup> m         |
| ω <sub>21</sub> (low mode, rear)                | 1.87 Hz                 | 2.06 Hz                 | 1.62 Hz                        | 2.68 Hz                        | 1.50 Hz                        |
| ξ <sub>21</sub> (low mode, rear)                | 12.3%                   | 12.0%                   | 11.1%                          | 10.4%                          | 16.3%                          |
| ω <sub>22</sub> (high mode, rear)               | 13.34 Hz                | 13.92 Hz                | 12.28 Hz                       | 14.86 Hz                       | 10.13 Hz                       |
| ξ <sub>22</sub> (high mode, rear)               | 19.7%                   | 20.6%                   | 21.3%                          | 17.4%                          | 24.5%                          |

**Table 9.20 Truck 19 Estimates**

| <b>Parameter</b>                                | <b>True Value</b>       | <b>0 Noise</b>          | <b>10<sup>-6</sup> m Noise</b> | <b>10<sup>-5</sup> m Noise</b> | <b>10<sup>-4</sup> m Noise</b> |
|---|-------------------------|-------------------------|--------------------------------|--------------------------------|--------------------------------|
| Front Axle Weight                               | 97,000 N                | 97,028 N                | 97,041 N                       | 97,285 N                       | 97,285 N                       |
| Rear Axle Weight                                | 152,185 N               | 152,282 N               | 152,328 N                      | 152,564 N                      | 152,403 N                      |
| Speed   | 35 m/s                  | 35 m/s                  | 35 m/s                         | 35.2 m/s                       | 35.1 m/s                       |
| Axle Spacing                                    | 5 m                     | 5 m                     | 5 m                            | 5.1 m                          | 5.1 m                          |
| R <sub>11</sub><br>(low mode amplitude, front)  | 2.41×10 <sup>-3</sup> m | 2.06×10 <sup>-3</sup> m | 2.95×10 <sup>-3</sup> m        | 1.30×10 <sup>-3</sup> m        | 0.95×10 <sup>-3</sup> m        |
| R <sub>12</sub><br>(high mode amplitude, front) | 1.79×10 <sup>-2</sup> m | 2.20×10 <sup>-2</sup> m | 0.86×10 <sup>-2</sup> m        | 3.34×10 <sup>-2</sup> m        | 3.81×10 <sup>-2</sup> m        |
| ω <sub>11</sub> (low mode, front)               | 2.09 Hz                 | 2.37 Hz                 | 1.68 Hz                        | 3.26 Hz                        | 1.50 Hz                        |
| ξ <sub>11</sub> (low mode, front)               | 7.4%                    | 6.8%                    | 7.9%                           | 6.1%                           | 5.4%                           |
| ω <sub>12</sub> (high mode, front)              | 12.49 Hz                | 11.52 Hz                | 11.04 Hz                       | 14.37 Hz                       | 15.85 Hz                       |
| ξ <sub>12</sub> (high mode, front)              | 49.8%                   | 51.1%                   | 53.0%                          | 53.8%                          | 54.2%                          |
| R <sub>21</sub><br>(low mode amplitude, rear)   | 3.18×10 <sup>-3</sup> m | 3.72×10 <sup>-3</sup> m | 2.36×10 <sup>-3</sup> m        | 2.18×10 <sup>-3</sup> m        | 5.23×10 <sup>-3</sup> m        |
| R <sub>22</sub><br>(high mode amplitude, rear)  | 1.46×10 <sup>-2</sup> m | 1.85×10 <sup>-2</sup> m | 0.84×10 <sup>-2</sup> m        | 1.0×10 <sup>-2</sup> m         | 0.68×10 <sup>-2</sup> m        |
| ω <sub>21</sub> (low mode, rear)                | 1.83 Hz                 | 1.61 Hz                 | 2.37 Hz                        | 2.46 Hz                        | 3.04 Hz                        |
| ξ <sub>21</sub> (low mode, rear)                | 5.9%                    | 6.3%                    | 5.2%                           | 4.9%                           | 7.2%                           |
| ω <sub>22</sub> (high mode, rear)               | 13.38 Hz                | 14.17 Hz                | 14.31 Hz                       | 11.75 Hz                       | 11.32 Hz                       |
| ξ <sub>22</sub> (high mode, rear)               | 34.1%                   | 35.7%                   | 33.2%                          | 32.6%                          | 30.3%                          |

**Table 9.21 Truck 20 Estimates**

| <b>Parameter</b>                                | <b>True Value</b>       | <b>0 Noise</b>          | <b>10<sup>-6</sup> m Noise</b> | <b>10<sup>-5</sup> m Noise</b> | <b>10<sup>-4</sup> m Noise</b> |
|---|-------------------------|-------------------------|--------------------------------|--------------------------------|--------------------------------|
| Front Axle Weight                               | 98,000 N                | 98,017 N                | 97,991 N                       | 98,049 N                       | 98,680 N                       |
| Rear Axle Weight                                | 124,100 N               | 124,173 N               | 124,194 N                      | 123,772 N                      | 122,392 N                      |
| Speed   | 35 m/s                  | 35 m/s                  | 34.9 m/s                       | 35 m/s                         | 34.9 m/s                       |
| Axle Spacing                                    | 5 m                     | 5 m                     | 5 m                            | 4.9 m                          | 5.1 m                          |
| R <sub>11</sub><br>(low mode amplitude, front)  | 2.78×10 <sup>-3</sup> m | 3.46×10 <sup>-3</sup> m | 3.61×10 <sup>-3</sup> m        | 1.82×10 <sup>-3</sup> m        | 1.47×10 <sup>-3</sup> m        |
| R <sub>12</sub><br>(high mode amplitude, front) | 2.03×10 <sup>-2</sup> m | 2.82×10 <sup>-2</sup> m | 1.52×10 <sup>-2</sup> m        | 3.26×10 <sup>-2</sup> m        | 1.14×10 <sup>-2</sup> m        |
| ω <sub>11</sub> (low mode, front)               | 1.79 Hz                 | 1.92 Hz                 | 2.23 Hz                        | 1.52 Hz                        | 2.68 Hz                        |
| ξ <sub>11</sub> (low mode, front)               | 6.0%                    | 6.4%                    | 6.6%                           | 5.0%                           | 4.6%                           |
| ω <sub>12</sub> (high mode, front)              | 10.38 Hz                | 10.04 Hz                | 11.39 Hz                       | 12.41 Hz                       | 12.79 Hz                       |
| ξ <sub>12</sub> (high mode, front)              | 30.3%                   | 31.2%                   | 28.6%                          | 33.4%                          | 26.2%                          |
| R <sub>21</sub><br>(low mode amplitude, rear)   | 3.36×10 <sup>-3</sup> m | 3.02×10 <sup>-3</sup> m | 4.26×10 <sup>-3</sup> m        | 2.86×10 <sup>-3</sup> m        | 2.14×10 <sup>-3</sup> m        |
| R <sub>22</sub><br>(high mode amplitude, rear)  | 1.12×10 <sup>-2</sup> m | 1.41×10 <sup>-2</sup> m | 1.74×10 <sup>-2</sup> m        | 0.45×10 <sup>-2</sup> m        | 3.18×10 <sup>-2</sup> m        |
| ω <sub>21</sub> (low mode, rear)                | 1.70 Hz                 | 1.84 Hz                 | 1.53 Hz                        | 2.38 Hz                        | 2.86 Hz                        |
| ξ <sub>21</sub> (low mode, rear)                | 6.9%                    | 6.4%                    | 5.5%                           | 7.8%                           | 8.3%                           |
| ω <sub>22</sub> (high mode, rear)               | 11.69 Hz                | 12.02 Hz                | 10.78 Hz                       | 12.81 Hz                       | 13.42 Hz                       |
| ξ <sub>22</sub> (high mode, rear)               | 36.1%                   | 37.0%                   | 37.6%                          | 38.3%                          | 29.5%                          |

## 9.7 Conclusions and Contributions

The identification of truck parameters using the dynamic bridge and dynamic truck models is the culmination of the work described in the previous chapters. The algorithm described in Chapter 9 cannot only determine truck axle weights from the deflection profiles, but also gives accurate information about the dynamic properties of the truck, including the natural frequencies and damping ratios of each axle. The transformation of the truck system to depend on the parameters in the assumed homogeneous solution allows the integration of the coupled bridge/truck equations of motion without the introduction of additional optimization parameters. This transformation also eliminates the spring constant  $ku$  as an optimization parameter since it can be determined from the other terms in the truck model.

Twenty simulated trucks were used to evaluate the performance of the algorithm. Their configurations are given in Table 3.2. The front axle weights of the trucks ranged from  $9.7 \times 10^4 \text{N}$  to  $1.32 \times 10^5 \text{N}$ , and the rear axle weights ranged from  $9.8 \times 10^4 \text{N}$  to  $1.93 \times 10^5 \text{N}$ . The natural frequencies of each axle ranged from 1.5 Hz-2.6 Hz (low mode) and 10.4 Hz-18.7 Hz (high mode). The damping ratios varied from 5.4%-12.9% (low mode) and 16.7%-50% (high mode). Different initial conditions were also used with each axle.

Estimates of the axle weights for the different levels of measurement noise are given in Figures 9.3-9.12 and Table 9.1. The maximum magnitude of the percent error in axle weight estimate for zero measurement noise was 0.019%. With the addition of measurement noise of  $\pm 1 \times 10^{-6} \text{m}$ , estimates of axle weights remained within 0.03%. For

measurement noise of  $\pm 1 \times 10^{-5}$  m, the maximum error in axle weight estimates was 0.6%, and for noise of  $\pm 1 \times 10^{-4}$  m, the error remained below 1.15%.

Estimates of the dynamic properties of each axle were also quite accurate. For zero measurement noise, the natural frequency and damping ratio of the low mode could be estimated to within 0.5 Hz and 0.8% (of critical damping) respectively. The properties of the high mode could also be estimated; the natural frequency could be determined to within 1.3 Hz and the damping ratio to within 3.1% (of critical damping).

These dynamic properties could also be found when measurement noise was added to the deflection profiles. For measurement noise of  $\pm 1 \times 10^{-6}$  m, the natural frequency and damping ratio of the low mode could be found within 0.85 Hz and 2.1% (of critical damping) respectively. The high mode could be identified to within 1.9 Hz and 3.4% (of critical damping). For measurement noise of  $\pm 1 \times 10^{-5}$  m, the low mode could be found to within 1.8 Hz and damping to within 3% (of critical damping). The high mode could be identified to within 3.6 Hz and damping ratio to within 8.4%. For the largest measurement noise of  $\pm 1 \times 10^{-4}$  m, the low mode's natural frequency and damping ratio could be determined to within 2 Hz and 3.6%, and the high mode to within 4.4 Hz and 14% (of critical damping).

The ability to identify not only axle weights, but also the dynamic properties of each axle is unique to this algorithm and provides useful information regarding the passing truck. Assuming a form of the homogeneous solution of each axle and then transforming the truck equations of motion to depend on the parameters in this solution allows the integration of the coupled system inside the optimization routine. The integration produces the bridge deflection profiles due to each estimate of the truck

**parameters at each iteration of the optimization routine. This transformation and identification technique could also be applied to other systems with similar behavior.**

# Chapter 10

## Conclusions and Future Work

### 10.1 Conclusions

The goal of this dissertation was to develop an algorithm to estimate truck axle weights to within 1% using the deflection of a bridge due to that truck. Currently there are bridge weigh-in-motion (WIM) systems in limited use, but they are only able to predict axle weights to within 10-15%. Other authors have developed algorithms to determine axle weights, but they do not predict the dynamic properties of the truck or the interaction between the truck and the bridge. The algorithm described in this work can not only predict axle weights much more accurately than the other methods, but also provides useful information on the dynamic properties of the truck. The addition of measurement noise to the deflection profile is also examined to more accurately represent a realistic measured signal. Measurement noise of magnitude  $\pm 1 \times 10^{-6}$  m to  $\pm 1 \times 10^{-4}$  m was added to assess the algorithm's performance using imperfect deflection measurements.

To identify the truck crossing the bridge, it was first necessary to accurately represent the coupled bridge/truck system, including the interaction between the two. The coupled bridge/truck system of equations are developed and integrated to determine the deflection of the bridge due to the force of the truck. This representation of the bridge/truck system determined the interaction between the two explicitly rather than approximating it as is done by many other authors.

Several assumptions were made throughout this work. First, it was assumed that the truck traveled at a constant speed across the bridge. It was also assumed that the truck's total time on the bridge was known-that the entrance time of the front axle and the exit time of the rear axle were determined by another source. This allowed the truck's speed to be determined from the truck's total time on the bridge and the axle spacing and eliminated speed as an optimization parameter. It was also assumed that the material and bending properties of the bridge were known precisely.

While the accurate estimation of the truck's axle weights was the primary goal of this work, it became necessary to estimate the dynamic properties of each axle as well. An approximate model of the force applied by each axle was assumed which consisted of the superposition of the truck's static weight and the homogeneous solution of the differential equations of motion of the 'quarter-car' model. The homogeneous solution was the superposition of two damped oscillatory modes in which the natural frequencies, damping ratios, and initial conditions were unknown. This approximate force model was then applied to the coupled bridge/truck system. The system was integrated to determine the interaction between the two and the response of the bridge.

Because the bridge/truck system of equations had to be integrated inside the optimization routine, it was necessary to transform the truck system of equations from depending on physical parameters (stiffness, damping, and mass) to the modal parameters expressed in the homogeneous solution. This transformation allowed the integration of the truck equations without adding additional optimization parameters. Using this transformed system, the natural frequencies, damping ratios, and initial conditions of

each mode of each axle were unknown, as well as the static axle weight and axle spacing. Each of these parameters was estimated by the optimization routine.

Twenty simulated trucks were used to evaluate the optimization routine's performance. The configuration of each of these trucks is given in Table 3.2. The front axle weights of the trucks ranged from  $9.7 \times 10^4 \text{N}$  to  $1.32 \times 10^5 \text{N}$  and the rear axle weights ranged from  $9.8 \times 10^4 \text{N}$  to  $1.93 \times 10^5 \text{N}$ . The lower mode's natural frequencies ranged from 1.5-2.6 Hz and the damping ratios ranged from 5.4%-12.9% (of critical). The higher mode's natural frequencies ranged from 10.4-18.4 Hz and the damping of this mode ranged from 16.7%-50%. The axle spacing varied from 4-10m and the speed from 25-35 m/s.

With zero measurement noise, the estimates of axle weights were very accurate. The average magnitude of the percent error in weight estimates was 0.007% with maximum errors less than 0.019%. The dynamic properties of each axle were also determined very accurately. The frequency and damping of the lower mode could be determined to within 0.5 Hz and 0.8% respectively. The high mode's frequency and damping could be found to within 1.3 Hz and 3.1%.

Accurate estimates of the truck parameters could also be found when measurement noise was added to the deflection profile. For measurement noise of magnitude  $\pm 1 \times 10^{-6} \text{m}$ , the error in axle weight estimates remained below 0.029%. The natural frequency of the low mode could be found to within 0.85 Hz and the damping to within 2.1%. For the high mode, the frequency could be found to within 1.9 Hz and the damping to within 3.4%. For the largest level of measurement noise,  $\pm 1 \times 10^{-4} \text{m}$ , the axle weights could be determined to within 1.15%. The frequency and damping of the low

mode could be found to within 2 Hz and 3.6%. The high mode's frequency and damping could be determined to within 4.4 Hz and 14%.

One limitation of this method is the time required to identify each truck. Inside the optimization routine, the coupled bridge/truck equations must be integrated with each set of approximate truck parameters. This integration requires approximately 5 seconds to complete. The optimization routine requires as many as 7,000 iterations to accurately identify all of the relevant truck parameters, resulting in 10-12 hours of computation time per truck. This time scale makes real-time identification of truck parameters impossible, although off-line computations would still be feasible.

The final stage of the algorithm described in Chapter 9 was developed using a series of simpler models which are described in Chapters 6-8. The first treated the static bridge and the static, or moving point force, model of the truck. The use of a random sampling method eliminated the problems associated with the discontinuous nature of the bridge/truck system and resulted in weight estimates with error less than  $4.5 \times 10^{-3}\%$  for zero measurement noise.

The second combination of models used the dynamic bridge model and the static truck model. It was found in this section that the use of three rather than one measurement location was necessary to estimate axle weights without prior knowledge of the truck's speed and axle spacing. Using the three deflection profiles to formulate the objective function resulted in less than 0.003% error in axle weight estimates.

The third combination of models was the first to use the dynamic, or 'quarter-car' model of the truck. The static bridge model was used to simplify the system for this stage. Using these models, the damped oscillatory form of the homogeneous solution of the

truck motion was adopted and used to represent the force imparted by the truck. An approximation of the interaction effects was used to eliminate the need to integrate the equations of motion. Using the three measurement locations and the approximate force model, the axle weights could be estimated to within 0.018%. Accurate estimates of the dynamic properties of the truck were also obtained and are given in Chapter 8.

In conclusion, the work described in this dissertation has two significant contributions. The first is the transformation of the truck system from the physical parameters to its modal ones. This transformation allowed the integration of the coupled bridge/truck equations without the requiring additional optimization parameters. Not only was such a transformation useful in this work, the method could be applied to other systems with similar properties.

The second major contribution is the ability to estimate not only axle weights very accurately, but also to be able to gain very good estimates of the dynamic properties of the truck as well. The axle weight estimates are very accurate even with the addition of measurement noise, but the ability to predict the natural frequencies and damping ratios of each axle is unique to this work.

## **10.2 Future Work**

Several things could be done to expand upon the work described here. One of the most obvious would be to eliminate the need to measure the truck's total time on the bridge. The use of more complex models of both the truck and the bridge could also be explored. Plate-type bridge models which include the torsional behavior of an actual bridge could be useful in implementing such a WIM system on a bridge with multiple or

off-center lanes. Truck models which include pitch and/or roll could be used to more accurately represent the load-sharing properties between the axles. Three-dimensional truck models that model each end of each axle separately could also be used, although the computational complexity of such a model could outweigh the benefit of greater detail.

Although the initial conditions of the truck entering the bridge were included in this work, the surface roughness of the bridge was not. The addition of surface roughness to the bridge model could be explored to determine whether the superposition of solutions used in the approximate truck model would be adequate when the truck was excited by not only the bridge deflection, but also small disturbances due to the variation in bridge surface.

Probably the most beneficial addition to this work would be the development of an approximate closed form solution to the coupled dynamic bridge/dynamic truck system. In the static bridge/dynamic truck case, an approximate solution for the deflection under each axle was used to determine the driven part of the truck's motion, and an analytic expression was evaluated to obtain the deflection profiles. An acceptable approximate solution was not found in this work for the dynamic bridge/dynamic truck case which could eliminate the need to integrate the coupled bridge/truck equations at each iteration of the optimization routine. An approximate solution for the driven portion of the truck's motion or the deflection profile due to the truck would greatly reduce the time required to identify each truck and make the algorithm more practical for real-time calculations.

# References

Ali, N., Trogon, J., Bergan, A.T., "Evaluation of Piezoelectric Weigh-in-Motion System"  
Canadian Journal of Civil Engineering, Vol. 21, No. 1, Feb 1995, pp. 34-47.

Beshears, D., Capps, G., Jordan, J., LaForge, J., Muhs, J., Nodine, R., Scudiere, M., White, C.,  
'System and Methods for Accurately Weighing and Characterizing Moving Vehicles', U.S.  
Patent No. US5998741, Dec. 1999.

Broyden, C.G., 'The Convergence of a Class of Double-rank Minimization Algorithms', Journal  
of Inst. Mathematics Applications, Vol. 6, 1970, pp. 76-90.

Cebon, D. Handbook of Vehicle-Road Interaction, Swets & Zeitlinger Publishers, Exton, Pa,  
USA, 1999.

Chan, T.H.T, Law, S.S, Yung, T.H., Yuan, X.R., "An Interpretive Method for Moving Force  
Identification", Journal of Sound and Vibration, Vol. 219, No. 3, 1999, pp. 503-524.

Chatterjee, P.K, Datta, T.K., Surana, C.S, "Vibration of Continuous Bridges Under Moving  
Vehicles", Journal of Sound and Vibration, Vol. 169, No. 5, 1994, pp. 619-632.

Chompooming, K., Yener, M., "The Influence of Roadway Surface Irregularities and Vehicle  
Deceleration on Bridge Dynamics Using Method of Lines", Journal of Sound and Vibration, Vol.  
183, No. 4, 1995, pp. 567-589.

Cole, D.J., Cebon, D., "Validation of an Articulated Vehicle Simulation", *Vehicle System Dynamics*, Vol. 21, 1992, pp. 197-223.

de Henau, A., "Weigh-in-Motion of Wheel, Axle, and Vehicle Loads", *Heavy Vehicle Systems, International Journal of Vehicle Design*, Vol. 1 No. 2, 1994, pp. 21-29.

"Exclusive Bridge Inventory Update", *Better Roads*, Vol. 59, No. 11, 1989, p. 20.

Fafard, M., Bennur, M. "A General Multi-Axle Vehicle Model to Study the Bridge/Vehicle Interaction", *Engineering Computation*, 1997, Vol. 14, No. 5, pp. 491-507.

Fafard, M., Laflamme, M., Savard, M., Bennur, M. "Dynamic Analysis of Existing Continuous Bridge", *Journal of Bridge Engineering*, Vol. 3, No. 1, Feb. 1998, pp. 28-37.

Fafard, M., Malliarjuna, B., Savard, M., 'A General Multi-Axle Vehicle Model to Study the Bridge-Vehicle Interaction', *Engineering Computations*, Vol. 14, No. 5, 1997, pp. 491-507.

Fletcher, R., 'A New Approach to Variable Metric Algorithms', *Computer Journal*, Vol. 13, 1970, pp. 317-322.

Forsen, A., "Parameter Identification in Heavy Vehicle Simulation", *Vehicle System Dynamics Supplement*, 1999, pp. 350-361.

**“Fragile Foundations: a Report on America’s Public Works”, National Council on Public Works Improvement (NCPWI), Washington, D.C., 1988.**

**Gere, J., Timoshenko, S., Mechanics of Materials, PWS Publishing, Boston, MA, USA, 1997.**

**Goldfarb, D., ‘A Family of Variable Metric Updates Derived by Variational Means’, Mathematics of Computing, Vol. 24, 1970, pp. 23-26.**

**Green, M.F., Cebon, D., “Dynamic Interaction Between Heavy Vehicles and Highway Bridges”, Computers and Structures ,Vol. 62, No.2, pp. 253-264, 1997.**

**Green, M.F., Cebon, D., Cole, D.J., “Effects of Vehicle Suspension Design on Dynamics of Highway Bridges”, Journal of Structural Engineering, Vol. 121, No. 2, Feb., 1995, pp. 34-41.**

**Henchi, K., Fafard, M., Talbot, M., Dhatt, G., “An Efficient Algorithm for Dynamic Analysis of Bridges Under Moving Vehicles Using a Coupled Modal and Physical Components Approach”, Journal of Sound and Vibration, Vol. 212, No. 4, 1998, pp. 663-683.**

**Hilal, M., Zibdeh, H., “Vibration Analysis of Beams with General Boundary Conditions Traversed by a Moving Force”, Journal of Sound and Vibration, Vol. 229, No. 2, 2000, pp. 377-388.**

Ibanez, P., Stoessel, J., Barrett, D., 'Method and Apparatus for Measuring the Weight of a Vehicle While the Vehicle is in Motion', U.S. Patent No. US4560016, Dec. 1985.

Judd, J., Appley, K., Yi, H., 'Method and Apparatus for Monitoring Multiple Points on a Vibrating Structure', U.S. Patent No. US5255565, Oct. 1993.

Law, S. Fang, Y., "Moving Force Identification: Optimal State Estimation Approach", Journal of Sound and Vibration, Vol. 201, No. 1, 1997, pp. 233-254.

Law, S., Chan, T, Zeng, Q., "Moving Force Identification: A Time Domain Method", Journal of Sound and Vibration, Vol. 201, No. 1, 1997, pp. 1-22.

Law, S., Zhu, X., "Study on Different Beam Models in Moving Force Identification", Journal of Sound and Vibration, Vol. 234, No. 4, 2000, pp. 661-679.

Loshbough, R., Hall, D., 'Vehicle Weighing in Motion Apparatus and Method', U.S. Patent No. US1989000447795, March, 1991.

Mills, N., 'Weigh-in-Motion Scale', U.S Patent No. US4957178, Sept 1990.

Muhs, J.D., Jordan, J.K., Tobin, K.W., LaForge, J.V., 'Apparatus for Weighing and Identifying Characteristics of a Moving Vehicle', U.S. Patent No. US199200086488, Nov. 1993.

Papagiannakis, A.T., "Calibration of Weigh-in-Motion Systems Through Dynamic Vehicle Simulation", *Journal of Testing and Evaluation*, Vol. 25, No. 2, 1997, pp. 197-204.

Papagiannakis, A.T., Senn, K., Huang, H., "On-Site Calibration Evaluation Procedures for WIM System", *Transportation Research Record* 1536, Nov. 1996, pp. 1-11.

Patten, W., Sack, R., He, Q. "Controlled Semiactive Hydraulic Vibration Absorber For Bridges", *Journal of Structural Engineering*, Feb. 1996, Vol. 122, No. 2, pp. 187-192.

Patten, W.N., Sun, J., Li, G., Kuehn, J., Song, G., "Field Test of an Intelligent Stiffener for Bridges at the I-35 Walnut Creek Bridge", *Earthquake Engineering and Structural Dynamics*, Vol. 28, 1999, pp. 109-126.

Pesterev, A., Bergman, L.A., "An Improved Series Expansion of the Solution to the Moving Oscillator Problem", *Transactions of the ASME, Journal of Vibration and Acoustics*, Vol. 122, Jan., 2000, pp. 54-61.

Pesterev, A.V., Bergman, L.A., "Response of a Nonconservative Continuous System to a Moving Concentrated Load", *Transactions of the ASME, Journal of Applied Mechanics*, Vol 65, June, 1998, pp. 436-444.

Pesterev, A.V., Bergman, L.A., "Response of Elastic Continuum Carrying Moving Linear Oscillator", *Journal of Engineering Mechanics*, Vol. 123, No. 8, August, 1997, pp. 886-889.

Pesterev, A.V., Bergman, L.A., "Vibration of Elastic Continuum Carrying Accelerating Oscillator", *Journal of Engineering Mechanics*, Vol. 123 No. 8, August, 1997, pp. 878-884.

Pesterev, A.V., Tan, C.A., Bergman, L.A., "A New Method for Calculating Bending Moment and Shear Force in Moving Load Problems", *Transactions of the ASME, Journal of Applied Mechanics*, Vol. 68, March 2001, pp. 252-259.

Pesterev, A.V., Tavrizov, G.A., "Vibrations of Beams with Oscillators I: Structural Analysis Method for Solving the Spectral Problem", *Journal of Sound and Vibration*, Vol. 170 No. 4, 1994, pp. 521-536.

Pesterev, A.V., Tavrizov, G.A., "Vibrations of Beams With Oscillators II: Generalized Static Green Operator", *Journal of Sound and Vibration*, Vol. 170, No. 4, 1994, pp. 537-544.

Pesterev, A.V., Yang, B, Bergman, L.A., Tan, C.A., "Response of Elastic Continuum Carrying Multiple Moving Oscillators" *Journal of Engineering Mechanics*, Vol. 127, No. 3, March 2001, pp. 260-265.

Shanno, D.F., 'Conditioning of Quasi-Newton Methods for Function Minimization', *Mathematics of Computing*, Vol. 24, 1970, pp. 647-656.

Snyder, R.E., Moses, F., Burke, B., Kennedy, D., Bridge Weigh-in-Motion, United States Patent No. 5,111,897, May 12, 1992.

Snyder, R., Moses, F., 'Application of In-Motion Weighing Using Instrumented Bridges', *Transportations Research Record*, Issue 1048, 1985, pp. 83-88.

Stalford, H., working papers on "Development of Equations of Motion for Dynamic Bridge/Dynamic Truck", Sept. 6, 2002.

Stalford, H., working papers on "Development of Truck State Matrices in Terms of its Modal Parameters", Oct. 15, 2002.

Stalford, H., Kullback, J., 'Identifying an Unknown Process by Utilizing Randomly Chosen Inputs.', *Information and Control Journal*, Vol. 23, No. 5, pp. 393-406, Dec. 1973.

Sun, J., Pang, J. Song, G., Patten, W. "Experimental Validation and Modal Analysis For A Highway Bridge", *Proceedings of DETC '97, 1997 ASME Design Engineering Technical Conferences*, Sept 14-17, 1997, Sacramento, CA, pp. 1-4

Tamamura, R., Yamanaka, M., 'Device for Weighing Running Vehicle', U.S. Patent No. US4049069, Sept. 1977.

Tan, G.H., Brameld, G.H, Thambiratnam, D.P., “Development of an Analytical Model for Treating Bridge-Vehicle Interaction”, *Engineering Structures*, Vol. 20, No. 1-2, 1998, pp. 54-61.

Thater, G., Chang, P., Schelling, D.R, Fu, C.C, “Estimation of Bridge Static Response and Vehicle Weights by Frequency Response Analysis”, *Canadian Journal of Civil Engineering*, Vol. 25, No. 4, August 1991, pp. 76-89.

Transportation Research Board, ‘WIM Technology’, National Research Council, 1986, pp. 16-34.

Vlasek, M., Stejskal, V., Sika, Z., Vaculin, O., Kovanda, J., “Dynamic Model of Truck for Suspension Control”, *Vehicle System Dynamics Supplement 28*, 1999, pp. 496-505.

Yamanaka, M., Masuda, Y., ‘Device for Weighing Running Vehicle’. United States Patent No. US3835945, Sept. 17, 1974.

Yang, F., Fonder, G., “An Iterative Solution Method for Dynamic Response of Bridge-Vehicle Systems”, *Earthquake Engineering and Structural Dynamics*, Vol. 25, 1996, pp. 195-215.

Yang, Y., Yau, J. “Vehicle-Bridge Interaction Element for Dynamic Analysis”, *Journal of Structural Engineering*, Nov., 1997, Vol. 123, No. 11, pp. 1512-1518.

**Yang, Y.B, Lin, B.H., “Vehicle-Bridge Interaction Analysis by Dynamic Condensation Method”,  
Journal of Structural Engineering, Vol. 121, No. 11, Nov., 1995, pp. 13-19.**